# CHAPTER IV

# ANALYSIS OF DATA

## A. Meteorology

### 1. Representativeness of Study Period

Hourly coast to inland station pressure gradients (reduced to mean sea level), mean Fresno 0400 PST 850 mb temperature and Fresno ozone concentrations were selected to compare the study period with the long-term records. Pressure gradients influence the air flow in the San Joaquin Valley and are affected by the synoptic pattern. The 850 mb temperature indicates the amount of stability which is also affected by the synoptic pattern. Ozone concentrations exceeding the federal and state standards indicate periods of stagnation within the San Joaquin Valley.

The surface pressure gradients (millibars, corrected to sea level) between San Francisco, California, and Las Vegas, Nevada, for the study period are shown in the table below. These locations roughly represent the pressure gradient between the coast and the Great Basin. Also included in the table below are the bulk Richardson (BR) numbers for 0500 PDT in Fresno. On average, the pressure gradient maxima occurred in the late afternoon at 1800 PDT and the minima occurred in the morning at 0800 PDT. As can be seen, the 13th, 14th, 17th, 18th and 19th were less stable (larger maximum, minimum and average pressure gradients) than the remaining days. These days also had

lower bulk Richardson numbers. The 21st was the only day where the maximum pressure gradient was low yet the bulk Richardson number was low also compared to the other days.

| Day | SF-LV Minimum | SF-LV Maximum | SF-LV Average | BR |
|---|---|---|---|---|
| 13 | 6.4 | 10.0 | 8.3 | 5.02 |
| 14 | 6.1 | 9.6 | 8.1 | 4.50 |
| 15 | 5.1 | 8.0 | 6.8 | 26.81 |
| 16 | 5.0 | 8.5 | 6.7 | 19.34 |
| 17 | 6.0 | 10.2 | 7.7 | 9.40 |
| 18 | 5.9 | 9.5 | 7.9 | 5.78 |
| 19 | 5.8 | 9.8 | 7.8 | 6.25 |
| 20 | 4.7 | 7.9 | 6.5 | 46.13 |
| 21 | 5.4 | 7.5 | 6.3 | 7.00 |
| 22 | 4.9 | 7.7 | 6.1 | 25.60 |

The average 0500 PDT pressure gradient for the ten days was 6.5 millibars whereas the long term average for August, 1972 to 1984, is 4.2 millibars (388 observations). This would possibly indicate less stability during the study period than average. Of the 388 observations, 3 percent were negative and 0.5 percent were zero. During the study period, no negative or zero gradients occurred.

The average 850 mb 0500 PDT temperature over Fresno for the study period was 17.6 degrees celcius. The long-term average for the month of August (1972 to 1984) was 19.8 degrees celcius (California Air Resources Board, Meteorological Division). This would indicate less stability than normal during the study period unless surface temperatures were cooler as well. The average 0500 PDT surface temperature for Fresno for the study period was 17.9 degrees celsius and the average for August, 1972 to 1984, was 18.9 degrees celcius.

The table below shows the number of days, followed by the

number of hours in August, the ozone concentrations exceeded 0.12 (federal standard) and 0.10 (state standard) parts per million (ppm) at three locations in Fresno (California Air Resources Board, 1978-1985). The data do not indicate that August, 1985, was more or less unstable than usual.

| | >0.12 ppm | | | >0.10 ppm | | |
|---|---|---|---|---|---|---|
| Year | Cal State | Olive Drive | Butle Street | Cal State | Olive Drive | Butle Street |
| 1978 | 10/23* | 6/13 | 6/19* | 14/81* | 9/35 | 9/53* |
| 1979 | 6/12* | 4/6 | 7/12* | 14/56* | 8/24 | 14/55* |
| 1980 | 10/19 | 5/8 | 6/10* | 21/84 | 10/39 | 18/71* |
| 1981 | 5/16 | 0/0* | 6/16 | 18/57 | 2/6* | 15/54 |
| 1982 | 4/5 | 0/0 | 3/7 | 12/40 | 1/2 | 16/47 |
| 1983 | 2/2 | 0/0 | 2/2 | 10/25 | 5/11 | 16/52 |
| 1984 | 6/7 | 0/0 | 4/6 | 15/50 | 0/0 | 18/67 |
| 1985 | 4/7* | 1/1 | 5/7* | 9/32* | 7/14 | 17/56* |

* indicates monthly data with missing values.

On the 17th, Fresno had heavy cloud cover in the morning and lighter cloud cover the rest of the day (see Table 4). Cloudiness over the park was restricted to the lower two sites. The Fresno maximum temperature was 30.0 degrees celcius while the average maximum temperature for the 10 days was 33.4 degrees celcius. The minimum relative humidity was 43 percent while the average for the 10 days was 29 percent. August 15, 16, 18, 19, 20 and 21 also had some cloud cover over Fresno but the temperatures and relative humidities were normal. Ash Mountain, Wolverton and Emerald Lake all had lower afternoon maximum temperatures on the 17th as compared to the rest of the study period (see Table 5). Wolverton experienced higher relative humidities on the 17th while Ash Mountain showed

| | TIME (PDT) | | | | | | | |
|---|---|---|---|---|---|---|---|---|
| DATE | 0200 | 0500 | 0800 | 1100 | 1400 | 1700 | 2000 | 2300 |
| 8/13 | | | | | | | | |
| SFO | 2 | 9 | 10 | 1 | 0 | 0 | 0 | 0 |
| SCK | -- | -- | -- | 0 | 0 | -- | -- | -- |
| FAT | 0 | 0 | 0 | 0 | 0 | 0 | 0 | 0 |
| BFL | -- | -- | 0 | 0 | 0 | 0 | 0 | -- |
| AM | -- | -- | 0 | 0 | -- | 0 | 0 | -- |
| WV | -- | -- | 0 | 0 | -- | 0 | 0 | 0 |
| EL | -- | -- | -- | -- | -- | -- | -- | -- |
| 8/14 | | | | | | | | |
| SFO | 0 | 0 | 10 | 10 | 2 | 1 | 5 | 10 |
| SCK | -- | -- | -- | 0 | 0 | -- | -- | -- |
| FAT | 0 | 0 | 0 | 0 | 0 | 0 | 0 | 0 |
| BFL | -- | -- | 0 | 0 | 0 | 0 | 0 | -- |
| AM | -- | 0 | 0 | 0 | -- | 1 | 1 | 0 |
| WV | -- | 0 | 0 | 0 | -- | 1 | 0 | 0 |
| EL | -- | -- | -- | -- | -- | -- | -- | -- |
| 8/15 | | | | | | | | |
| SFO | 10 | 10 | 10 | 10 | 10 | 9 | 9 | 10 |
| SCK | -- | -- | -- | 0 | 0 | -- | -- | -- |
| FAT | 0 | 0 | 5 | 5 | 2 | 1 | 4 | 2 |
| BFL | -- | -- | 2 | 2 | 2 | 9 | 8 | -- |
| AM | -- | 0 | 1 | 1 | -- | 1 | 1 | -- |
| WV | -- | 0 | 2 | 2 | -- | 1 | 1 | 0 |
| EL | -- | -- | -- | -- | -- | -- | 0 | 0 |
| 8/16 | | | | | | | | |
| SFO | 10 | 10 | 10 | 10 | 9 | 9 | 6 | 10 |
| SCK | -- | -- | -- | 1 | 5 | -- | -- | -- |
| FAT | 2 | 5 | 5 | 2 | 1 | 0 | 0 | 0 |
| BFL | -- | -- | 0 | 0 | 0 | 3 | 2 | -- |
| AM | -- | -- | -- | -- | -- | 2 | 4 | -- |
| WV | -- | 0 | 0 | 1 | -- | 2 | 1 | -- |
| EL | -- | 0 | 0 | 1 | -- | 0 | 4 | -- |
| 8/17 | | | | | | | | |
| SFO | 10 | 10 | 10 | 10 | 9 | 1 | 0 | 0 |
| SCK | -- | -- | -- | 9 | 10 | -- | -- | -- |
| FAT | 0 | 5 | 10 | 10 | 3 | 1 | 2 | 0 |
| BFL | -- | -- | 0 | 0 | 0 | 0 | 1 | -- |
| AM | -- | -- | 8 | 1 | -- | 1 | 1 | -- |
| WV | -- | -- | 6 | 3 | -- | 2 | 1 | -- |
| EL | -- | -- | 0 | 0 | -- | 3 | 2 | -- |

Table 4: Cloud cover (tenths) for August 13th through 17th, 1985, at indicated hours (see next page).

| DATE | TIME (PDT) 0200 | 0500 | 0800 | 1100 | 1400 | 1700 | 2000 | 2300 |
|---|---|---|---|---|---|---|---|---|
| 8/18 | | | | | | | | |
| SFO | 0 | 0 | 0 | 0 | 0 | 4 | 0 | 4 |
| SCK | -- | -- | -- | 0 | 0 | -- | -- | -- |
| FAT | 0 | 0 | 0 | 1 | 0 | 5 | 0 | 0 |
| BFL | -- | -- | 10 | 10 | 5 | 5 | 10 | -- |
| AM | -- | -- | 0 | 4 | -- | <1 | 3 | 0 |
| WV | -- | -- | 0 | 2 | -- | 1 | 2 | 0 |
| EL | -- | -- | 0 | 0 | -- | 0 | 0 | 0 |
| 8/19 | | | | | | | | |
| SFO | 2 | 1 | 8 | 9 | 9 | 1 | 10 | 9 |
| SCK | -- | -- | -- | 5 | 3 | -- | -- | -- |
| FAT | 0 | 0 | 9 | 6 | 8 | 8 | 1 | 0 |
| BFL | -- | -- | 10 | 10 | 8 | 10 | 5 | -- |
| AM | -- | 0 | 4 | 1 | -- | 9 | 9 | -- |
| WV | -- | 0 | 9 | 2 | -- | 9 | 4 | -- |
| EL | -- | 0 | 0 | 1 | -- | 3 | 7 | -- |
| 8/20 | | | | | | | | |
| SFO | 4 | 8 | 4 | 0 | 0 | 0 | 0 | 5 |
| SCK | -- | -- | -- | 0 | 0 | -- | -- | -- |
| FAT | 0 | 0 | 7 | 4 | 6 | 2 | 1 | 0 |
| BFL | -- | -- | 6 | 10 | 0 | 0 | 0 | -- |
| AM | -- | -- | 1 | 1 | -- | 1 | <1 | 1 |
| WV | -- | -- | 7 | 3 | -- | 0 | <1 | 3 |
| EL | -- | -- | 4 | 0 | -- | 0 | 0 | 0 |
| 8/21 | | | | | | | | |
| SFO | 10 | 10 | 4 | 4 | 7 | 6 | 8 | 0 |
| SCK | -- | -- | -- | 1 | 4 | -- | -- | -- |
| FAT | 0 | 0 | 0 | 0 | 8 | 9 | 3 | 1 |
| BFL | -- | -- | 5 | 2 | 1 | 1 | 1 | -- |
| AM | -- | 0 | 0 | 2 | -- | 0 | 0 | -- |
| WV | -- | <1 | 1 | 3 | -- | 4 | 3 | -- |
| EL | -- | 0 | 0 | 2 | -- | 0 | 1 | -- |
| 8/22 | | | | | | | | |
| SFO | 0 | 6 | 10 | 0 | 0 | 5 | 10 | 7 |
| SCK | -- | -- | -- | 0 | 0 | -- | -- | -- |
| FAT | 0 | 0 | 0 | 0 | 0 | 0 | 0 | 0 |
| BFL | -- | -- | 0 | 0 | 0 | 0 | 0 | -- |
| AM | -- | -- | 0 | 0 | -- | 0 | 0 | -- |
| WV | -- | -- | 0 | 0 | -- | 0 | 0 | -- |
| EL | -- | -- | 0 | 0 | -- | 0 | -- | -- |

Table 4: (Cont'd) Cloud cover (tenths) for August 18th through 22nd, 1985, at indicated hours. SFO-San Francisco, SCK-Stockton, FAT-Fresno, BFL-Bakersfield, AM-Ash Mountain, WV-Wolverton, EL-Emerald Lake.

| | Min/Max T2 | | | | Min/Max T5 | | |
|---|---|---|---|---|---|---|---|
| Day | FAT | AM | WV | EL | AM | WV | EL |
| 13 | 18/32 | --/-- | --/23 | --/-- | --/-- | --/21 | --/-- |
| 14 | 18/34 | --/31 | 3/24 | --/-- | --/31 | 5/23 | --/-- |
| 15 | 19/34 | 18/34 | 4/23 | --/-- | 18/33 | 6/23 | --/-- |
| 16 | 19/34 | 20/34 | 4/24 | 11/20 | 20/33 | 6/23 | 12/20 |
| 17 | 18/29 | 19/31 | 4/20 | 10/16 | 19/30 | 5/18 | 10/15 |
| 18 | 17/32 | 16/30 | 2/20 | 6/16 | 16/29 | --/-- | 6/16 |
| 19 | 17/31 | 18/29 | -1/20 | 8/21 | 18/29 | --/19 | 8/19 |
| 20 | 17/33 | 17/32 | -1/22 | 9/19 | 17/31 | 1/21 | 9/19 |
| 21 | 18/34 | 19/33 | -1/22 | 8/19 | 19/32 | 1/20 | 8/18 |
| 22 | 18/35 | 19/33 | 2/22 | 11/20 | 20/33 | 4/21 | 11/18 |

| | Max/Min RH | | |
|---|---|---|---|
| Day | AM | WV | FAT |
| 13 | --/-- | ---/-- | 65/32 |
| 14 | --/17 | ---/-- | 68/25 |
| 15 | 48/12 | ---/19 | 63/26 |
| 16 | 45/13 | 100/21 | 73/27 |
| 17 | 53/15 | 100/58 | 73/43 |
| 18 | 81/30 | 100/38 | 75/35 |
| 19 | 61/27 | 92/16 | 70/34 |
| 20 | 58/17 | 97/15 | 75/25 |
| 21 | 55/12 | 99/22 | 54/24 |
| 22 | 40/12 | 93/30 | 65/22 |

Min/Max T2, Min/Max T5=minimum temperature/maximum temperature at 2 and 5 meters, respectively; Max/Min RH= maximum and minimum relative humidity.

Table 5: Daily weather station minimum and maximum temperature (celcius) and relative humidity (percent) data for Fresno (FAT), Ash Mountain (AM), Wolverton (WV) and Emerald Lake (EL) for August 13th to 22nd, 1985 (Fresno data obtained from the National Weather Service).

increased relative humidities on the 18th (relative humidity data not available for Emerald Lake). The 17th was influenced by the remnants of a tropical hurricane. Winds were southerly to southeasterly and laden with moist air. A record low of 19.4 degrees celcius (maximum afternoon temperature) occurred with rain in Sacramento on this day as well (Linse 1986).

The temperature and pressure gradient data for the study period, as compared to long term averages, suggest less stability than normal in the San Joaquin Valley. Less stability would reduce the pollutant levels and possibly lower the frequency of occurrence of the Fresno eddy or nocturnal jet. The ozone data did not indicate higher levels of pollutants and evidence of the nocturnal jet occurred every night of the study period (8-11 meters per second). Clear evidence of the Fresno eddy occurred on the mornings of the 14th, 20th, 21st and 22nd and less clearly on the 13th, 15th and 17th. In conclusion, during the study period, pollutant levels may have been slightly underestimated for normal August conditions and some unusual meteorology occurred on August 17th.

2. General Circulation

During the study period (August 13 to 22, 1985), the movement of the semi-permanent subtropical Pacific high pressure cell and migratory high and low pressure systems influenced the upper level winds of the study area. Surface isobar and 850, 700 and 500 millibar height charts

were obtained from the California Air Resources Board (Sacramento Office, Meteorological Division) and the National Weather Service.

a. Subtropical Pacific High Pressure Cell

The upper air charts showed the position of the summer Pacific high pressure cell to be south of Alaska centered of the west coast of Canada from August 13th to 15th. Figure 5 shows the 0500 PDT 500 millibar height charts for August 13th to 22nd, 1985. On the afternoon of the 15th, the high pressure center moved to the northwest at all levels. On the afternoon of the 17th, the high pressure center began to move back again (to the southeast). The influence of the Pacific high was overridden by a low pressure trough off the entire western coast which began forming on the 17th and became a cutoff low on the 21st. In addition, a high pressure area began developing over the southwestern states on the morning of the 21st and continued to strengthen through the 22nd.

b. Migratory Cells

Figure 6 shows the surface isobars (in millibars minus 1000; 0500 and 1100 PDT) and the 850 and 700 mb heights (in dekameters above sea level; 0500 and 1700 PDT). There is one row per day with the date located in the center of the figure. To distinguish the 850 and 700 mb heights, the lines are broken and solid, respectively. Rather than present a description of the complex synoptic movements of the migratory cells, Tables 6 and 7 contain a brief summary

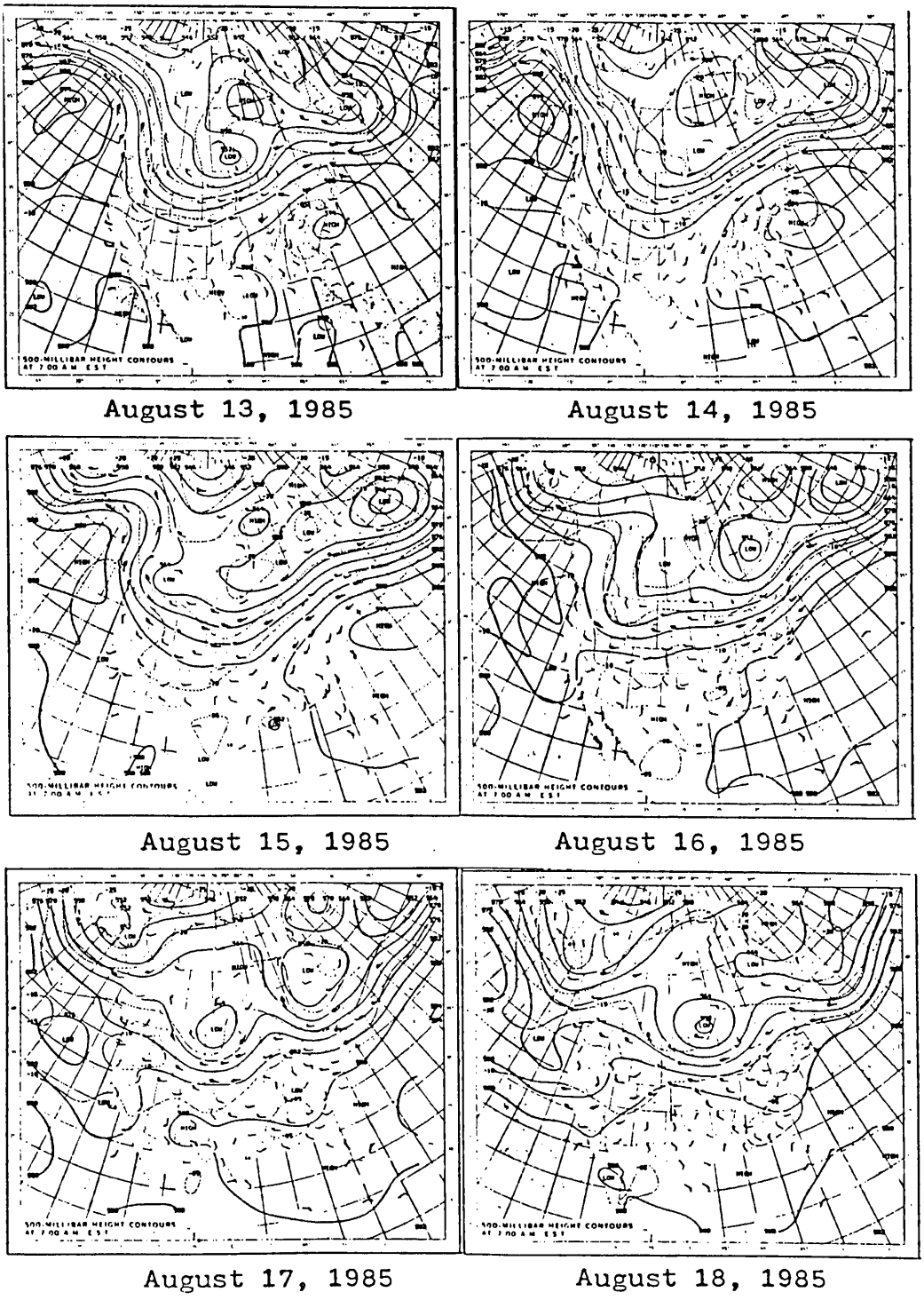


Figure 5: 0500 PDT 500 millibar height charts (dekameters) for August 13th to 18th, 1985.

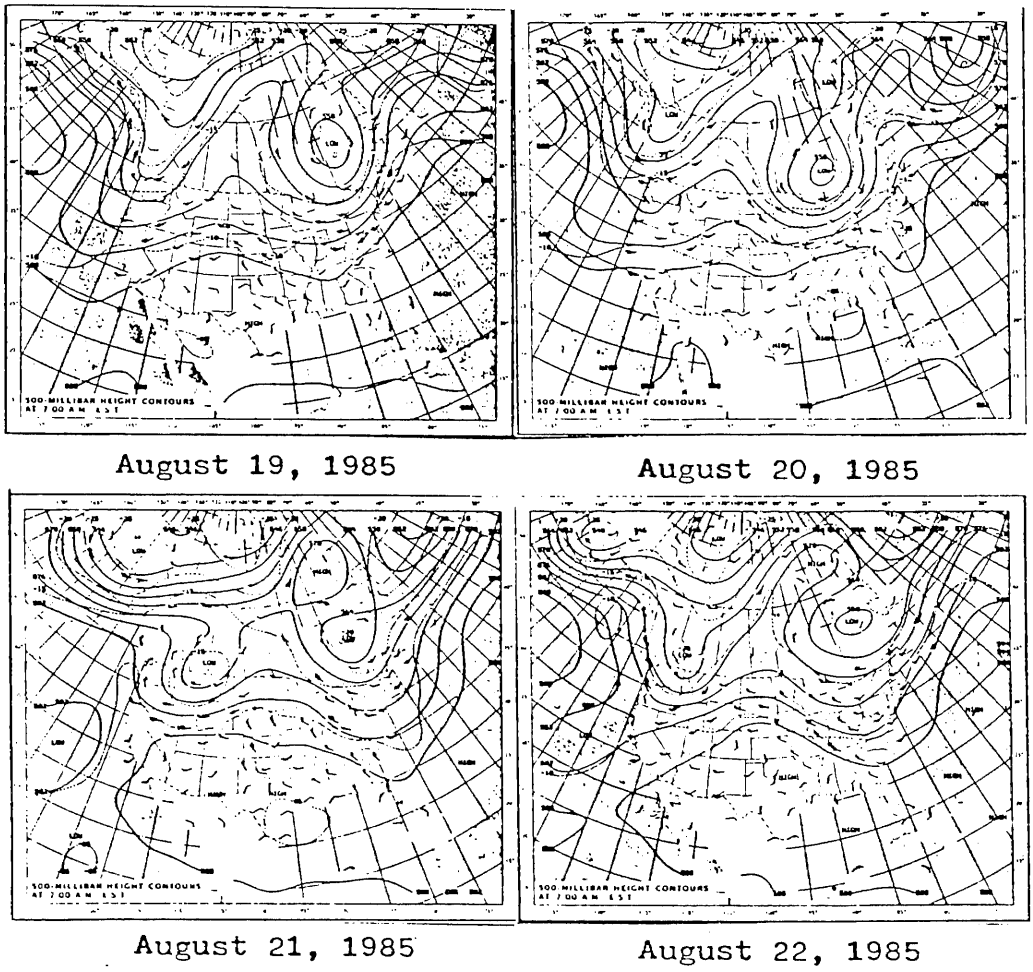

August 19, 1985 August 20, 1985

August 21, 1985 August 22, 1985

Figure 5: (Cont'd.) 0500 PDT 500 millibar height charts (dekameters) for August 19th to 22nd, 1985.

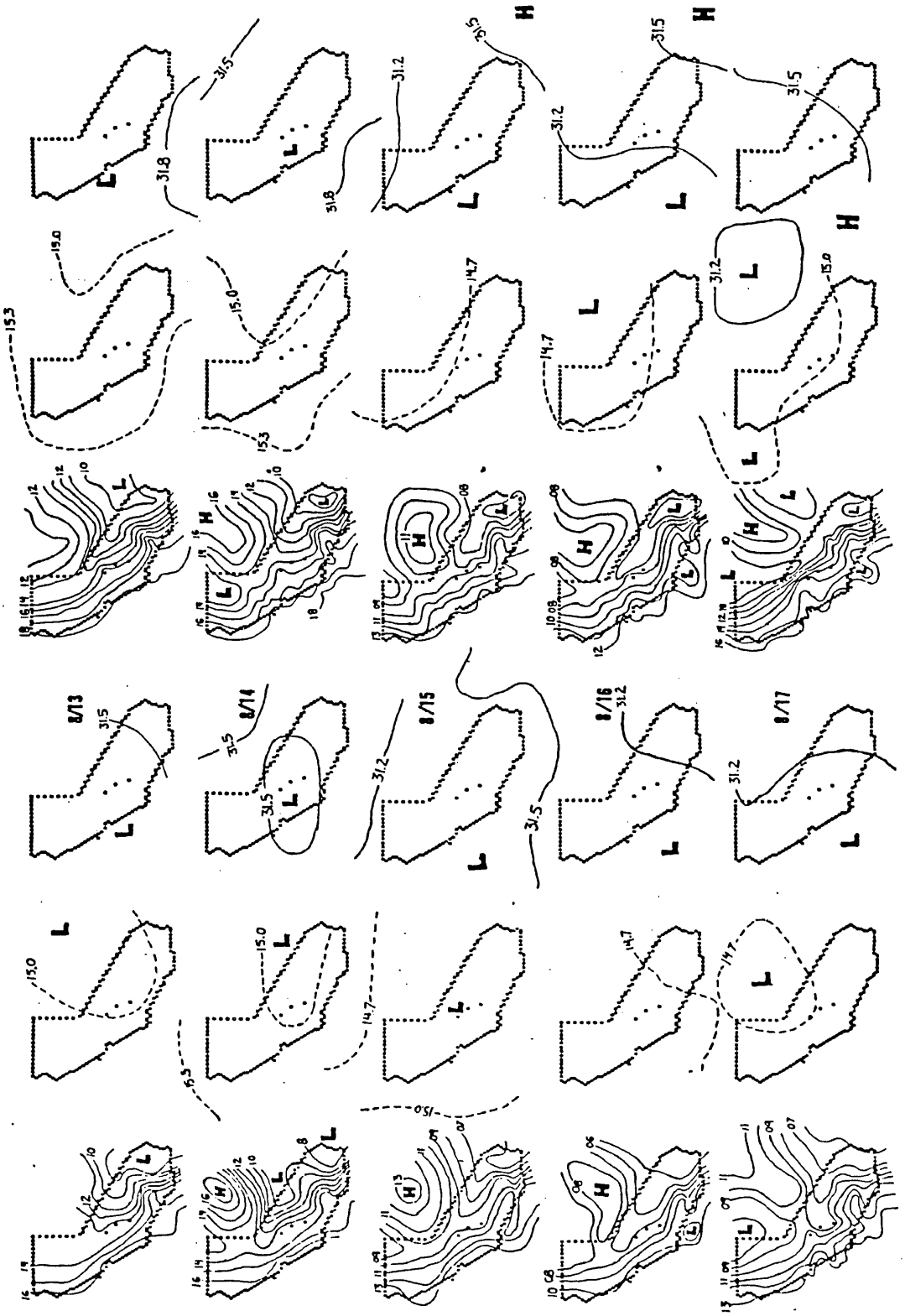


Figure 6: Surface isobar, 850 and 700 millibar height charts for August 13th to 17th, 1985.

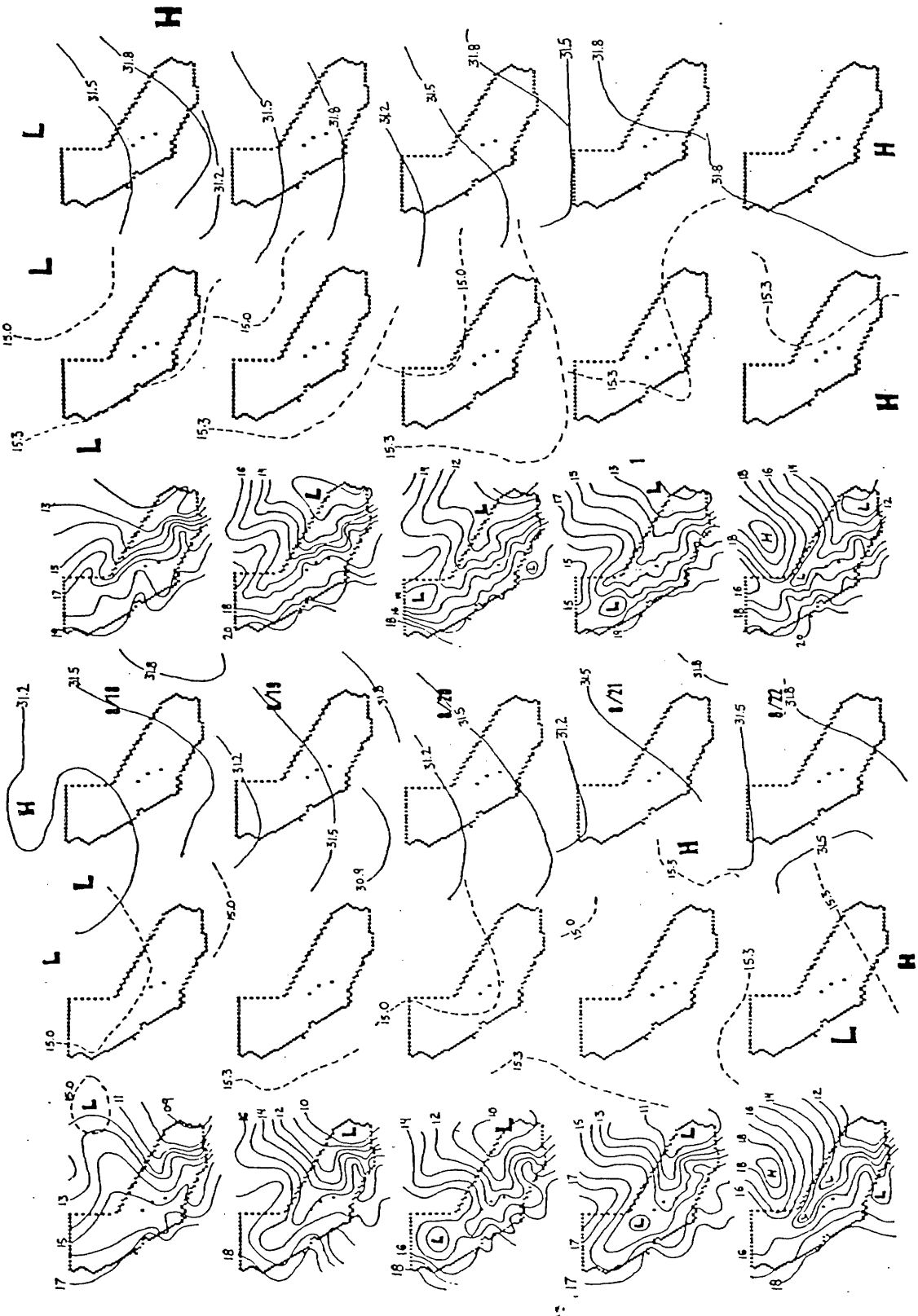


Figure 6: (Cont'd) Surface isobar, 850 and 700 millibar height charts for August 18th to 22nd, 1985.

| DATE | | DESCRIPTION |
|---|---|---|
| 13 | morning | low over Nevada and Utah border |
| 13 | afternoon | low east of Four Corners |
| 14 | morning | low over SE California and central New Mexico |
| 14 | afternoon | low over Four Corners |
| 15 | morning | low over central Sierra, dissipated by afternoon |
| 15 | afternoon | low over Wyoming |
| 16 | morning | low over Wyoming |
| 16 | afternoon | low over Nevada and Colorado, high over NW corner of Montana |
| 17 | morning | low over Nevada, high over Wyoming, low east of Four Corners |
| 17 | afternoon | low off northern coast of California and northeastern Nevada, high over Arizona |
| 18 | morning | low off northern coast of California |
| 18 | afternoon | same as morning, low over northern Mexico |
| 18-21 | | low moves north and south between Idaho and southern Saskatchewan, Canada, with trough extending to south and southwest |
| 19 | morning | low off northern coast of California dissipated |
| 21 | afternoon | high over central Arizona/New Mexico border and over central Baja |
| 21 | afternoon | high off central Baja coast |
| 22 | morning | high off northern Baja coast, low off central coast of California |
| 22 | afternoon | high off southern coast of California |

Table 6: Description of positions of migratory cells at 850 millibars influencing wind flow patterns of study area in August, 1985. Morning is at 0500 PDT and afternoon is at 1700 PDT.

| DATE | | DESCRIPTION |
|---|---|---|
| 13 | morning | low off central coast of California, high over Arizona, high off central Baja coast |
| 13 | afternoon | low over central coast of California, high off north central Baja coast |
| 14 | morning | low over central California, high off central Baja coast |
| 14 | afternoon | low over central California, high off northern Baja coast and over northern Mexico |
| 15-18 | | low off south central coast of California (at 500 mb as well), moved off northern coast of California morning of 18th |
| 15 | morning | low over southern Alberta, Canada, high off south central Baja coast |
| 15 | afternoon | high over northern Mexico, low over Wyoming |
| 16 | morning | high over central Baja, low over Wyoming |
| 16 | afternoon | high over SE Arizona, low over northern Wyoming/South Dakota border |
| 17 | morning | high over southern Arizona/New Mexico border |
| 17 | afternoon | high over central Arizona/New Mexico border |
| 18 | morning | high over central Washington/Oregon border, high over west central New Mexico |
| 18 | afternoon | low off northern coast of California moved east into Oregon, high over central Arizona |
| 19 | morning | low in northern Mexico Mexico |
| 19-21 | | trough centered in SW Canada extended south parallel and off western coast (at 500 mb as well) |
| 20-22 | | high developing over Texas, over Arizona/New Mexico border and off northern coast of Baja by 22nd |
| 22 | morning | trough moved eastward, cutoff low remained off central coast of California |

Table 7: Description of positions of migratory cells at 700 millibars influencing wind flow patterns of study area in August, 1985. Morning is at 0500 PDT and afternoon is at 1700 PDT.

for the 850 and 700 mb heights, respectively. Only those pressure systems influencing the study area are included.

3. Pilot Balloon Data

Appendix E contains the pilot balloon profiles (Figures 1 through 50) for Fresno, Ash Mountain, Wolverton and Emerald Lake during the August study period. Balloon releases were conducted every day within one-half hour of 0700, 1100, 1600 and 1900 PDT and half the time within one-half hour of 2300 and 0400 PDT. At the Emerald Lake site, balloons were released at 1830 rather than 1900 PDT. The Fresno schedule was slightly different. The morning releases were made between 0400 and 0600 PDT and the rest were made at 1100, 1700 and 2300 PDT. The Fresno early morning releases were plotted with either the 0400 or 0700 PDT releases for the park sites depending whether there were 0400 releases in the park or not. The Fresno 1700 PDT releases were plotted with the 1600 PDT releases for the other sites. Wind direction is toward the center line and the length of the line is proportional to the wind speed. The data has been edited for obvious reading or recording errors. In Figures 1 through 50, the vertical wind profiles were plotted directly over each site (meters above ground level). The length of the lines are proportional to wind speed (meters per second) and wind direction is toward the center lines with north being towards the top of the page. Throughout this section, all figure references will correspond to the figures in Appendix II-E.

The distinct layering was the dominant feature of the wind profiles. The topographic winds made up the layer closest to the ground. These winds moved up-valley and upslope during the day and down-valley and downslope during the night. The up-valley direction for Ash Mountain was south-southwesterly up the Middle Fork of the Kaweah River. The up-valley direction was west-southwesterly for Wolverton and westerly for Emerald Lake up the Marble Fork of the Kaweah River (see Table 2). The down-valley directions were simply the reverse of the up-valley directions. Fresno showed a more complex day/night wind pattern. At 1100 PDT, the flow was usually of low magnitude and westerly (up the western Sierran slope) becoming more northwesterly above or the flow had a southerly component (Fresno eddy) becoming northwesterly above. The Fresno eddy is particularly visible in Figures 8, 38, 44 and 48. Afternoon winds were stronger and northwesterly (sea-breeze). During the night, the winds were usually strongest and northwesterly (low level nocturnal jet).

The winds above the topographic wind layer (up to 5500 meters) corresponded well with the 700 and 500 mb height charts (approximately 3000 and 5500 meters above mean sea level). The 850 mb height chart is approximately 1500 meters above mean sea level and was approximately at the top of the topographic wind layer for Ash Mountain. Frequently, there was a layer in between the topographic

winds and the upper level winds that was highly variable. This layer was probably the transition layer where pressure gradient forces interacted with topographic effects. It was also the layer where there was evidence of compensation flow. This intermediate layer was more prominent at the Fresno and Ash Mountain sites.

The wind profiles were the result of a combination of shifting pressure cells interacting with topography on both large and small distance and time scales. The next two sections discuss the topographic and upper level winds in relation to the synoptic weather charts. While the limited number of synoptic weather maps were useful for understanding the upper level winds as observed by pilot balloons, many apects of the profiles remain open to interpretation.

a. Topographic Winds

In contrast to many previous reports (Defant 1951; Thyer 1966; Buettner 1967; Orgill 1981), the hourly topographic winds for the study sites were mostly constant in direction, speed and depth from day to day although upper air patterns were constantly changing. August 13th was a day with low upper level wind speeds (Figures 1-5) and August 18th had high upper level winds speeds (Figures 27-31) yet the topographic wind depths were similar (Appendix E). Emerald Lake was the only site where the winds would occassionally be up-valley rather than down-valley during night or early morning profiles or the topographic winds

would be indistinguishable from the upper level winds. This was probably due to the site being near the upper reaches of the drainage and in an open area relatively free of vegetation allowing more interaction with the upper level winds.

Although the pilot balloon data had a low vertical resolution (90 vertical meters per observation), it may be used as a gross estimate of the depth of the topographic winds. Only profiles with topographic winds in the direction of the drainage flow and distinguishable from the upper level or transition winds were used. The table below shows the range/average depth (meters) of the topographic winds by hour (PDT) for the study sites (including Fresno) for August. The Fresno and Ash Mountain topographic winds were deeper than those at Wolverton and Emerald Lake due to the drainages being much larger. They also showed a day/night pattern with the largest depth occurring in the afternoon (1600 PDT) and the smallest depth occurring at night (2300 PDT). A day/night difference in depth was not as apparent for Wolverton and Emerald Lake. The height of

| Time (PDT) | Fresno | Ash Mountain | Wolverton | Emerald Lake |
|---|---|---|---|---|
| 0400 | 540-1080/774 | 270-810/574 | 90-450/210 | 135-540/315 |
| 0700 | -- | 180-810/559 | 90-630/255 | 90-540/310 |
| 1100 | 720-2250/1202 | 675-1260/920 | 180-900/405 | 90-450/288 |
| 1600 | 900-1980/1314 | 630-1350/1044 | 180-450/347 | 360-540/441 |
| 1900 | -- | 810-1170/950 | 45-630/284 | 180-540/370 |
| 2300 | 720-1260/995 | 450-630/570 | 270-360/315 | 360-405/383 |

the maximum topographic wind depth was approximately ridge height except for Emerald Lake where it was below the ridge height (see Table 2). This was probably due to Emerald

Lake being at the top of the drainage and more exposed than the other sites.

Evidence of compensation winds was frequently seen above the topographic winds at Fresno and Ash Mountain. Occassionally, winds resembling compensation winds were observed at Wolverton and Emerald Lake. Since the depth of compensation wind layer has been reported to be approximately equal to the topographic winds below, it is possible that, given the 90 meter observation intervals, the compensation winds were not as readily discernable as for Fresno and Ash Mountain (Buettner and Thyer 1966). Another possible explanation for the apparent lack of compensation winds at the higher elevation sites may be that upper level winds more readily penetrate below the surrounding topography and dominate the wind flow patterns. Figures 9, 15 and 45 and Figures 3, 14 and 34 are examples of compensation winds for Fresno and Ash Mountain, respectively. Figures 44, 45 and 46 show evidence of compensation winds for all sites. It is interesting to note that except for August 16 and 17, evidence of compensation winds were observed regularly. Although there were fewer nighttime observations, compensation winds seemed to occur just as frequently as during the daytime.

b. Upper Level Winds

In this section, unless otherwise specified, upper level winds refer to winds at 700 and 500 mb levels (approximately 3000 and 5500 meters above sea level,

respectively). Reference to Figures 5 and 6 and Tables 6 and 7 may be useful in the following discussion. From the 13th to the 15th, the 700 mb winds were mostly southeasterly and the 500 mb winds were mostly westerly (Figures 1-17). The 500 mb westerlies were due to a dominating low pressure center over southwestern Ontario, Canada, and the Pacific high pressure cell off the western coast of Canada funneling winds to the east. The 700 mb southeasterlies were due to a low pressure area centered to the west of the study area. On the 15th (Figures 12-17), the upper level winds were highly variable, shifting between southeasterly and southwesterly and on the 16th (Figures 18-22), the upper level winds were southeasterly again. The 15th was characterized by a low pressure area moving off the central coast of California (700 mb) and a low pressure area moving over the central Sierra (850 mb). The high pressure area off the Baja coast weakened and moved south. This shifting around of high and low pressure areas resulted in the wind variability seen in Figures 12-17. The low pressure area over the central Sierra dissipated by the afternoon of the 15th. The major feature on the 16th at 700 and 500 mb levels was the low pressure area off the south-central coast of California causing upper level winds to be southeasterly. By late morning of the 16th, the upper level wind speeds increased (Figure 20) due to the higher pressure gradients. The highest wind speeds of the ten day period occurred on the 17th and 18th

(Figures 23-31). High wind speeds persisted until the evening of the 21st. The upper level winds shifted to southwesterly on the 17th (Figures 23-26). This wind shift was the result of low pressure systems to the north over Nevada (850 mb) and off the northern coast of California. Although the low off the northern coast of California moved into Oregon and dissipated by the morning of the 19th, the southwesterly winds persisted until the 21st due to a trough centered over southwestern Canada which extended southward parallel to and off the coast of California. By late afternoon of the 21st, the upper level winds began to shift again. A cutoff low pressure area remained off the central coast of California. The trough in Canada moved eastward and the Pacific high pressure cell moved east. On the afternoon of the 22nd, a high pressure area centered off the south coast of California (over Texas at 500 mb) extended into California causing winds to be westerly.

4. Wolverton Tethersonde Data

While pilot balloon data were useful for investigating the general wind patterns, the Wolverton tethersonde data allowed a more detailed look at the topographic winds. Figures 7 to 22 show the vertical profiles (meters above ground level) of absolute humidity (x1000), virtual potential temperature (Kelvin), wind speed and wind direction. Wind direction is towards the center line and wind speed (meters per second) is proportional to the

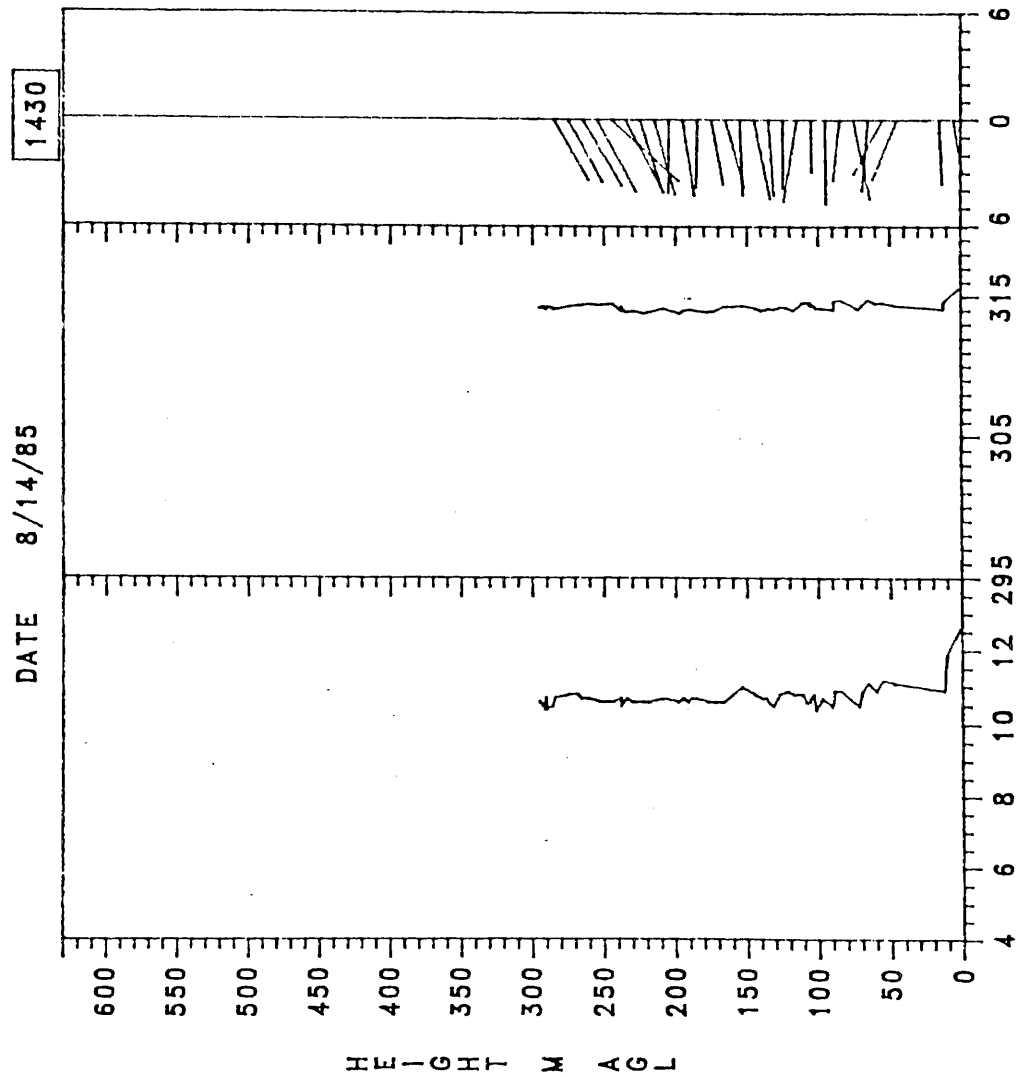


Figure 7: Tethersonde profile for August 14, 1985 at 1430 PDT for Wolverton.

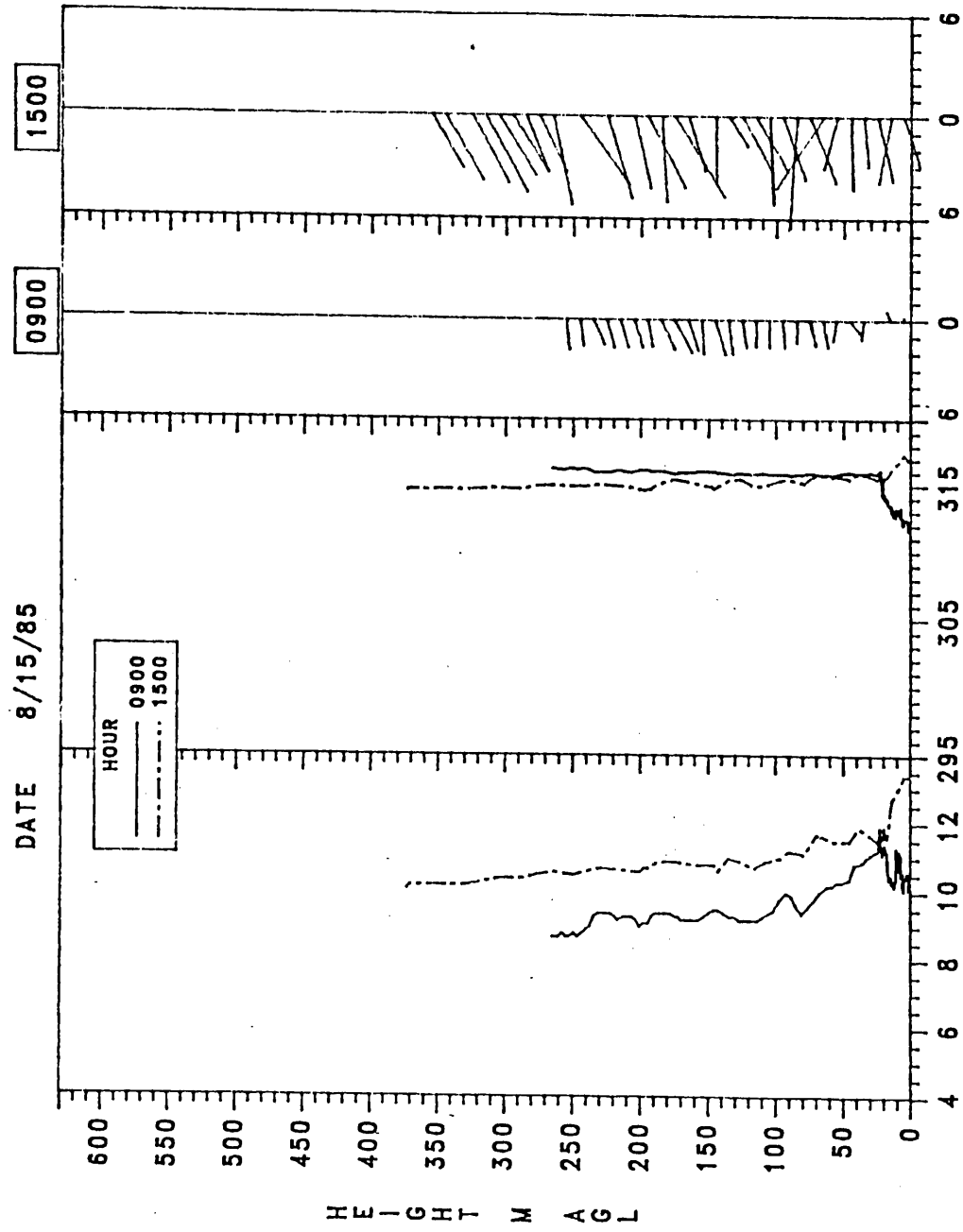


Figure 8: Tethersonde profile for August 15, 1985, at 0900 and 1500 PDT for Wolverton.

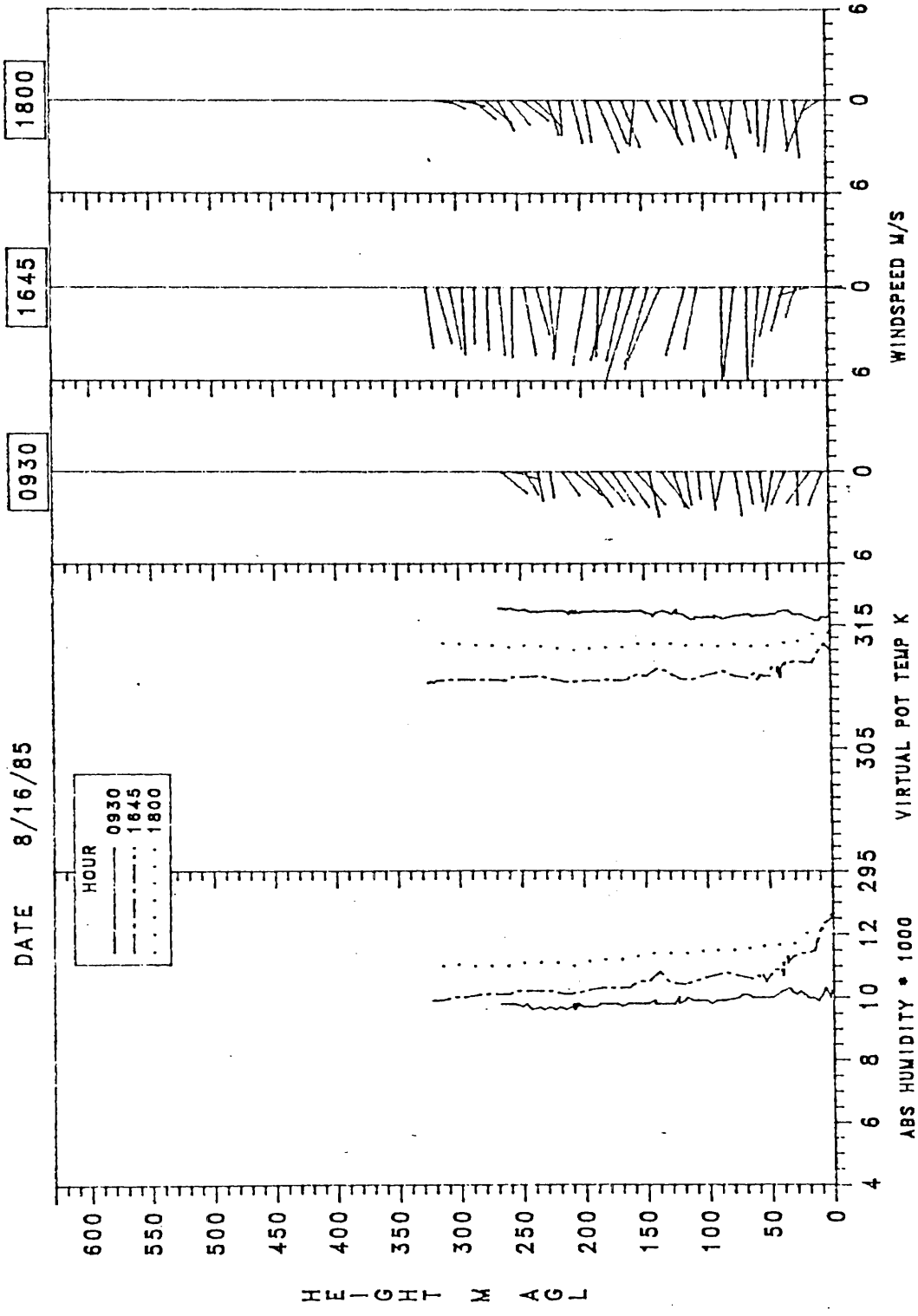


Figure 9: Tethersonde profile for August 16, 1985, at 0930, 1645 and 1800 PDT for Wolverton.

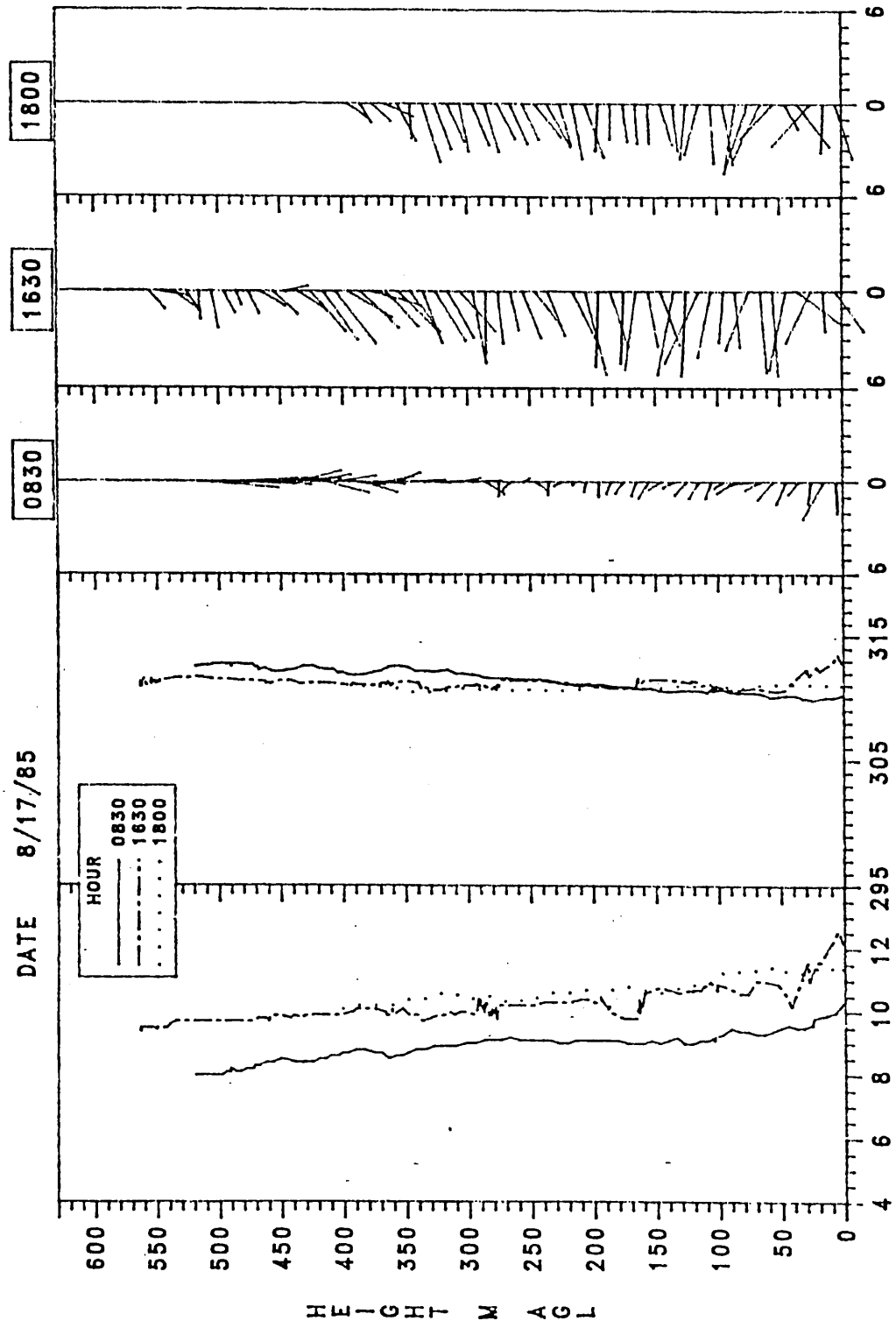


Figure 10: Tethersonde profile for August 17, 1985, at 0830, 1630 and 1800 PDT for Wolverton.

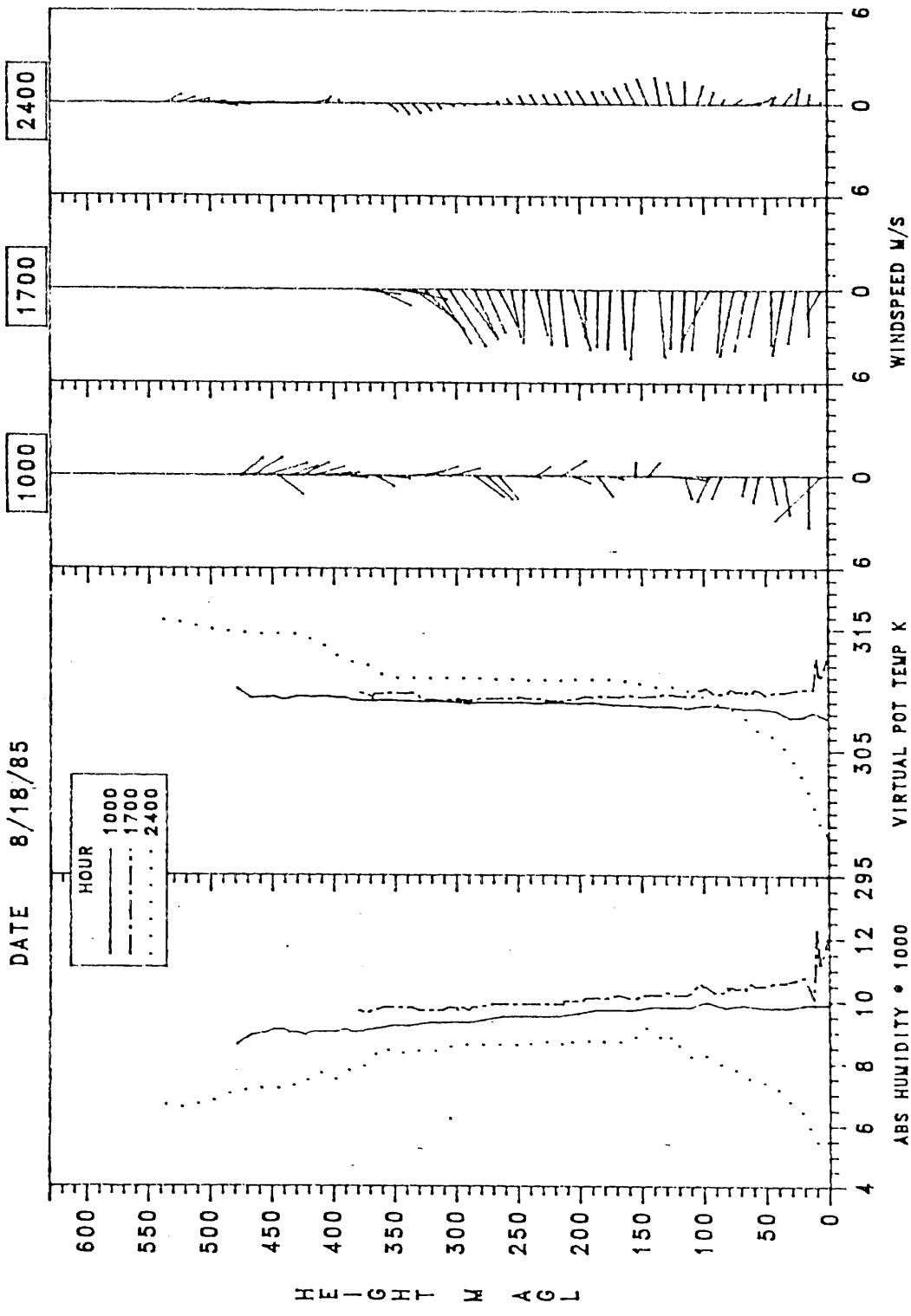


Figure 11: Tethersonde profile for August 18, 1985, at 1000, 1700 and 2400 PDT for Wolverton.

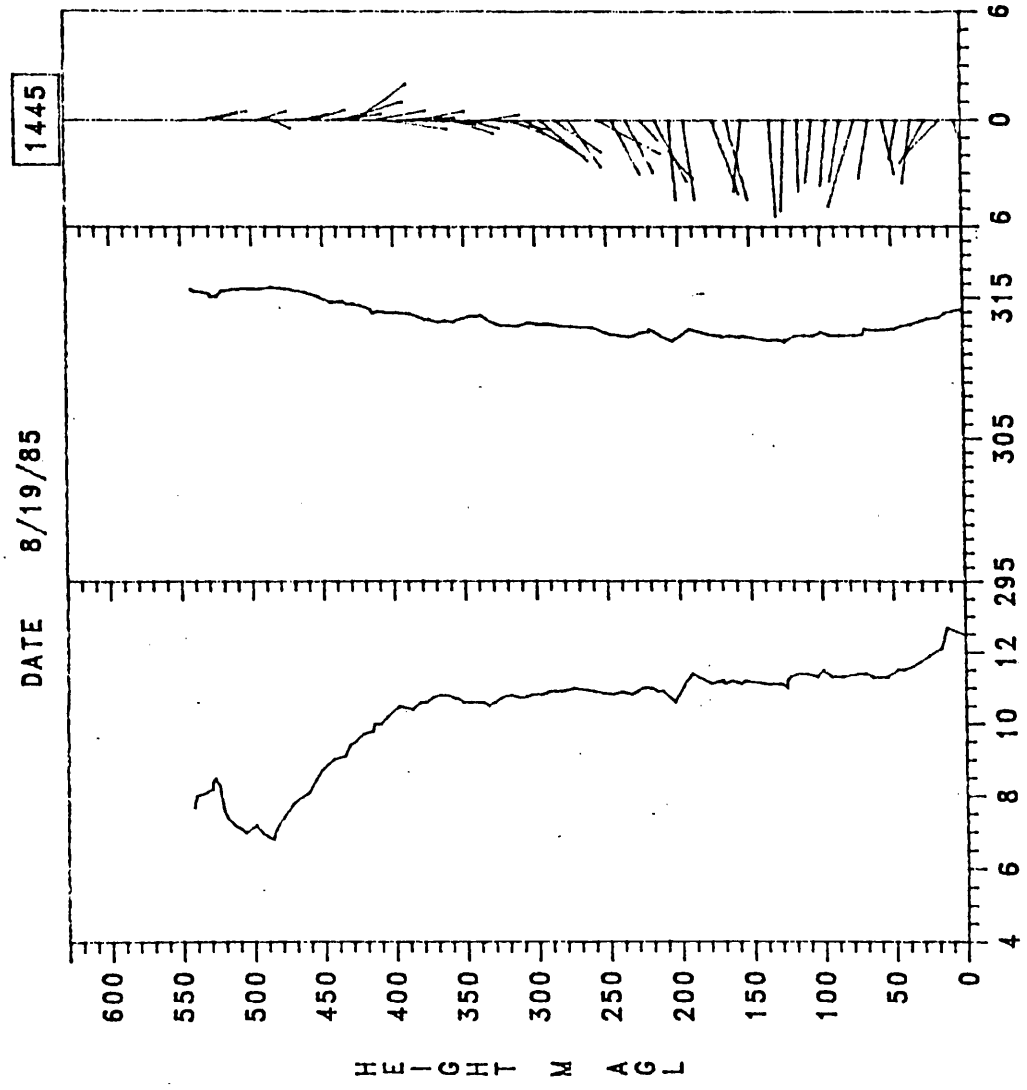


Figure 12: Tethersonde profile for August 19, 1985, at 1445 PDT for Wolverton.

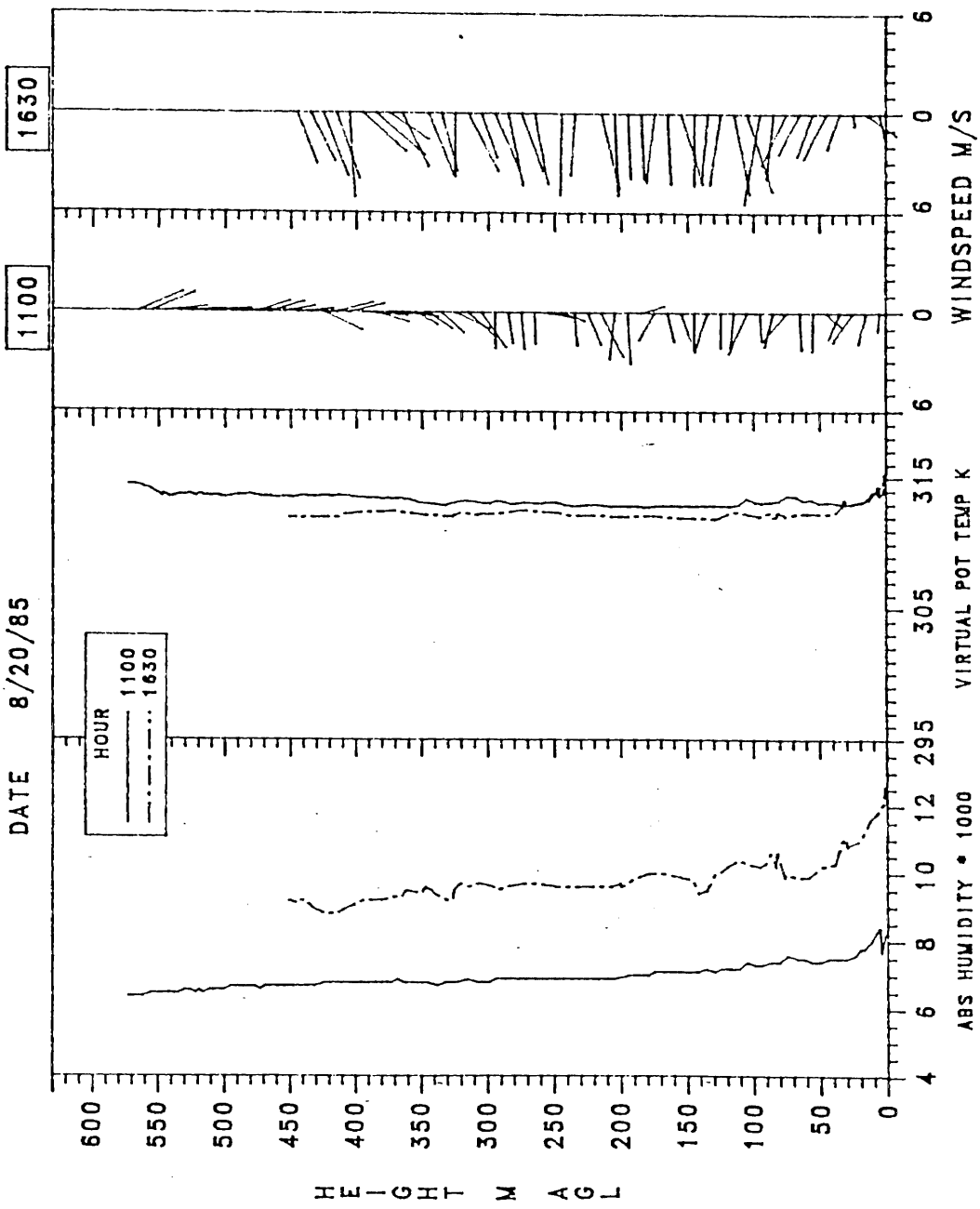


Figure 13: Tethersonde profile for August 20, 1985, at 1100 and 1630 PDT for Wolverton.

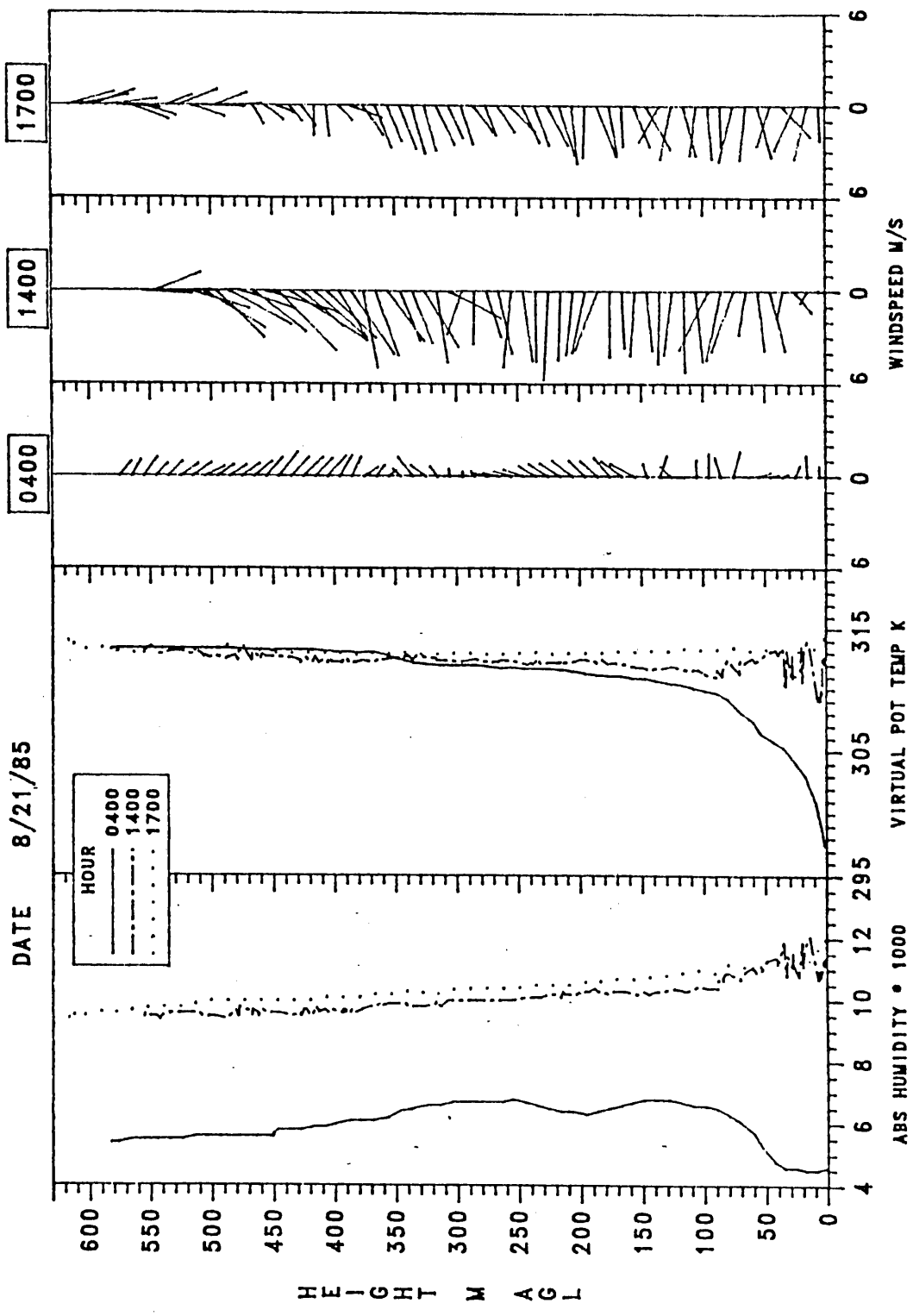


Figure 14: Tethersonde profile for August 21, 1985, at 0400, 1400 and 1700 PDT for Wolverton.

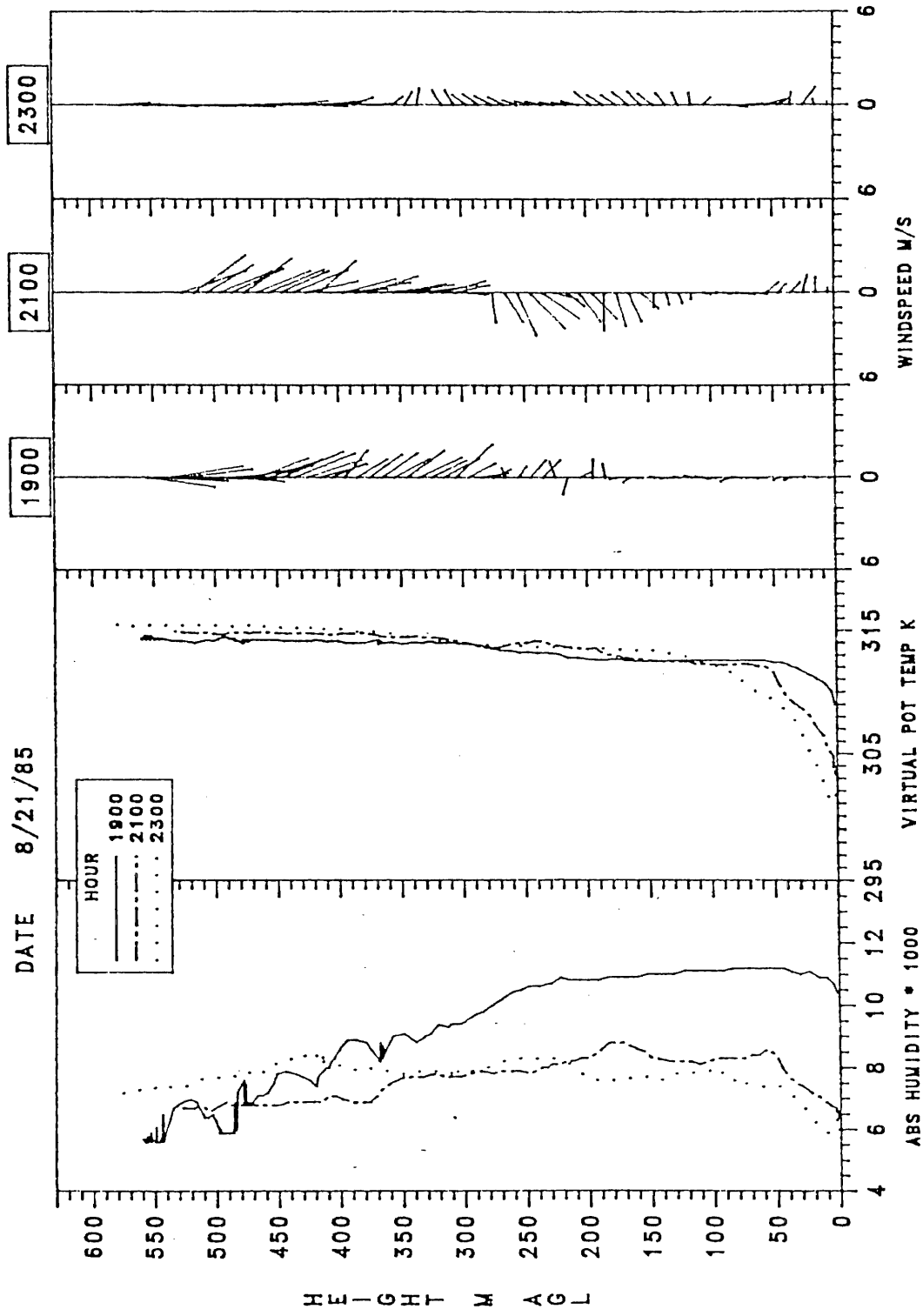


Figure 15: Tethersonde profile for August 21, 1985, at 1900, 2100 and 2300 PDT for Wolverton.

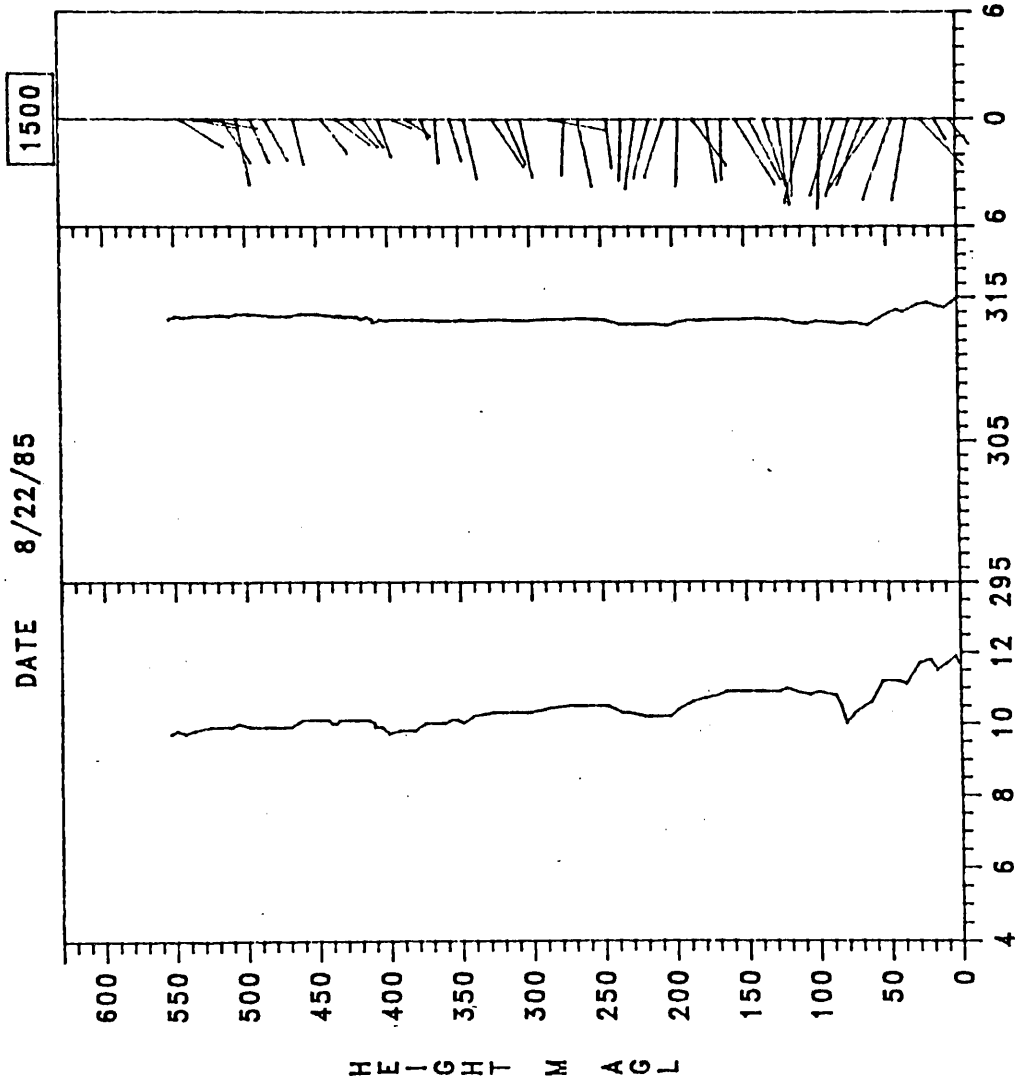


Figure 16: Tethersonde profile for August 22, 1985, at 1500 PDT for Wolverton.

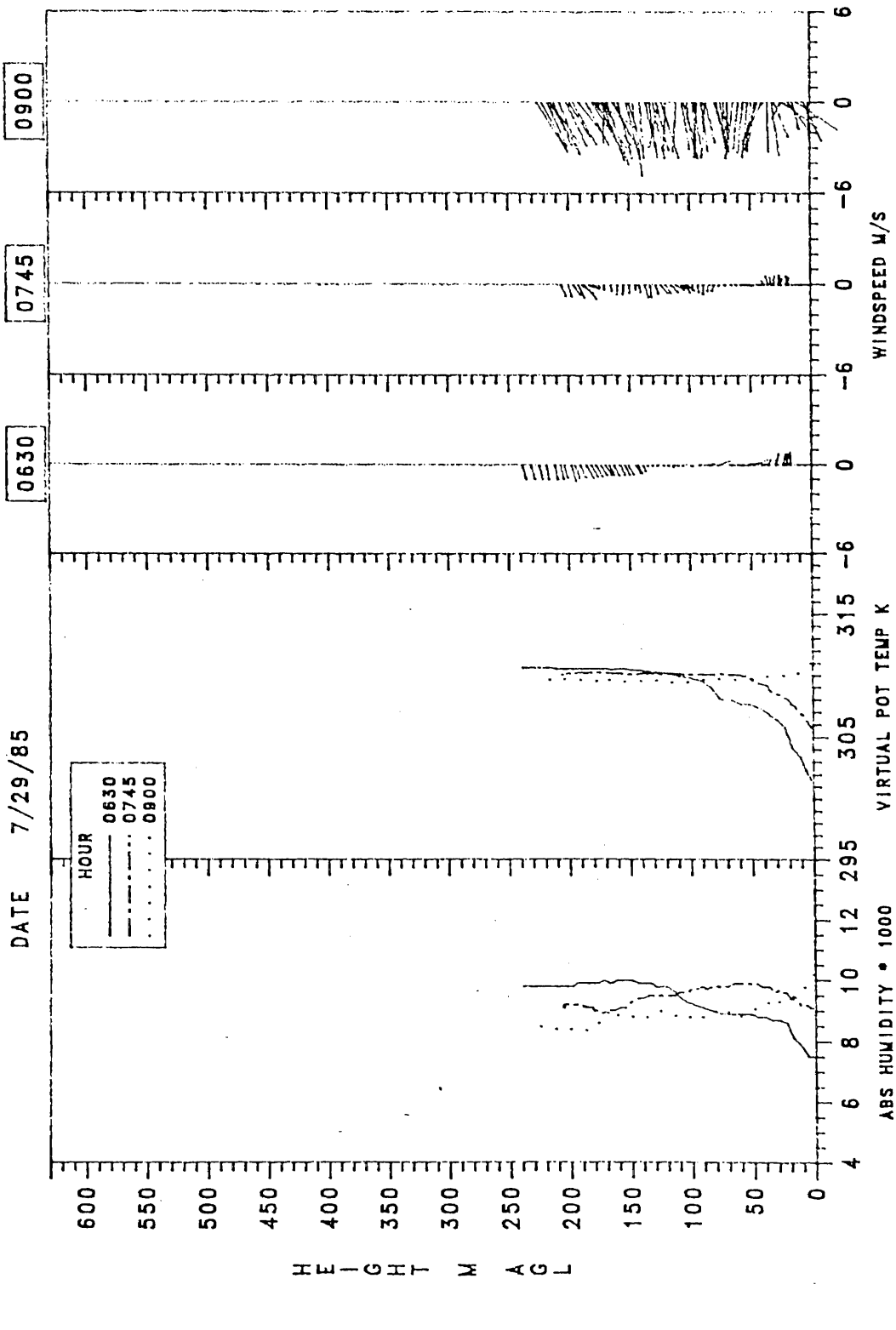


Figure 17: Tethersonde profile for July 29, 1985, at 0630, 0745 and 0900 PDT for Wolverton.

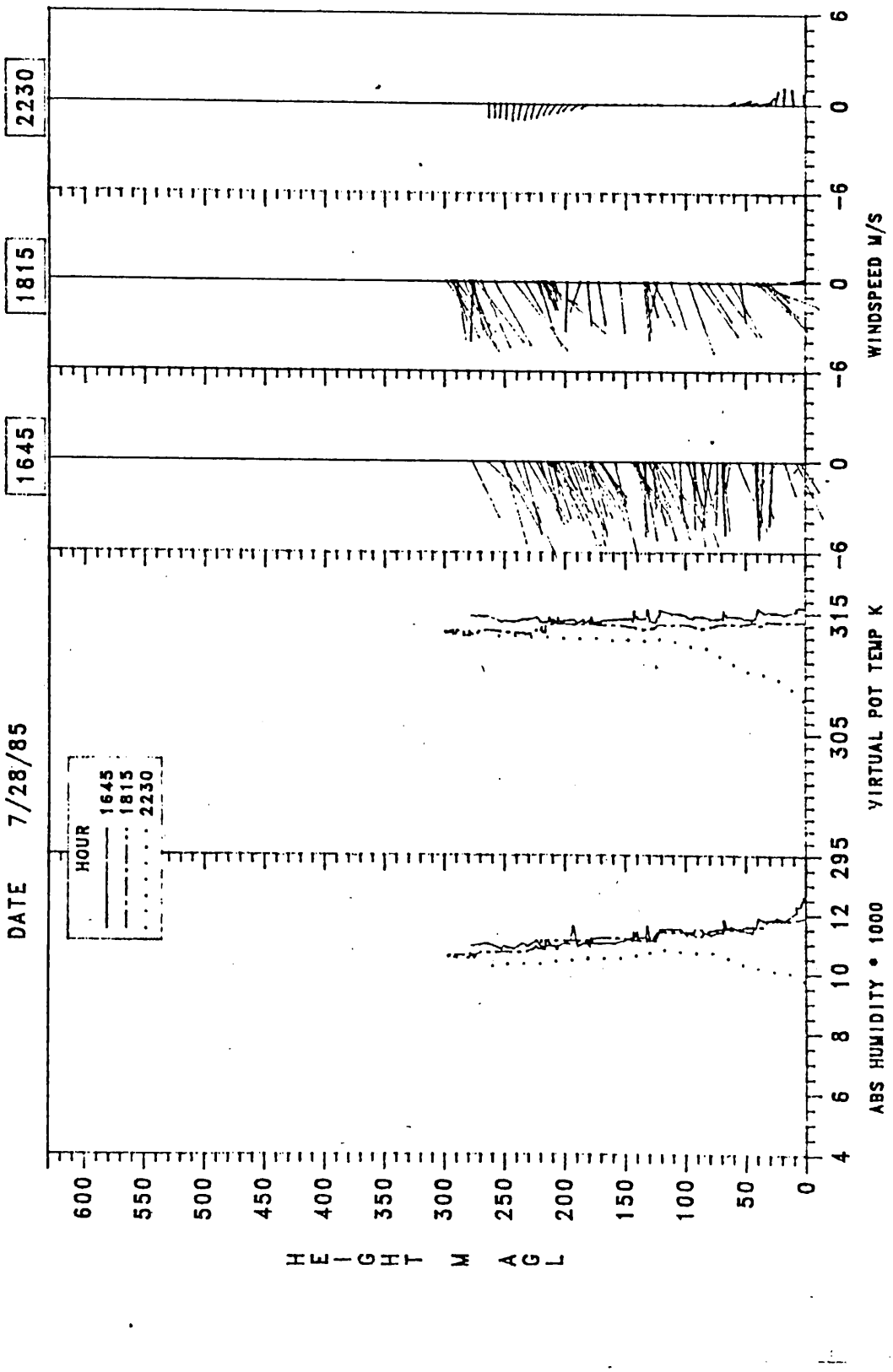


Figure 18: Tethersonde profile for July 28, 1985, at 1645, 1815 and 2230 PDT for Wolverton.

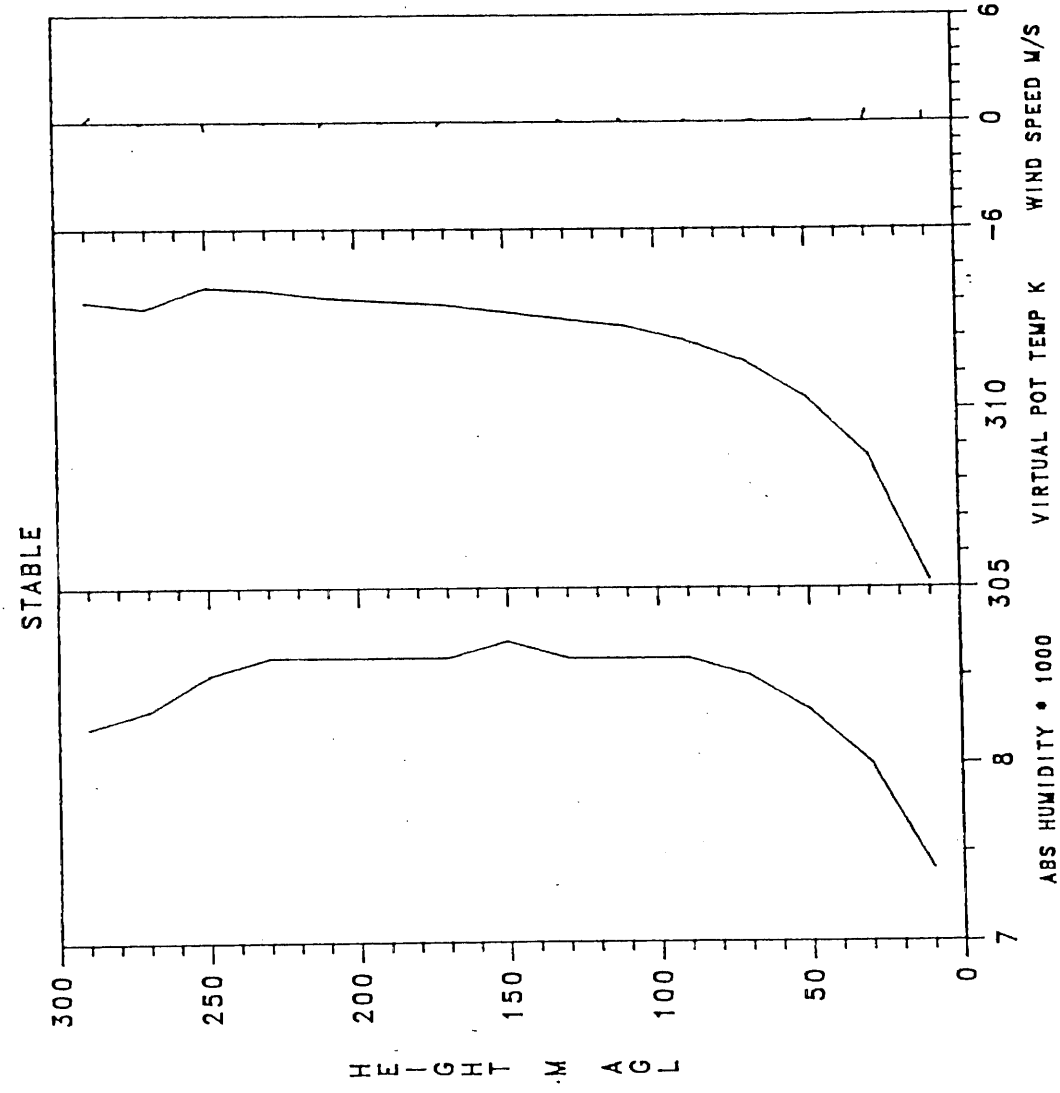


Figure 19: Tethersonde stability profile for the stable category.

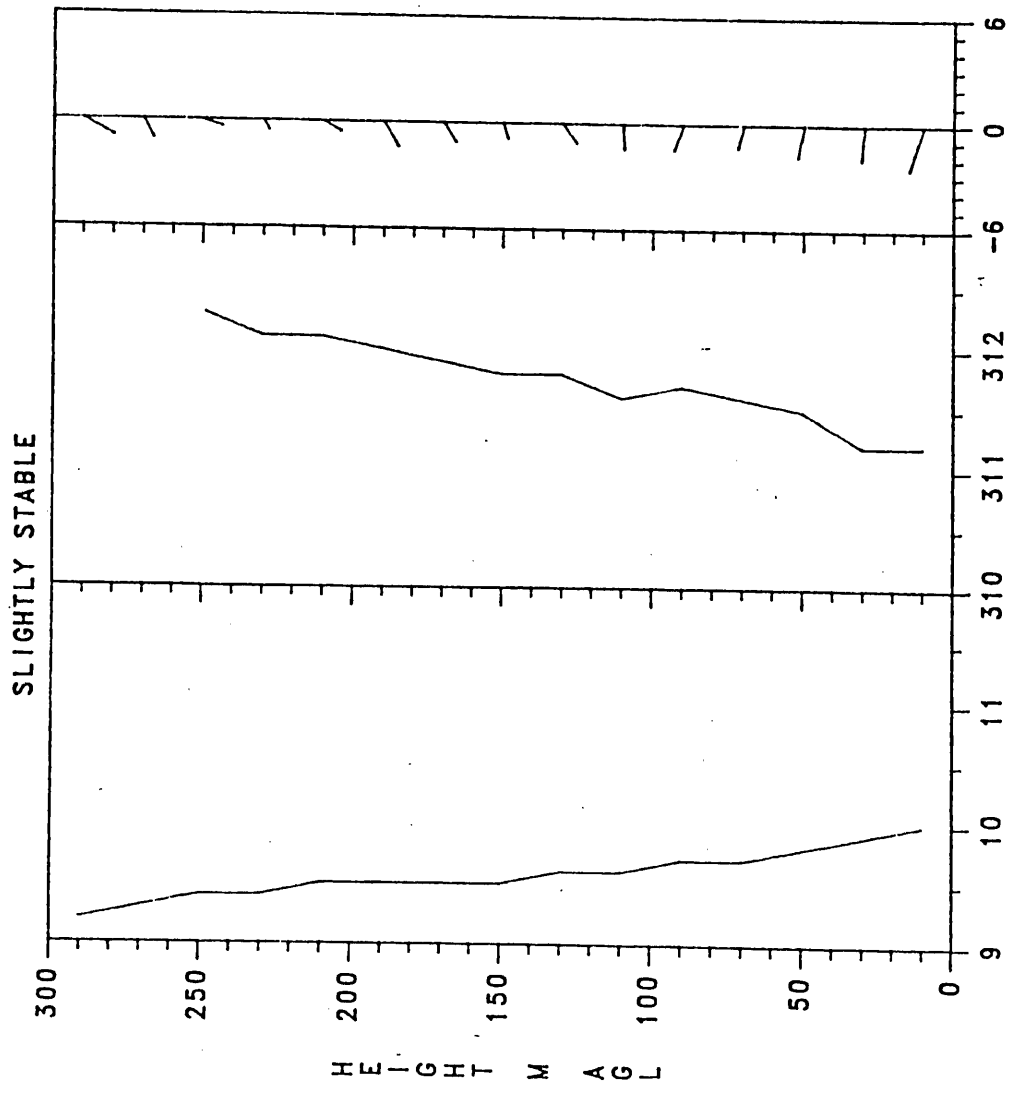


Figure 20: Tethersonde stability profile for the slightly stable category.

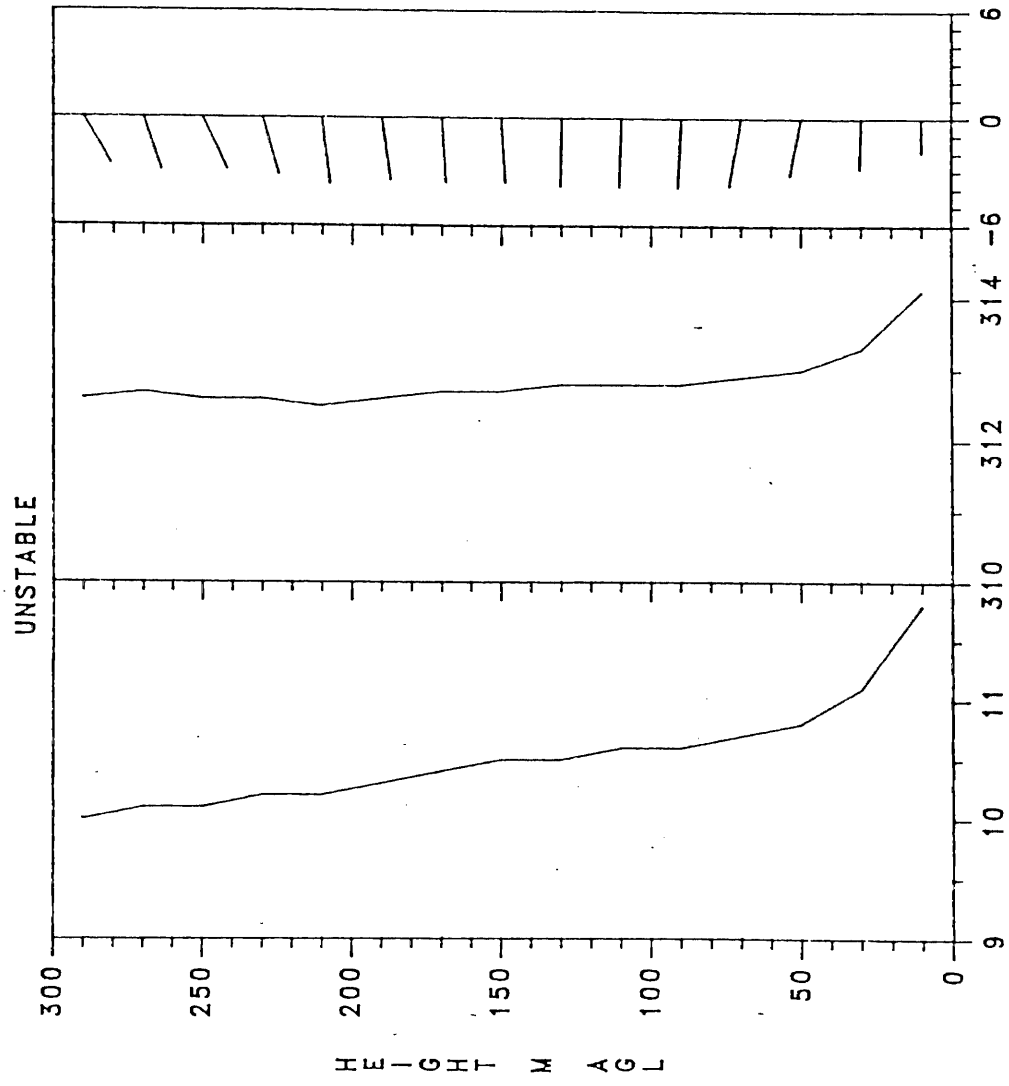


Figure 21: Tethersonde stability profile for the unstable category.

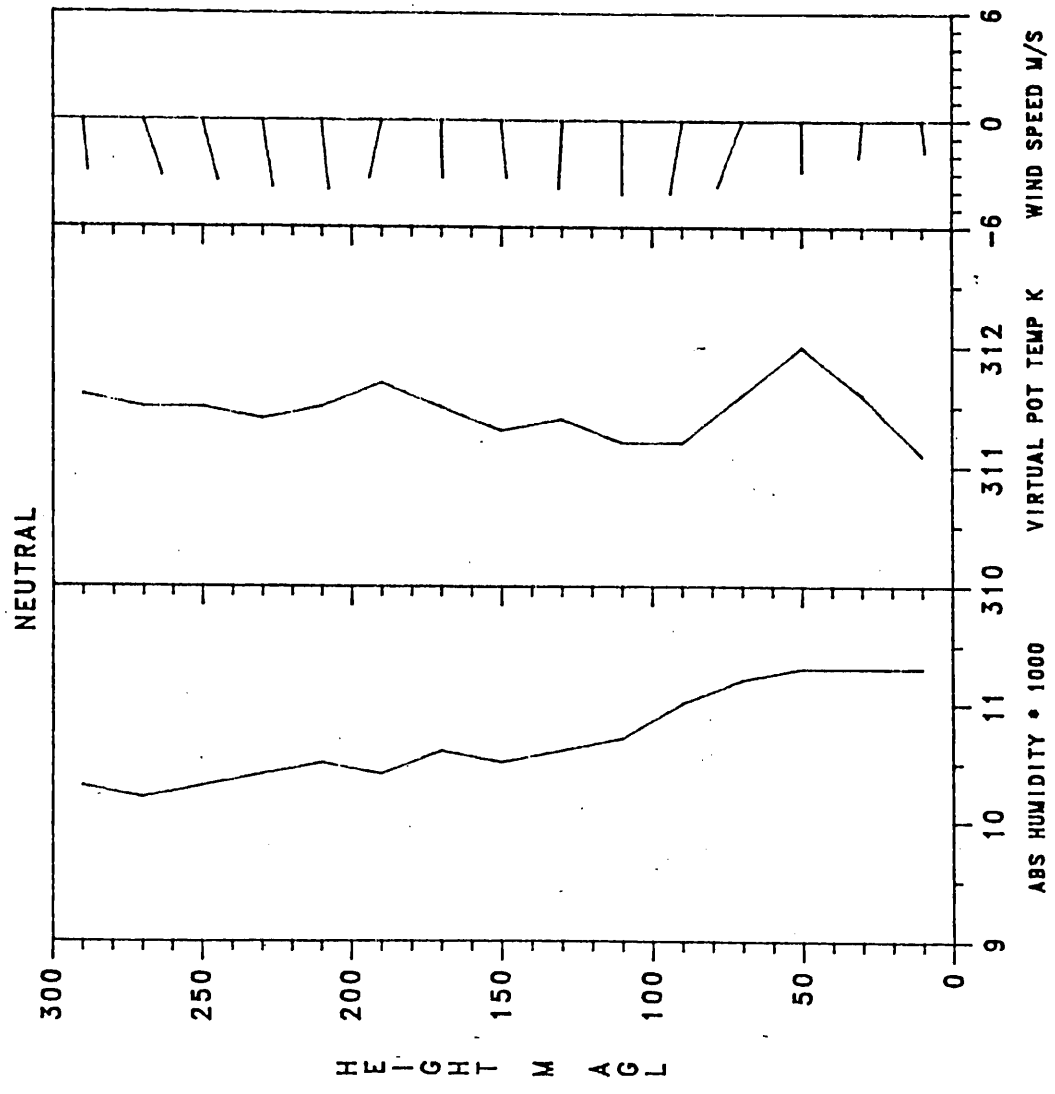


Figure 22: Tethersonde stability profile for the neutral category.

length of the line.

The wind profiles from the tethersonde and pilot balloon data agreed relatively well even though the vertical resolutions were less than 1 meter and 90 meters, respectively. The tethersonde profiles and pilot balloon releases were not always simultaneous but were within two hours of each other (see Table 1). The largest difference between the two when estimating the depth of the topographic winds was approximately 180 meters (less than 35 percent of time). The tethersonde data confirms, as indicated earlier, that there was not a distinct difference between the depth of the up- and down-valley flow depths. This was also found to be true by Whiteman (1980) in valleys in the Rocky Mountains of Colorado. The up-valley winds tended to reach maximum depth soon after sunrise and increase in speed until mid-afternoon (1600 PDT) whereas the down-valley winds increased in depth more slowly and growth continued until sunrise the next day with wind speeds remaining low the entire time.

The inversion breakup appeared to follow Whiteman's (1980) pattern number two (see Figure 1). In pattern two, the inversion top descends to the ground with minimal convective boundary layer growth from the ground up (Figure 17). The winds are down-valley below the inversion top and are replaced by the up-valley winds above as the inversion top reaches the ground. The inversion formation was the reverse case. The inversion began at the ground and

ascended with down-valley winds below and up-valley winds above (Figures 15 and 18).

Daytime wind speeds were not greater than seven meters per second and averaged around four meters per second. There were insufficient number of consecutive soundings done during the evening transition to document low level jet occurrence (Myrup et al. 1986). The virtual potential temperature profile was neutral (vertical) during the day with a small unstable layer next to the ground. During the day, the absolute humidity profile increased at all levels and frequently there was a sharp decrease next to the ground in the afternoon, resembling of a super adiabatic profile.

Nighttime wind speeds were less than two meters per second and variable direction although maintaining a general down-valley direction. One exception was Figure 15 where an up-valley layer appeared between 100 and 280 meters above ground level with speeds greater than 3 meters per second. This did not appear in other nighttime profiles and remains unexplained. There was an insufficient number of nighttime profiles to detect a wind speed maxima in the wind profiles as described by many authors (Buettner 1967; Davidson and Roa 1963; Horst and Doran 1986; Manins and Sawford 1979; Orgill 1981; Whiteman 1980) although it was indicated in Figure 11. Profiles were stable at night (virtual potential temperature increased with height) and slightly stable in the morning.

During the night, the absolute humidity profile decreased at all levels. This was due to the tethersonde being located directly over a moist meadow with a creek running through it. At night the moisture in the air condensed onto the vegetation and during the day it evaporated into the air.

Figures 19 to 22 show the average tethersonde profiles as categorized by bulk Richardson (BR) number. These figures summarize the features discussed above for the individual profiles. The data fell into four categories: stable, slightly stable, neutral and unstable. The BR numbers were calculated using the difference between the ground and 200 meter potential temperature and the average wind speed and potential temperature for the entire 200 meters. The stable category included 6 profiles with and average BR of 221.01 (hours between 1900 and 0900 PDT). This category showed the strongest temperature inversion, the lightest and most variable winds and the lowest absolute humidity. The slightly stable category included 3 profiles with an average BR of 2.99 (hours between 0800 and 1000 PDT). This category showed intermediate conditions between the stable and unstable categories. Compared to the stable profile, the winds were stronger and decidely up-valley, the absolute humidity was higher and the potential temperature profile was almost neutral. The unstable category included 12 profiles with an average BR of -1.02 (hours between 1100 and 1800 PDT). This category showed the highest wind

speeds, highest absolute humidity and a super-adiabatic lapse rate near the ground level. The neutral category included 2 profiles with and average BR of 0.01 (1800 and 1400 PDT). This category most likely represents the transition period between unstable and stable profiles. Neutral profiles were observed in the morning probably due to the limited number of profiles and the rapid conversion from stable to unstable profiles in the morning hours.

5. Ground Weather Station Data

The three ground weather stations located at each site recorded data continuously (averaged over one-half hour periods) over the ten days in August. Scatter plots for wind speed (meters per second) and wind direction (degrees) are shown in Figures 23, 25 and 27. Scatter plots for absolute humidity (x1000) or relative humidity (percent) and temperature (celcius) are shown in Figures 24, 26 and 28. All parameters show extreme regularity, especially temperature and wind direction. The Emerald Lake relative humidity sensor malfunctioned which is readily apparent in Figure 28.

Bulk Richardson (BR) numbers (x100) were calculated from the average temperature and the temperature difference between two and five meters and the five meter wind speed. The resulting scatter plots are shown in Figure 29. The larger and infrequent BR numbers have been left out so that the day/night (negative/ positive) pattern may be more readily seen. The change from positive to negative bulk

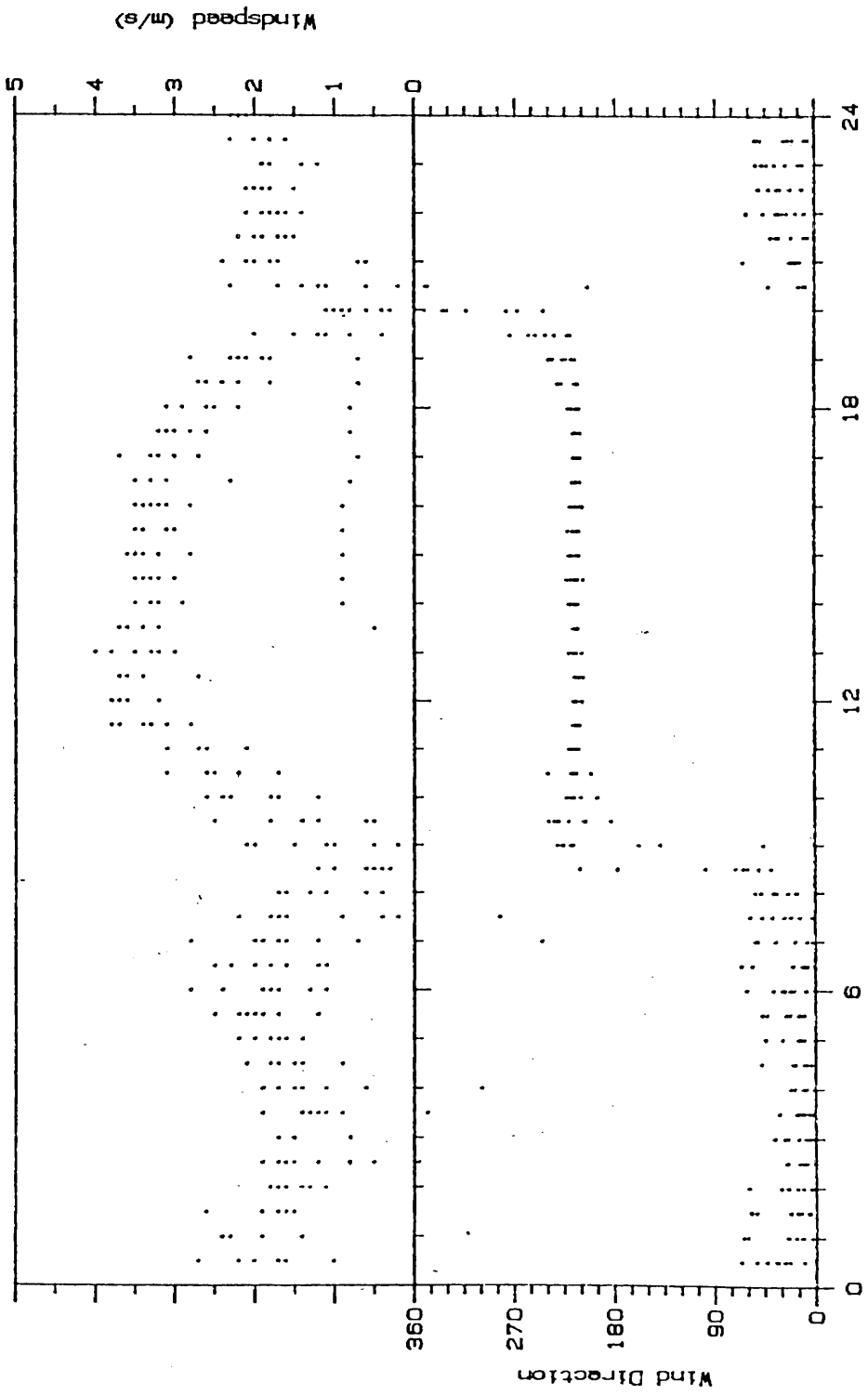


Figure 23: Ash Mountain ground weather station scatter plots for wind speed (meters/second) and wind direction (degrees) by time of day.

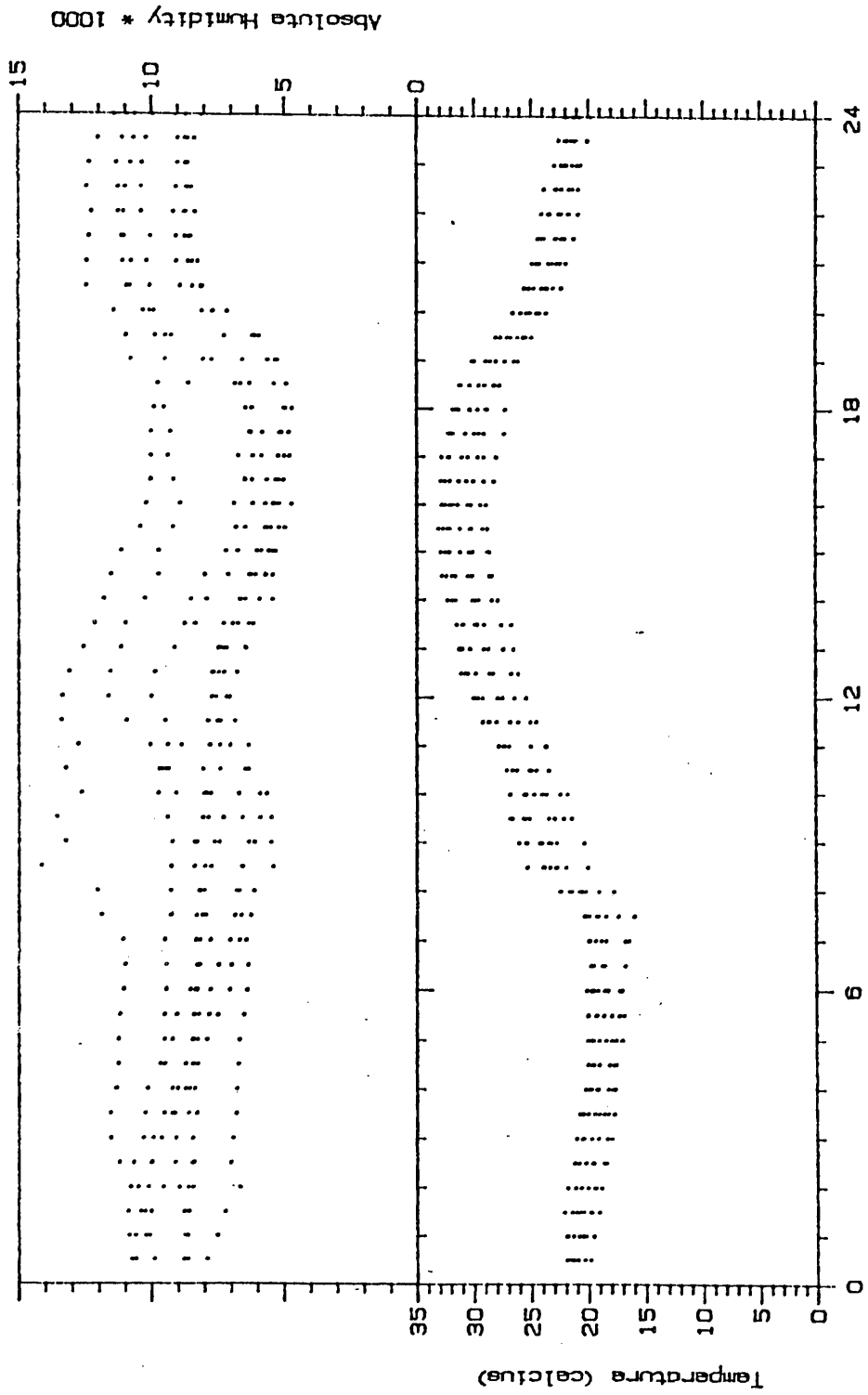


Figure 24: Ash Mountain ground weather station scatter plots for absolute humidity (x1000) and temperature (celcius) by time of day.

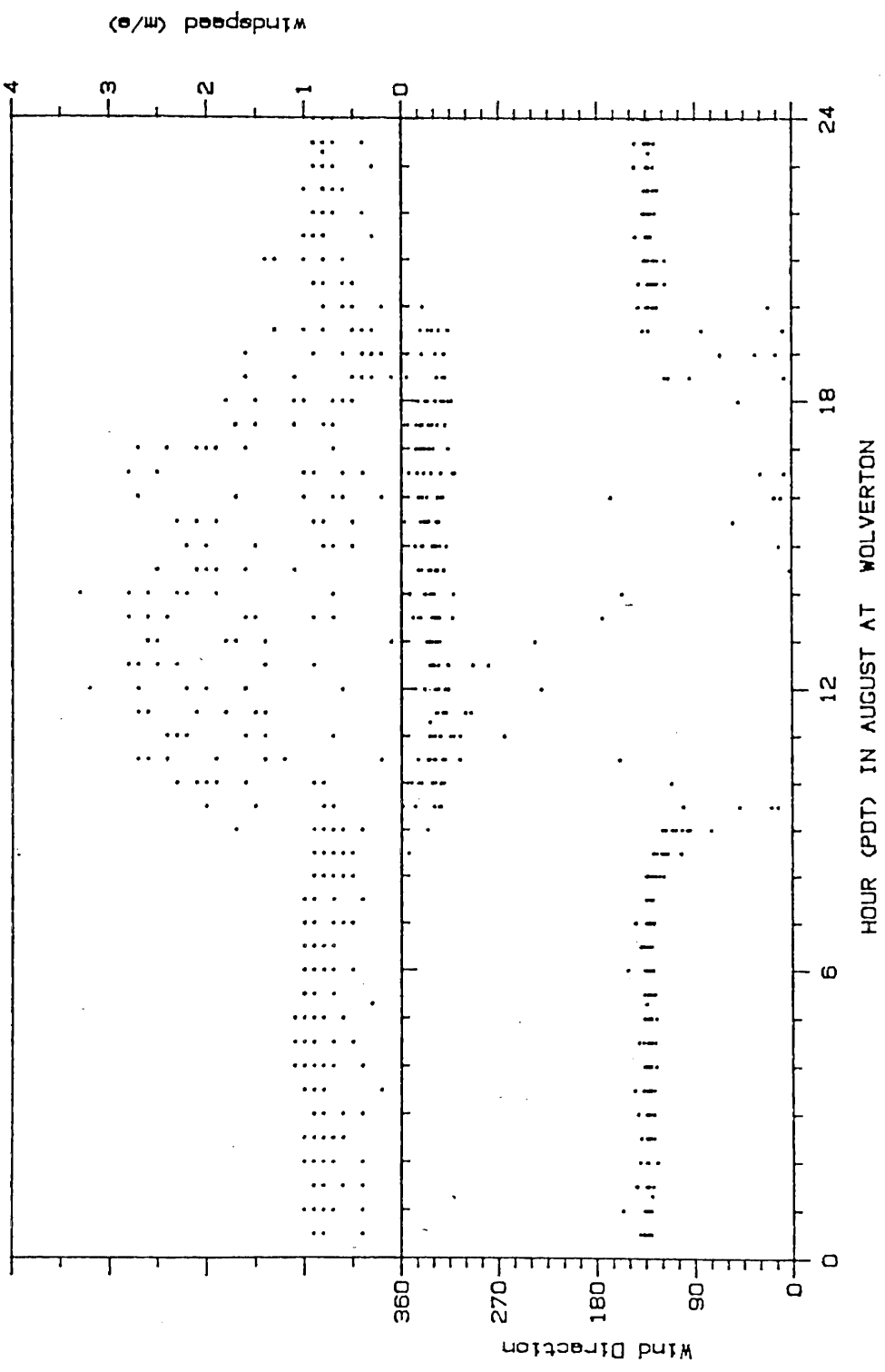


Figure 25: Wolverton ground weather station scatter plots for wind speed (meters/second) and wind direction (degrees) by time of day.

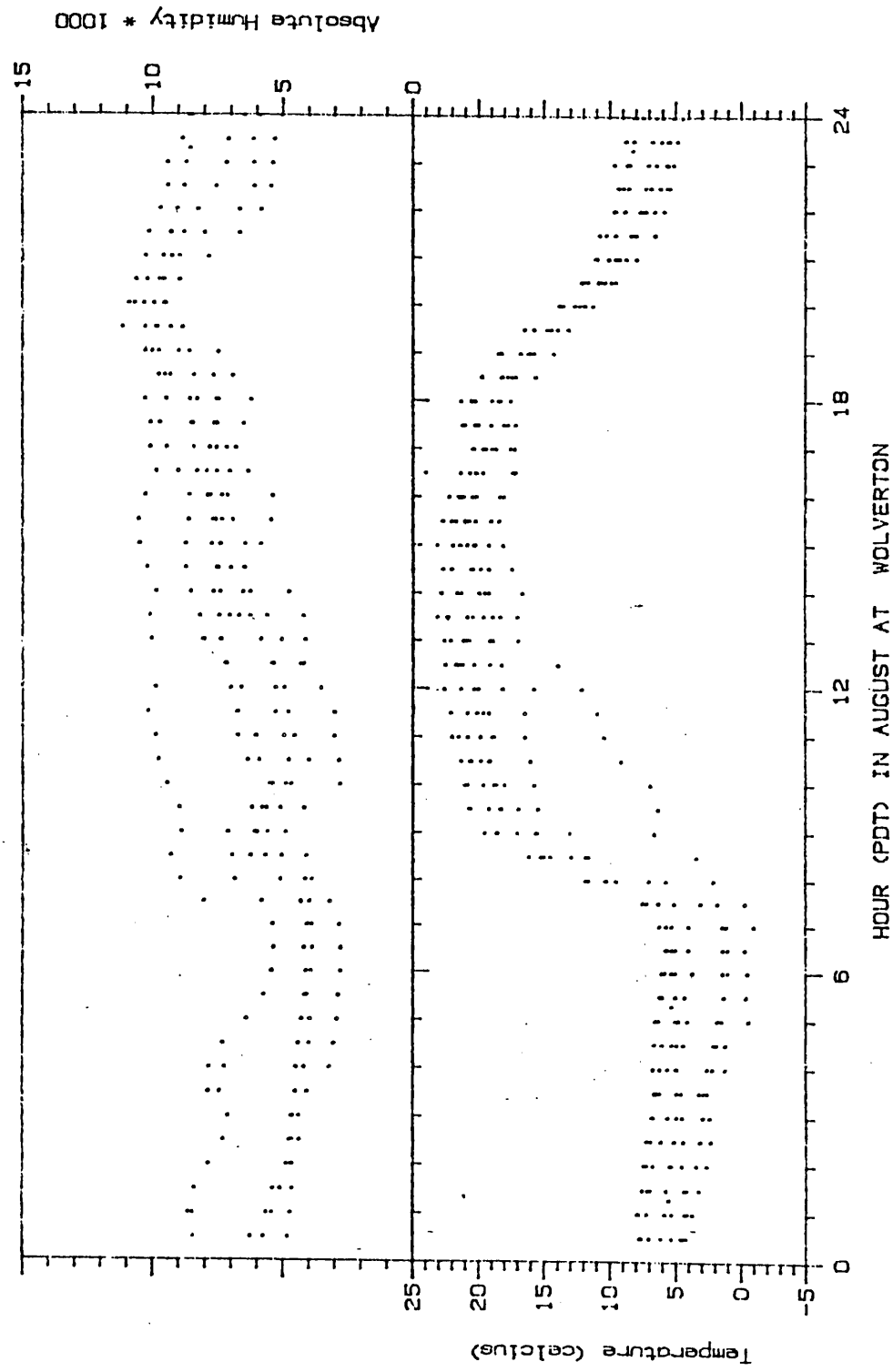


Figure 26: Wolverton ground weather station scatter plots for absolute humidity (x1000) and temperature (celcius) by time of day.

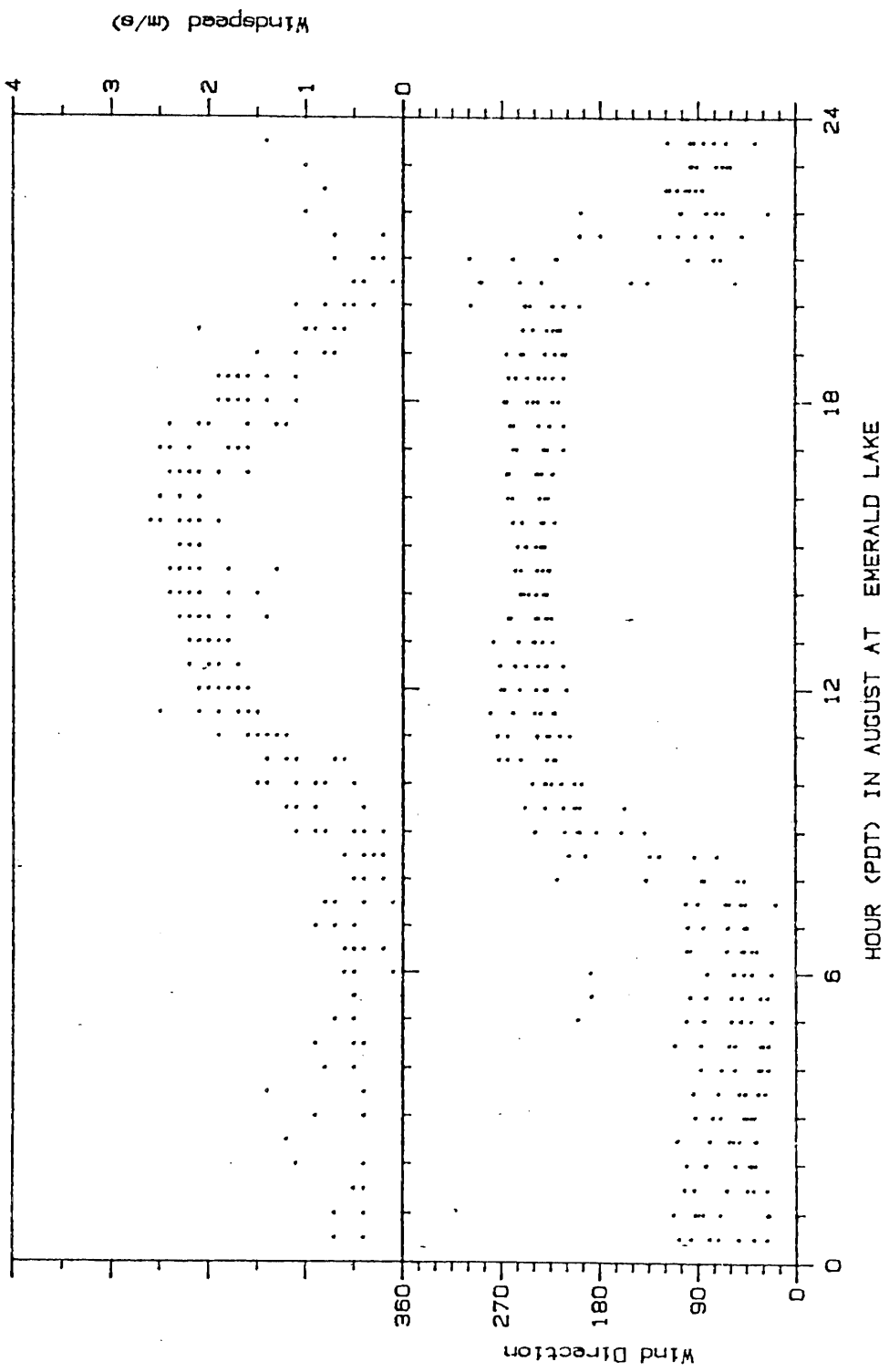


Figure 27: Emerald Lake ground weather station scatter plots for wind speed (meters/second) and wind direction (degrees) by time of day.

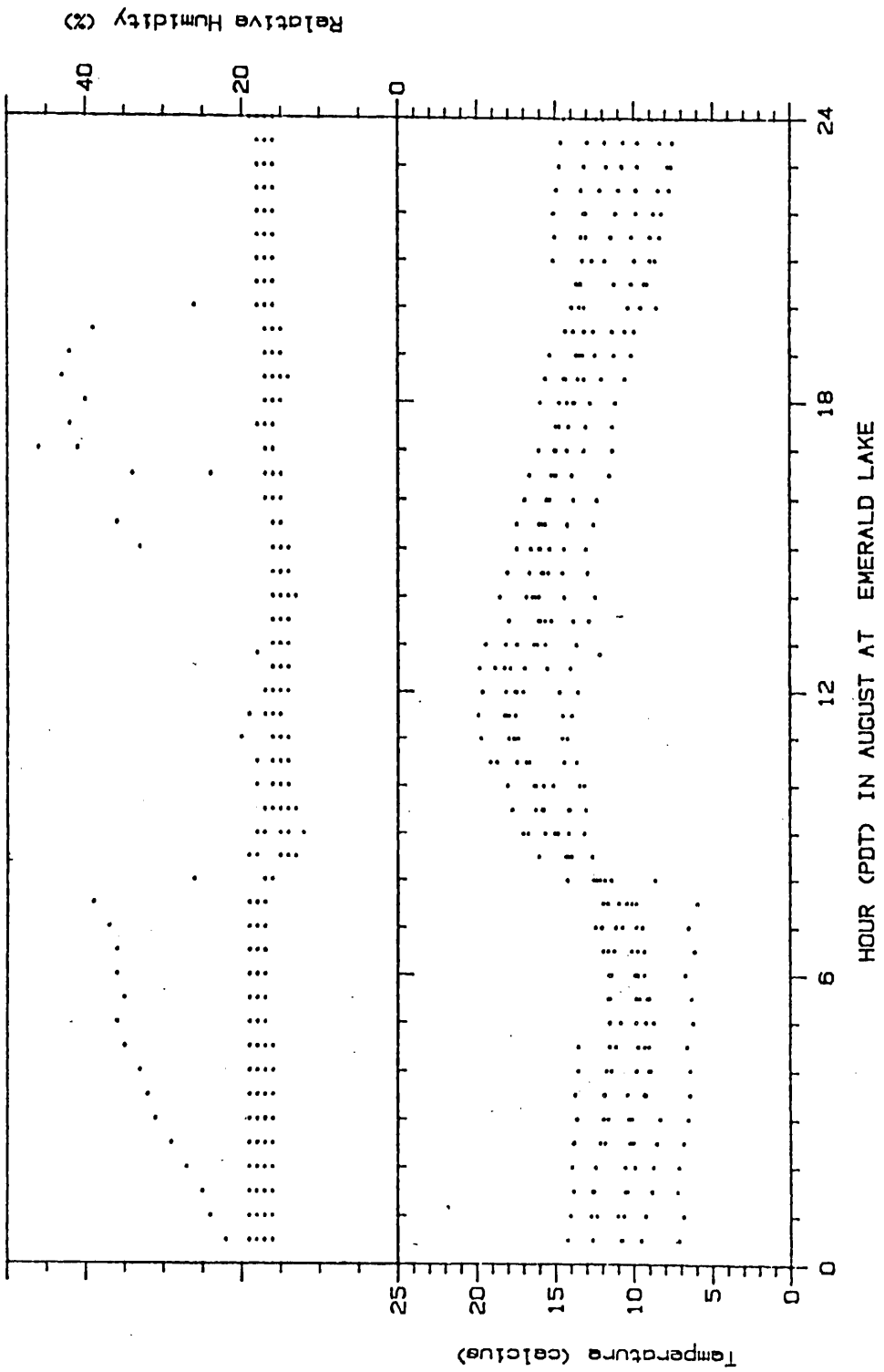


Figure 28: Emerald Lake ground weather station scatter plots for relative humidity (percent) and temperature (celcius) by time of day.

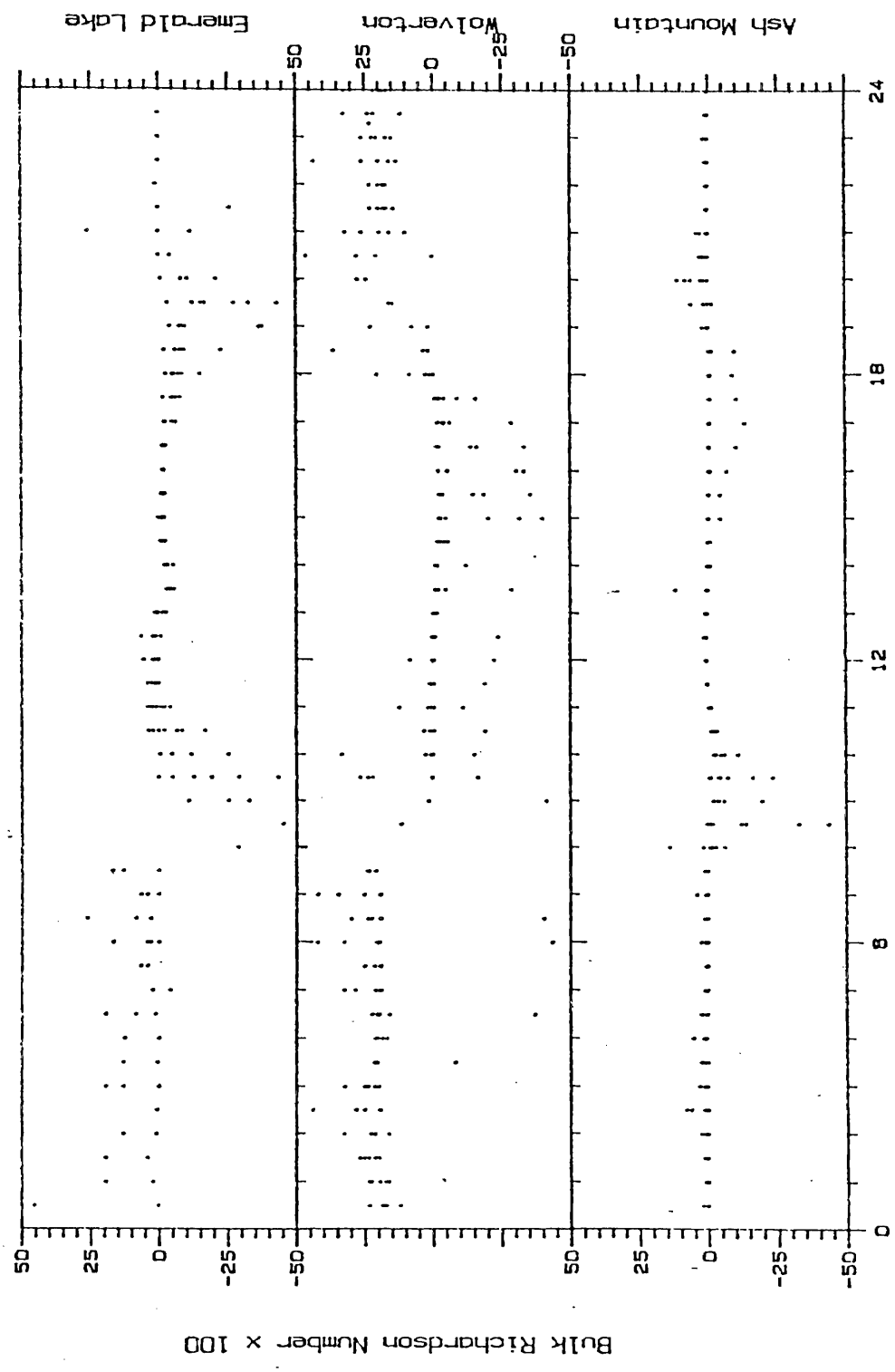


Figure 29: Bulk Richardson number (x100) scatter plots for Ash Mountain, Wolverton and Emerald Lake by time of day.

Richardson numbers and visa
versa corresponded to the times of inversion breakup and formation. At Ash Mountain, the BR number would revert back to small positive numbers (less than one) from 1130 to 1400 PDT every day. This may have been due to shading of the lower temperature sensor. It is probable that the cup anemometer assembly at Emerald Lake had a higher starting threshold than the instrument specifications (Appendix A) and therefore the BR numbers were underestimated during the day and were zero at night (between 2300 and 0800 PDT). The zero values were not plotted on Figure 29.

Table 8 summarizes the weather station data for the three sites. The first 5 rows indicate the day and night wind direction, topographic features influencing the wind direction and the time of up- and down-valley wind shifts. The wind direction for the three sites differ considerably compared to the wind direction listed in Table 2. The topographic features described in Table 2 reflected the general surroundings whereas the ground stations were influenced by the immediate surroundings. At Ash Mountain the wind followed the Middle Fork of the Kaweah River both day and night but at night the wind was also influenced by the east-southeast slope near the station. At Wolverton the daytime wind direction was influenced by both Wolverton creek and Long Meadow. At Emerald Lake, the wind direction was mostly along the Marble Fork of the Kaweah River with the south slope across the Marble Fork from the station

| Parameter | Ash Mountain | Wolverton | Emerald Lake |
|---|---|---|---|
| Daytime Wind Direction | 215 | 330 | 240 |
| Nighttime Wind Direction | 15 | 135 | 60 |
| Topographic Features | Middle Fork ESE Slope | Wolverton Ck. NW Slope | Marble Fork S Slope |
| Morning Wind Shift (PDT) | 0800-0900 | 0800-0930 | 0730-0900 |
| Evening Wind Shift (PDT) | 1900-2030 | 1930 | 2000-2130 |
| Wind Speed (m/s) | 0-4 | 0-3.5 | 0-2.5 |
| Temperature (°C) | 16-33 | -1-24 | 6-20 |
| RH (%) | 10-80 | 15-100 | -- |
| q x 1000 | 5-14 | 3-11 | -- |
| BR x 100 | -98-12 | -603-485 | -983-51 |
| Maximum Temperature (PDT) | 1530 | 1500 | 0830-1400 |
| Minimum Temperature (PDT) | 0430 | 0530 | 0500 |
| Inversion Formation (PDT) | 1900 | 1800 | 2030 |
| Inversion Destruction (PDT) | 0730 | 1200 | 0730 |

RH-relative humidity, q-absolute humidity, BR-bulk Richardson number

Table 8: Weather station data summary.

slightly influencing the direction both day and night. Wind direction was most variable at Emerald lake. Evening wind shifts occurred a few hours after temperatures began to drop. Emerald Lake experienced ealier morning and later evening wind shifts due to its position at the head of the Marble Fork drainage.

The next 5 rows in Table 8 indicate the range of values observed for wind speed, temperature, relative humidity, absolute humidity and bulk Richardson number. Wind speeds are lowest at Emerald lake. Again this was probably due to the problem with the starting speed for the cup anemometer. A higher starting speed would underestimate the average wind speed. As expected, the temperatures were much cooler at Wolverton and Emerald Lake than at Ash mountain. The coolest temperatures were at Wolverton because of the moisture from the meadow. It is interesting that while the Wolverton site was located next to a moist meadow, the absolute humidity range was lower than at Ash Mountain. As mentioned before, the absolute humidity at Wolverton would increase during the day and decrease at night. At Ash Mountain, the opposite was true. Larger positive and negative BR numbers were observed at Wolverton indicating Wolverton is more stable at night and more unstable during the day. The larger nighttime positive BR numbers were expected since the Wolverton station was located next to Long meadow which was in a depressed, horseshoe shaped area facing the north where cold area readily drained to and

accumulated. The smaller negative BR numbers at Ash Mountain indicate more uniform mixing of the air masses. The next 4 rows indicate the times of maximum and minimum temperatures and of inversion formation and destruction. A dead snag was used as the instrument tower at Emerald Lake. The "two meter" temperature probe was located on a rock on the ground and the "five meter" temperature probe was on a limb at four meters above the ground. The morning minimum temperatures were regular and the two probes agreed well but the afternoon temperatures were very inconsistent and the two probes peaked hours apart. It is probable that shading and radiation were the cause of the inconsistent data. On the average, however, the temperature maximum occurred before noon. The early maxima was probably the result of afternoon shading by steep walls surrounding the narrow valley. The inversion destruction at Wolverton was notably later when night temperatures were below freezing. Table 5 lists the minima and maxima temperatures for the three study sites plus Fresno and relative humidities for Fresno, Ash Mountain and Wolverton for each day of the August study period.

B. Aerosol Sampling

Vertical aerosol profiles were collected using a tethered balloon system. Two-staged aerosol samplers were spaced 50 meters apart along the tether line up to 250 meters above the ground level. A total of 5 morning, 9 afternoon and 3 evening profiles were made during the August field period

equaling 64 coarse and 64 fine filter samples (Table 2). The morning profiles were between 0800 and 1200 PDT, the afternoon profiles were between 1400 and 1800 and the evening profiles were between 2200 and 0500 PDT. In the following sections, "day" aerosol values refer to the afternoon profiles and "night" aerosol values refer to the morning and evening profiles combined.

1. Average Concentrations

The samples were analyzed for elemental concentrations of sodium to lead, gravimetric mass, hydrogen concentration and carbon absorption. Listed below are the fine and coarse average concentrations (averaged over all levels)

| | FINE | | | COARSE | | |
|---|---|---|---|---|---|---|
| | Al | Si | Fe | Al | Si | Fe |
| avg | 189 | 260 | 71 | 1217 | 1786 | 543 |
| s | 87 | 136 | 45 | 391 | 1239 | 533 |
| err | 21 | 19 | 22 | 16 | 25 | 24 |
| s | 10 | 9 | 10 | 17 | 10 | 11 |
| up | 19 | 33 | 34 | 9 | 33 | 34 |
| down | 11 | 28 | 25 | 19 | 27 | 27 |
| | S | K | Mass | S | K | Mass |
| avg | 630 | 61 | 36 | 320 | 284 | 27 |
| s | 299 | 33 | 33 | 146 | 199 | 15 |
| err | 14 | 33 | 6 | 68 | 51 | 7 |
| s | 8 | 19 | -- | 22 | 17 | -- |
| up | 33 | 33 | 34 | 8 | 19 | 33 |
| down | 29 | 28 | 29 | 6 | 28 | 30 |
| | Ca | H | C-S | Ca | | |
| avg | 34 | 495 | 1119 | 273 | | |
| s | 19 | 179 | 616 | 194 | | |
| err | 37 | 15 | 7 | 45 | | |
| s | 11 | -- | -- | 17 | | |
| up | 22 | 33 | 33 | 30 | | |
| down | 15 | 26 | 27 | 22 | | |

avg.=average concentration; s=standard deviation of the concentration; err=average error for concentration; s=standard deviation of the error; up=number of afternoon concentrations in average; down=number of morning and evening concentrations in average.

for the major elements aluminum (Al), iron (Fe), silicon

(Si), sulfur (S), potassium (K) and calcium (Ca) as well as gravimetric mass (Mass). Average fine hydrogen and carbon-soot concentrations are also listed. Elemental concentrations and carbon-soot are in nanograms per cubic meter and gravimetric mass is in micrograms per cubic meter.

2. Source Categories

The aerosol data were grouped into source categories. In the list below, the fine aerosols have been grouped into sulfate, smoke, soil, auto and ocean-salt categories (micrograms per cubic meter). These are categories used by Cahill et al. (1986b). The sulfate was calculated assuming the sulfur was in the form of ammonium sulfate. The smoke category is non-soil potassium and a multiplication factor of 20 has been used (low end of associated particle loading range). Non-soil potassium was determined by subtracting soil potassium from total potassium. Soil potassium was calculated by multiplying fine Fe with the ratio of coarse K to coarse Fe. Soil was calculated by an algorithm which accounts for 86 percent of the mass of a typical sediment and includes Al, Si, Ca, Fe and K. Titanium was excluded since it occurred infrequently and was in insignificant concentrations. An additional 16 percent was added to the elemental concentrations to account for other elements not included in algorithm. Chlorine was not included in the soil category since, in general, chlorine is present in typical soils at less than one percent of the other major

soil element levels. The auto category included lead (Pb) and bromine (Br) and ocean-salt included sodium (Na) and chlorine (Cl).

Fine Aerosol Concentration-Source Categories

| Sulfate | Smoke | Soil | Auto | Salt | H:S | Total Mass |
|---|---|---|---|---|---|---|
| 2.6 | 0.4 | 1.3 | 0.09 | 0.05 | 25 | 36 |

While the fine soil component was less than 5 percent of the total fine mass, the coarse soil was 33 percent of the total coarse mass (9 micrograms per cubic meter). Cahill et al. (1986a) reported that coarse soil was on average 60 percent of the total coarse mass for the National Park Service network. This difference was probably due to the samplers for the network being located at the ground level while the tethered samplers were located from 50 to 250 meters above the ground. Also included above is the hydrogen to sulfur molar ratio. The ratio for ammonium sulfate is 8:1. The ratio above indicates a large proportion of the hydrogen was associated with other elements besides sulfur. It is probable that nitrogen was the other major element associated with the hydrogen although nitrogen was not included in the elemental analysis (Cahill et al. 1986a).

3. Vertical Concentration Profiles

While 5 morning, 3 evening and 9 afternoon profiles were completed, data for all levels (50 to 250 meters) for every element were not available for every profile due to various difficulties. Some problems were battery pack failure or explosion, pump failure, sample elemental concentration

below detectable limits or too large of a concentration error. It is, therefore, difficult to compare the profiles. Figures 30 and 31 show average morning, afternoon and evening aerosol profiles for fine sulfur, potassium and silicon and coarse silicon, iron and calcium (nanograms per cubic meter). What is apparent from these two figures is the increase in concentration from 50 to 150 or 200 meters for the coarse aerosol evening profiles (Figure 31) and the lack of any gradient for all the fine aerosol profiles (Figure 30) and the afternoon and morning coarse aerosol profiles. This would indicate sedimentation of the coarse particles in the evening while fines remain well mixed. Apparently, morning and afternoon conditions were such that both coarse and fine elements were well mixed. Since the number of samples per level were not equal (see Table 1), these conclusions are only tentative at best and further investigation on this subject is needed. Figure 32 shows the individual profiles for fine sulfur. The numbers listed next to each vertical profile indicate the day in August. The two evening profiles on the 21st are further labeled with the time (PDT). Again, these profiles do not show a consistent pattern of increase nor decrease with height.

The table below shows the results from a standard pooled variance t-test comparing afternoon to morning and evening aerosol concentrations (averaged over all levels). All the afternoon profiles had significantly higher concentrations

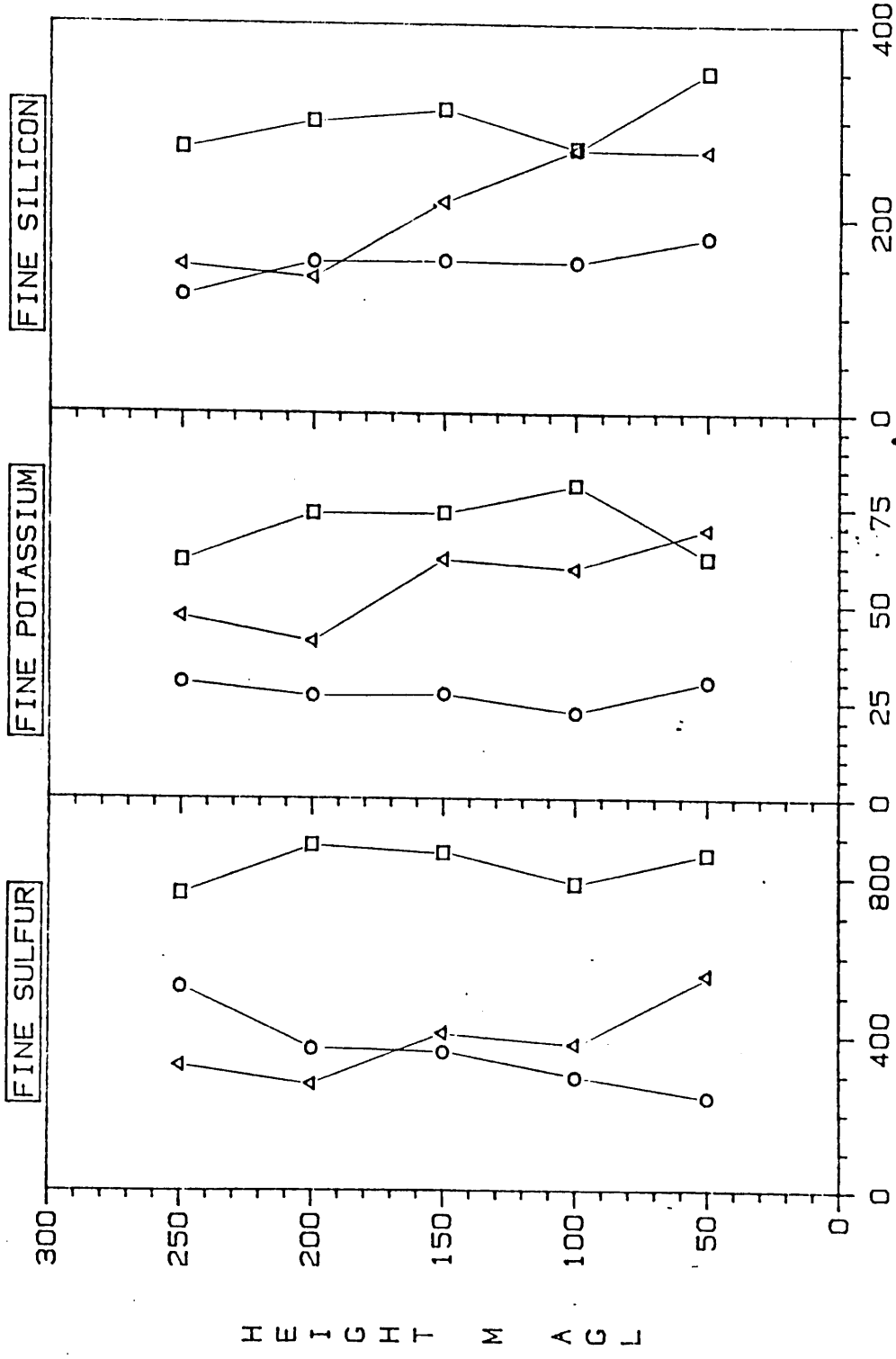


Figure 30: Average fine aerosol concentration profiles for sulfur, potassium and silicon.

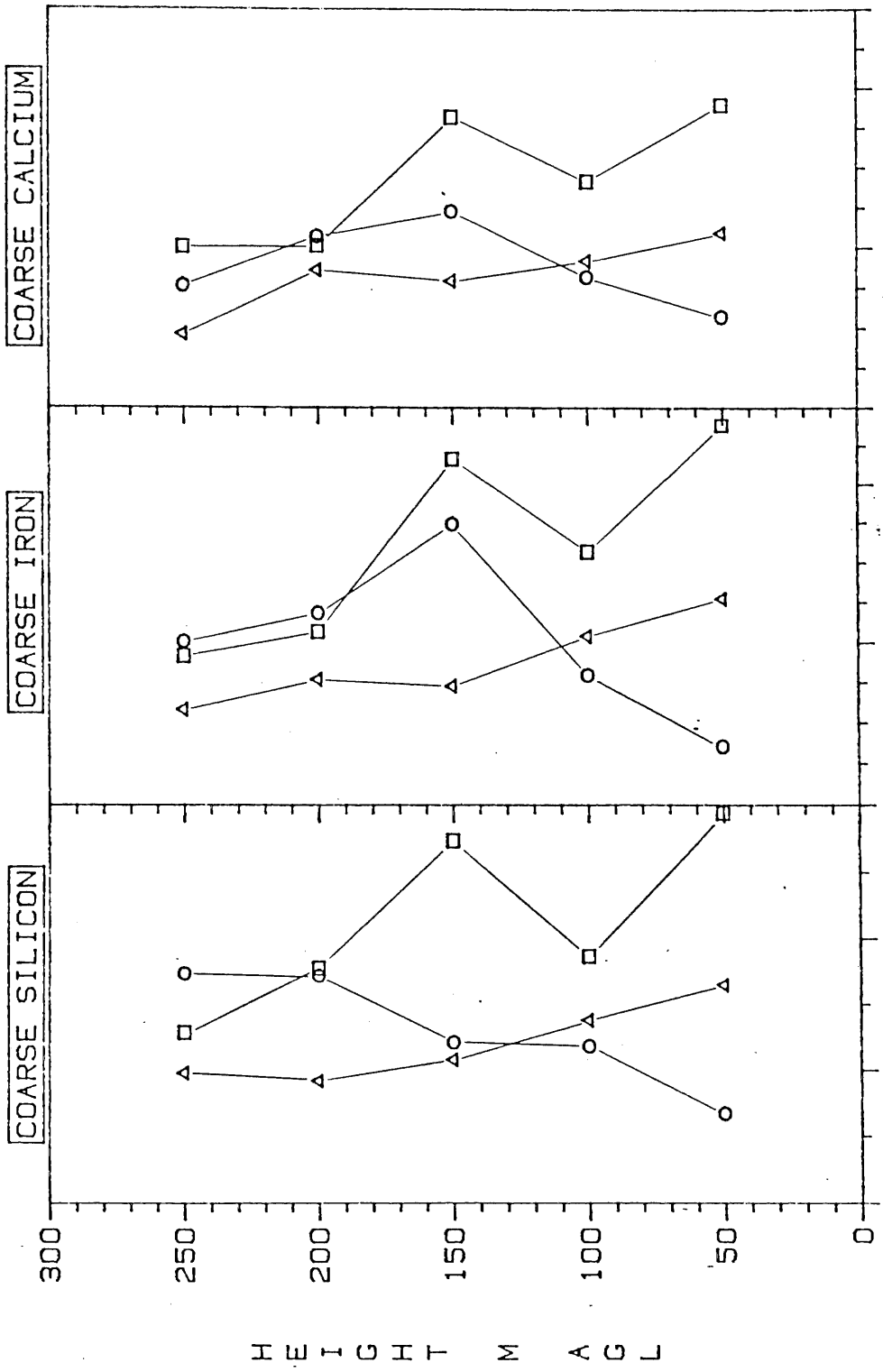


Figure 31: Average coarse aerosol concentration profiles for silicon, iron and calcium.

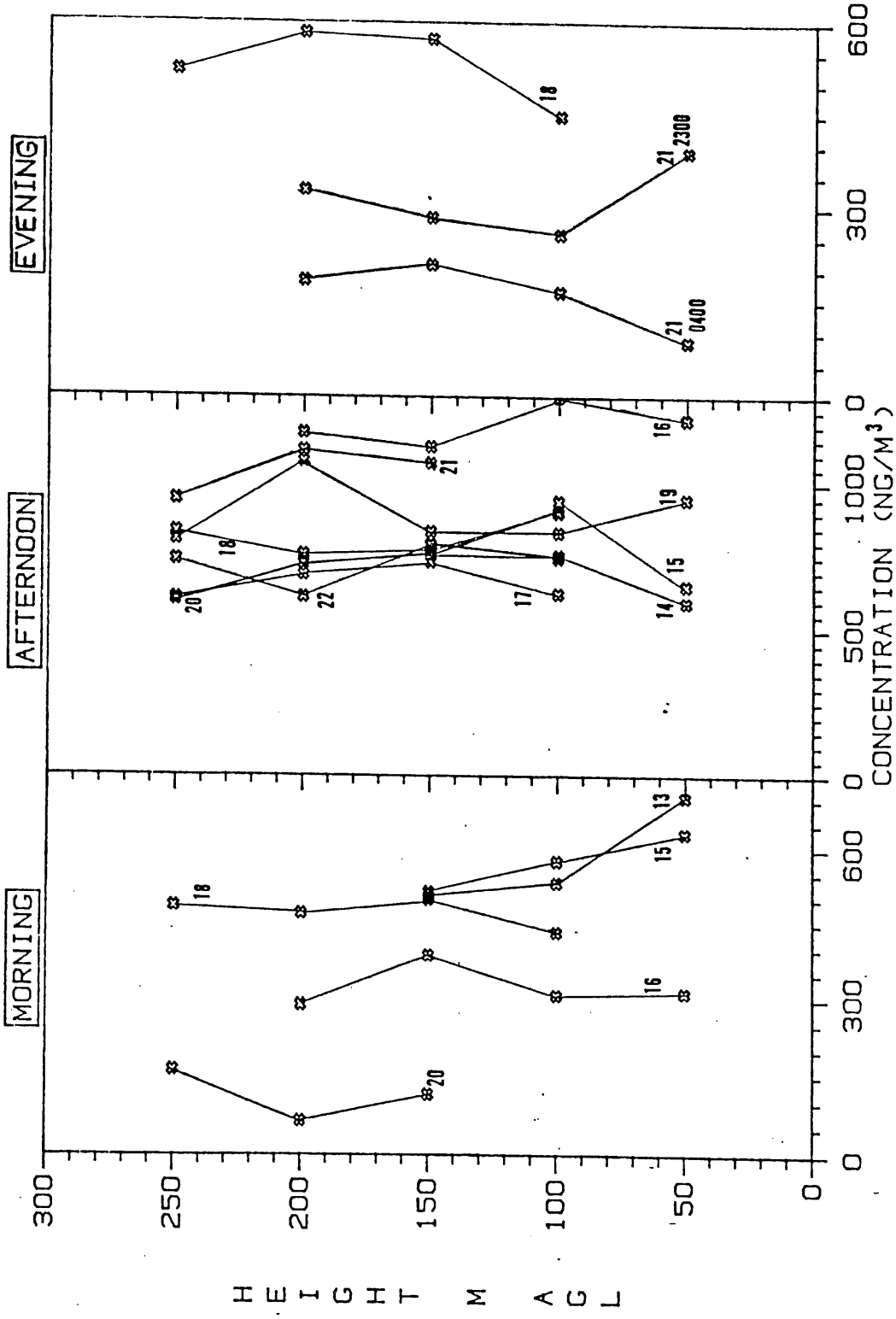


Figure 32: Individual fine aerosol concentration profiles for sulfur.

except for fine Ca, Pb and Al and coarse Al and mass. Fine mass and coarse K, Ca and Fe were not as significantly different as were the other elements. The most significant differences were for fine S, K, C-S and H.

| | afternoon | | | morning & evening | | | | |
|---|---|---|---|---|---|---|---|---|
| Element | mean | s | n | mean | s | n | df | percentile |
| FINE | | | | | | | | |
| Mass | 39.1 | 19.3 | 34 | 33.1 | 11.0 | 29 | 61 | .90 |
| S | 849.5 | 191.9 | 33 | 380.8 | 179.4 | 29 | 60 | >.9995 |
| K | 73.3 | 33.8 | 33 | 45.9 | 26.3 | 28 | 59 | .9995 |
| Si | 304.7 | 148.9 | 33 | 207.0 | 96.3 | 28 | 59 | .995 |
| C-S | 1474.3 | 705.6 | 33 | 684.7 | 434.7 | 27 | 58 | .9995 |
| Ca | 33.2 | 16.6 | 22 | 34.0 | 13.7 | 15 | 35 | NS |
| Fe | 84.3 | 50.8 | 34 | 52.5 | 23.7 | 25 | 57 | .995 |
| Pb | 61.7 | 37.0 | 12 | 58.1 | 30.5 | 11 | 21 | NS |
| H | 580.9 | 155.0 | 33 | 386.6 | 146.8 | 26 | 57 | .9995 |
| Al | 152.9 | 65.1 | 34 | 140.0 | 62.2 | 30 | 62 | NS |
| COARSE | | | | | | | | |
| Mass | 27.9 | 14.4 | 33 | 25.7 | 15.0 | 30 | 61 | NS |
| Si | 2137.2 | 1524.7 | 33 | 1356.1 | 521.3 | 27 | 58 | .99 |
| K | 332.6 | 247.7 | 27 | 211.9 | 67.7 | 21 | 46 | .975 |
| Ca | 312.1 | 234.4 | 30 | 218.6 | 101.2 | 22 | 50 | .95 |
| Fe | 636.2 | 634.9 | 34 | 426.1 | 342.8 | 27 | 59 | .90 |
| Al | 1333.9 | 958.8 | 29 | 1037.7 | 620.8 | 19 | 46 | NS |

df-degrees of freedom, s-standard deviation, n-number of data points, NS-not significant.

A concurrent study by Cahill et al. (1986a) showed possibly different results. They found that nighttime levels of accumulation mode size particles of sulfur and potassium (.10 to .6 microns) were higher than daytime values. Conclusive evidence as to whether total fine concentrations were higher (<2.5 microns) at night than during the day awaits further data analysis. Preliminary data from a nitrogen study conducted in the summer of 1986 showed higher nitrate and nitric acid concentrations during the day than at night (Jack Horrocks 1987).

Since aluminum is a major component of soil, it was

unexpected that the afternoon concentrations of coarse aluminum were not higher than the morning/night concentrations. The average fine and coarse aluminum to silicon ratios were 0.640 and 0.657, respectively, as compared to the crustal average of 0.292 (see Chapter III, Section E-4). Aluminum also had the lowest correlation to silicon of the soil related elements as well (see Section B-5). The source of excess aluminum is unknown at this time.

Figures 33 to 43 are scatter plots of major coarse and fine aerosol concentration profiles. All concentrations are in nanograms per cubic meter except for gravimetric mass which is in micrograms per cubic meter. On the top portion of each figure are the afternoon ("day") concentrations and on the bottom half are the morning and evening ("night") concentrations. As shown, the morning concentrations are plotted as open circles and the evening concentrations are plotted as filled in circles. The direction of the arrows indicate the wind direction with north being toward the top of the page. Unusually large values have been plotted as stars and are actually off scale. The wind direction for each sampling height was carefully determined and will be explained in more detail under Section B-6 below.

The most striking differences between the "day" and "night" concentrations are seen for fine carbon-soot and sulfur. Figure 33 shows coarse aluminum having high values

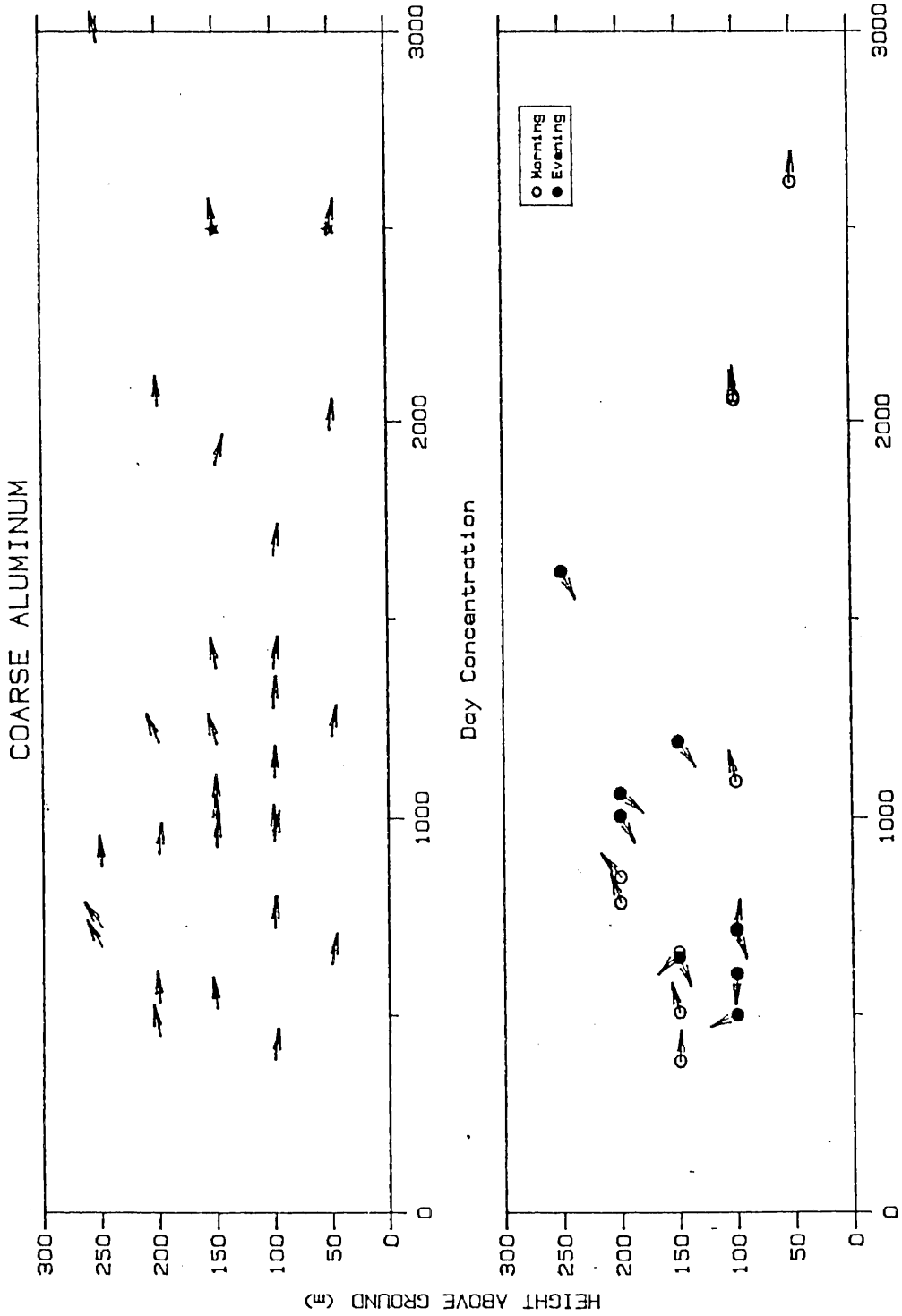


Figure 33: Scatter plot of coarse aluminum aerosol concentration profiles.

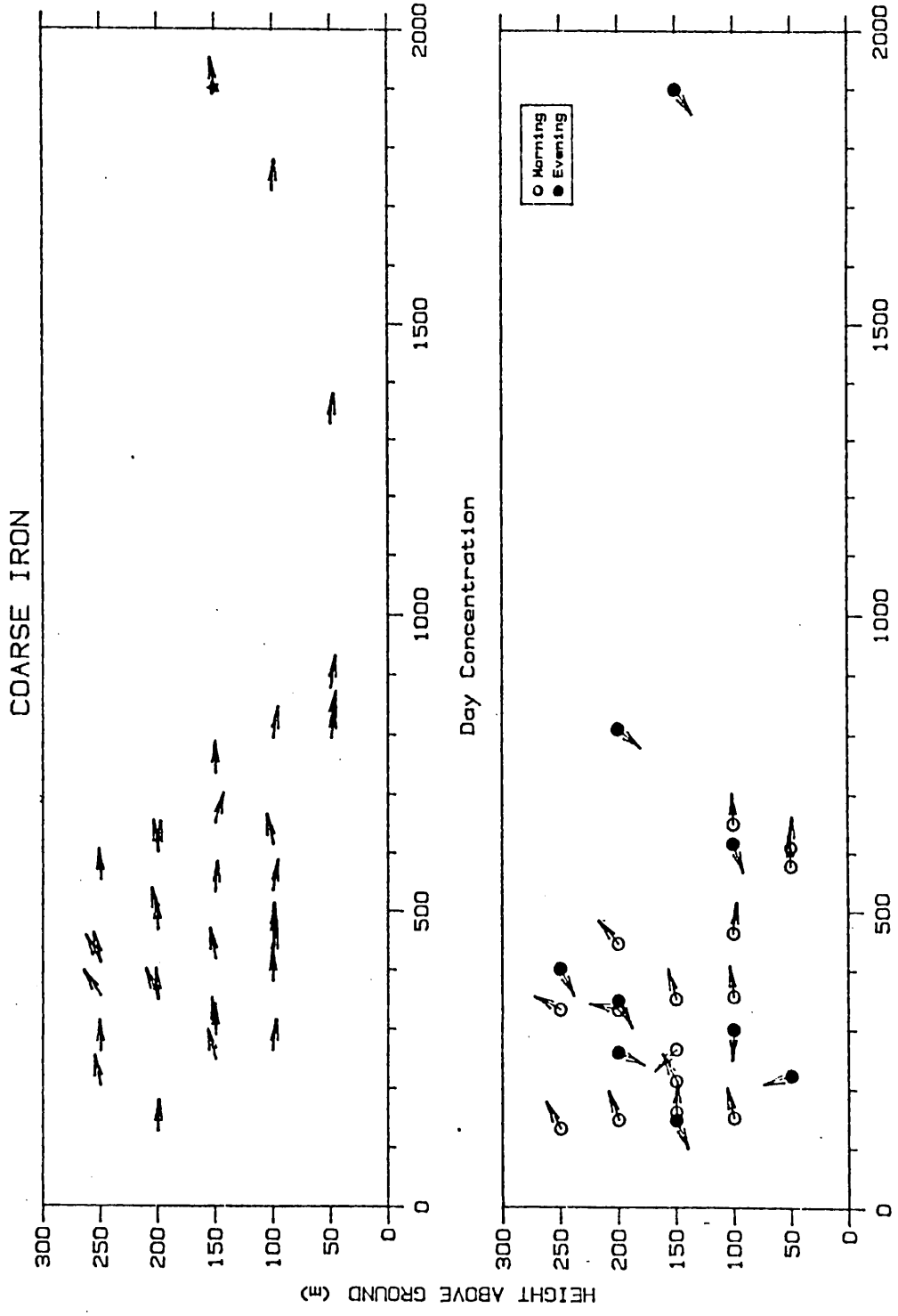


Figure 34: Scatter plot of coarse iron aerosol concentration profiles.

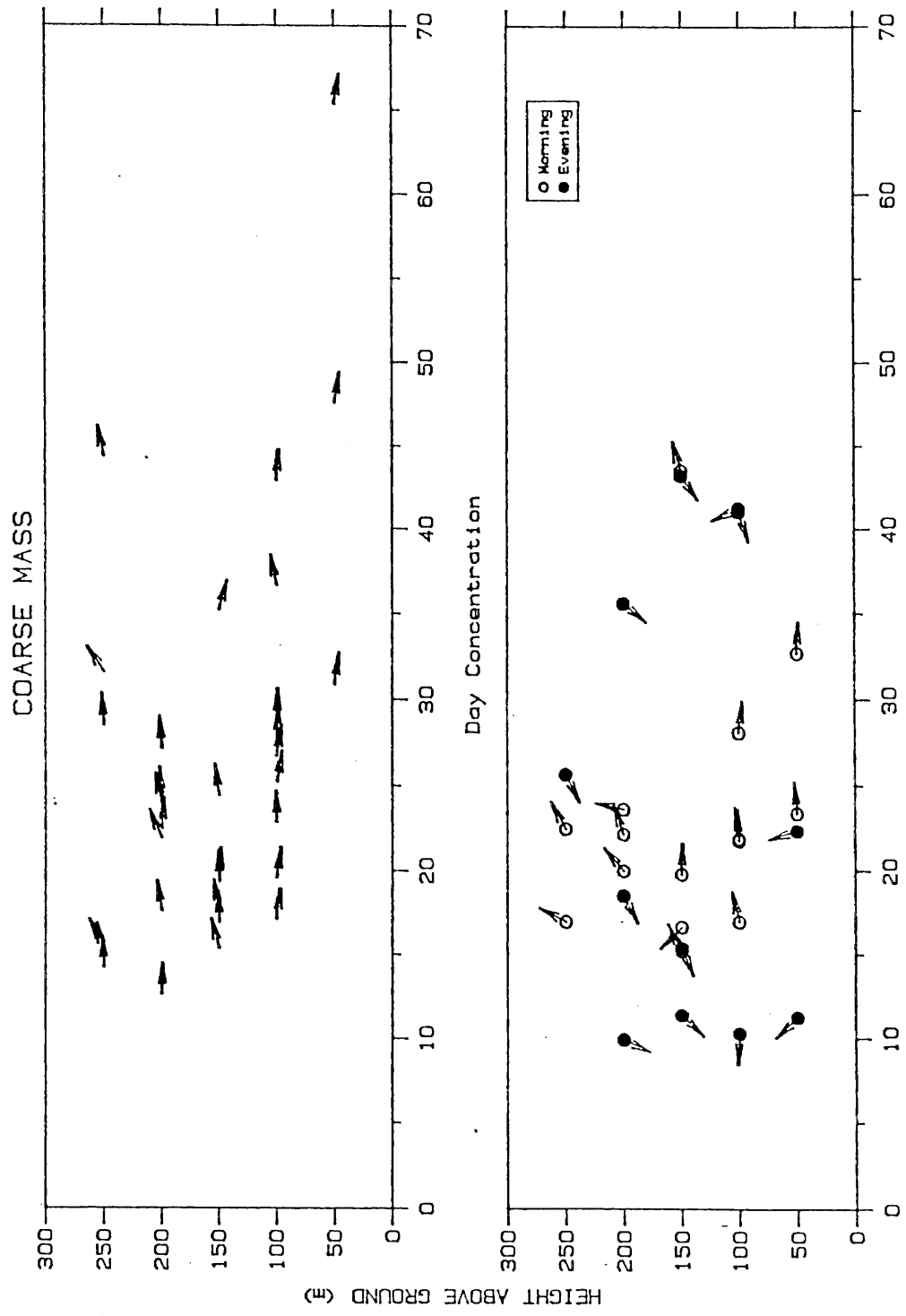


Figure 35: Scatter plot of coarse mass aerosol concentration profiles.

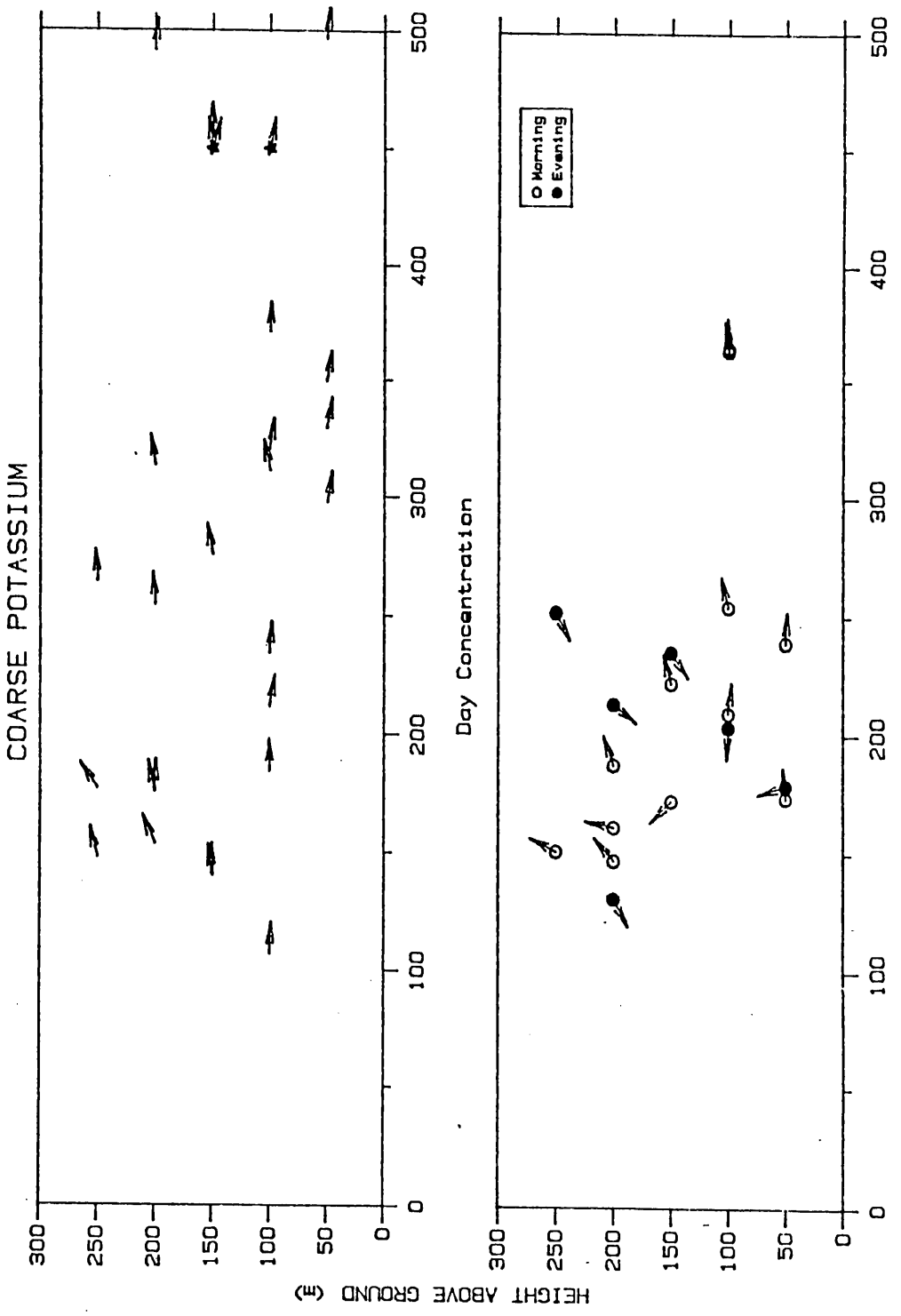


Figure 36: Scatter plot of coarse potassium aerosol concentration profiles.

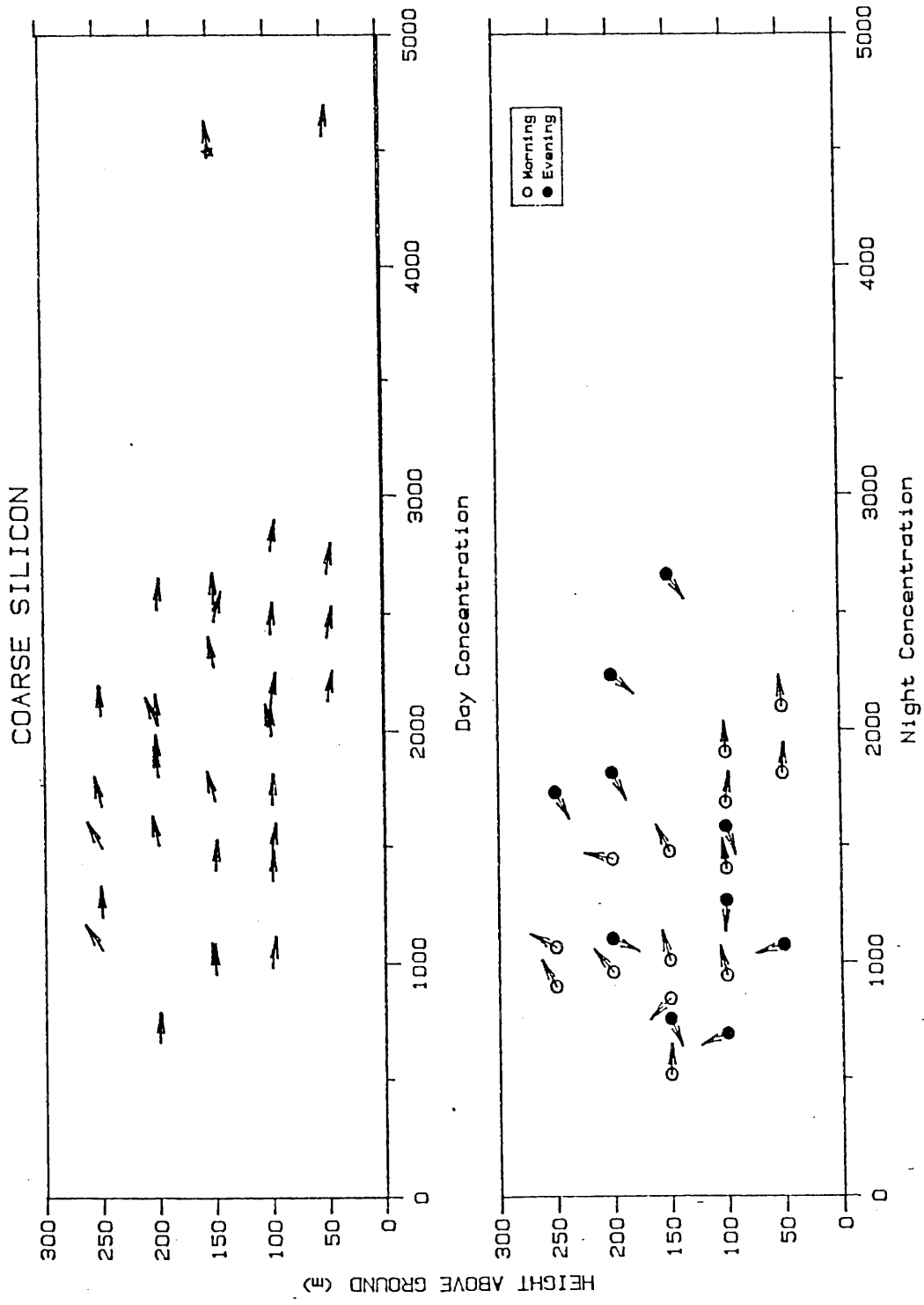


Figure 37: Scatter plot of coarse silicon aerosol concentration profiles.

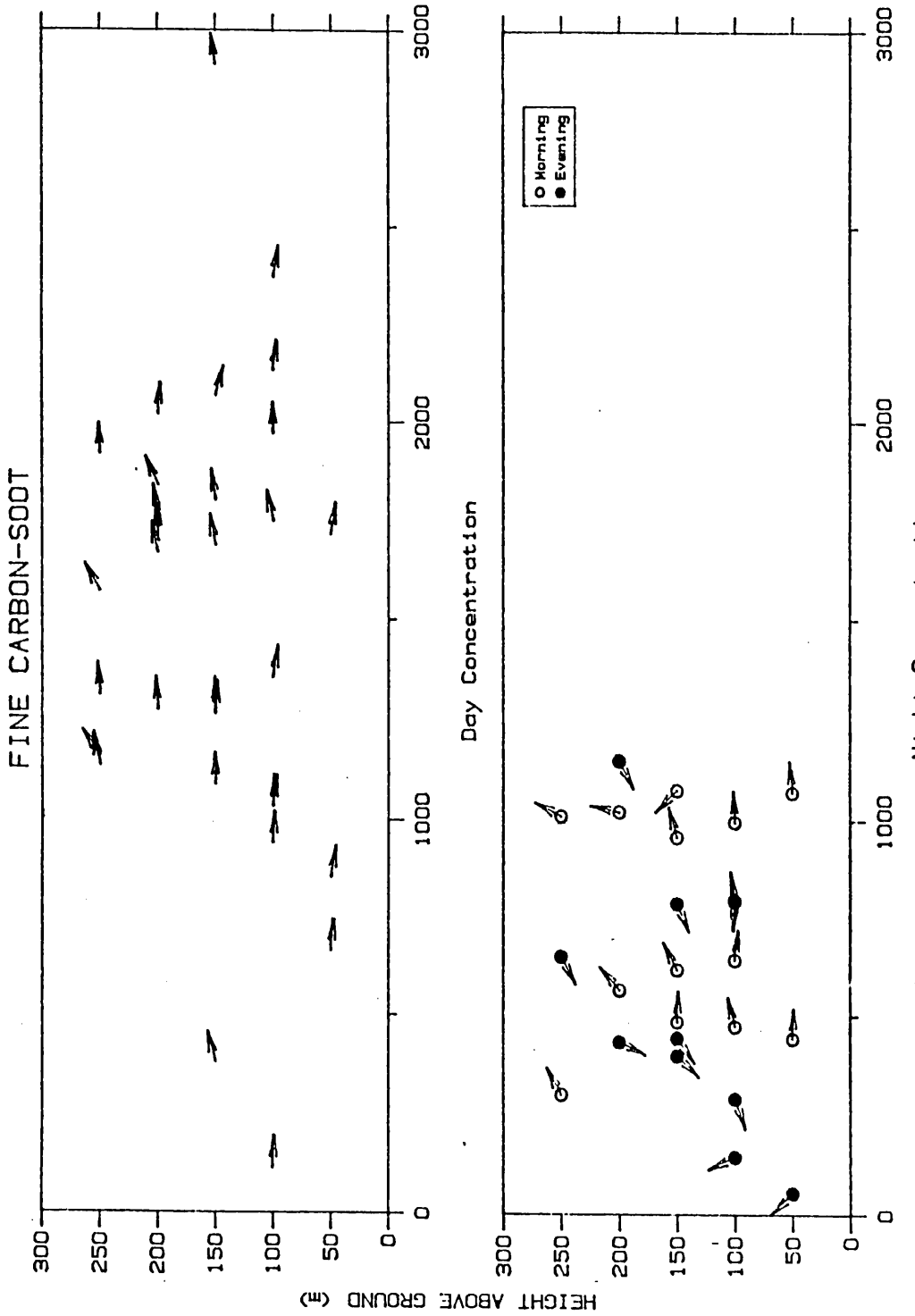


Figure 38: Scatter plot of fine carbon-soot aerosol concentration profiles.

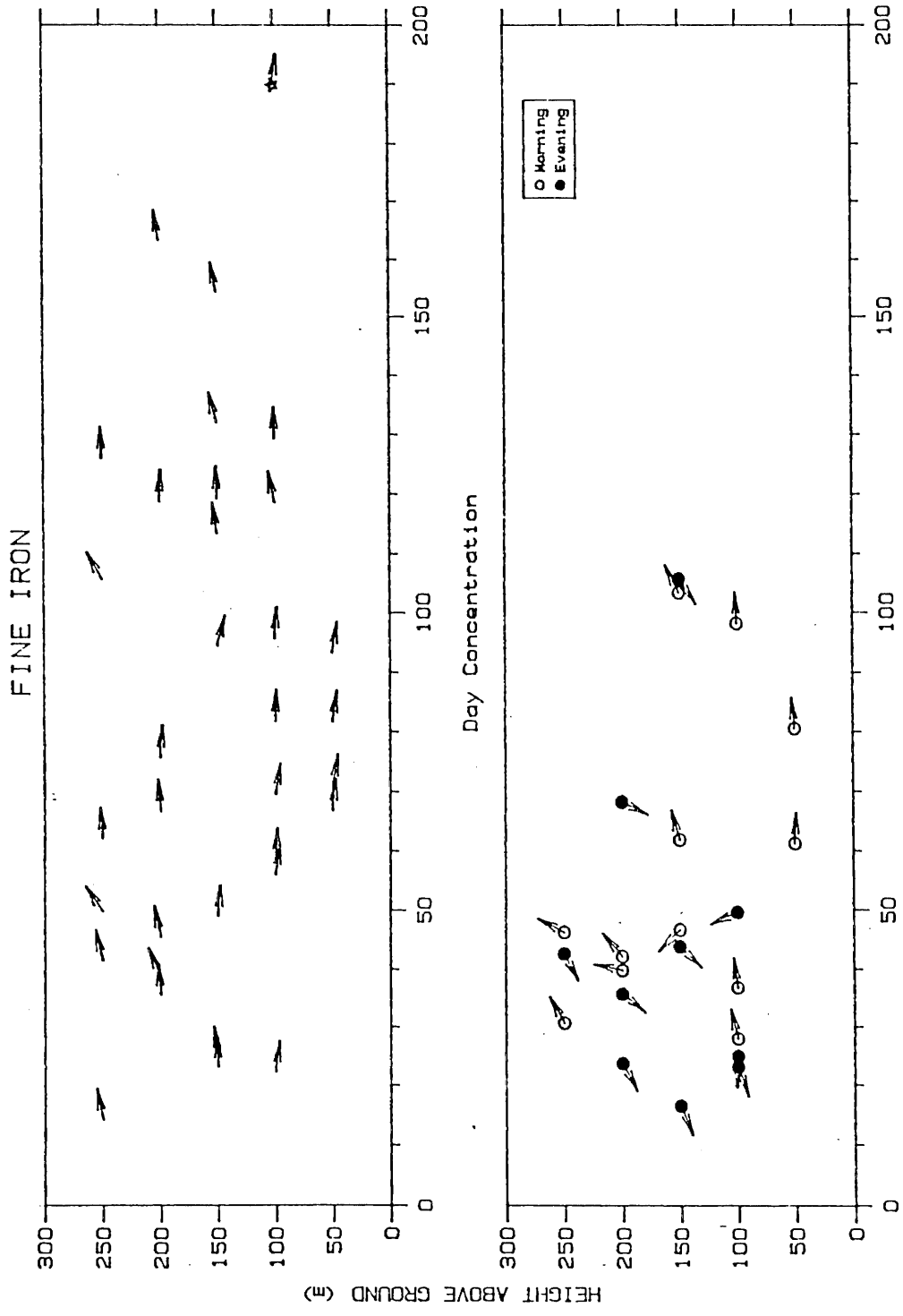


Figure 39: Scatter plot of fine iron aerosol concentration profiles.

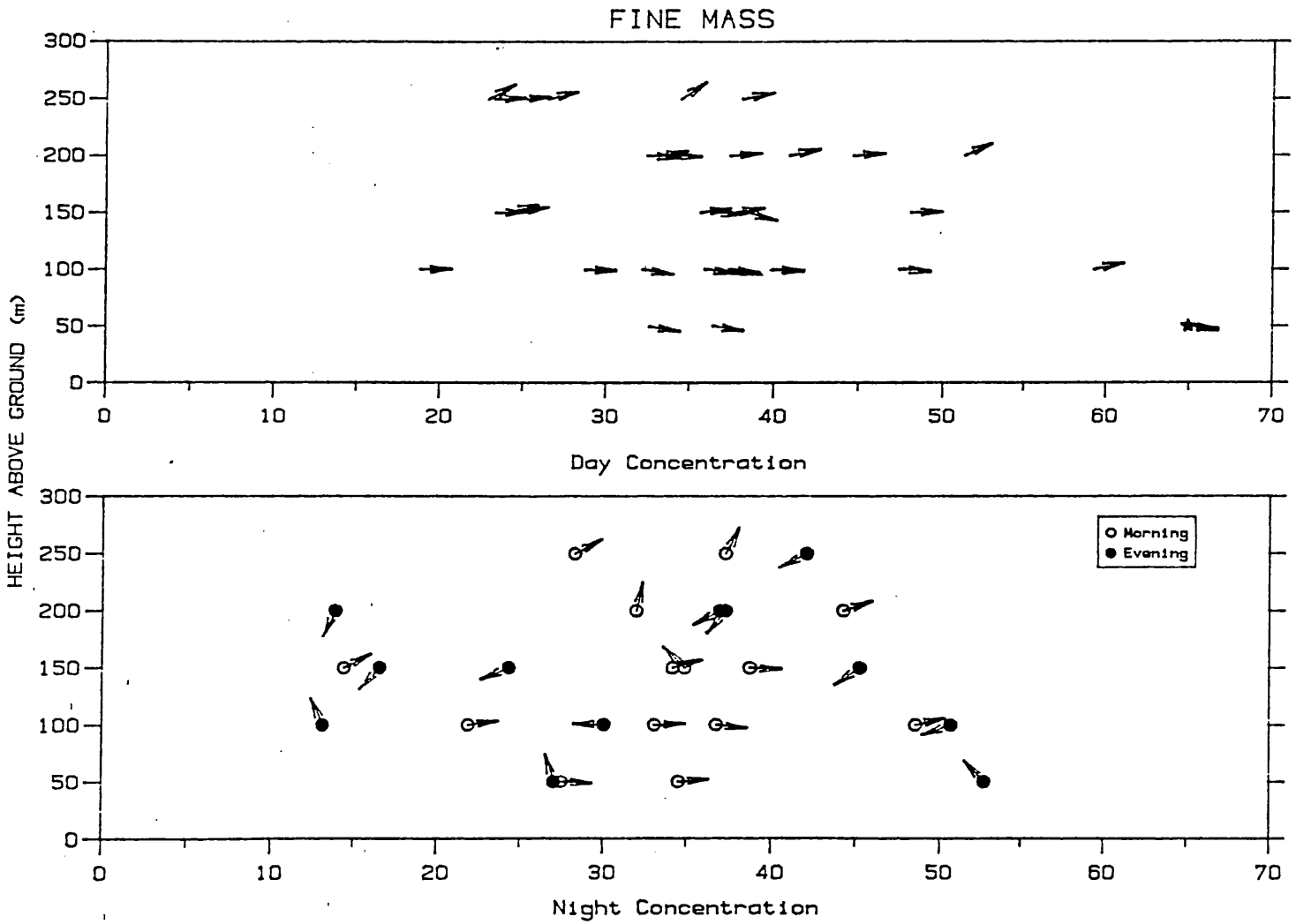


Figure 40: Scatter plot of fine mass aerosol concentration profiles.

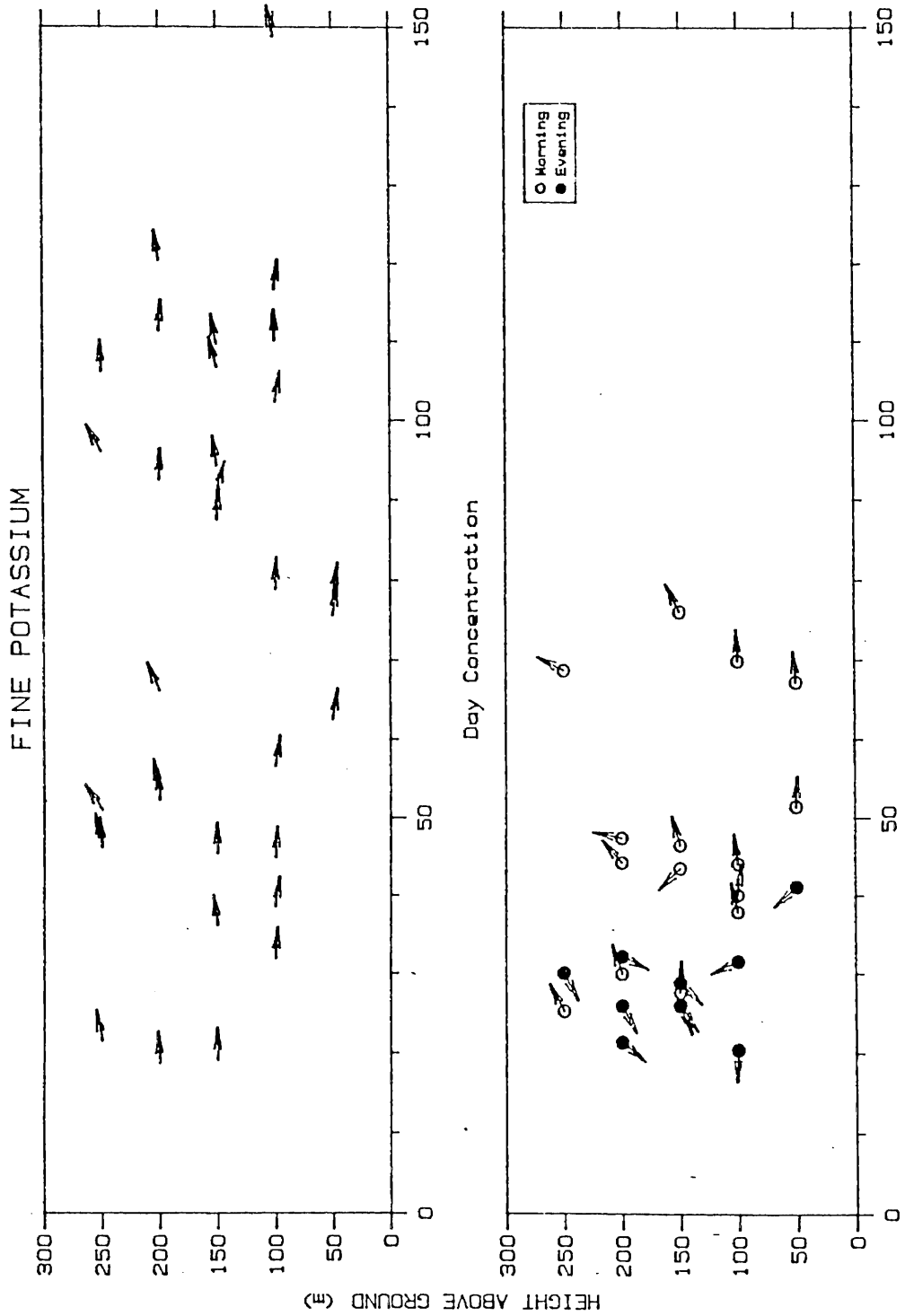


Figure 41: Scatter plot of fine potassium aerosol concentration profiles.

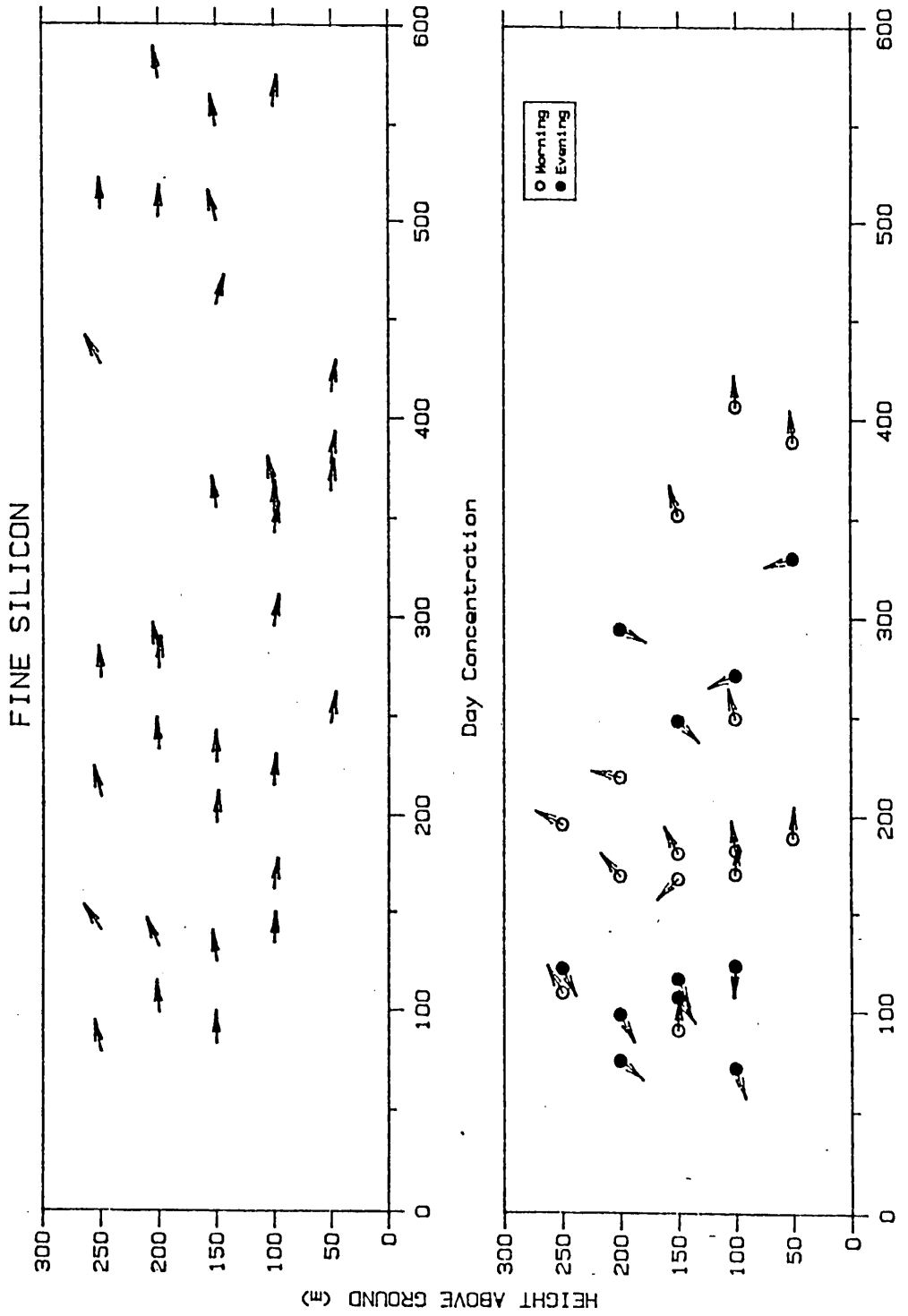


Figure 42: Scatter plot of fine silicon aerosol concentration profiles.

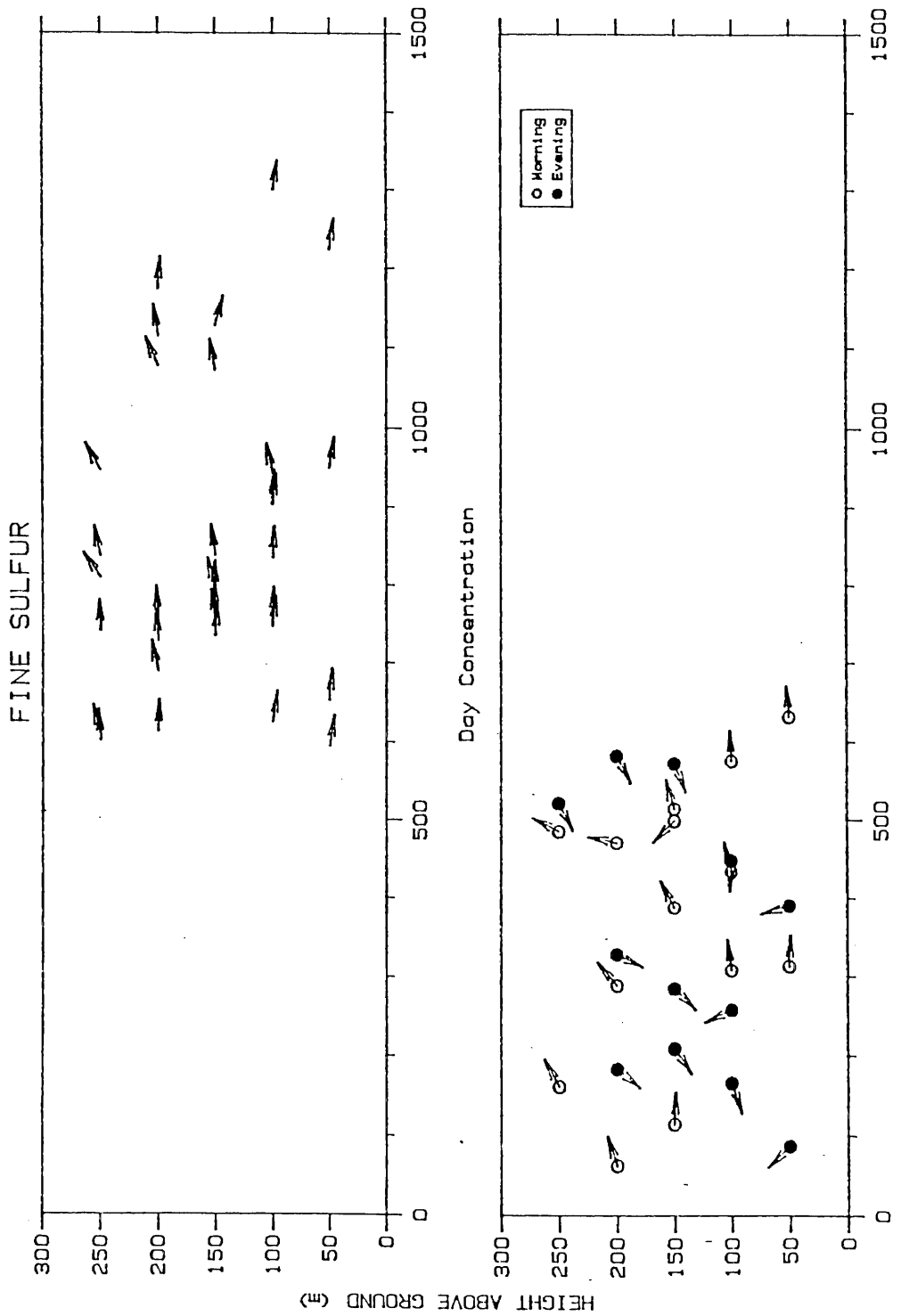


Figure 43: Scatter plot of fine sulfur aerosol concentration profiles.

both "day" and "night". Coarse iron had more high values during the "day" than "night" (Figure 34). Coarse and fine mass show little difference between "day" and "night" concentrations (Figures 35 and 40). Coarse potassium and silicon and fine iron, potassium and silicon also show higher "day" concentrations (figures 36, 37, 39, 41 and 42).

4. Case Study-August 16th and 17th

Upper level winds were mostly southeasterly at 700 millibars and westerly above from the 13th to the 16th. The 15th showed some variability but the upper winds returned to southeasterly at all levels by the 16th. On the 17th, upper level winds became very strong and southerly and brought in moisture from the remnants of a tropical hurricane. Figures 44, 45 and 46 show the afternoon satellite photographs for August 15th, 16th and 17th (obtained from the Meteorology Section, California Air Resources Board). The moisture from the hurricane can be tracked southwest of San Diego on the 15th, near Pt. Arguello on the 16th and covering a large portion of the state on the 17th. On the 16th, high concentrations were observed for elements typically transported from long distances. Below is a table with fine S, K, C-S and H afternoon concentrations averaged over the entire vertical profile for August 13th through 22th (nanograms per cubic meter). Concentrations on the 17th were the lowest of the ten days (except for potassium). This decrease in

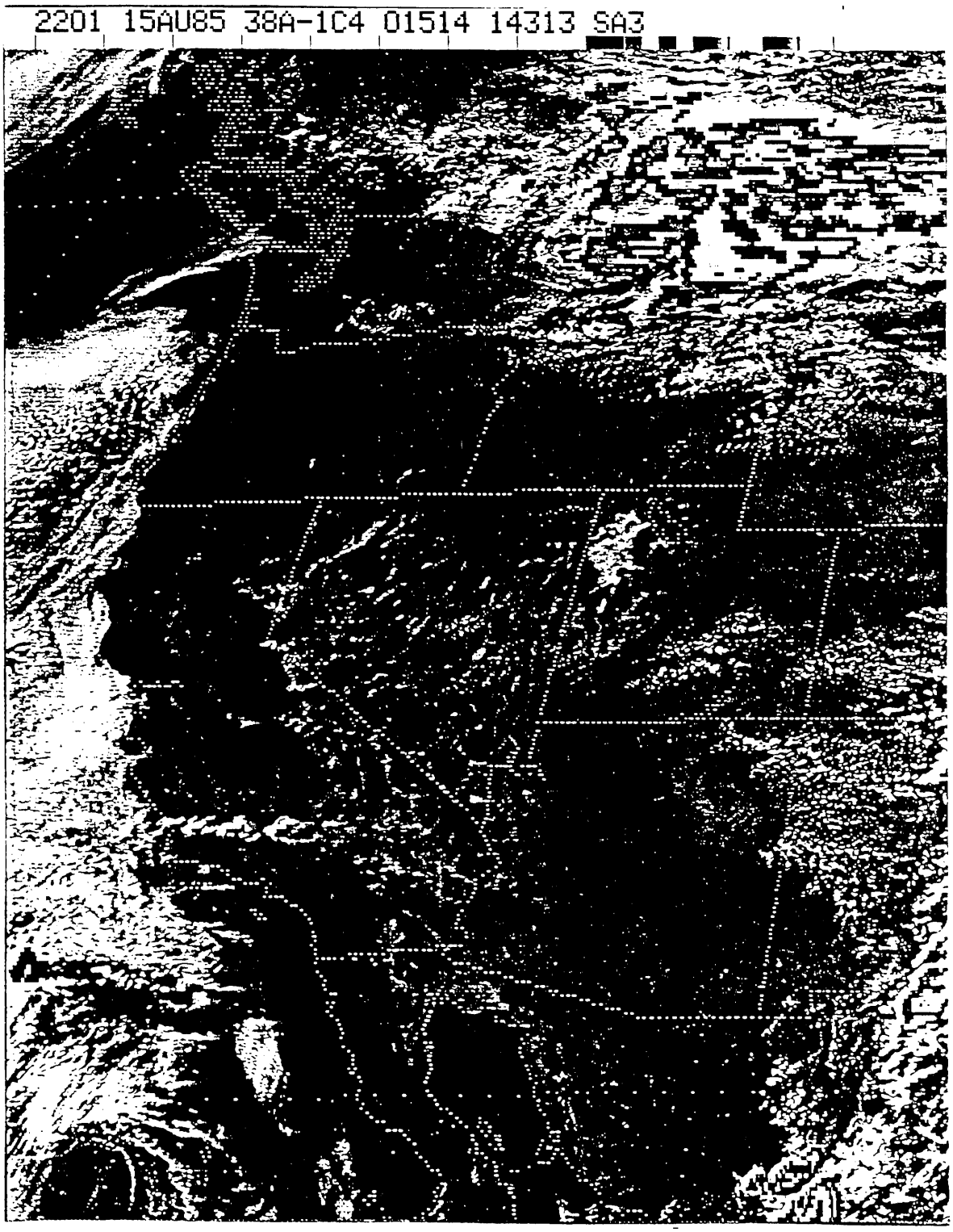


Figure 44: Satellite photograph for August 15th, 1985, at 1501 PDT, of the western United States.


Figure 45: Satellite photograph for August 16th, 1985, at 1431 PDT, of the western United States.


Figure 46: Satellite photograph for August 17th, 1985, at 1431 PDT, of the western United States.

concentrations is most likely due to the increase in wind speeds and instability causing greater dilution of pollutants.

| Day | S | K | C-S | H |
|---|---|---|---|---|
| 8/14 | 703 | 84 | 973 | 499 |
| 8/15 | 799 | 149 | 1207 | 434 |
| 8/16 | 1207 | 95 | 2045 | 735 |
| 8/17 | 665 | 61 | 1358 | 390 |
| 8/18 | 823 | 25 | 1136 | 486 |
| 8/19 | 902 | 52 | 1507 | 613 |
| 8/20 | 750 | 44 | 1310 | 565 |
| 8/21 | 1045 | 109 | 1747 | 787 |
| 8/22 | 725 | 106 | 1535 | 581 |

5. Correlation Analysis

Simple correlation coefficients between two elements indicate a common source. Below are the correlation coefficients for the major elements.

Of the major soil-derived elements, fine silicon correlated with fine iron and potassium. Fine aluminum and calcium were slightly correlated to fine silicon but not as much as in the coarse mode. This indicates these elements

| FINE | Al | Fe | Si | S | K | Mass | H | Ca | C-S |
|---|---|---|---|---|---|---|---|---|---|
| Al | 1.00 | .39 | .53 | .34 | .61 | -.15 | .29 | .39 | .12 |
| Fe | .39 | 1.00 | .79 | .34 | .70 | .01 | .41 | .47 | .36 |
| Si | .53 | .79 | 1.00 | .42 | .73 | -.07 | .48 | .43 | .40 |
| S | .34 | .34 | .42 | 1.00 | .54 | .15 | .80 | .17 | .75 |
| K | .61 | .70 | .73 | .54 | 1.00 | .00 | .60 | .67 | .51 |
| Mass | -.15 | .01 | -.07 | .15 | .00 | 1.00 | .12 | .15 | .02 |
| H | .29 | .41 | .48 | .80 | .60 | .12 | 1.00 | .46 | .62 |
| Ca | .39 | .47 | .43 | .17 | .67 | .15 | .46 | 1.00 | .27 |
| C-S | .12 | .36 | .40 | .75 | .51 | .02 | .62 | .27 | 1.00 |

| COARSE | Mass | Si | K | Ca | Fe | Al |
|---|---|---|---|---|---|---|
| Mass | 1.00 | .47 | .24 | .40 | .53 | .14 |
| Si | .47 | 1.00 | .86 | .93 | .91 | .77 |
| K | .24 | .86 | 1.00 | .82 | .76 | .76 |
| Ca | .40 | .93 | .82 | 1.00 | .93 | .75 |
| Fe | .53 | .91 | .76 | .93 | 1.00 | .61 |
| Al | .14 | .77 | .76 | .75 | .61 | 1.00 |

were less soil-related than in the coarse mode. Fine

sulfur correlated well with fine hydrogen and carbon-soot suggesting sulfur's anthropogenic origins. Fine potassium was slightly correlated with hydrogen and calcium verifying potassium's association with smoke and soil, respectively. Gravimetric mass did not correlate well with any of the fine or coarse elements. The highest mass correlations were with coarse iron and silicon (0.53 and 0.47, respectively) which are major soil components. A poor correlation between mass and fine elements was not unexpected since much of the fine mass is typically unaccounted for (Cahill 1986b). Soil related coarse elements, however, generally contribute the majority of the mass in the coarse fraction. Correlation coefficients for the 50 and 100 meter sample heights were calculated for the coarse elements. All of the correlations coefficients except aluminum improved by excluding the upper levels. The correlation coefficients for coarse silicon, potassium, calcium, iron and aluminum were 0.65, 0.37, 0.64, 0.70 and 0.11, respectively. Potassium's low correlation with mass was expected since it is also associated with smoke. All of the coarse elements correlated well with each other except iron and aluminum (0.61).

6. Vertical Flux Profiles

The mass and elemental fluxes have been calculated by multiplying the elemental and mass concentrations by the corresponding wind speed. All fluxes are in nanograms per square meter per second except for gravimetric mass which

is in micrograms per square meter per second. Flux indicates the amount of pollutant passing through a fixed point at a given time. The samplers were located approximately every 50 meters on the tether line while the meteorological package was moved up and down during the sampling period on a seperate tether line. To obtain a representative wind speed and wind direction for each sampling height, a running average was calculated. Depending on the number of consecutive readings, either three, four or five data points centered around the sampling height were used at ten meter intervals. Tables 9 and 10 show the wind speed and wind direction, number of running points and sample height for the "day" (afternoon) and "night" (morning and evening) profiles, respectively.

The coarse and fine flux for selected elements are shown in Figures 47 to 55. The "day" flux refers to afternoon profiles (top of each figure) and the "night" flux refers to the morning and evening profiles (bottom of each figure). Morning and evening fluxes are plotted with open and filled in circles, respectively. Unusually large values are shown as stars and are off scale. The arrows indicate the wind direction with north being towards the top of the page. The standard pooled variance t-test was used to compare the "day" and "night" fluxes and the results are shown in the table below.

All of the "day" fine and coarse elemental fluxes listed above were significantly larger than the "night" fluxes.

| Date | Sampling Height | Wind Speed | Wind Direction | Running Average | Number of Observations |
|---|---|---|---|---|---|
| Morning | | | | | |
| 8/15 | 50 | 1.2 | 264 | 5 | 11 |
| | 100 | 1.5 | 267 | 5 | 12 |
| | 150 | 2.1 | 253 | 5 | 14 |
| 8/16 | 50 | 2.3 | 272 | 5 | 14 |
| | 100 | 2.1 | 262 | 5 | 16 |
| | 150 | 2.8 | 242 | 5 | 12 |
| | 200 | 2.2 | 228 | 5 | 31 |
| 8/18 | 100 | 1.2 | 256 | 4 | 4 |
| | 150 | 0.8 | 137 | 3 | 3 |
| | 200 | 1.3 | 192 | 3 | 3 |
| | 250 | 1.4 | 206 | 4 | 4 |
| 8/20 | 100 | 2.0 | 277 | 5 | 9 |
| | 150 | 1.9 | 272 | 5 | 8 |
| | 200 | 1.9 | 250 | 5 | 7 |
| | 250 | 1.6 | 240 | 5 | 9 |
| Evening | | | | | |
| 8/18 | 100 | 1.1 | 93 | 5 | 13 |
| | 150 | 1.4 | 66 | 5 | 15 |
| | 200 | 0.9 | 60 | 5 | 16 |
| | 250 | 0.4 | 61 | 5 | 15 |
| 8/21 | 50 | 0.8 | 138 | 4 | 5 |
| | 100 | 1.1 | 69 | 5 | 6 |
| | 150 | 1.3 | 53 | 5 | 5 |
| | 200 | 1.6 | 37 | 5 | 5 |
| 8/21 | 50 | 1.1 | 163 | 5 | 11 |
| | 100 | 0.7 | 157 | 5 | 21 |
| | 150 | 1.2 | 42 | 5 | 14 |
| | 200 | 1.1 | 25 | 5 | 9 |

Table 9: Morning and evening running averages for wind speed and wind direction at specified sampling heights. Sampling height is in meters, wind speed is in meters per second and wind direction is in degrees.

| Date | Sampling Height | Wind Speed | Wind Direction | Running Average | Number of Observations |
|---|---|---|---|---|---|
| Afternoon | | | | | |
| 8/14 | 50 | 3.8 | 280 | 4 | 7 |
| | 100 | 3.6 | 272 | 5 | 15 |
| | 150 | 4.1 | 261 | 5 | 10 |
| 8/15 | 50 | 3.4 | 276 | 5 | 7 |
| | 100 | 4.5 | 257 | 5 | 5 |
| 8/16 | 50 | 3.9 | 279 | 5 | 24 |
| | 100 | 4.7 | 280 | 4 | 4 |
| | 150 | 5.2 | 287 | 5 | 9 |
| | 200 | 4.5 | 275 | 4 | 6 |
| 8/17 | 100 | 4.4 | 280 | 5 | 10 |
| | 150 | 4.4 | 274 | 5 | 9 |
| | 200 | 4.1 | 257 | 4 | 9 |
| | 250 | 3.0 | 256 | 5 | 11 |
| 8/18 | 100 | 3.8 | 278 | 5 | 11 |
| | 150 | 4.1 | 269 | 4 | 8 |
| | 200 | 3.5 | 265 | 5 | 10 |
| | 250 | 3.0 | 258 | 5 | 8 |
| 8/19 | 50 | 3.4 | 280 | 5 | 8 |
| | 100 | 4.3 | 273 | 5 | 10 |
| | 150 | 4.5 | 262 | 4 | 8 |
| | 200 | 4.1 | 245 | 4 | 8 |
| | 250 | 3.4 | 234 | 4 | 6 |
| 8/20 | 100 | 4.3 | 274 | 5 | 13 |
| | 150 | 4.2 | 268 | 5 | 6 |
| | 200 | 4.4 | 265 | 4 | 7 |
| | 250 | 4.0 | 266 | 4 | 5 |
| 8/21 | 100 | 3.2 | 269 | 5 | 6 |
| | 150 | 2.7 | 259 | 5 | 6 |
| | 200 | 3.3 | 261 | 5 | 7 |
| | 250 | 2.3 | 240 | 5 | 7 |
| 8/22 | 100 | 4.6 | 277 | 5 | 8 |
| | 150 | 3.6 | 254 | 5 | 6 |
| | 200 | 3.3 | 272 | 5 | 5 |
| | 250 | 3.3 | 267 | 4 | 5 |

Table 10: Afternoon running averages for wind speed and wind direction at specified sampling heights. Sampling height is in meters, wind speed is in meters per second and wind direction is in degrees.

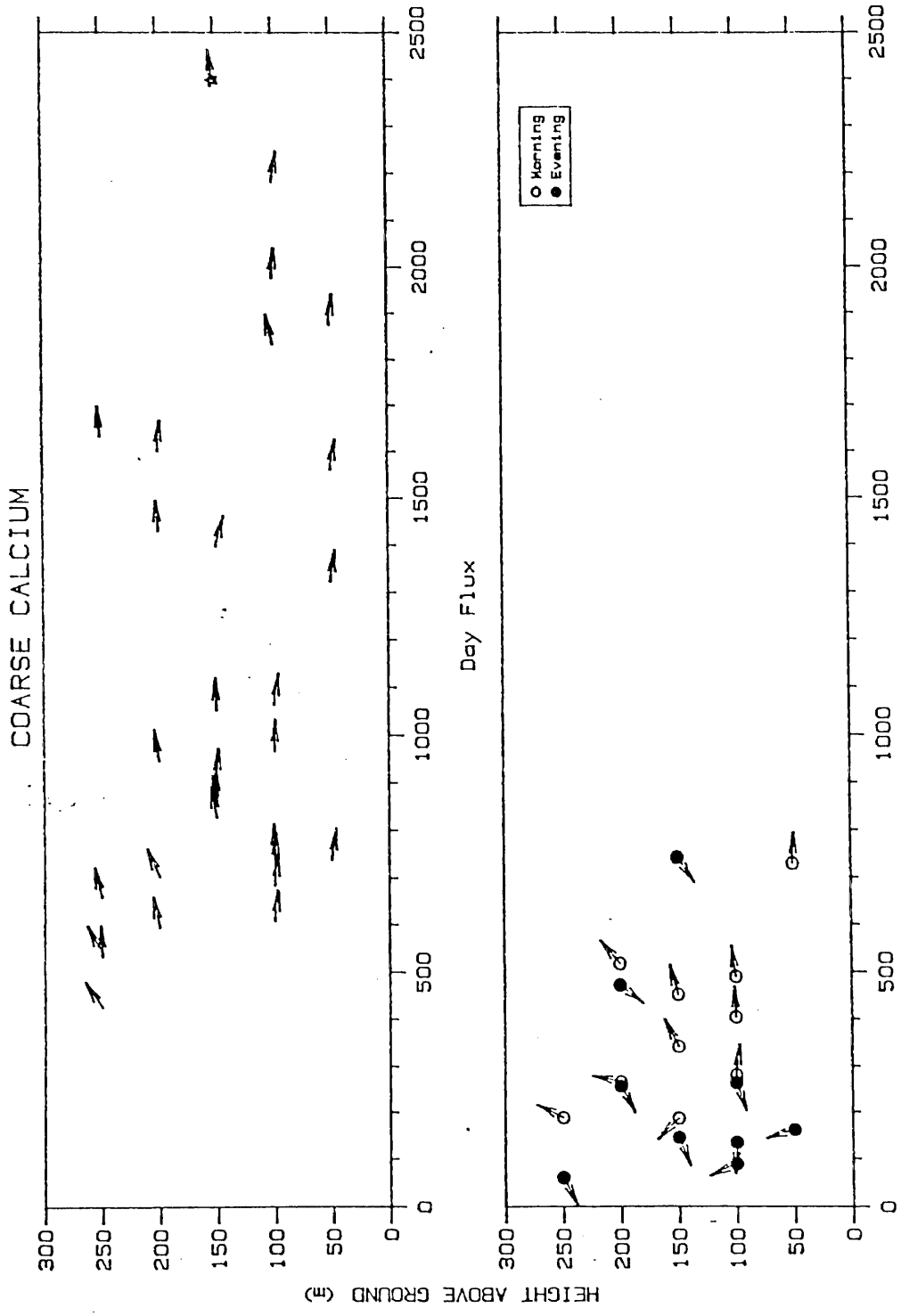


Figure 47: Scatter plot of coarse calcium aerosol flux profiles.

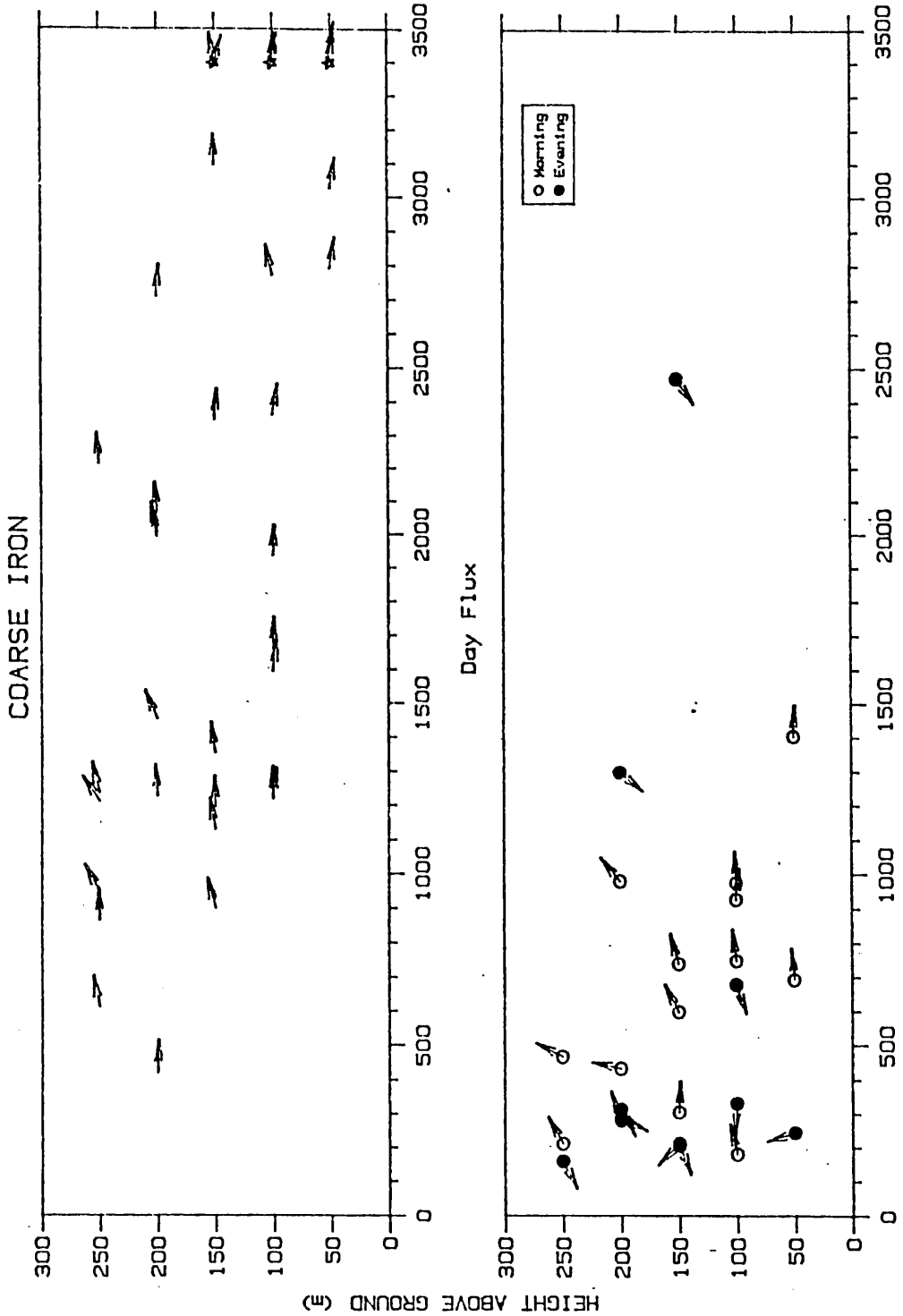


Figure 48: Scatter plot of coarse iron flux profiles.

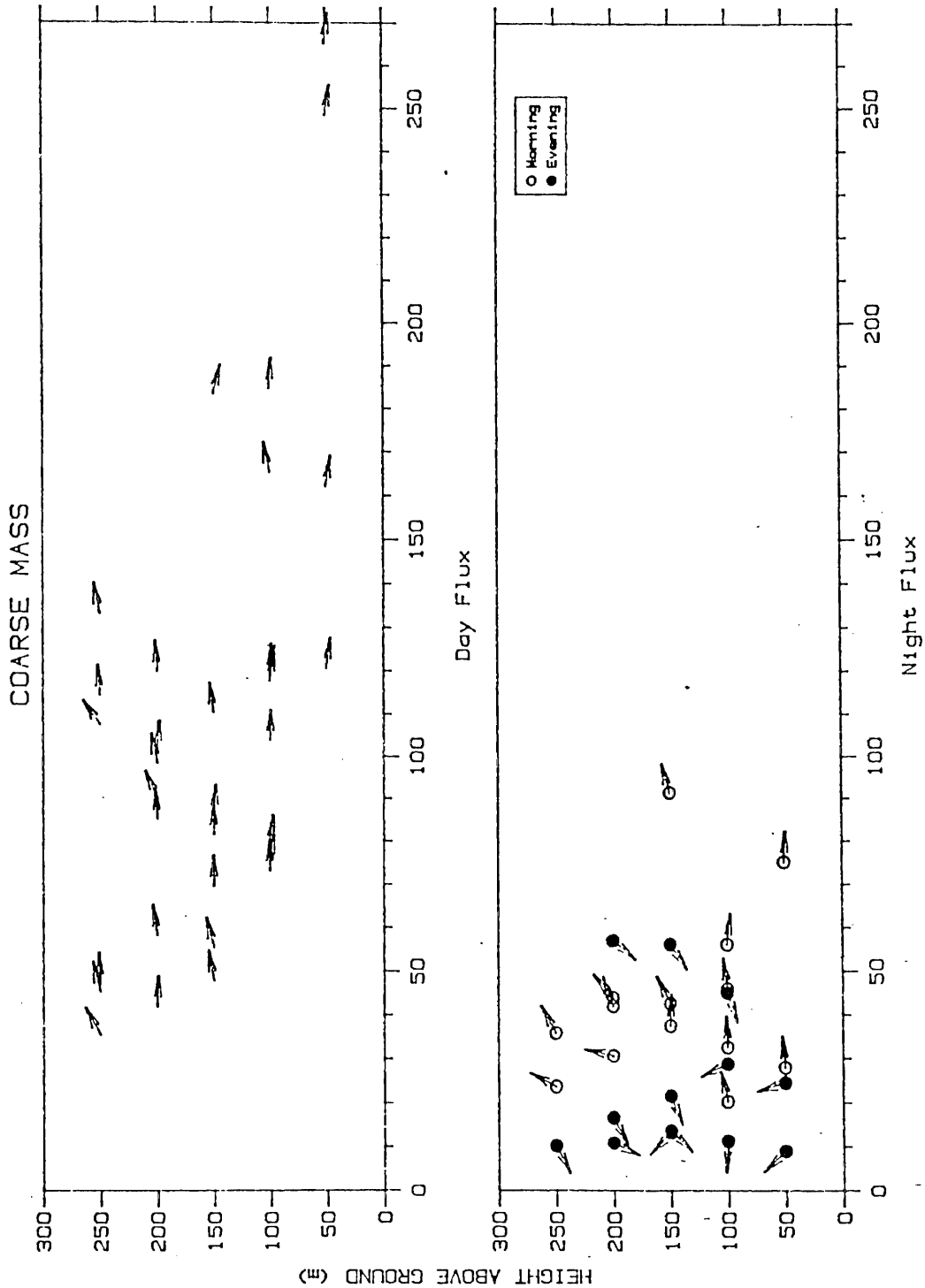


Figure 49: Scatter plot of coarse mass aerosol flux profiles.

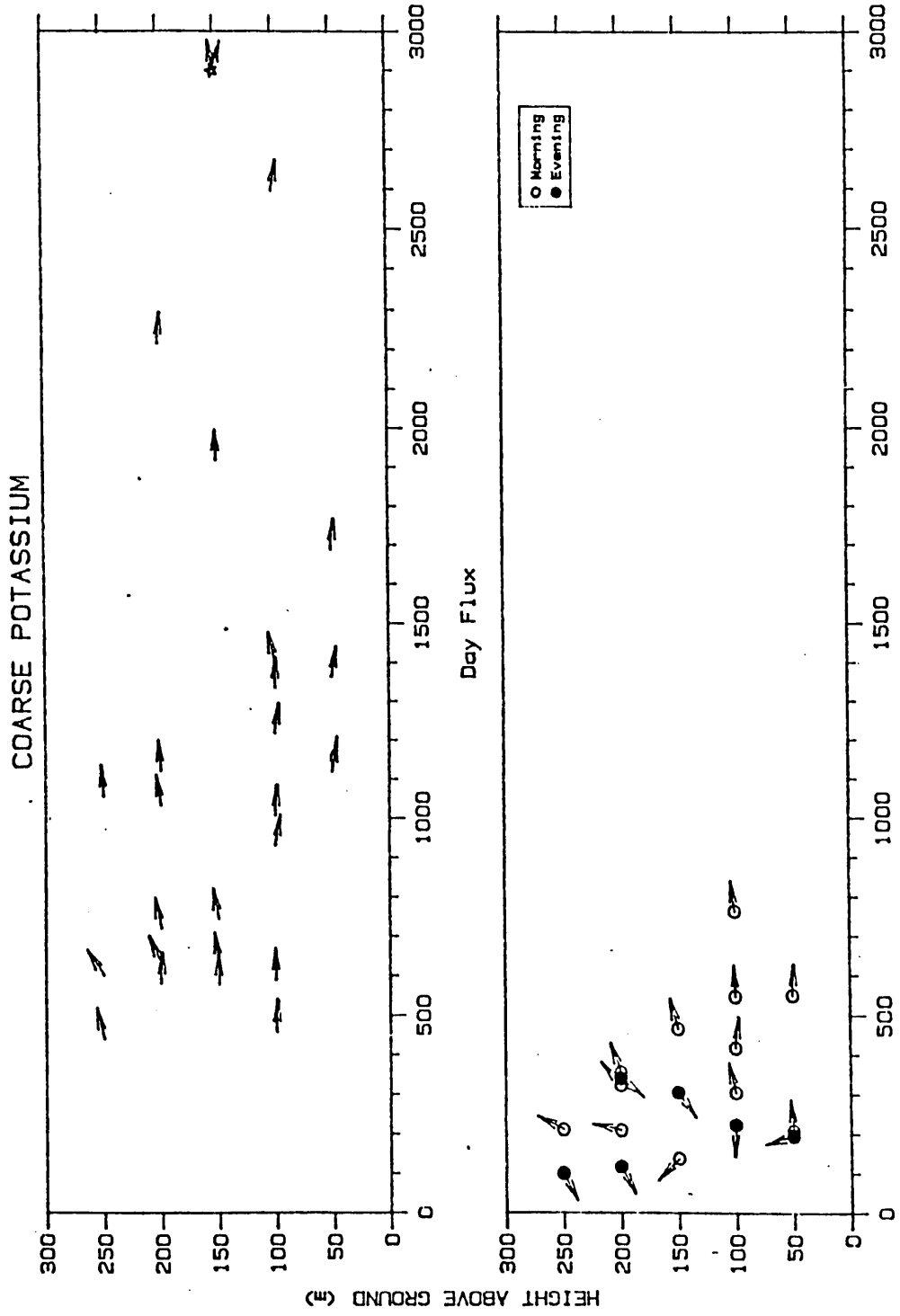


Figure 50: Scatter plot of coarse potassium aerosol flux profiles.

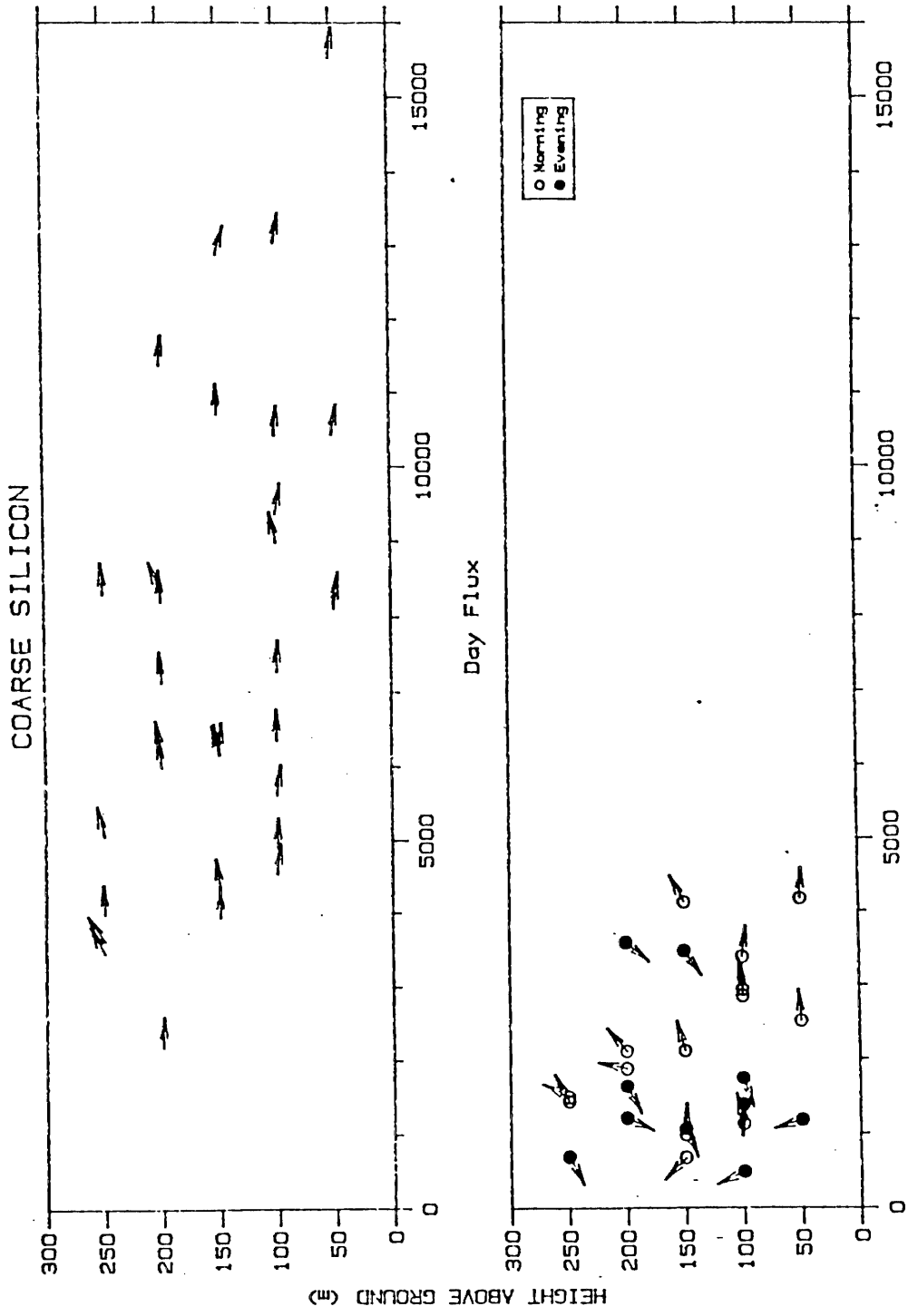


Figure 51: Scatter plot of coarse silicon aerosol flux profiles.

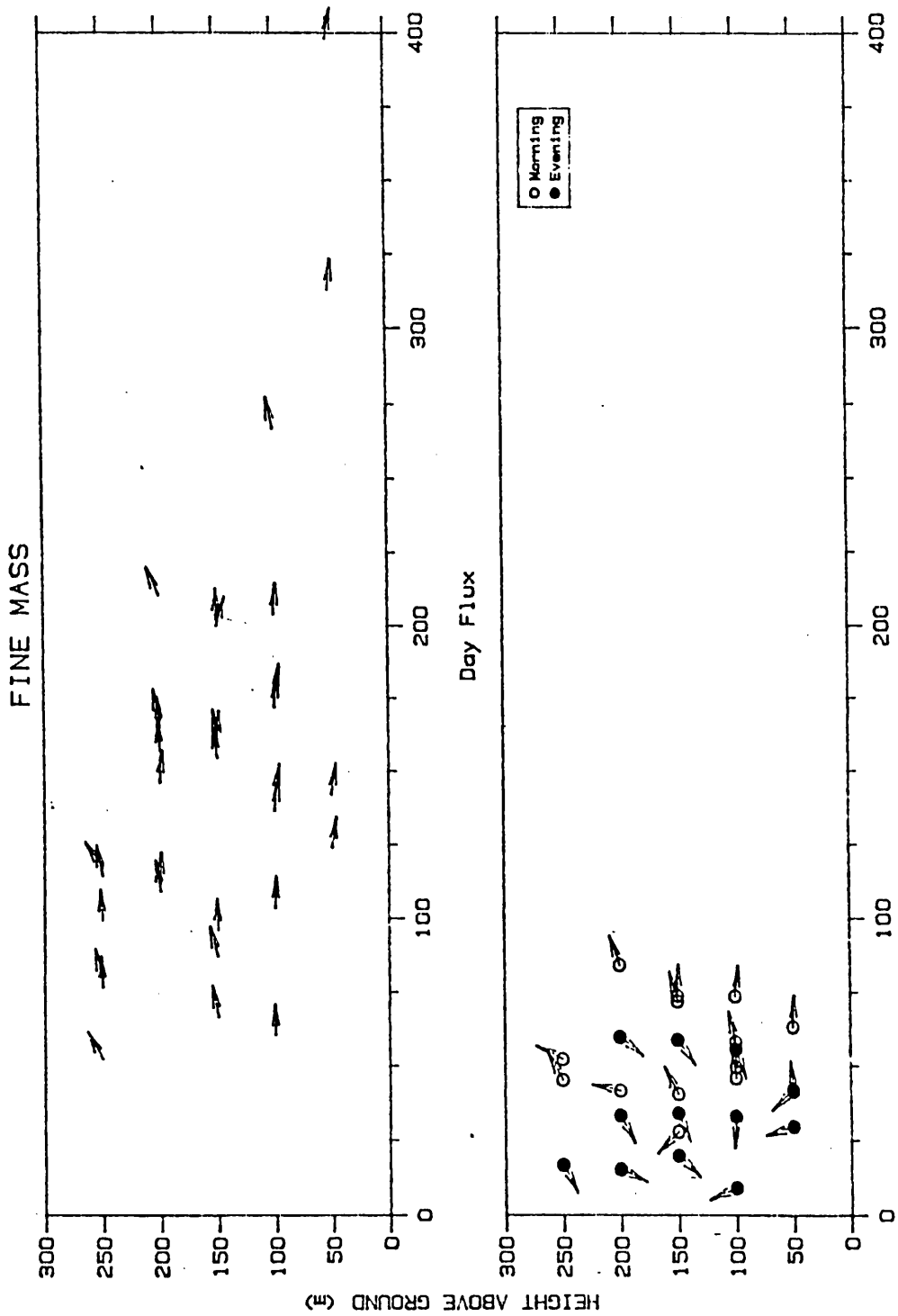


Figure 52: Scatter plot of fine mass aerosol flux profiles.

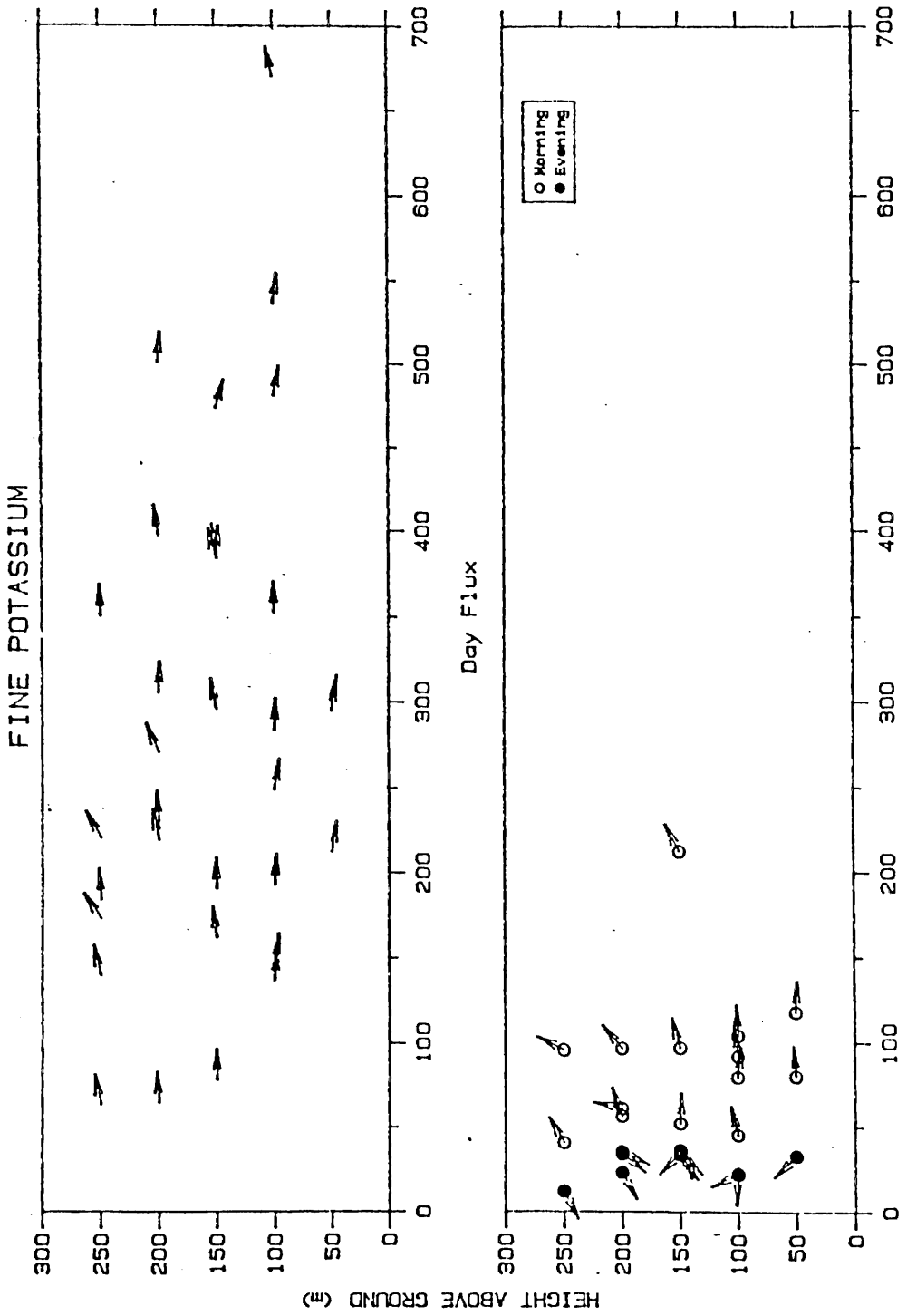


Figure 53: Scatter plot of fine potassium aerosol flux profiles.

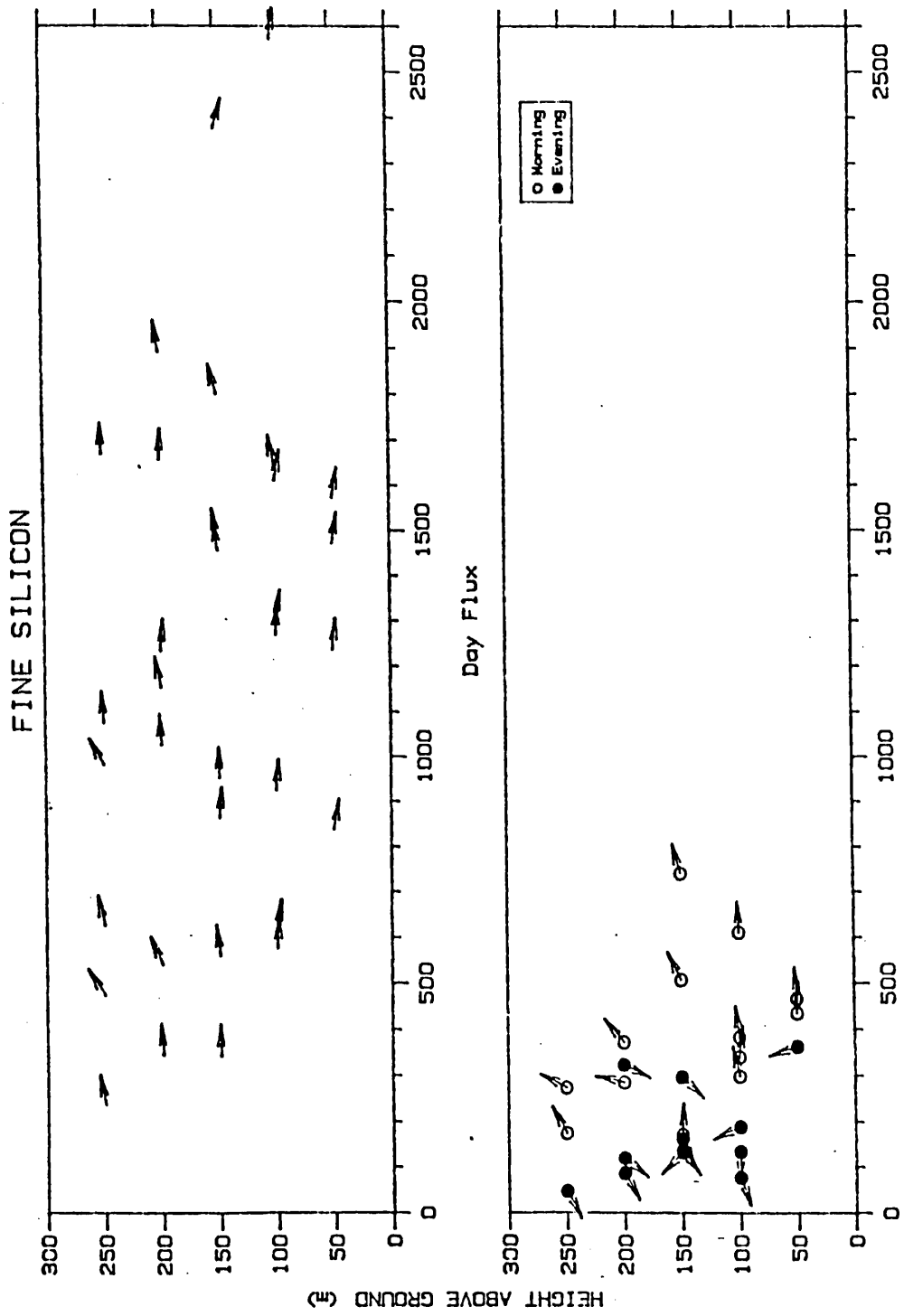


Figure 54: Scatter plot of fine silicon aerosol flux profiles.

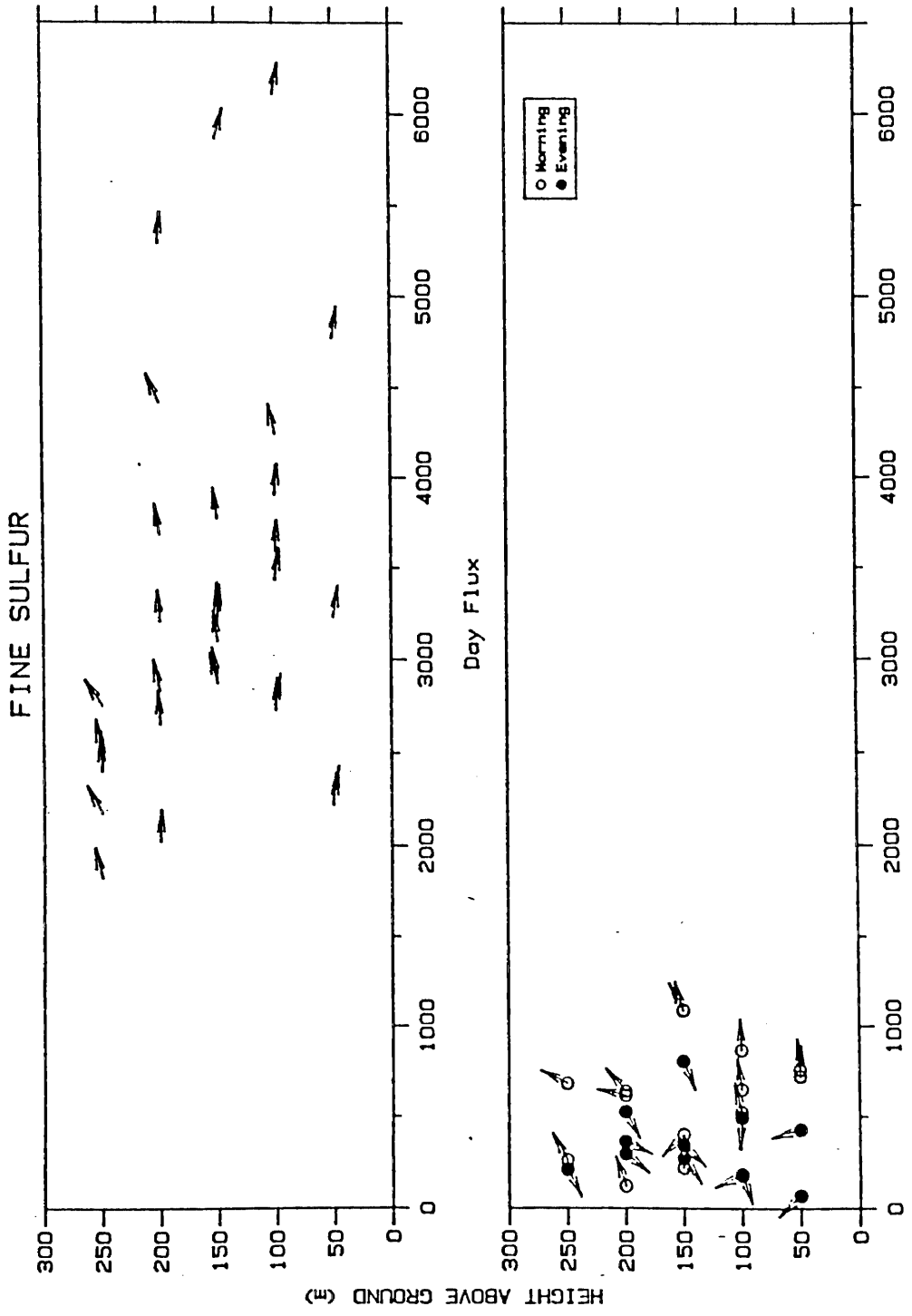


Figure 55: Scatter plot of fine sulfur aerosol flux profiles.

Fine and coarse gravimetric mass "day" fluxes were also significantly larger than the "night" fluxes even though the coarse mass concentration was not and the fine mass

| | afternoon | | | morning & evening | | | | |
|---|---|---|---|---|---|---|---|---|
| FINE | mean | s | n | mean | s | n | df | percentile |
| Mass | 151.4 | 71.4 | 34 | 45.4 | 19.6 | 26 | 58 | >.9995 |
| S | 3306.6 | 1046.3 | 33 | 491.4 | 283.8 | 26 | 57 | >.9995 |
| K | 282.8 | 143.5 | 33 | 62.4 | 44.0 | 25 | 56 | >.9995 |
| Si | 1164.1 | 573.1 | 33 | 286.1 | 173.9 | 25 | 56 | >.9995 |
| COARSE | | | | | | | | |
| Mass | 107.5 | 54.9 | 33 | 34.3 | 20.6 | 27 | 58 | >.9995 |
| Si | 8370.9 | 6362.6 | 33 | 2015.2 | 1115.9 | 24 | 55 | >.9995 |
| K | 1344.3 | 1104.5 | 27 | 321.4 | 174.4 | 18 | 43 | >.9995 |
| Ca | 1236.1 | 986.2 | 30 | 326.4 | 199.6 | 19 | 47 | >.9995 |
| Fe | 2515.3 | 2646.2 | 34 | 632.6 | 531.5 | 24 | 56 | .995 |

df-degrees of freedom, s-standard deviation, n-number of data points.

concentration was only slightly larger. These relationships are clearly seen in Figures 47 to 55, especially for fine sulfur (Figure 55).

# CHAPTER V

## SUMMARY AND CONCLUSIONS

An intensive, ten day field program was conducted along an elevational gradient in Sequoia National Park to characterize the meteorology and transport of aerosols. Pilot balloons were released at Ash Mountain, Wolverton and Emerald Lake (560, 2222, 2719 meters elevation) four times per day and 2 times per night one half the time. Additional releases were made at the University of Fresno by the Geography Department. Continuous ground meteorological data were collected at the three park sites. Boundary layer meteorology and aerosol vertical profiles were also measured at the middle elevation site (Wolverton).

To determine the representativeness of the study period, inland station pressure gradients, morning 850 millibar mean temperature and ozone concentrations for the study period were compared to long term averages. The temperature and pressure gradient data for the study period, as compared to the long term averages, may have been less stable than normal in the San Joaquin Valley. Less stability would reduce pollutant levels yet the Fresno ozone data did not indicate this. During August 17th, moisture from a tropical hurricane caused below average temperatures and above average relative humidities in the study area.

The data from the pilot balloon releases were very useful

for interpreting the synoptic scale weather charts. While the upper level winds varied from 3 to 18 meters per second during the study period, the topographic winds remained uniform in direction and speed throughout the ten days. The prominent feature of the vertical wind profiles was the distinct layering. For the three park sites, the topographic winds made up the layer closest to the ground. These winds moved up-valley and upslope during the day and down-valley and downslope during the night. Fresno showed a more complex day/night topographic wind pattern which included down-valley in the early morning (Fresno eddy), upslope by mid-morning (western slope of the Sierra), up-valley by late morning or early afternoon and strong up-valley by midnight (low level nocturnal jet). Winds above the topographic wind layer corresponded well with the 700 and 500 millibar synoptic height charts. Frequently, there was a layer between the topographic winds and the upper level winds which were possibly transition or compensation winds.

The lower pilot balloon observations were used to estimate the depth of the topographic winds. Fresno and Ash Mountain had much deeper topographic winds than Wolverton and Emerald Lake and showed a tendency to be deeper in the day than at night. Topographic winds at Wolverton and Emerald Lake were much shallower and did not show a distinct day/night pattern.

At Wolverton, the tethersonde data profiled absolute

humidity, virtual potential temperature, wind speed and wind direction as a function of height up to 630 meters above ground level. Estimates of the topographic wind depth from the tethersonde data compared well with the pilot balloon data estimates. The 23 tethersonde profiles were categorized by bulk Richardson numbers (BR) into the four following stability classes: stable, slightly stable, unstable and neutral. The average BR numbers were 222.01, 2.99, -1.02 and 0.01, respectively. Stable conditions included the hours between sunset and sunrise. Wind speeds averaged less than one meter per second with wind direction variable but generally down-valley. Virtual potential temperature and absolute humidity increased with height. Slightly stable conditions included the early morning hours after sunrise where wind speeds were less than three meters per second and wind direction was up-valley. Virtual potential temperature still slightly increased and absolute humidity slightly decreased with height. Unstable conditions included the hours from late morning to sunset. Wind speeds were less than five meters per second and wind direction was up-valley. Virtual potential temperature was super adiabatic below 50 meters and vertical above. Absolute humidity echoed the virtual potential temperature profile. Neutral conditions represented the transition period from afternoon unstable to evening stable conditions. Wind speed and wind direction were the same as the unstable conditions. The virtual potential temperature

profile was generally vertical and the absolute humidity profile decreased slightly with height.

The ground weather station at each park site allowed continuous observation of temperature (two and five meters), wind speed, wind direction and absolute humidity (five meters). The wind directions were more dependent on the immediate surroundings rather than the general topographic features. Wolverton was more unstable during the day and more stable at night compared to Ash Mountain and Emerald Lake. Emerald Lake experienced earlier morning and later evening wind shifts compared to Ash Mountain and Wolverton. The shift from positive to negative bulk Richardson numbers, and visa versa, corresponded to the inversion breakup and formation.

Average coarse and fine elemental, gravimetric mass and carbon-soot concentrations averaged over the entire vertical profile and over all samples were presented. Source categories for fine aerosols were also presented. Average morning, afternoon and evening profiles for fine aerosols did not show a gradient increase nor decrease with height. This was also true for the coarse aerosols except for the evening profiles where concentrations increased from 50 to 150 or 200 meters above ground level. The afternoon aerosol concentration profiles had significantly higher concentrations than morning and evening profiles except for fine calcium, lead, aluminum and coarse aluminum and mass. The most significantly different were fine

sulfur, potassium, carbon-soot and hydrogen. The day/night differences are indicative of long distance transport. The lack of day/night differences in coarse aluminum concentrations was unexpected since aluminum is a major component of soil. On the 17th of August, 1985, aerosol concentrations were the lowest in the ten day study period. This was attributed to an upper level wind shift which also brought moisture into the area from the remnants of a tropical hurricane.

A simple correlation coefficient analysis was done for the fine and coarse elemental, gravimetric mass and carbon-soot concentrations. In general, the fine and coarse soil elements were highly correlated to one another (iron, potassium, silicon, etc) except for fine calcium, fine sulfur correlated well with fine hydrogen and fine carbon-soot, fine potassium was slightly correlated to fine hydrogen and fine and coarse gravimetric mass did not correlate well with anything. Coarse gravimetric mass correlations with the coarse elements were improved by using the 50 and 100 meter sample heights only. Vertical flux profiles were presented for gravimetric mass and some of the major elements. Flux was calculated by multiplying the concentration by the running average of the wind speed for each sampling level. All afternoon fluxes were significantly different from the morning and evening fluxes.

# CHAPTER VI

## SUGGESTIONS FOR FUTURE RESEARCH

The research on meteorology and aerosol transport in the southern Sierra as reported here is preliminary and has raised many questions. Further research is needed to determine the day/night variation in aerosols as related to the synoptic and meso-scale meteorology. More days of data are needed to determine the interaction of synoptic air flow with the San Joaquin Valley meso-scale meteorology (Fresno eddy, marine air penetration, nocturnal jet) and Sierran mountain/valley wind flow and the resulting aerosol transport into the Sierra. For example, on a cool day with deep marine air penetration, would sulfur transport by the Fresno eddy from Bakersfield northward be absent during the night and result in low sulfur concentrations in the Sierra the next day? Would a very stable morning in Fresno mean reduced pollutants into the Sierra during the day?

In addition to aerosol measurements, ozone profiles would be very enlightening. Ozonesondes are available that can be tethered and give a continuous profile of concentrations immediately (see Chapter II, Section A). The advantages of knowing the concentrations at the moment of collection are great. The timing, number and height of the profiles could be designed given current conditions. Ozone is a good indicator of air quality and also a threat to forest vegetation.

Since tethered balloon systems are not commonly used,

the following suggestions should help future research efforts involving their use. The tethersonde and aerosol sampling balloon systems are discussed seperately. For both balloon systems, Federal Aviation Administration (FAA) standards must be followed.

A. Tethersonde Tethered Balloon System

1. The meterological package and Follmer balloon were described in Morris et al. (1975). A study making great use of this system was done by Whiteman (1980) and was tested in the laboratory as well as used in the field. Both of these publications are very useful and should be consulted.

2. During this study it was found that the Follmer balloon (Morris et al. 1975) was much too fragile and did not have enough free lift. This study utlilized a blimp shaped balloon (JK20) purchased from Pie in the Sky (San Mateo, California). The tethersonde package was suspended below the front of the balloon. The problem of the tethersonde being in the wake of the balloon was avoided and the package was more stable due to the reduced length of the suspension lines. The JK20 balloon was let out to 630 meters above ground level. In the afternoon, this was not high enough to reach the top of the boundary layer. It is suggested that the wind direction and temperature data be monitored as the balloon ascends to ensure the entire boudary layer is included (if possible) in the profile if this is

desireable information.

3. If virtual potential temperature, mixing ratio and other meteorological parameters are to be calculated from the tethersonde data, it is advisable to have a barometer at the ground level rather than use the hydrostatic approximation utilizing data from an established National Weather Service weather station. Surface pressure should be taken at the beginning and end of each profile.

4. The tethersonde should be allowed to equilibriate at each level of observation to account for the lag time in the instruments.

5. Relative humidity and wind speed measuring devices for checking the tethersonde instruments at the surface are recommended.

6. It can not be emphasized how important a log book is on a project of this type. All pertinent information should be written down for every profile including: time and date of ascent, barometric surface pressure and dry/wet bulb temperature from ground and tethersonde instruments, cloud and weather observations, local sunset and sunrise, equipment problems, etc.

B. Aerosol Sampling Tethered Balloon System

1. Aerosol Samplers

a. If possible, have a ground sampler operating for every profile.

b. Use a one stage filter cassette for the exhaust to eliminate risk of contamination from carbon vane pump.

c. Design stack for cassette to avoid large particles.

d. Tape or glue intake tube to pump intake and remove and replace just the filter cassette to avoid pump intake damage.

e. Warm up batteries in sun before use for more accurate beginning flow readings.

f. Leak test pumps regularly using small rotometer and non-leaking filter cassette. Epoxy worked well to seal the leaks around the edges of the pump barrel.

g. A pump maintenance kit should include extra carbon vanes, graphite lubricant or spray, emery paper, extra intake and exhaust tubes (metal), epoxy, extra belts, vice and pliers or vice grips.

h. Have extra samplers, filter cassettes and tubing.

2. Tethered Balloon

a. Develop a better system for sampler attachment to tether line. A possibility might be modification of ascent jumars used for rock climbing.

b. During windy conditions, the tether line tends to resonate with the samplers acting as "walls". The resonating places undue stress on the line and shakes the samplers. Pulling on the line stops the resonance but a design to prevent this would greatly improve the system.

c. During windy conditions, the lowest sampler should not be used since it pulls the line too close to the ground level.

d. When operating the samplers at night, lights should be attached to the samplers and balloon.

e. The ascent and descent of the sampling balloon should be made as quickly as possible to reduce the differences in operation time of the samplers at different levels. A remote controlled sampler would be ideal and many have been developed.

f. Keep a log book on the conditions the balloon is flown under, record the angle of the tether line and note any problems.

g. Always wear a hard hat when standing underneath samplers.

# CHAPTER VII

## REFERENCES

American Meteorological Society, 1974. Proceedings of the Symposium on Atmospheric Diffusion and Air Pollution. Sept. 19-13, 1974, Santa Barbara, California. World Meteorology Organization.

American Meteorological Society, 1976. Proceedings of the Third Conference on Atmospheric Turbulence, Diffusion and Air Quality. Oct. 19-22, 1976, Rayleigh, North Carolina. American Meteorological Society, Boston, Massachusetts.

American Meteorological Society, 1978a. Proceedings of the Conference on Sierra Nevada Meteorology. June 19-21, 1978, South Lake Tahoe, California. American Meteorological Society, Boston, Massachusetts, and U.S. Dept. Agriculture-Forest Service.

American Meteorological Society, 1978b. Proceedings of the Fifth National Conference on Fire and Forest Meteorology. March 14-16, 1978, Atlantic City, N.J. American Meteorological Society, Boston, Massachusetts. 99 pp.

American Meteorological Society, 1979. Proceedings of the Fourth Symposium on Atmospheric Turbulence, Diffusion and Air Quality. Jan. 15-18, 1979, Reno, Nevada. American Meteorological Society, Boston, Massachusetts.

American Meteorological Society, 1981a. Proceedings of the Fifth Symposium on Turbulence, Diffusion, and Air Pollution. Atlanta, Georgia, March 9-13, 1981. American Meteorological Society, Boston, Massachusetts.

American Meteorological Society, 1981b. Proceedings of the Second Conference on Mountain Meteorology. Nov. 9-12, 1981, Steamboat Springs, Colorado. American Meteorological Society, Boston, Massachusetts, and U.S. Dept. Agriculture-Forest Service.

American Meteorological Society, 1983a. Proceedings of the Seventh Conference on Fire and Forest Meteorology. April 25-28, 1983, Ft. Collins, Colorado. American Meteorological Society, Boston, Massachusetts. 173 pp.

Amercian Meteorological Society, 1983b. Proceedings of the Sixth Symposium on Turbulence, Diffusion, and Air Pollution. Boston, Massachusetts, March 22-25, 1983. American Meteorological Society, Boston, Massachusetts.

American Meteorological Society, 1984. Proceedings of the Third Conference on Sierra Nevada Meteorology. Oct. 16-21, 1984, Portland, Oregon. American Meteorological Society,

Boston, Massachusetts, and U.S. Dept. Agriculture-Forest Service.

Armstrong, J.A. and P.A. Russell, 1979. The monitoring of particulates using a balloon-borne sampler. In: Proceedings of the Symposium on the Transfer and Utilization of Particulate Control Tech. Volume 4: Fugitive Dusts and Sampling, Analysis and Characterization of Aerosols. EPA-600/7-79-044D, NTIS PB-295229, U.S. Environmental Protection Agency, Febuary, 1979. pp. 357-376.

Armstrong, J.A., P.A. Russell, L.E. Sparks and D.C. Drehmel, 1981. Tethered balloon sampling systems for monitoring air pollution. J. A.P.C.A., 31(7):735-743.

Atkinson, B.W., 1981. Meso-Scale Atmospheric Circulations. Acad. Press, New York. p. 218.

Blackadar, A.K., 1957. Boundary Layer wind maxima and their significance for the growth of nocturnal inversions. Bull. Amer. Meteor. Soc., 38(5):283-290.

Blumenthal, D.L., T.B. Smith, D.E. Lehrman, R.A. Rasmussen, G.Z. Whitten and R.A. Baxter, 1985. Southern San Joaquin Valley Ozone Study, Final Report. Prep. for Western Oil & Gas Assoc. (WOGA), Los Angeles, California, Contract No. 84-8.0.05(2)-07-01 by Sonoma Tech., Inc., and Systems Applications, Inc., STI Report 94100-510-FR. 143 pp.

Buettner, K.J.K. and N. Thyer, 1966. Valley winds in the Mount Ranier area. Archives for Meteorology, Geophysics and Bioclimatology, Ser. B;14(2):125-160.

Buettner, K.J.K., 1967. Valley wind, sea-breeze, and mass fire: Three cases of quasi-stationary airflow. In: Proceedings of the Symposium on Mountain Meteorolgy. E.R. Reiter and J.L. Rasmussen (Eds.), June 26, 1967, Ft. Collins, Colorado, Atmospheric Science Paper No. 122, Dept. Atmospheric Science, Colorado State University, Colorado. pp. 104-129.

Cahill, T.A., L.L. Ashbaugh, J.B. Barone, R.A. Eldred, P.J. Feeney, R.G. Flocchini, C. Goodart, D.J. Shadoan and G.W. Wolfe, 1977. Analysis of respirable fractions in atmospheric particulated via sequential filtration. J. A.P.C.A., 27(7):675-678.

Cahill, T.A., R.A. Eldred, J. Barone and L.L. Ashbaugh, 1979. Ambient Aerosol Sampling With Stacked Filter Units, Final Report. Prep. for Federal Highway Administration, Office of Research and Development, Washington D.C., Rep. No. FHWA-RD-78-178, by the Air Quality Group, Crocker Nuclear Laboratory, University of California, Davis, Febuary, 1979.

Cahill, T.A., R.A. Eldred, D. Shadoan, P.J. Feeney, B.H. Kusko and Y. Matsuda, 1984. Complete elemental analysis of aerosols: PIXE, FAST, LIPM, and MASS. Nuclear Instruments and Methods in Physics Research B3. Elsevier Science Publishers B.V. pp. 291-295.

Cahill, T. A., 1986a. Particulate Monitoring for Acid Deposition Research in the Sierra Nevada, California, Final Report, June 1985-May 1986. Prep. for the California Air Resources Board, Grant No. A4-124-32, by the Air Quality Group, Crocker Nuclear Laboratory, University of California, Davis, California. 134 pp.

Cahill, T.A., R.A. Eldred and P.J. Feeney, 1986b. Particulate Monitoring and Data Analysis for the National Park Service, 1982-1985. Prep. for the National Park Service, Contract No. USDICX-0001-3-0056, by the Air Quality Group, Crocker Nuclear Laboratory, University of California, Davis, California, 130 pp.

California Air Resources Board, 1978-1985. California Air Quality Data, Gaseous and Particulate Pollutants. Annual summaries for 1978 to 1985. Aerometric Data Division of the California Air Resources Board, Sacramento, California. Vol. 7-16.

Carroll, J.J. and R.L. Baskett, 1979. Dependence of air quality in a remote location on local and mesoscale transports. J. Appl. Meteor., 18:474-486.

Cleeves, G.A., T.J. Lemmons and C.A. Clemons, 1966. A low-level air sampling and meteorological sounding system. J. A.P.C.A., 16(4):207-211.

Countryman, C.M. and M.J. Schroeder, 1959a. Prescribed Burn Fireclimate Survey 2-57. Tech. Paper No. 31, Pacific Southwest Forest and Range Experiment Station, U.S. Dept. Agriculture-Forest Service. 18 pp.

Countryman, C.M. and M.J. Schroeder, 1959b. Prescribed Burn Fireclimate Survey 3-57. Tech. Paper No. 34, Pacific Southwest Forest and Range Experiment Station, U.S. Dept. Agriculture-Forest Service. 15 pp.

Cramer, O.P. and R.E. Lynott, 1961. Cross-section analysis in the study of windflow over mountainous terrain. Bull. Amer. Meteor. Soc., 42:693-702.

Davidson, B., 1961. Valley wind phenomena and air pollution problems. J. A.P.C.A., 11:364-368.

Davidson, B., 1963. Some turbulence and wind variability observations in the lee of mountain ridges. J. Appl.

Meteor., 2:463-472.

Davidson, B. and P.K. Rao, 1963. Experimental studies of the valley-plain wind. Int. J. Wat. Poll., 7:907-923.

Defant, F., 1951. Compendium of Meteorology. T.M. Malone (Ed), American Meteorological Society, Boston. pp. 655-675.

DeMarrais, G.A., G.L. Downing and H.E. Meyer, 1968. Transport and Diffusion of an Aerosolized Insecticide in Mountainous Terrain. ESSA Research Laboratories Tech. Memo. ARL6, Silver Spring, Maryland. 46 pp.

Dickerson, M.H. and P.H. Gudiksen, (Eds), 1983. ASCOT Technical Progress Report FY-1979 Through FY-1983. Lawrence Livermore National Laboratory (ASCOT 84-1), University of California (UCID-19851), Livermore, California. 367 pp.

Dunsmore, H. and P. Fransioli, 1978. Observations of multiple layer inversions with gravity waves in a Sierra basin. In: Proceedings of the Conference on Sierra Nevada Meteorology. June 19-21, 1978, South Lake Tahoe, California. American Meteorological Society, Boston, Massachusetts, and U.S. Dept. Agriculture-Forest Service. pp. 91-96.

Edinger, J.G. and R.A. Helvey, 1961. The San Fernando convergence zone. Bull. Amer. Meteor. Soc., 42:626-635.

Edinger, J.G., 1963. Modification of the marine layer over coastal Southern California. J. Appl. Meteor., 2:706-712.

Estoque, M.A., 1961. A theoretical investigation of the sea breeze. Quart. J. R. Meteor. Soc., 87:136-146.

Estoque, M.A., 1962. The sea breeze as a function of the prevailing situation. J. Atmos. Sci., 19:244-250.

Feeney, P., T.A. Cahill, J. Olivera and R. Guidara, 1984. Gravimetric determination of mass on lightly loaded membrane filters. J. A.P.C.A., 34(4):376-378.

Fischer, E.L., 1960. An observational study of the sea breeze. J. Meteor., 17:645-660.

Fischer, E.L., 1961. A theoretical study of the sea breeze. J. Meteor., 17:645-660.

Flocchini, R.G., 1984. A particle sampler for tethered balloon systems (extended abstract). In: Proceedings of the First International Aerosol Conference on Aerosols Science, Technology and Industrial Applications of Airborne Particles. Liu, Pai and Fissan (Eds). Sept. 17-21, 1984, at

Minneapolis, Minnesota, Elsevier Science Publishers B.V. pp. 321-324.

Flocchini, R. and L. Myrup, 1986. Assessment of Aerosol Transport into the Mojave Desert. Prep. for the California Air Resources Board by the University of California, Dept. Land, Air and Water Resources, Davis, California. 89 pp.

Forrest, J., S.E. Schwartz and L. Newman, 1979. Conversion of sulfur dioxide to sulfate during the Da Vinci flights. Atmos. Environ., 13:157-167.

Fosberg, M.A. and M.J. Schroeder, 1963. A Warm Sea Breeze? U.S. Pacific Southwest Forest and Range Experimental Station, U.S. Forest Service Research Note PSW-N18. 8 pp.

Fosberg, M.A. and M.J. Schroeder, 1966. Marine air penetration in Central California. J. Appl. Meteor., 5:573-589.

Frenzel, C.W., 1962. Diurnal wind variations in Central California. J. Appl. Meteor., 1:405-412.

Galbally, I., 1968. Some measurements of ozone variation and destruction in the atmospheric surface layer. Nature, 218:456-457.

Garland, J.A. and J.R. Branson, 1976. The mixing height and mass balance of $SO_2$ in the atmosphere above Great Britain. Atmos. Enviro., 10:353-362.

Giroux, H.D., W.R. Knuth and J.A. Anderson, 1981. Nocturnal central valley pollution dynamics. In: Proceedings of the Conference on Sierra Nevada Meteorology. June 19-21, 1981, South Lake Tahoe, California. American Meteorological Society, Boston, Massachusetts. pp. 165-170.

Gleeson, T.A., 1951. On the theory of cross-valley winds arising from differential heating of the slopes. J. Meteor., 8:398-405.

Graham, H.E., 1955. Fire whirls. Bull. Amer. Meteor. Soc., 36(3):99-103.

Green, H. L. and W. R. Lane, 1964. Particulate Clouds: Dust, Smokes and Mists, 3rd Edition. E.&F.N. Spon Ltd., London.

Haugen, D.A., J.C. Kaimal, C.J. Readings and R. Rayment, 1975. A comparison of balloon-borne and tower-mounted instrumentation for probing the atmospheric boundary layer J. Appl. Meteor., 14:540-545.

Hawkes, H.B., 1947. Mountain and Valley Winds. Doctoral

Dissertation, Dept. of Geography, Ohio State University, Columbus, Ohio.

Henderson, Don, 1987. Personal Communication. Research Branch of the Air Quality Division for the National Park Service, Lakewood, Colorado.

Horrocks, J., 1987. Unpublished preliminary data from summer, 1986. California Air Resources Board, Haagen-Smit Laboratory, El Monte, California.

Hindman, E.E., 1973. Air currents in a mountain valley deduced from the breakup of stratus deck. Monthly Weather Review, 101(3):195-200.

Huschke, R.E. (Ed.), 1959. Glossary of Meteorology. American Meteorological Society, Boston, Massachusetts. p. 355.

John, W., S. Herring, G. Reischl and J. Wesolowski, 1980. Investigation of the Filtration Characteristics of the Stacked Filter Unit, Final Report. Prep. for the California Air Resources Board, Contract No. A7-139-30, by California Dept. of Health Services CA/DOH/AIHL/SP-21, Air and Industrial Hygiene Laboratory Section, Laboratory Services Branch, Berkeley, California, Feb. 1980. 48pp.

Kobayashi, J. and Y. Toyama, 1966a. On various methods of measuring the vertical distribution of atmospheric ozone (II). Papers in Meteorology and Geophysics (Tokyo, Japan), 17(2):97-112.

Kobayashi, J. and Y. Toyama, 1966b. On various methods of measuring the vertical distribution of atmospheric ozone (III). Papers in Meteorology and Geophysics (Tokyo, Japan), 17(2):113-125.

Kobayashi, J., M. Kyozuka and H. Muramatsu, 1966. On various methods of measuring the vertical distribution of atmospheric ozone (I). Papers in Meteorology and Geophysics (Tokyo, Japan), 17(2):76-95.

Lamb, B.K. and F.H. Shair, 1977. Atmospheric Tracer Studies to Characterize the Transport and Dispersion of Pollutants in the California Delta Region: Volume 1, Presentation and Discussion of Results. Prep. for California Air Resources Board, Contract No. ARB-A5-065-87, by California Institute of Technology, Div. of Chemistry and Chemical Engineering, Pasadena, California. 266 pp.

Lehrman, D., T.B. Smith and S. Gouze, 1980. Upper San Joaquin River Valley Impact Study. Prep. for U.S. Forest Service, San Francisco, California, Contract No. 53-9158-9-6251 by Meteorology Research, Inc., Altadena, California,

MRI Tech. Rep. 80 FR-1745. 121pp.

Linse, E.W., 1986. Climate '85 meridional patterns over California. Preprints of Conference on the Human Consequences of 1985's Climate. Sponsored by the Amercian Meteorological Society. Aug. 4-7, 1985, Ashville, North Carolina. pp. 174-177.

Lorenzen, A., 1979 (Ed). Summary of California Upper Air Meteorological Data. California Air Resources Board, Tech. Serv. Div., Sacramento, California. 125 pp.

Lowry, W.P., 1963. Observations of atmospheric structure during summer in a coastal mountain basin in Northwest Oregon. J. Appl. Meteor., 2:713-721.

MacHattie, L.B., 1968. Kanasis valley winds in summer. J. Appl. Meteor., 7:348-352.

Mandrioli, P. and F. Tampieri, 1978. Vertical profiles of biological particle concentrations under convective conditions. Boundary-Layer Meteor., 14:331-340.

McHattie, L.B., 1968. Kananaskis Valley winds in summer. J. Appl. Meteor., 7:348-352.

McMahon, T.A., 1986. Personal Communication. U.S. Dept. of Agriculture, Southeastern Forest Experiment Station, Dry Branch, Georgia.

Miller, P.R., 1969. Air pollution and the forests of California. Calif. Air Environ. 1(4):1-3.

Miller, P.R., M.H. McCutchan and H.P. Milligan, 1972. Oxidant air pollution in the Central Valley, Sierra Nevada foothills, and Mineral King Valley of California. Atmos. Environ., 6:623-633.

Morgan, D., 1974. Jet Winds in the San Joaquin Valley. Prep. for the Pacific Southwest Forest and Range Experiment Station, Berkeley, California, U.S. Dept. Agric., Forest Service, PSW Grant No. 13. by the Dept. of Geography, California State University, Fresno, California, Oct. 31, 1974. 39 pp.

Morgan, D.L. and W.F. Slusser, 1978. A pilot study of upslope winds in the Sierra Nevada. In: Proceedings of the Conference on Sierra Nevada Meteorology. June 19-21, 1978, South Lake Tahoe, California. Sponsored by the American Meteorological Society, Boston, Massachusetts, and U.S. Dept. Agriculture-Forest Service. pp. 55-60.

Morgan, D.L. and W.F. Slusser, 1979. Wind Measurements in the River Canyons of the Southcentral Sierra Nevada: Final

Report, Volume 1. Prep. for the California Energy Commission, Sacramento, California, Contract NO. 500-128 (7/8), by the Dept. of Geography, California State University, Fresno, California. 54 pp.

Morgan, D.L., 1987. Personal Communication. Geography Department, University of Fresno, California.

Morris, A.L., D.B. Call and R.B. McBeth, 1975. A small tethered balloon sounding system. Bull. Amer. Meteor. Soc., 56(9):964-969.

Myrup, L.O., D.L. Morgan and R.L. Boomer, 1983. Summertime three-dimensional wind field above Sacramento, California. J. C. Appl. Meteor., 22:256-265.

Myrup, L.O., D.L. Morgan and R. Boomer, 1986. An analysis of mesoscale transport phenomena during the evening transition period near Sacramento, California. J. C. Appl. Meteor., 25(4):405-417.

Orgill, M.M., 1981. Atmospheric Studies in Complex Terrain: A Planning Guide for Future Studies. U.S. Dept. of Energy, Contract No. DE-AC06-76RLO 1830, by the Pacific Northwest Laboratory, Richland, Washington.

Palmer, C.E., 1957. Some Kinematic aspects of frontal zones. J. Meteor., 14:403-409.

Palmer, T.Y. and J.A. Watrous, 1978. Gravity wave and turbulent dispersion in a Sierra Nevada valley. In: In: Proceedings of the Conference on Sierra Nevada Meteorology. June 19-21, 1978, South Lake Tahoe, California. American Meteorological Society, Boston, Massachusetts, and U.S. Dept. Agriculture-Forest Service. pp. 101-103.

Pearce, R.P., 1955. The calculation of a sea-breeze circulation in terms of differential heating across the coastline. Quart. J. R. Meteor. Soc., 81:351-381.

Pearce, R.P., 1962. A simplified theory of the generation of sea breezes. Quart. J. R. Meteor. Soc., 88:20-29.

Perroud, P., G. Pleyber and M. Sylvestre-Baron, 1973. The use of captive balloons for air pollution study in the lower layers of the atmosphere. In: Proceedings of the AERALL 1973 Colloquium. Nov. 12-14, 1973, Paris, France, NTIS:CEA-CONF-2491.

Petkovsek, Z., 1973. Vergleichungen der lokalen temperaturanderungen im Gebirgsgebiete, Flachland und freie atmosphare. Meteorologie, 10-11:135-150.

Ranzieri, Andrew, 1987. Personal Communication. California Air Resources Board, Technical Support Division, Sacramento, California.

Regener, V.H., 1960. On a sensative method for the recording of atmospheric ozone. J. Geophys. Res., 65(12):3975-3977.

Regener, V.H., 1963. Ozone Measuring Devices, Final Report. Air Force Cambridge Research Laboratories, Bedford, Massachusetts. Contract No. AF19(604)-7211. December 10, 1963.

Regener, V.H., 1964. Measurement of atmospheric ozone with the chemiluminescent method. J. Geophys. Res., 69(18):3795-3800.

Reiter, E.R. and J.L. Rasmussen (Eds), 1967. Proceedings of the Symposium on Mountain Meteorolgy. June 26, 1967, Ft. Collins, Colorado. American Meteorological Society, Boston, Massachusetts.

Ryan, B.C. and J.G. Brown, 1978. Influences on winds in moutainous terrain. In: Proceedings of the Conference on Sierra Nevada Meteorology. June 19-21, 1978, South Lake Tahoe, California. American Meteorological Society, Boston, Massachusetts, and U.S. Dept. Agriculture-Forest Service. pp. 46-52.

Ryan, P.W., C.D. Tangren and C.K. McMahon, 1979. A balloon system for profiling smoke plumes from forest fires. In: Proceedings of the 72nd Annual Mtg. of the A.P.C.A. Cincinnati, Ohio, June 24-29, 1979. pp. 2-24.

Schroeder, M.J., 1961. Down-canyon afternoon winds. Bull. Amer. Meteor. Soc., 42(8):527-542.

Schroeder, M.J., M.A. Fosberg, Cramer, O.P. and C.A. O'Dell, 1967. Marine air invasion of the Pacific Coast: A problem analysis. Bull. Amer. Meteor. Soc., 48(11):802-808.

Scorer, R.S., 1958. Natural Aerodynamics. Pergamon Press. 313 pp.

Sekihara, K., Y. Suzuki, I. Akita, T. Suzuki and W. Yagihashi, 1977. Ozone concentrations in the lower atmosphere. J. of Meteor. Res. Japan, 29(5-6):105-111.

Sentell, R.J., R.W. Storey, J.J.C. Chang and S.J. Jacobson, 1976. Tethered Balloon-Based Measurements of Meteorological Variables and Aerosols. NASA-TM-X-73999, NTIS N77-15586, December, 1976. 317 pp.

Shair, F.H., 1986. Atmospheric Tracer Experiments Aimed at

Characterizing the Transport and Dispersion of Airborne pollutants in Sequoia and Kings Canyon National Parks. California Institute of Technology, Div. of Chemistry and Chemical Engineering, Pasadena, California. Unpublished presentation at National Park Service and California Air Resources Board meeting on Acid Deposition held at Sequoia National Park, January, 1986.

Smith, T.B., D.E. Lehrman, D.D. Reible and F.H. Shair, 1981. The Origin and Fate of Airborne Pollutants Within the San Joaquin Valley, Volumes 1-7. Prep. for the California Air Resources Board by Meteorology Research, Inc., Altadena, California and California Institute of Technology, Pasadena, California, MRI FR-1838.

Spurny, K.R., J.P. Lodge, Jr., E.R. Frank and D.C. Sheesley, 1969. Aerosol filtration by means of nucleopore filters structural and filtration properties. Enviro. Sci. Tech., 3(5):453-464.

Sommers, W.T., 1978. Strong mountain downslope wind field experiment using surface station, monostatic acoustic sounder, and rawinsonde observations. In: Proceedings of the Fourth Symposium on Meteorological Observations and Instrumentation. April 10-14, 1978, Denver, Colorado. American Meteorological Society, Boston, Massachusetts. pp. 339-344.

Staley, D.O., 1957. The low-level sea breeze of Northwest Washington. J. Meteor., 14:458-470.

Sterten, A.K. and J. Knudsen, 1961. Local and Synoptic Meteorology Investigations of the Mountain and Valley Wind System. Intern Rapport K-242, Forsvarets Forsknings-institutt, Norwegian Defence Research Establishment, Kjeller-Lillestrom, Norway. 139 pp.

Swanson, R.N., M.L. Mooney and L. Langan, 1981. Pibal ascent rate uncertainties in the planetary boundary layer. In: Proceedings of the Fifth Symposium on Turbulence, Diffusion, and Air Pollution. March 9-13, 1981, Atlanta, Georgia. American Meteorological Society, Boston, Massachusetts. pp. 63-64.

Taylor, S.R., 1964. Abundance of chemical elements in the continental crust: A new table. Geochimical et Cosmochimical Acta, 28:1273-1285.

Thompson, N., 1972. Turbulence measurements over the sea by a tethered-balloon technique. Quart. J. R. Meteor. Soc., 98:745-762.

Thompson, Philip D. and Robert O'Brien (Eds), 1965. Weather. Time Inc., New York. p. 61.

Thyer, N.H., 1962. Double theodolite pibal evaluation by computer. J. Appl. Met. 1:66-68.

Thyer, N.H., 1966. A theoretical explanation of mountain and valley winds by numerical method. Archives for Meteorology, Geophysics and Bioclimatology. Ser. A;15(3/4): 318-348.

Tyson, P.D., 1968. Velocity fluctuations in the mountain wind. J. Atmos. Sci., 25(3):381-384.

Unger, C.D., 1978. The transport of photochemical smog in the Central Valley and Sierra Nevada Mountains of California. In: Proceedings of the Conference on Sierra Nevada Meteorology. June 19-21, 1978, South Lake Tahoe, California. American Meteorological Society, Boston, Massachusetts. pp. 38-45.

Wagner, 1938. Theorie und beobachtung der periodischen gebirgswinde. Gerlands Beitr. Geophys., (Liepzig), 52:408-449.

Wanta, R.C. and W.P. Lowry, 1976. Airflow through rough terrain and built-up areas. In: Air Pollution, 3rd Edition: Volume 1. A.C. Stern (Ed), Acad. Press, San Francisco, California. pp. 386-390.

Warren, J.C., J.H. Smalley and A.L. Morris, 1971. Aerostatic Lift of Helium and Hydrogen in the Atmosphere. NCAR Tech. Note, NCAR-TN/IA-69, National Center for Atmospheric Research, Boulder, Colorado, December, 1971. 79 pp.

Whiteman, C.D., 1980. Breakup of Temperature Inversions in Colorado Mountain Valleys. Doctoral Dissertation, Atmos. Sci. Pap. No. 328, Colorado State University, 250 pp.

Whiteman, D.C., 1981. Temperature inversion buildup in valleys of the Rocky Mountains. In: Proceedings of the Second Conference on Mountain Meteorology. Nov. 9-12, 1981, Steamboat Springs, Colorado. American Meteorological Society, Boston, Massachusetts, and U.S. Dept. Agriculture-Forest Service. pp. 276-282.

Whiteman, D.C., 1982. Breakup of temperature inversions in deep mountain valleys: Part I; Observations. J. Appl. Meteor., 21:270-289.

Willis, R.A. and P. Williams, Jr., 1972. A Study of the Low Level Jet Stream of the San Joaquin Valley (Project Lo-Jet). NOAA Tech. Memorandum NWS WR-75, Western Region Headquarters, Salt Lake City, Utah. 43 pp.

Yokoyama, O., 1969. Measurement of wind fluctuations by a

vane mounted on a captive balloon cable. J. Meteor. Soc. Japan, 47:159-165.

Zak, B.D., 1981. Lagrangian measurements of sulfur dioxide to sulfate conversion rates. Atmos. Environ., 15(12):2583-2591.

# Glossary of Abbreviations and Symbols

## Aerosol Abbreviations:

| | |
|---|---|
| Al | aluminum |
| Br | bromine |
| Ca | calcium |
| Cl | chlorine |
| C-S | carbon-soot |
| Fe | iron |
| H | hydrogen |
| K | potassium |
| Mass | gravimetric mass |
| Na | sodium |
| S | sulfur |
| Si | silicon |
| Pb | lead |

## Abbreviations of Units and Terms, Symbols:

| | |
|---|---|
| agl | above ground level |
| cm | centimeter |
| g | gram |
| km | kilometer |
| m | meter |
| mb | millibar |
| mg | microgram |
| msl | meters above sea level |
| ng | nanogram |
| q | absolute humidity |
| s | second |
| μm | micron or micrometer |

| | |
|---|---|
| AM | Ash Mountain |
| BFL | Bakersfield (Kern County Air Terminal) |
| BR | bulk Richardson number |
| EL | Emerald Lake |
| FAT | Fresno (Air Terminal) |
| K | Kelvin |
| LIPM | Lasar Integrating Plate Method (carbon-soot) |
| PDT | Pacific Daylight Time (Pacific Standard Time plus one hour) |
| PIXE | Particle Induced X-ray Emission |
| RH | relative humidity |
| SCK | Stockton (Metropolitan Airport) |
| SFO | San Francisco (International Airport) |
| WV | Wolverton |

# APPENDIX II

"Meteorology and Aerosol Transport in the Southern Sierra Nevada as Measured with Tethered Balloon Systems" A Master's Thesis by Diane E. Ewell, 1987.

All thesis data on weather station instrument specifications, flow rates and aerosol cut-points, and tethersonde data processing are included as Appendix II.

# APPENDIX II-A

APPENDIX II-A: Weather station instrument specifications.

All instrumentation was acquired from Campbell Scientific, Inc., Logan, Utah, however the individual components had seperate manufacturers. The thermistor was manufactured by Fenwal in Massachusettes, the relative humidity sensor by Phys-Chemical Research Corp. in New York and windspeed and direction sensors by Met-one, Inc., in Sunnyvale, California. The specifications listed here are taken from the users manual accompanying the instrumentation or from information supplied by the manufacturers. Specified accuracy is for normal operating conditions.

1. Model 201 Thermistor and Relative Humidity Probe

Sensor is a sulfonated polystyrene plate plus a thermistor (for temperature compensation) encased in a slotted plastic shield. Thermistor is waterproof, heat-shrink encapsulated and non-aspirated. The resistance of the sulfonated plate is inversely proportional to the humidity (more moisture, more conductance) and the output is temperature compensated in the CR21 software.

Relative Humidity Probe (PCRC-11)
- Range: 10 to 95 percent
- Time Constant (double for descending RH): 30 seconds still air, 1 to 5 seconds moving air
- Accuracy: ±3 percent

Thermistor (Fenwal UUT-51J1)
(temperature is not a source of error under normal operating range)
- Calibration Range: 5 to 95 degrees celcius
- Time Constant: <5 seconds
- Calibration: 1 percent
- Accuracy: ±0.1 degrees celcius

2. Model 101 Thermistor (Fenwal UUT-51J1)

Thermistor design same as above except it is not shielded and specifications are same except calibration range.
- Calibration Range: -40 to 60 degrees celcius

3. Model 024A Met-One Wind Direction Sensor

Light weight, air-foil vane and potentiometer producing an output that varies proportionally to the wind direction.
- Threshold: 0.4 meters per second
- Range: 0 to 360 degrees
- Accuracy: ±5 degrees
- Damping Ratio: 0.25
- Delay Distance: <1.5 meters

4. Model 14A Met-One Wind Speed Sensor

Aluminum 3-cup contact anemometer assembly using a magnet-read switch assembly producing a series of contact closures whose frequency is proportional to the wind speed
- Range: 0 to 60 meters per second
- Accuracy: ±0.1 meters per second
- Starting Speed: 0.5 meters per second
- Distance Constant: <4.6 meters

# APPENDIX II-B

## Flow Rates and Aerosol Cut-Points

# APPENDIX II-B

## Flow Rates and Aerosol Cut Points

### I. Volume Estimate Methodology

The flow rates were measured by a field audit device (corrected for elevation) calibrated with an integrating spirometer at the University of California, Davis. The beginning and ending flow rates were measured for each air sample and the total volume of air sampled was estimated using the following procedure:

F=Change in flow rate.
F1= Beginning flow rate.
F2= Ending flow rate.
S = Slope of the latter part of the flow versus time curve (.0725).
T= Total Sample time.
V = Total volume.

1. If the beginning flow rate was less than the ending flow rate (F1 < F2):

   F=F2 - F1
   V=((F/2) x 10) + (F2 x (T - 10))

2. If the beginning flow rate was greater than the ending flow rate (F1 > F2):

   F=F1 - F2
   V=(F1 + (.05 x F1)) x (T - F/S) + ((F/2) x (F/S))

The above procedure was devised from the results of a series of tests that were performed to characterize the flow rate variation. Two tests using four samplers each were run at the University of California, Davis, measuring the flow rate every 10 minutes. One test used batteries that had been in the freezer for 3 hours and the other used batteries that had been in the sun for 30 minutes. The variation in the flow rates was dependent on the batteries and not on the individual pump and motor. Temperature did not appear to effect the flow rate variation.

Flow rate versus time curves were graphed and a regular pattern appeared. In general, the flow rate initially increased on average by 10 percent and would continue at this level for a period of time until the flow rate would drop at a fairly constant rate until the batteries lost all charge. The average of the 2 flow rates used for the first 10 minutes in procedure 1 and the addition of 5 percent to the inicial flow rate for procedure 2 was used to compensate for this initial increase. The average slope

from where the flow rate had decreased to its initial value until the batteries stopped was calculated to be 0.0725 (±0.03) liters per minute squared.

In the field, samplers were not always run as long as two hours or the batteries performed better than average so the ending flow rate was greater than the initial flow rate. In this case (40 percent of the time), procedure one above was used. On the other hand, 60 percent of the time, the ending flow rate was less than the initial value and procedure two was used. Comparison of the Simson's Rule estimates to estimates following procedure 2 above indicated for the worst case an uncertainty of 15 percent but on average it was 4 percent.

One test was run in the field the last day of the August period. The slope was 0.12 liters per minute squared and the uncertainty was 13 percent. The results of this one test more than likely indicate the upper end of the uncertainty. More tests in the field would have improved the estimate of the uncertainty but expense and time precluded this decision. Only five samplers were available for the project and one of the five failed during the August period. Future projects should have at least ten samplers available for the above reasons.

II. Coarse Filter Cut-Point Calculations

The lower cut-point calculations for the coarse filter were made following equations presented by Spurny et al. (1969). The upper cut-point was determined by assuming the flow rate had to be equal to or exceed the settling velocity of the particle and following equations from Green and Lane (1964).

1. Lower Cut-Point

D=Slip corrected aerosol particle diffusivity (cm /s).
Eff=The effiency of particle collection given the particle aerodynamic diameter and density.
L=Filter thickness (0.0001 cm).
m=Mass of aerosol (cm).
n=Viscosity of air (0.000181 g/cm/s).
P=Porosity of filter (.05).
pie=3.14159.
q=Face velocity (46.05 cm/s).
Ro=Filter pore radius (0.0004 cm).
s=Particle density ($g/cm^3$).

$$Eff = Ei + Ed + (0.15 \times Er) - (Ei \times Ed) - (0.15 \times Ei \times Er)$$

$$Ei = 2Ei'/(1 + e) - Ei'^2/(1 + e)^2$$

$$Ei' = 2 \times Stk \times \sqrt{e} + 2 \times Stk^2 \times e \times \exp(1/(-Stk \times \sqrt{e})) - 2 \times Stk^2 \times e$$

$e=\sqrt{P}/(1-\sqrt{P})$

$Stk=(m \times q)/(6 \times pie \times n \times r \times Ro)$

$m=(4/3) \times (pie \times r^3 \times s)$

$Ed=1 - 0.81904 \times \exp(-3.6568 \times Nd) -$
$0.09752 \times \exp(-22.3045 \times Nd) -$
$0.03248 \times \exp(-56.95 \times Nd) -$
$0.0157 \times \exp(-107.6 \times Nd) - \ldots$, etc.

$Nd=(L \times D \times P)/(Ro^2 \times q)$

$Er=r/Ro \times (2 - (r/Ro))$ $Nr \leq 1$ (if $Nr>1$ then $Eff=1$)

Results:

| Particle Diameter(μm) | D ($\times 10^{-7}$) | Eff x 100 (%) |
|---|---|---|
| 1 ($s=1$ g/cm$^3$) | 2.741 | 46 |
| ($s=2.2$ g/cm$^3$) | | 67 |
| 1.5 ($s=1$ g/cm$^3$) | 2.007 | 68 |
| ($s=2.2$ g/cm$^3$) | | 82 |

1. average particle density is 1 g/cm$^3$ and average soil particle density is 2.2 g/cm$^3$.

Figure 1 shows the experimental results for three different nucleopore filters as a function of face velocity (Cahill et al. 1979). It can be seen that the 50 percent cut-point is approximately 1.5 μm at the face velocity of 46.05 cm/s (average face velocity for the August field season) which agrees well with the theoretical calculations. The curves in Figure 1 were derived from experiments using un-coated nucleopore filters. The effect of coating the filter would be to lower the cut-point due to an increase in the face velocity by as much as 15 percent (John et al. 1980). This would drop the 50 percent cut-point to approximately 1.3 μm for the 8 μm filter curve in Figure 1.

2. Upper Cut-Point

d=Particle aerodynamic diameter
g=Acceleration due to gravity (981 cm/s$^2$)
n=Viscosity of air (0.000181 g/cm/s)
s=Particle density (g/cm$^3$)
s'=Air density (0.001205 g/cm$^3$)
v=Sedimentation velocity=Face velocity (46.05 cm/s)

Equation: $v=((s - s') \times g \times d^2)/(18 \times n)$ For Reynold's number up to 0.05

Results:

| Particle Density(g/cm$^3$) | Particle Diameter(μm) |
|---|---|
| 1 | 123 |
| 2.2 | 83 |

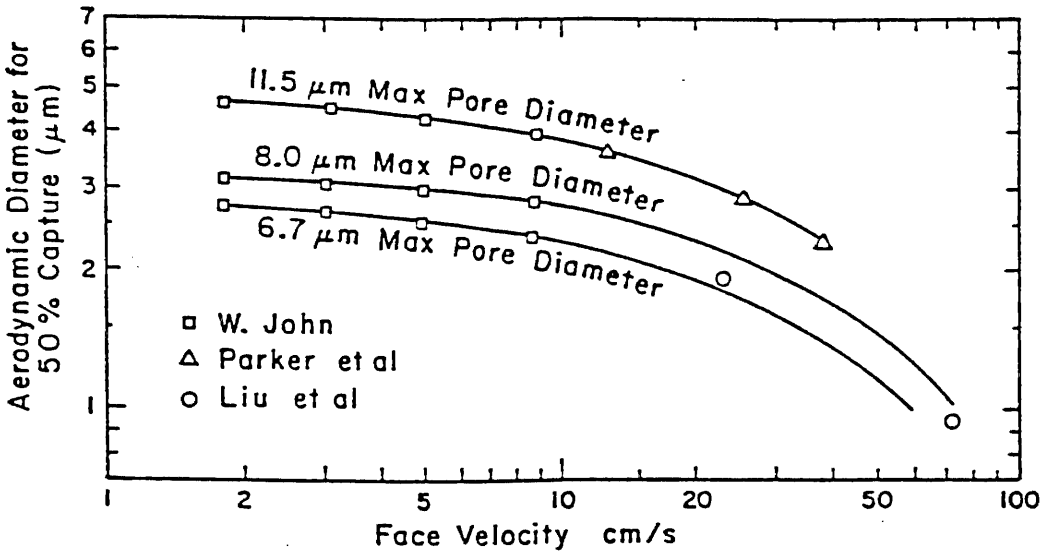


Figure 1: Variation of aerodynamic diameter for 50 percent ccapture by nuclepore filters as a function of face velocity for 3 pore diameters (from Cahill et al. 1979).

# APPENDIX II-C

## Tethered Balloons and Tethersonde Specifications

# APPENDIX II-C

## Tethered Balloons and Tethersonde Specifications

The 1 kilogram tethersonde package includes a windspeed sensor, 3-cup anemometer, fan-aspirated tubular radiation shield with two bead thermistors (one in middle of airstream and the other covered by a wetted wick), a pressure aneroid transducer (temperature compensated) and a potentiometric compass. The system was purchased from Atmospheric Instrument Research Co., Boulder, Colorado. The tethered balloons were purchased from Pie In The Sky, Division of J-KAM, Inc., San Mateo, California.

The tethersonde system consists of the re-chargeable battery operated telemetry meteorological package, receiver and EPSON printer ground station powered by 12 volts DC or 110 volts AC, antennae and 12 volt DC or 110 volt AC variable-speed powered winch. A review of the system can be found in Morris et al. (1975).

The following are specifications from the Operations Manual for the TS-2A Tethersonde/Airsonde. In parenthesis are values from tests on the system conducted at the National Center For Atmoshpheric Research (NCAR) facilities (Whiteman 1980).

Dry Bulb Temperature Sensor
Miniature bead thermistor (two non-linear thermistors)
- Range: -50 to 50 degrees celcius
- Accuracy: ±0.5 degrees celcius (±0.8)
- Time Constant: (13 seconds)

Pressure
Temperature-compensated aneroid transducer
- Range: 0 to 100 millibars
- Accuracy: ±1 millibar (±1.5)

Horizontal Windspeed
3-cup anemometer
- Range: 0.5 to 20 meters per second
- Accuracy: ±0.25 meters per second (±0.3)
- Starting Speed (0.4 to 0.7 meters per second)
- Stopping Speed: (0.3 meters per second)
- Time Constant: (0.3 to 0.5 seconds)

Wind Direction
Magnetic compass
- Range: 0 to 360 degrees
- Accuracy: ±5 degrees (±4)

Transmitter
Frequency: 400 to 420 megahertz FM
Frequency Stability: 0.0005 percent between -30 to 60 degrees celcius
Modulation: 16 F3
Power Output: 5 megawatts

Ground Receiver
Frequency Range: 400 to 420 megahertz FM
Number of Channels: 4
Frequency Stability: 0.0005 percent between 0 to 60 degrees celcius
Channel Spacing: 25 kilohertz
Sensitivity: 0.5 microvolts
Selectivity: 60 decibells
Audio Output: 500 megawatts
Antenna: 15 centimeter whip with ground plain

Winch
Line Capacity: 1000 meters
Power: 12 volts DC or 110 volts AC

Telemetry Balloon
Model: JK20
Shape: blimp
Volume: 10.2 cubic meters
Weight: 6.8 kilograms
Available Lift at Sea Level: 4 kilograms
Available Lift at 500 Meters Above Site (2722 meters above sea level): 1.4 kilograms

Particle Sampling Balloon
Model: "10 foot diameter" balloon
Shape: Spherical
Volume: 14.8 cubic meters
Weight: 5.9 kilograms
Available Lift at Sea Level: 9.7 kilograms
Available Lift at 500 Meters Above Site (2722 meters above sea level): 6 kilograms

*Note: Available lift calculated using U.S. Standard Atmosphere values from Warren et al. 1971 and does not include weight of tether line (0.8 grams per meter, 120 pound test).

# APPENDIX II-D

## Tethersonde Data Processing

# APPENDIX II-D

## Tethersonde Data Processing

I. Calculation of Wolverton surface pressure (SP):

Parameters:
If not specified, the parameter in question refers to the initial readings from the tethersonde at Wolverton at approximately 1.5 meters above ground level (excluding meteorological constants).

e=Mass of water vapor/mass of dry air (0.622).
E=vapor pressure (mb).
EF=vapor pressure at Fresno (mb).
ES=Saturated vapor pressure at wet bulb temperature (mb).
eso=Saturation vapor pressure at 0 degrees celsius (6.1078 mb).
g=Acceleration due to gravity (9.81 $m/s^2$).
Lv=Latent heat of vaporization at 0 degrees celsius ($2.5 \times 10^6$ J/kg).
P=Standard atmospheric pressure at 2222 meters mean sea level (770.66 mb).
PF=Pressure at Fresno (mb).
R=Mixing ratio.
Rd=Dry gas constant (287 J/K/kg).
RF=Mixing ratio at Fresno.
Rv=Gas constant for water vapor (461 J/K/kg).
SP=Surface pressure (mb).
T=Dry bulb temperature (degrees celsius).
T'=Wet bulb temperature (degrees celcius).
TDF=Dewpoint temperature at Fresno (degrees celcius).
TF=Dry bulb temperature at Fresno (degrees celcius).
TV=Virtual temperature (K).
TVF=Virtual temperature at Fresno (K).
z1=Elevation (2222 m).
z2= Elevation at Fresno (100 m).

Equations:
(**= indicate "to the power of")

ES=eso x 10 ** ((7.5 x T')/(237.3 + T'))
EF=eso x exp((Lv/Rv) x (1/273.15 -1/(TDF + 273.15)))
E=ES - .00066 x (1 + .00115 x T') x P x (T - T')
R=e x E/(P - E)
RF=e x EF/(PF - EF)
TV=(273.15 + T) x ((1 + 1/e x R)/(1 + R))
TVF=(273.15 + TF) x ((1 + 1/e x RF)/(1 + RF))
SP=PF x exp((g x (z1 - z2))/(Rd x ((TV + TVF)/2)))

II. Calculation of profile parameters:

Parameters:
All parameters (excluding meteorological constants) refer to readings from the tethersonde at Wolverton.

Cp=Specific heat at constant pressure (1004 J/K/kg).
e=Mass of water vapor/mass of dry air (0.622).
eso=Saturation vapor pressure at 0 degrees celsius (6.1078 mb).
ESz=Saturated vapor pressure at wet bulb temperature at height Z (mb).
Ez=vapor pressure at height Z (mb).
p1=Inicial pressure change reading at 1.5 meters (mb).
pz=Pressure change reading at height Z (mb).
Pz=Pressure at height Z (mb).
Rd=Dry gas constant (287 J/K/kg).
Rz=Mixing ratio at height Z.
SP=Surface pressure (mb).
TVoz=Virtual potential temperature at height Z (K).
TV1=Virtual temperature at 1.5 meters (K).
TVz=Virtual temperature at height Z (K).
Tz=Dry bulb temperature at height Z (degrees celcius).
Tz'=Wet bulb temperature at height Z (degrees celcius).
Z=Height of tethersonde (meters).

Equations:
First reading is assumed to be at 1.5 meters above ground level (**= indicate "to the power of").

Pz=SP - (pz - p1)
ESz=eso x 10 **((7.5 x Tz')/(237.3 + Tz'))
Ez=ESz - .00066 x (1 + (.00115 x Tz')) x Pz x (Tz - Tz')
Rz=(e x ESz)/(Pz - ESz)
TVz=(273.15 + Tz) x ((1 + (1/e x Rz))/(1 + Rz))
TVoz=(TVz + 273.15) x ((1000/Pz) ** (Rd/Cp))
Z=14.636 x (TV1 + TVz) x ln (SP/Pz) + 1.5

# APPENDIX II-E

## Pilot Balloon Profiles

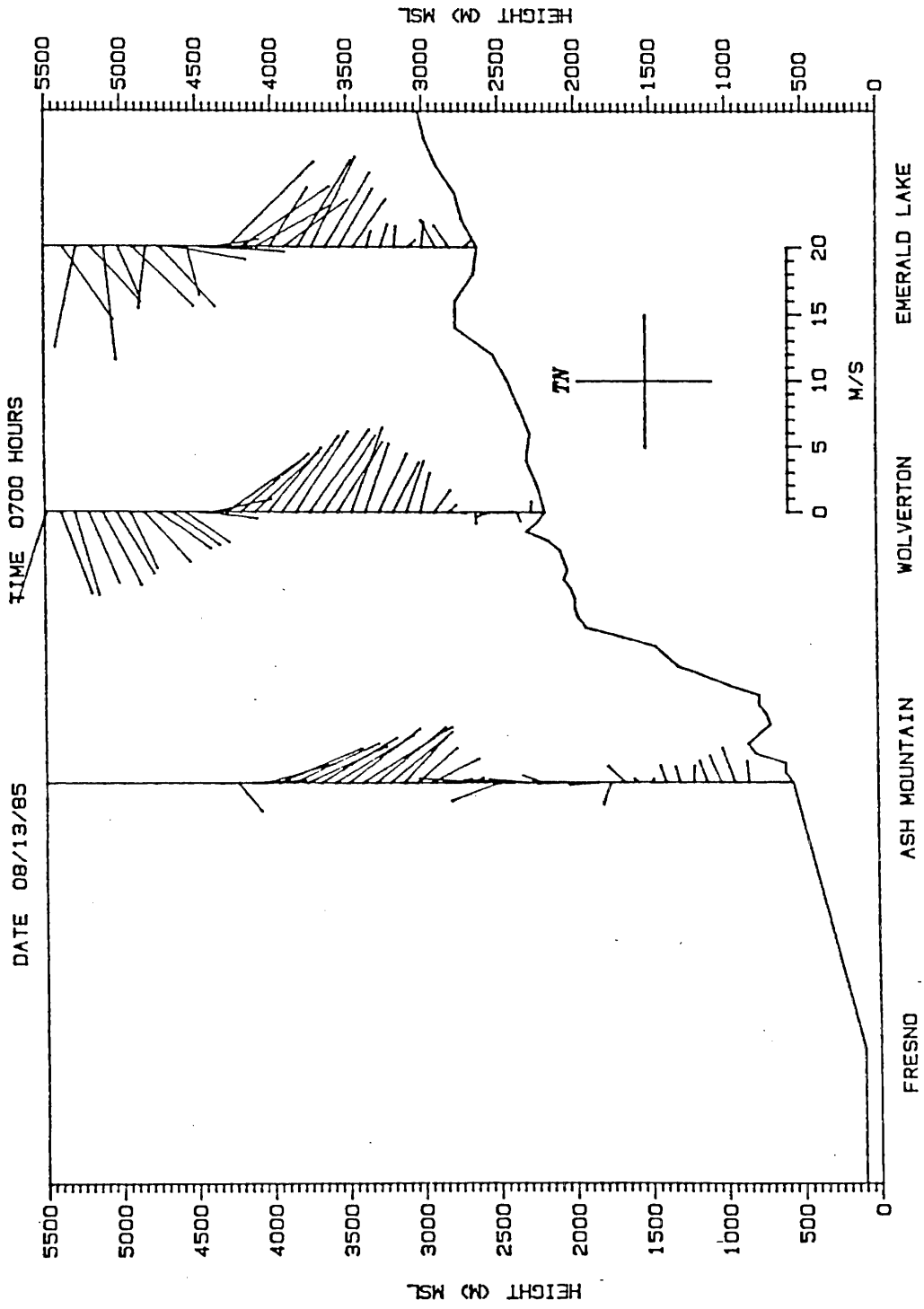


Figure 1: Pilot balloon wind profiles for August 13th, 1985, at 0700 PDT.

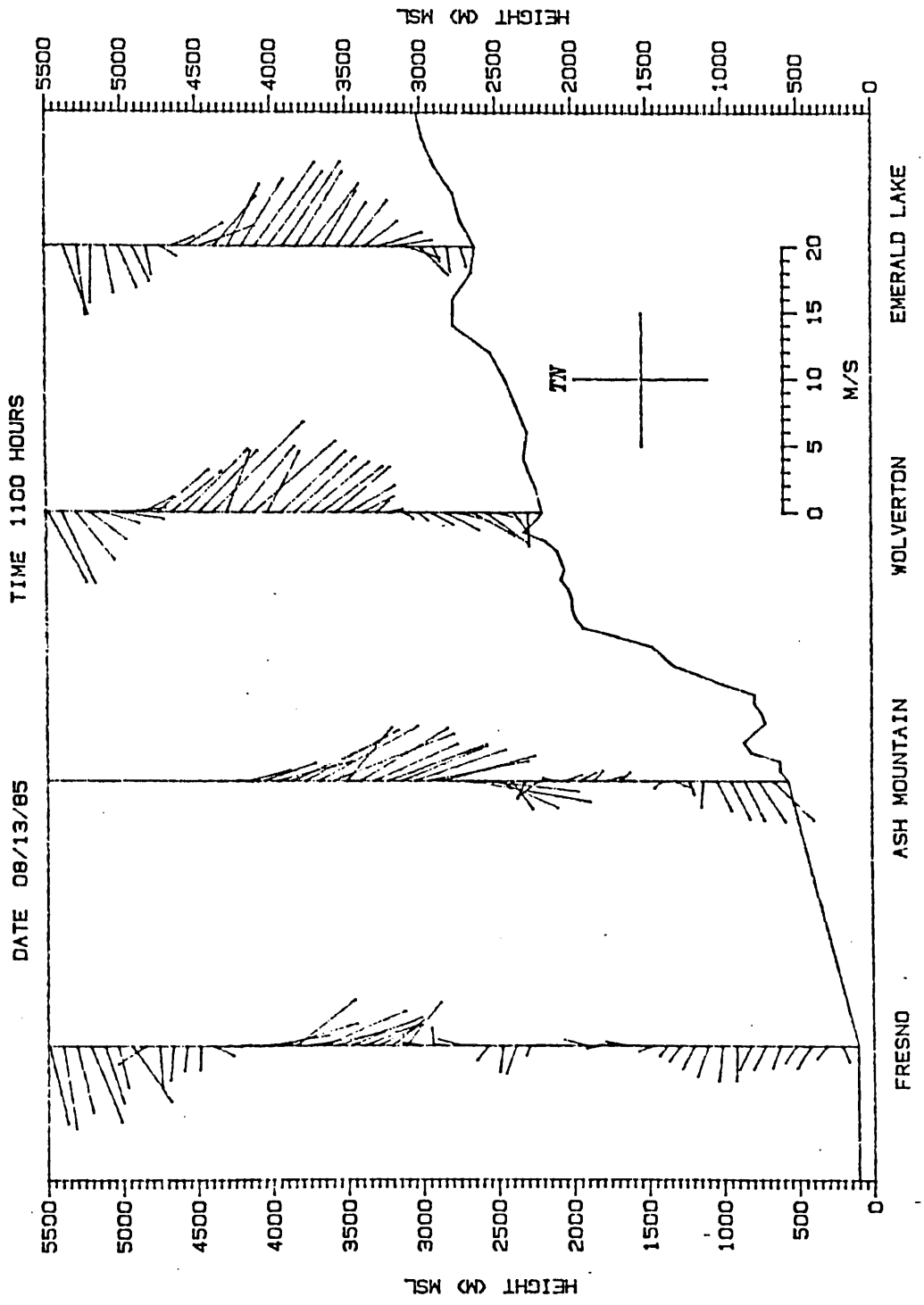


Figure 2: Pilot balloon wind profiles for August 13th, 1985, at 1100 PDT.

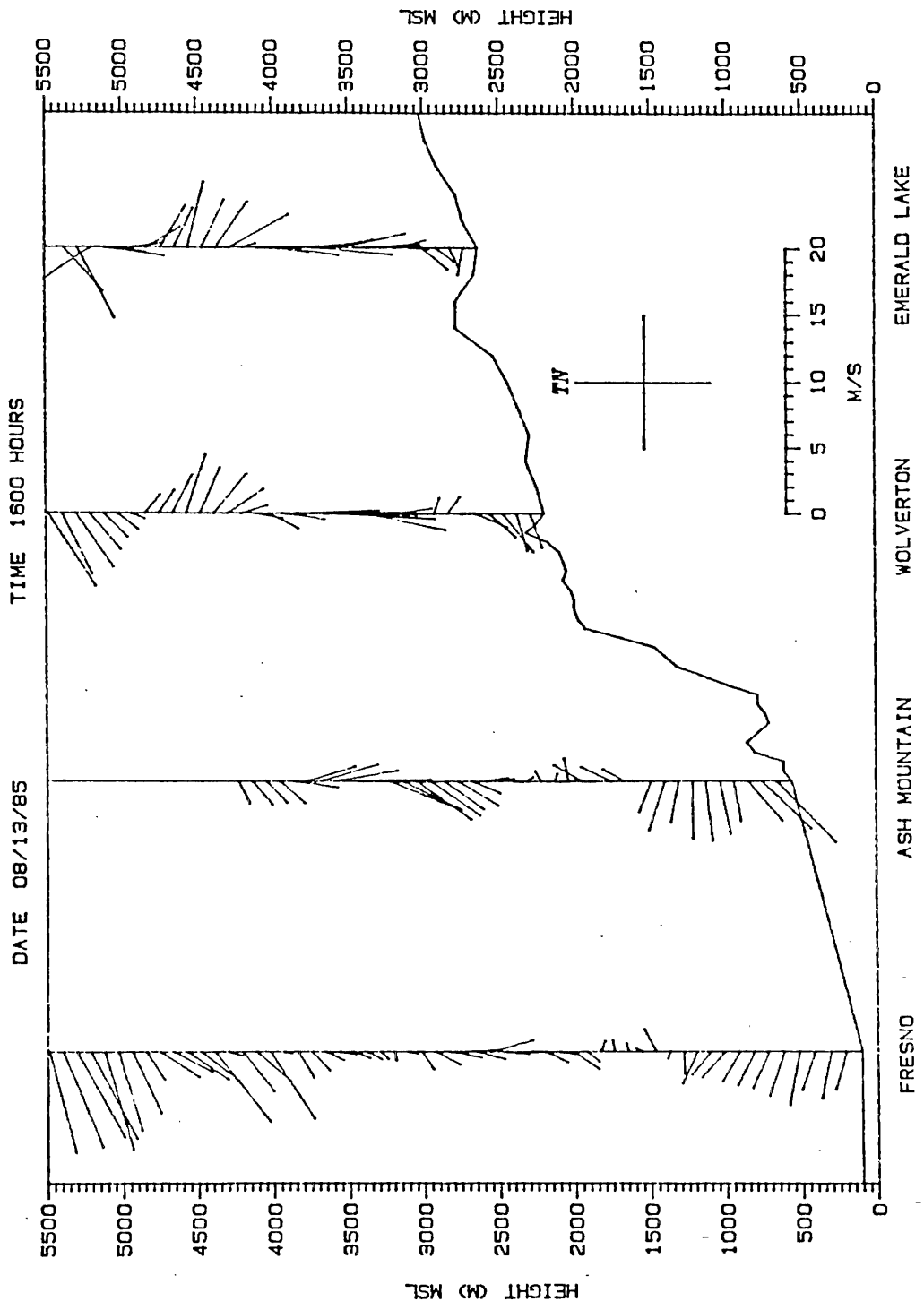


Figure 3: Pilot balloon wind profiles for August 13th, 1985, at 1600 PDT.

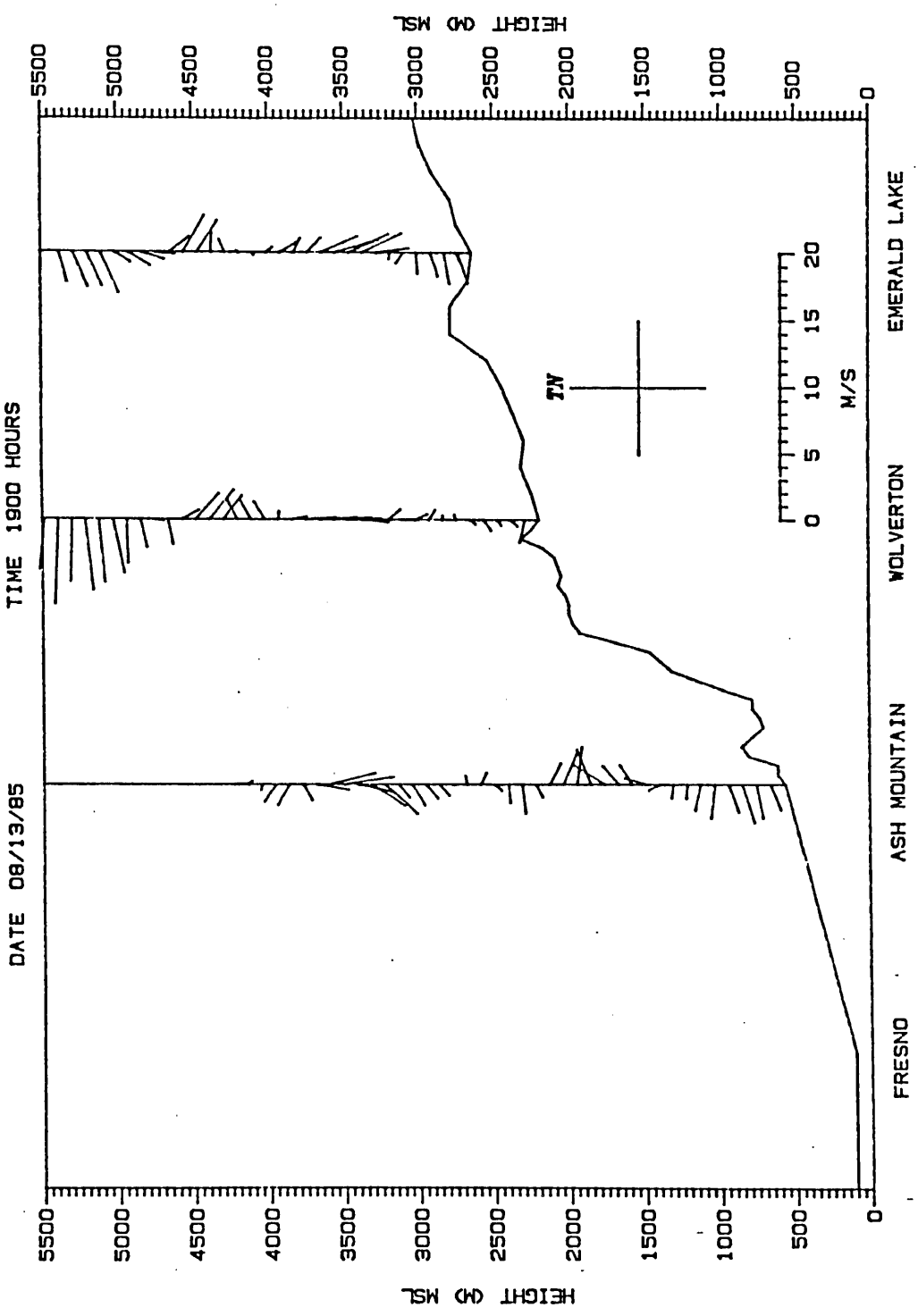


Figure 4: Pilot balloon wind profiles for August 13th, 1985, at 1900 PDT.

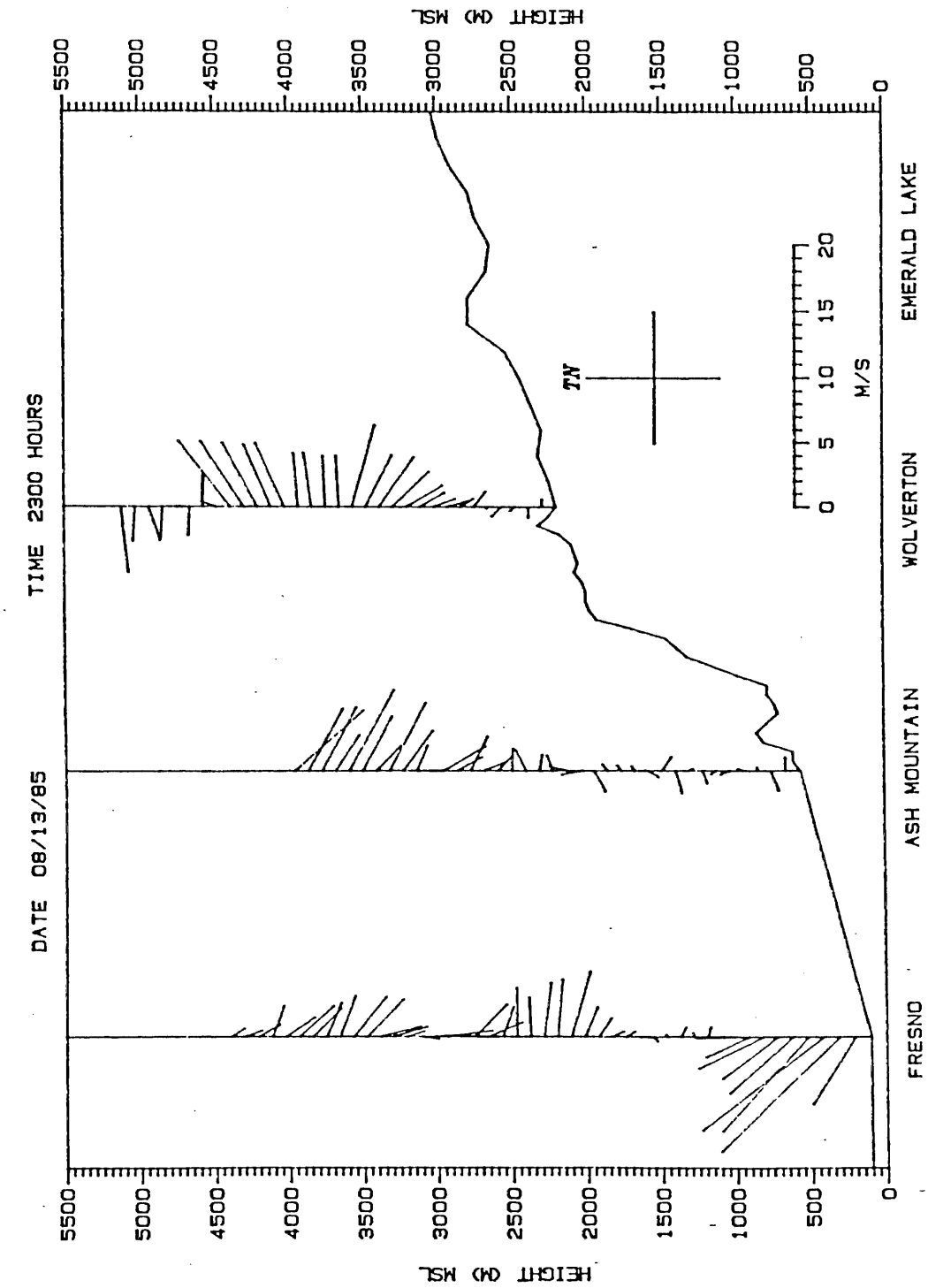


Figure 5: Pilot balloon wind profiles for August 13th, 1985, at 2300 PDT.

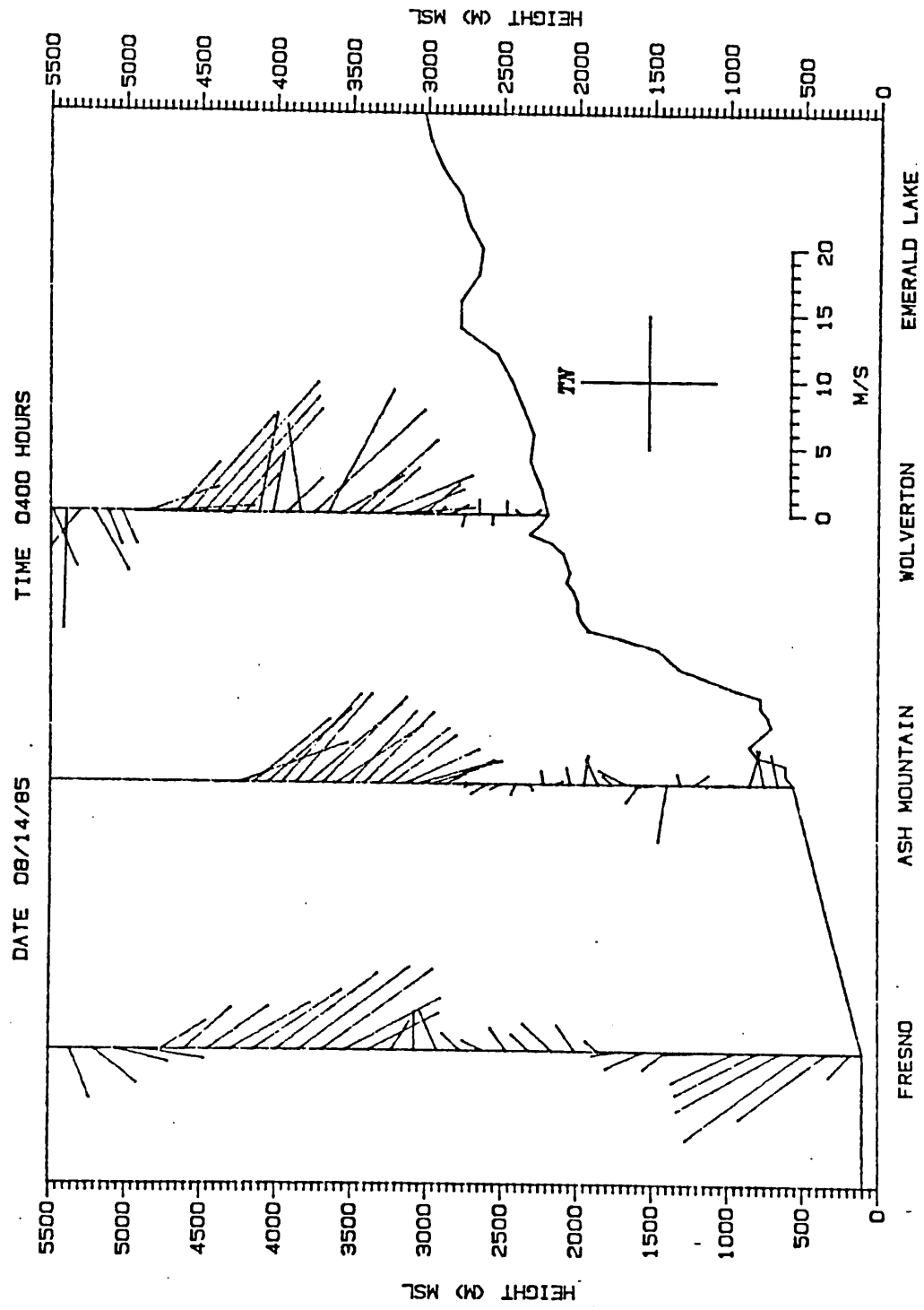


Figure 6: Pilot balloon wind profiles for August 14th, 1985, at 0400 PDT.

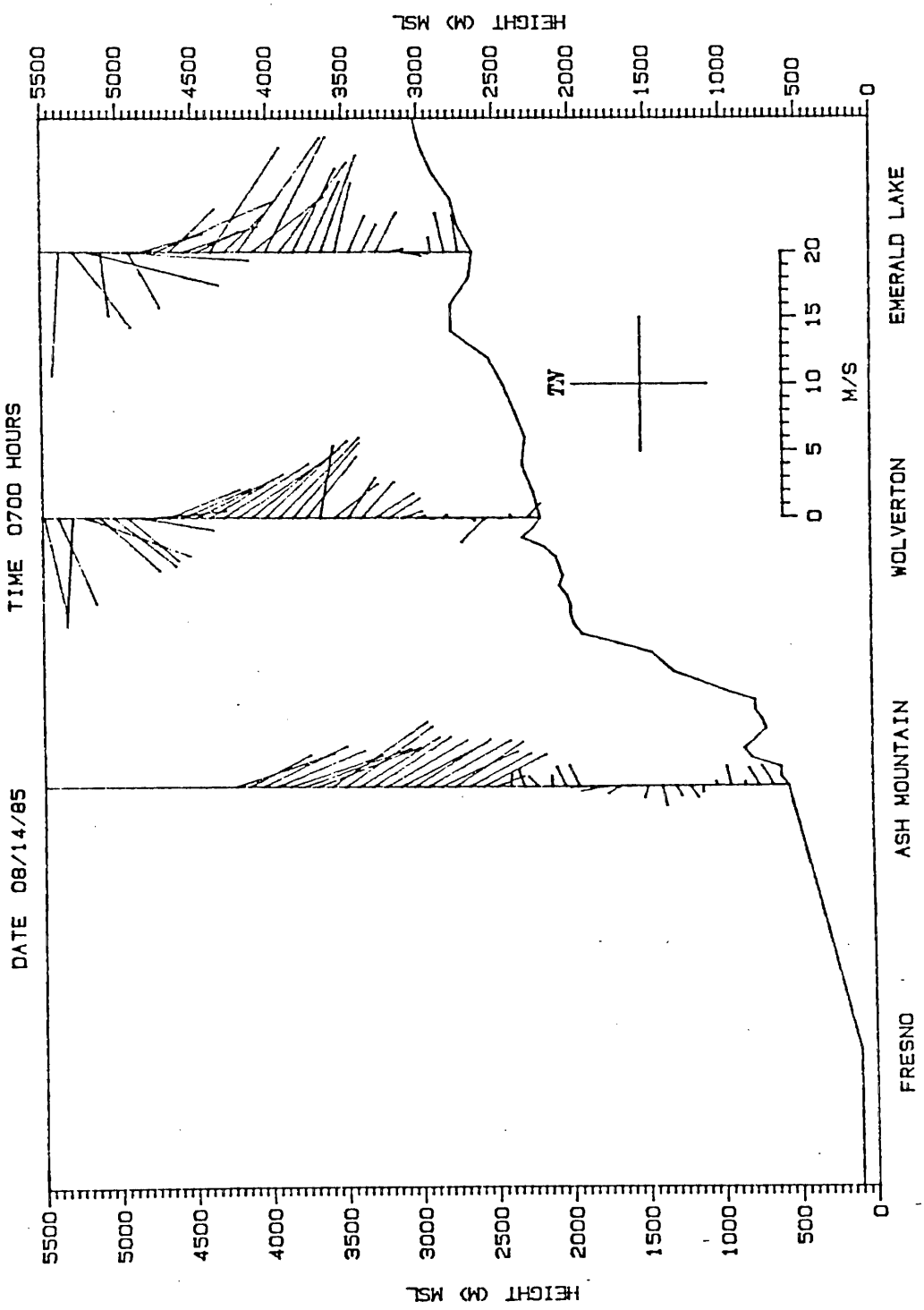


Figure 7: Pilot balloon wind profiles for August 14th, 1985, at 0700 PDT.

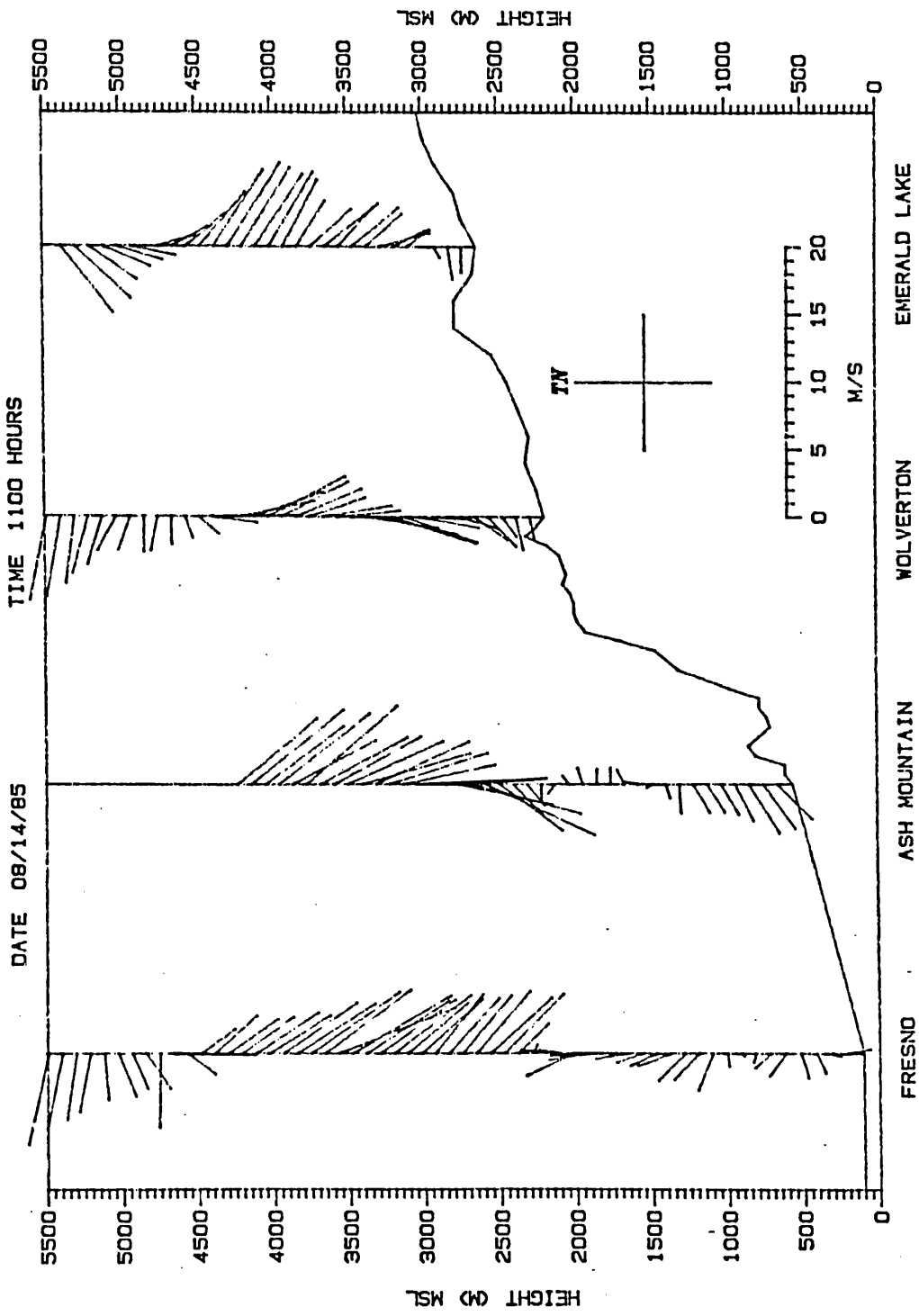


Figure 8: Pilot balloon wind profiles for August 14th, 1985, at 1100 PDT.

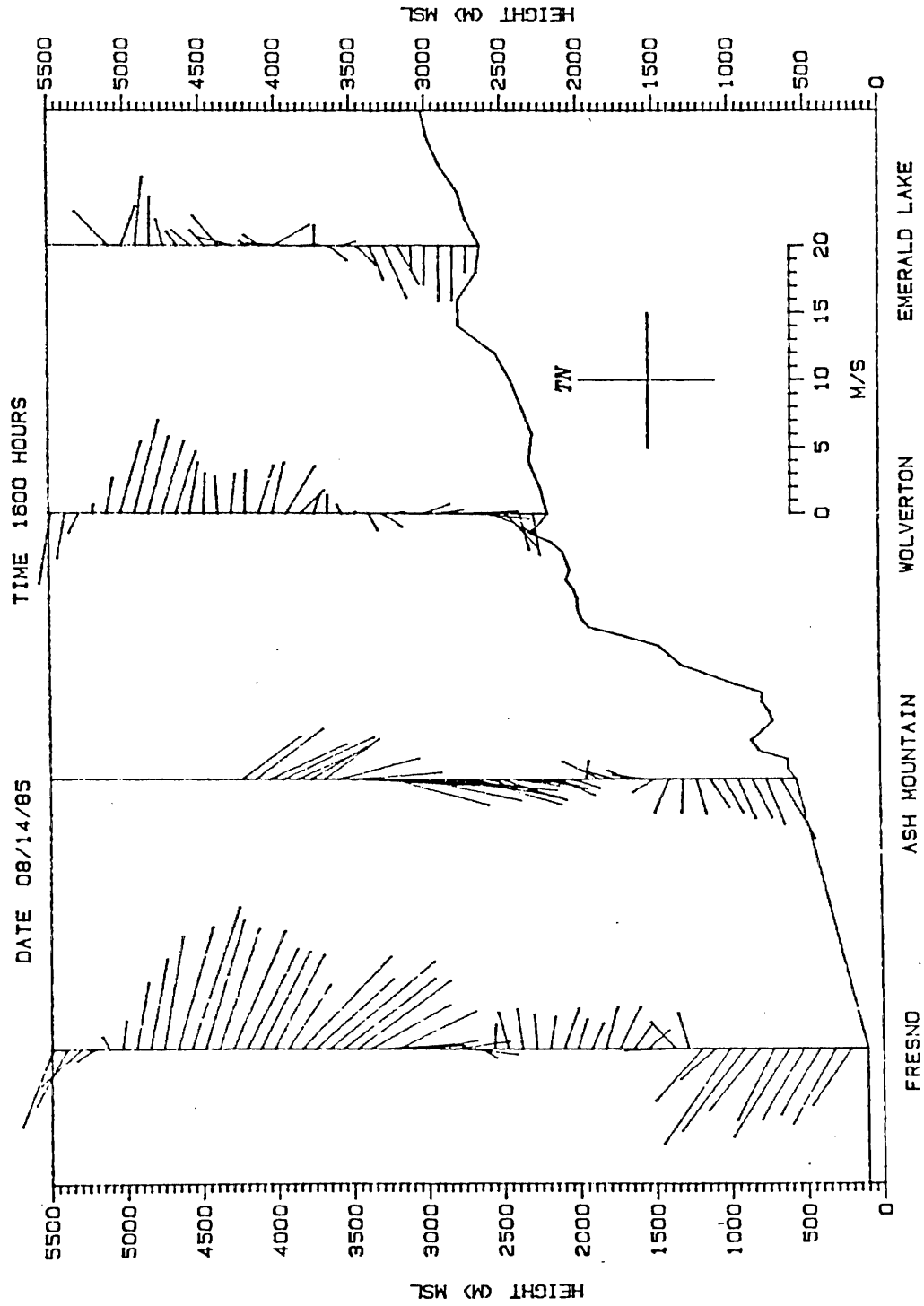


Figure 9: Pilot balloon wind profiles for August 14th, 1985, at 1600 PDT.

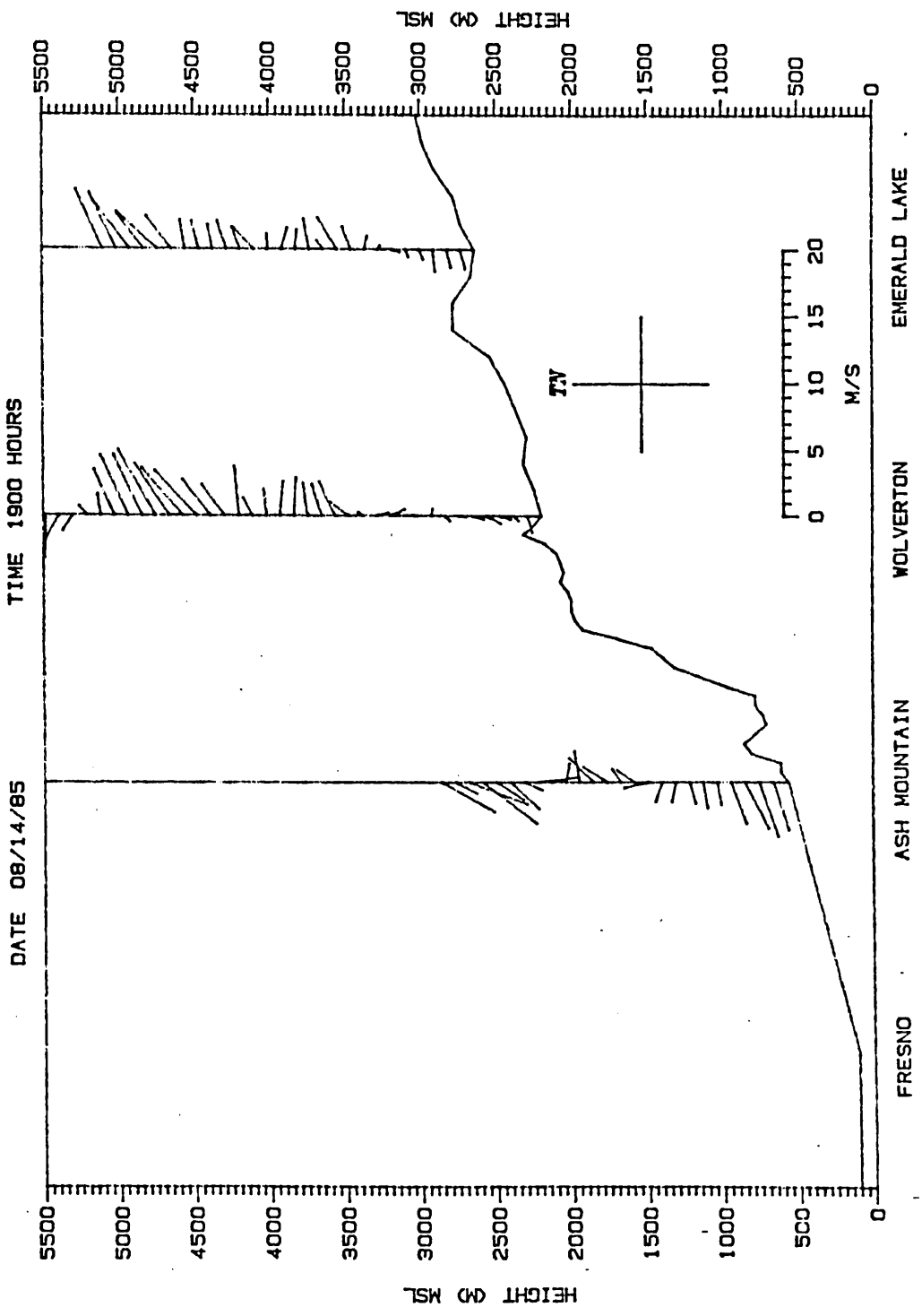


Figure 10: Pilot balloon wind profiles for August 14th, 1985, at 1900 PDT.

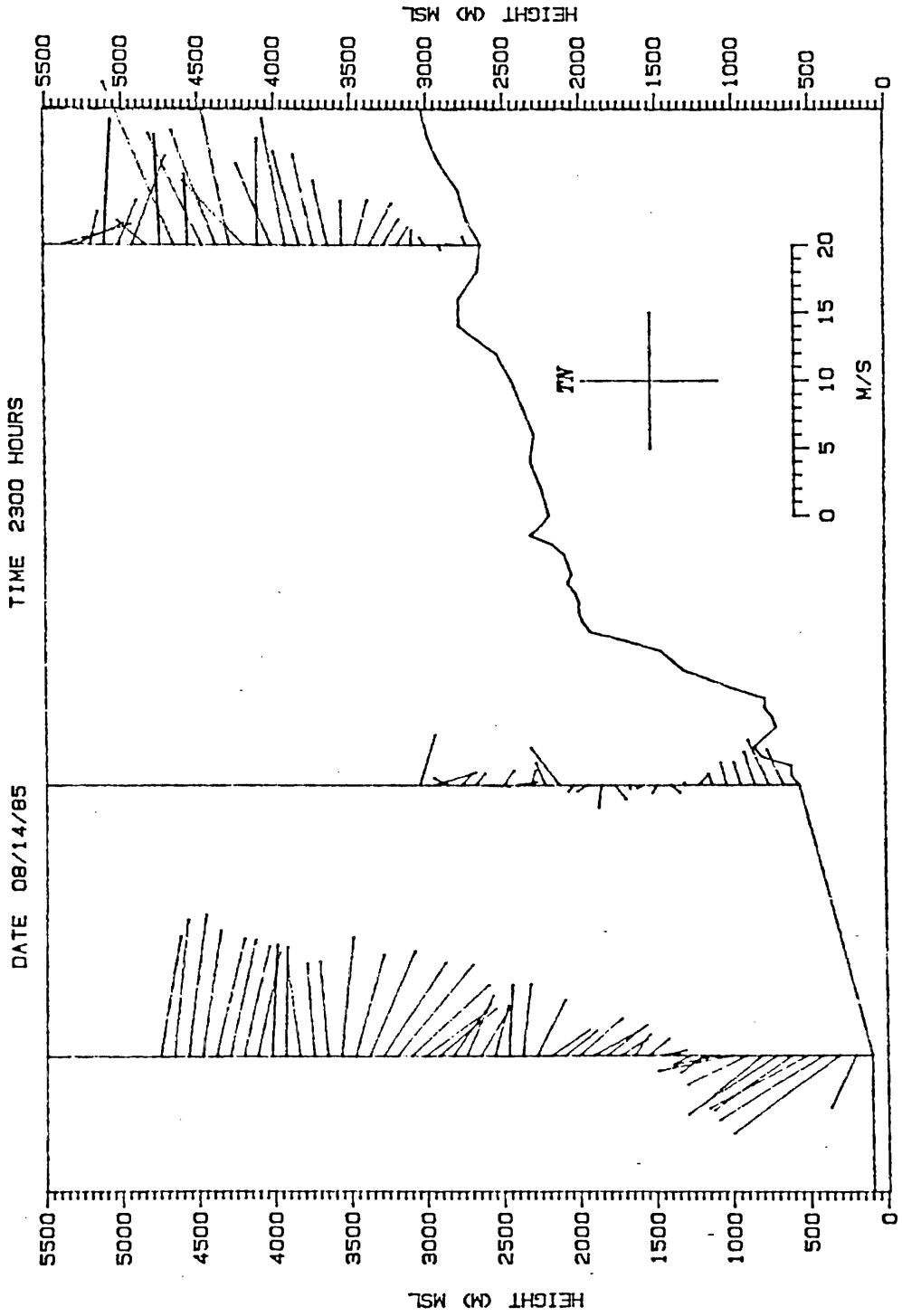


Figure 11: Pilot balloon wind profiles for August 14th, 1985, at 2300 PDT.

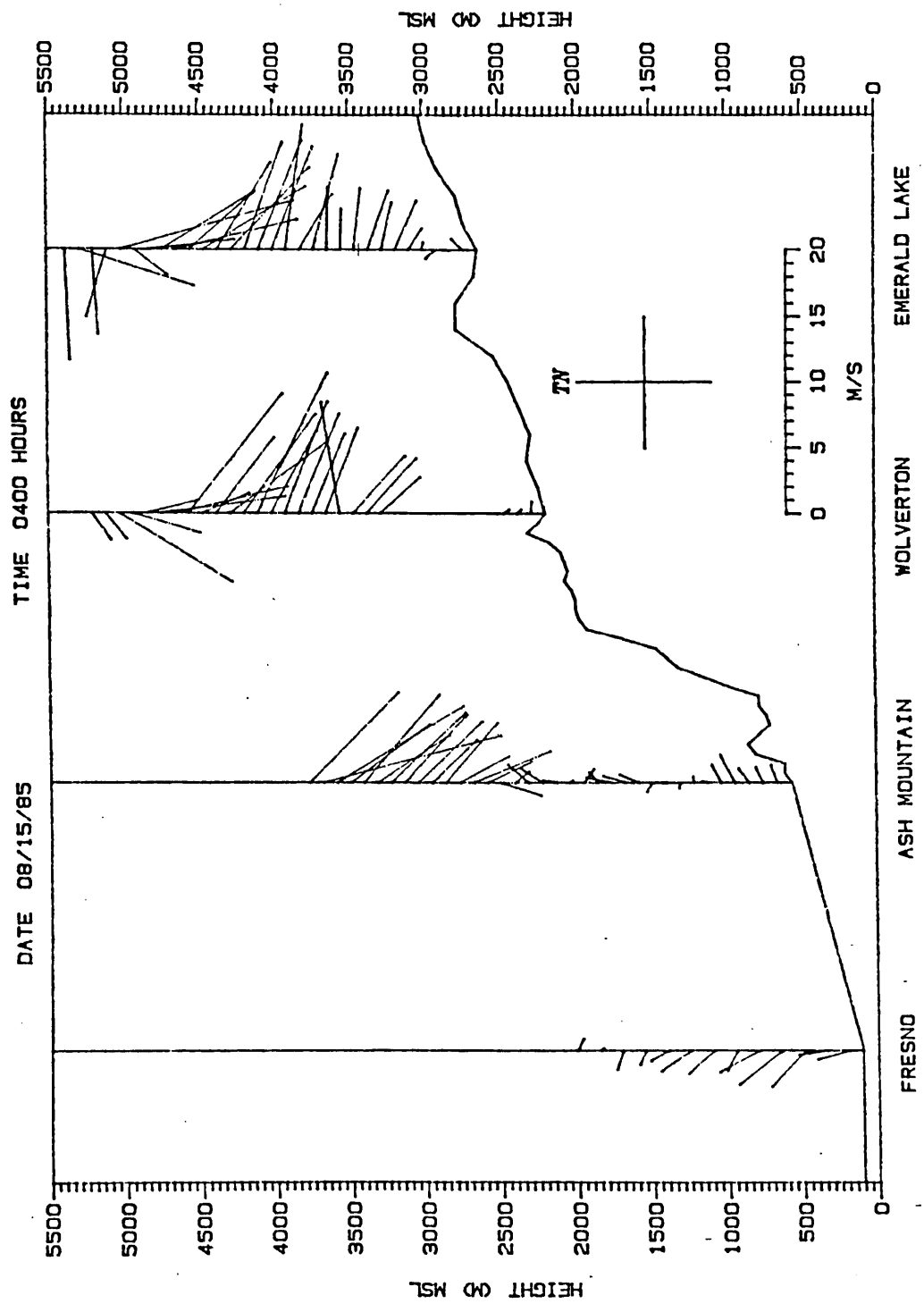


Figure 12: Pilot balloon wind profiles for August 15th, 1985, at 0400 PDT.

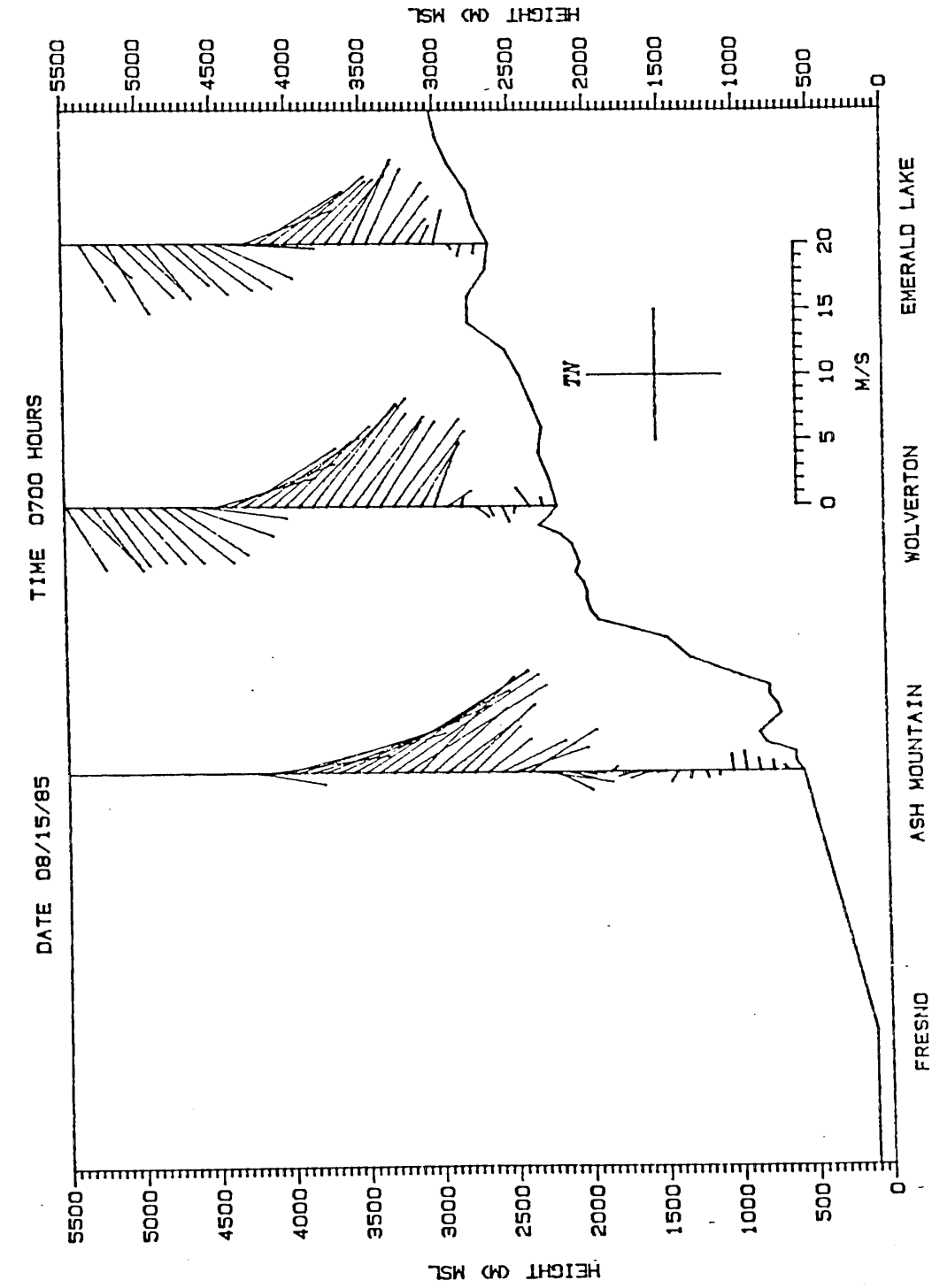


Figure 13: Pilot balloon wind profiles for August 15th, 1985, at 0700 PDT.

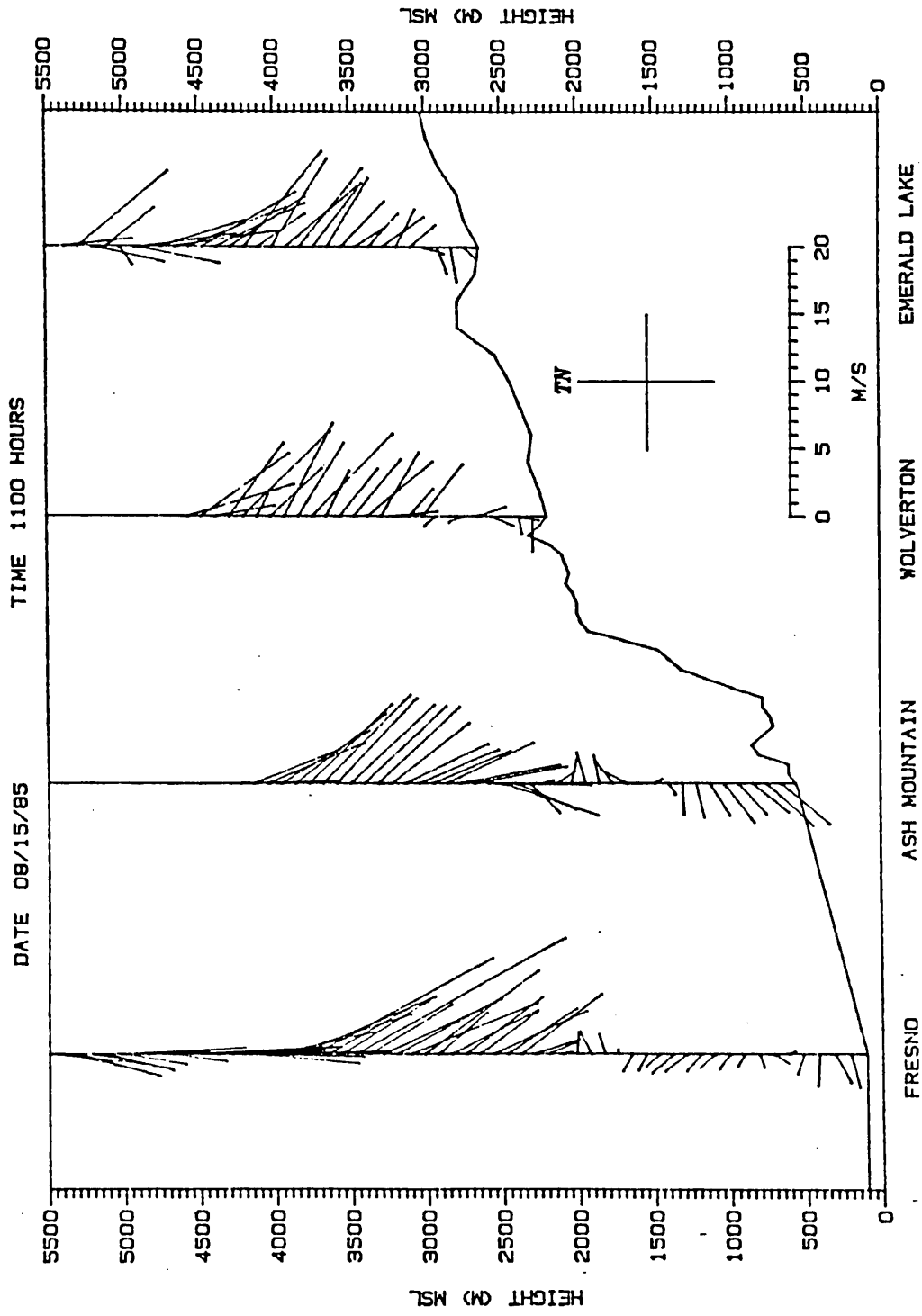


Figure 14: Pilot balloon wind profiles for August 15th, 1985, at 1100 PDT.

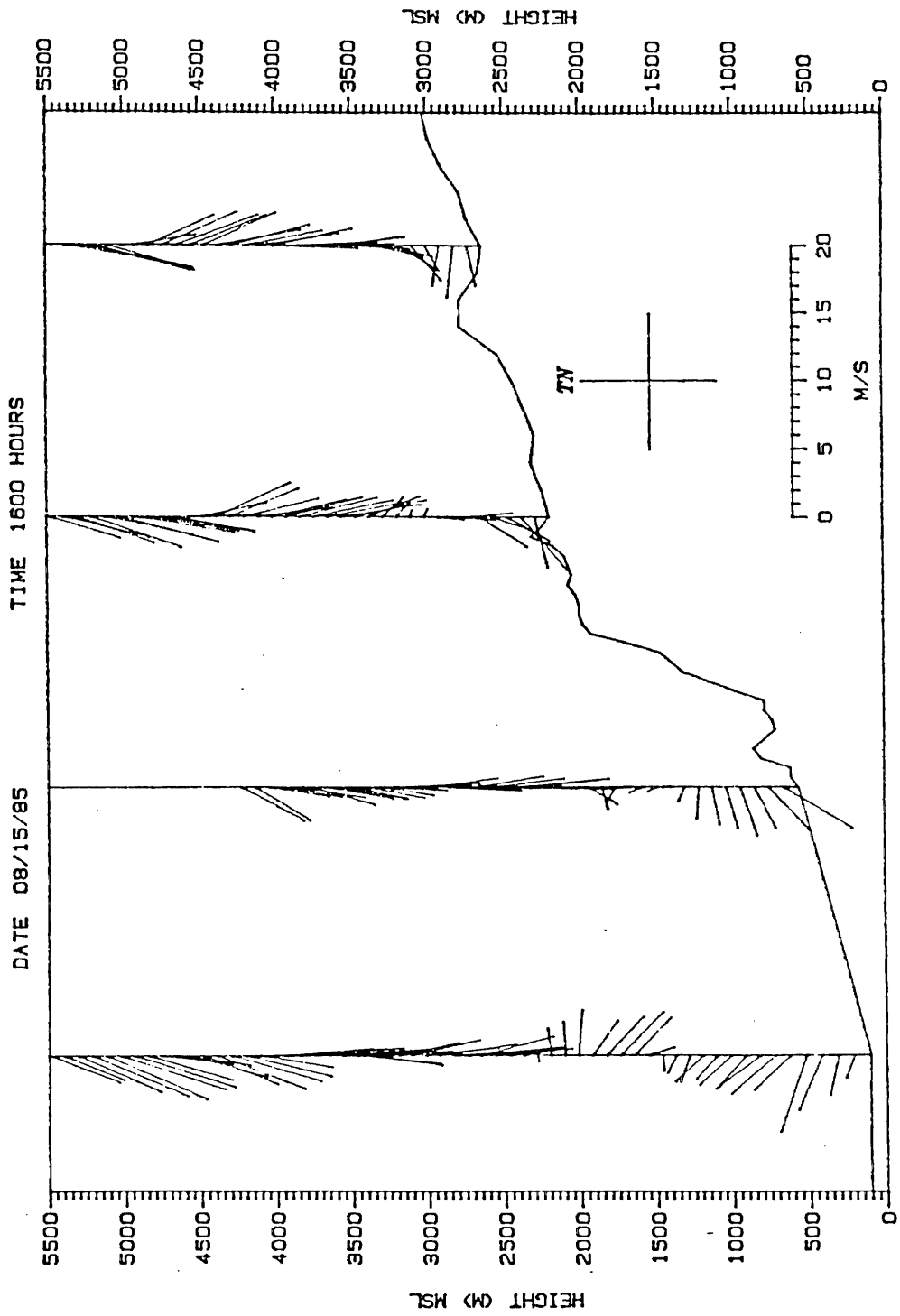


Figure 15: Pilot balloon wind profiles for August 15th, 1985, at 1600 PDT.

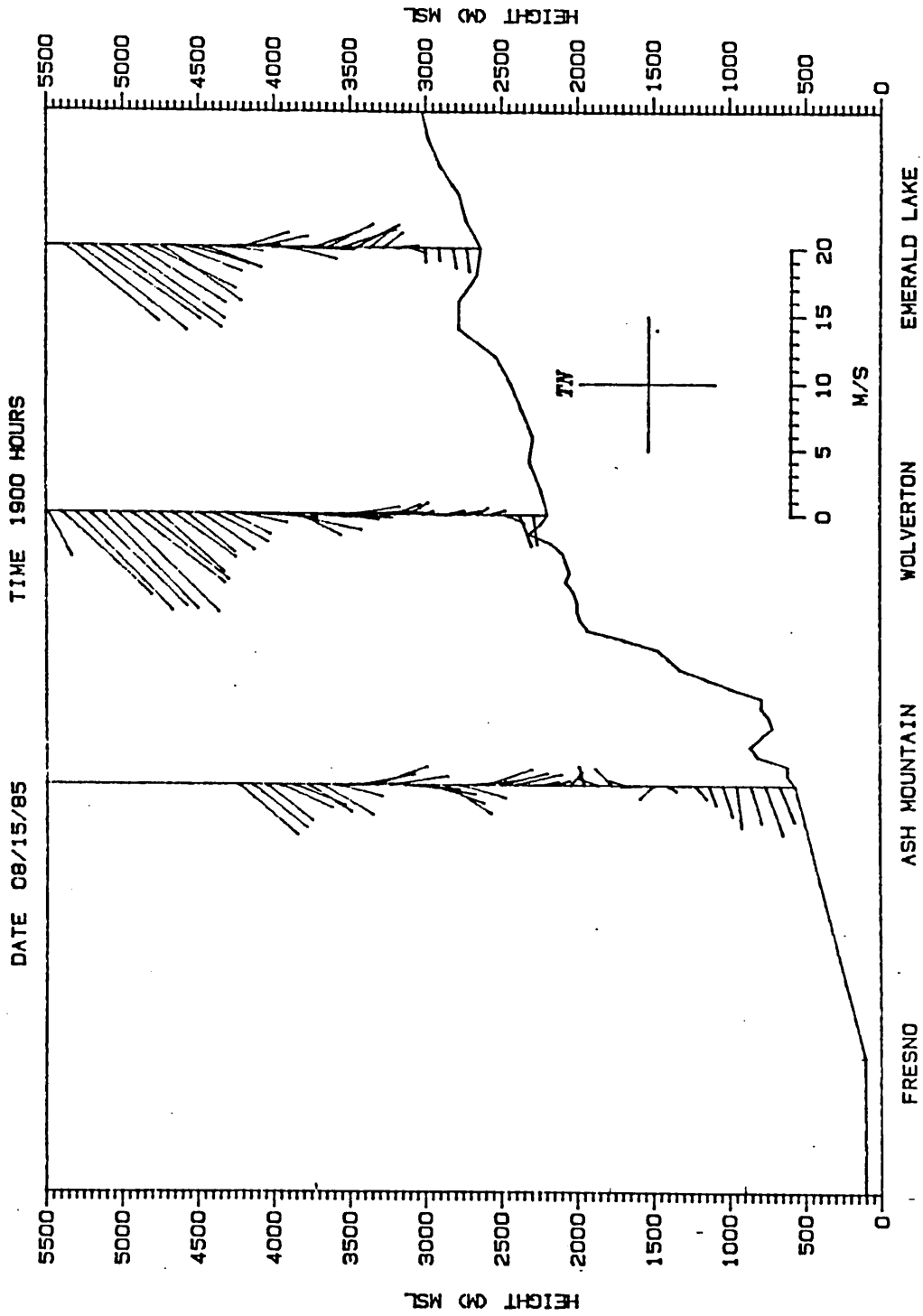


Figure 16: Pilot balloon wind profiles for August 15th, 1985, at 1900 PDT.

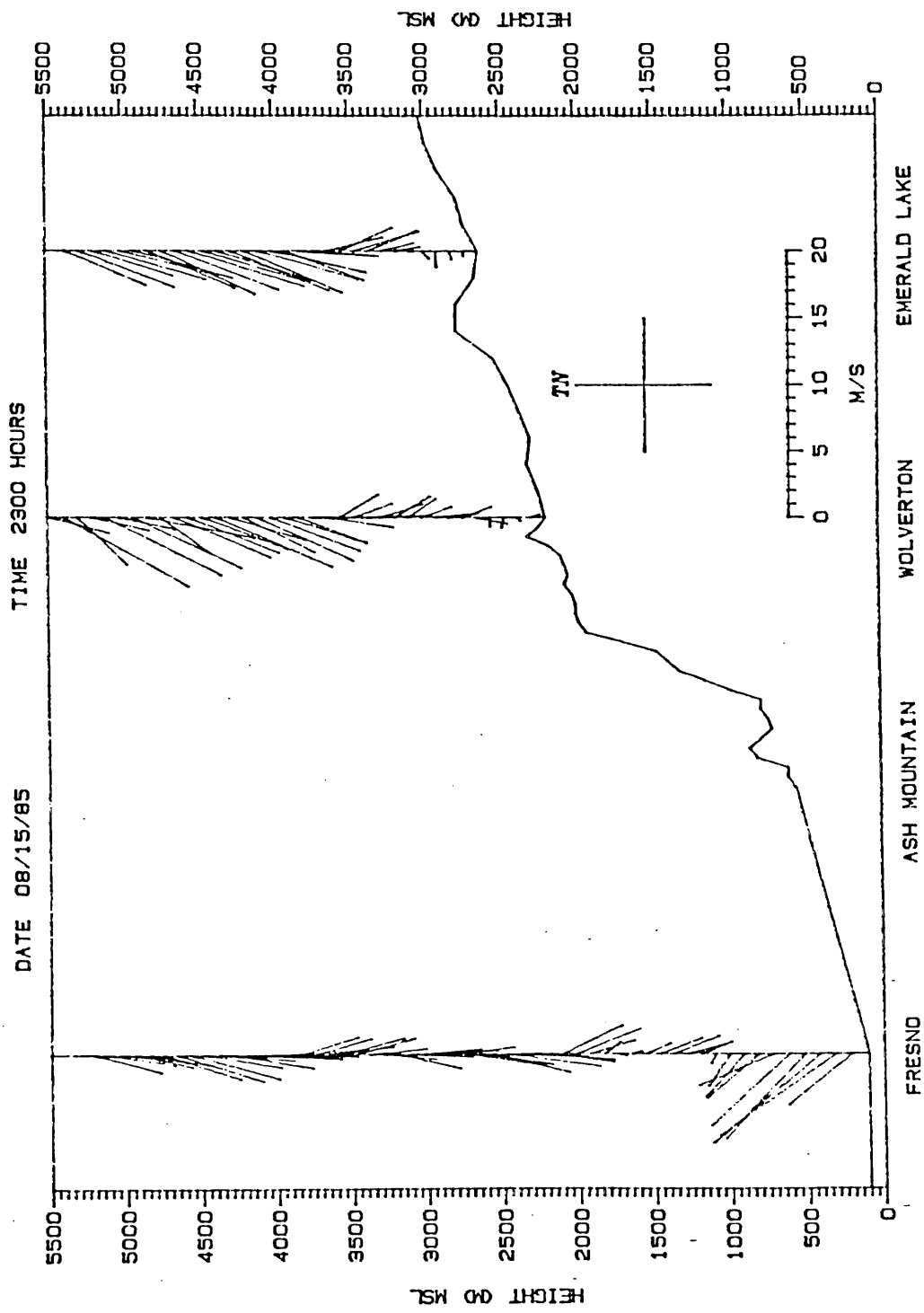


Figure 17: Pilot balloon wind profiles for August 15th, 1985, at 2300 PDT.

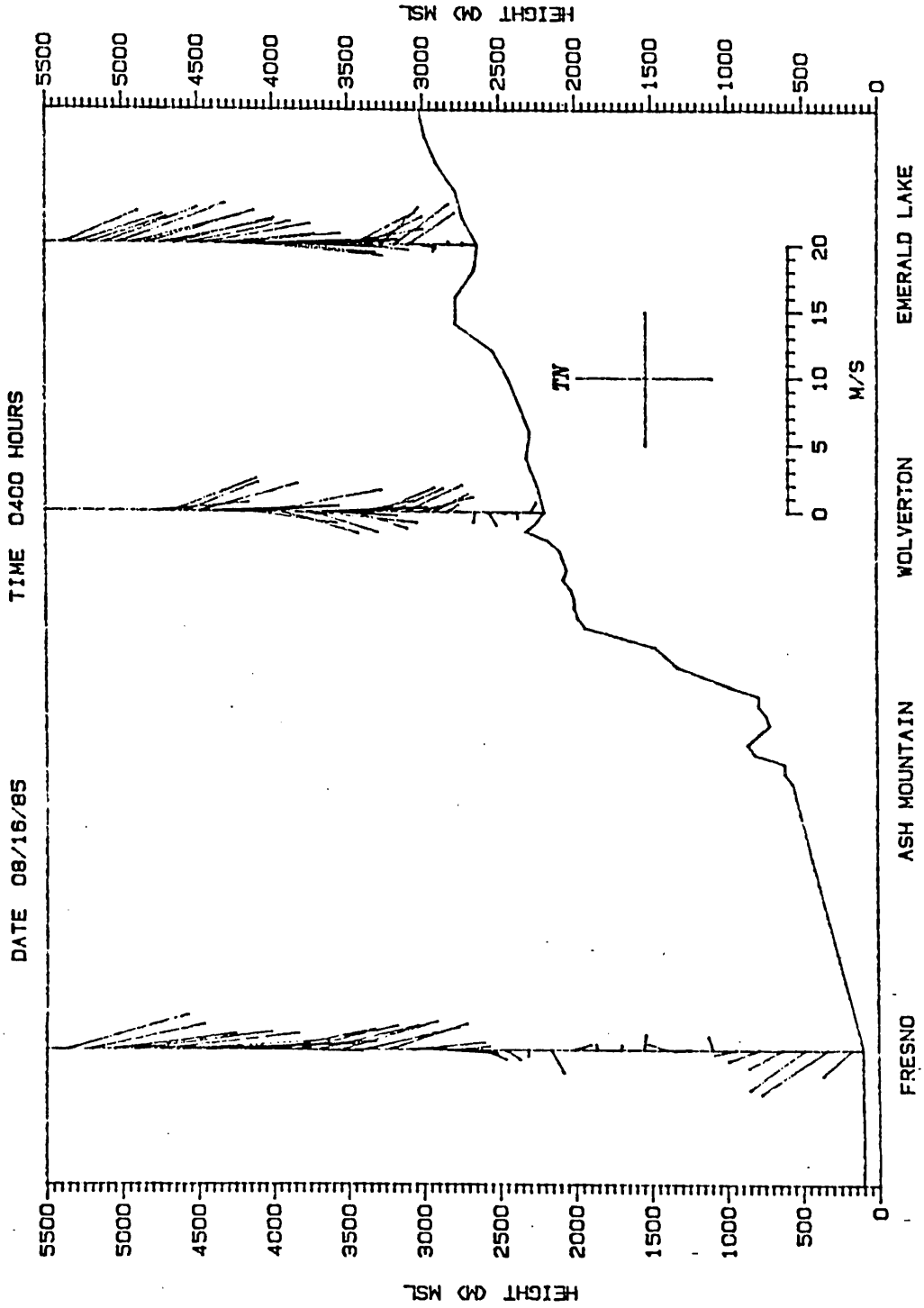


Figure 18: Pilot balloon wind profiles for August 16th, 1985, at 0400 PDT.

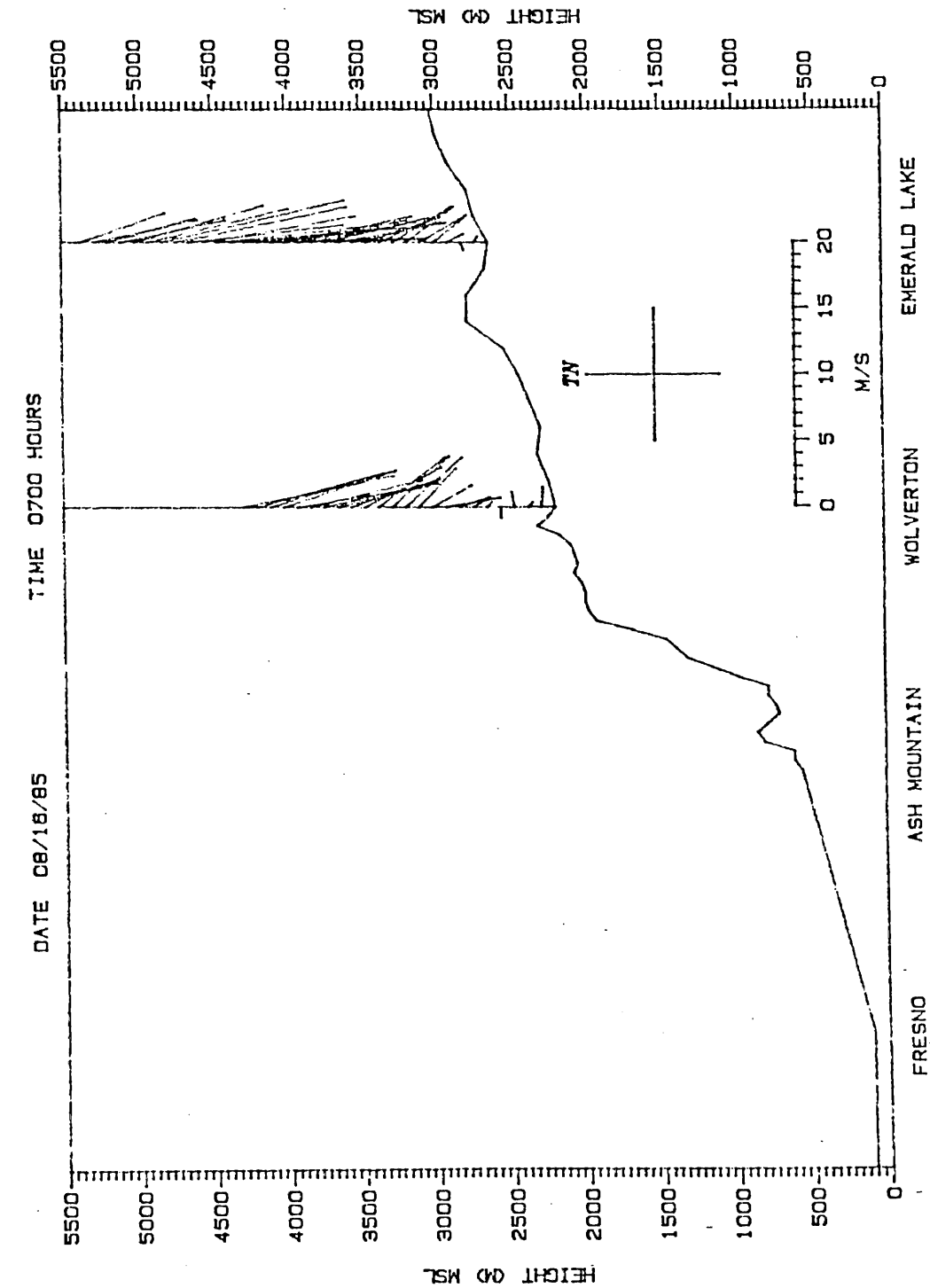


Figure 19: Pilot balloon wind profiles for August 16th, 1985, at 0700 PDT.

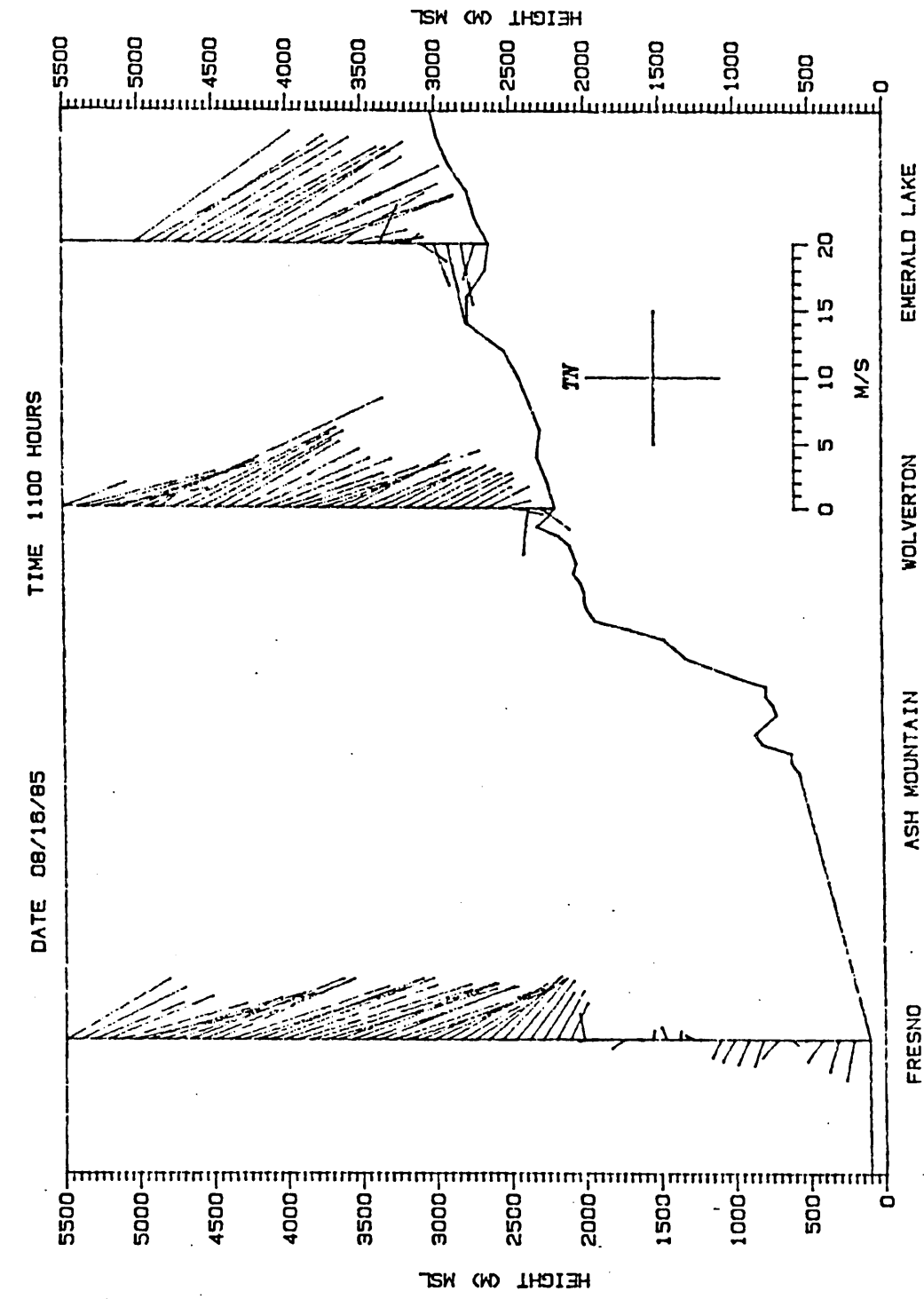


Figure 20: Pilot balloon wind profiles for August 16th, 1985, at 1100 PDT.

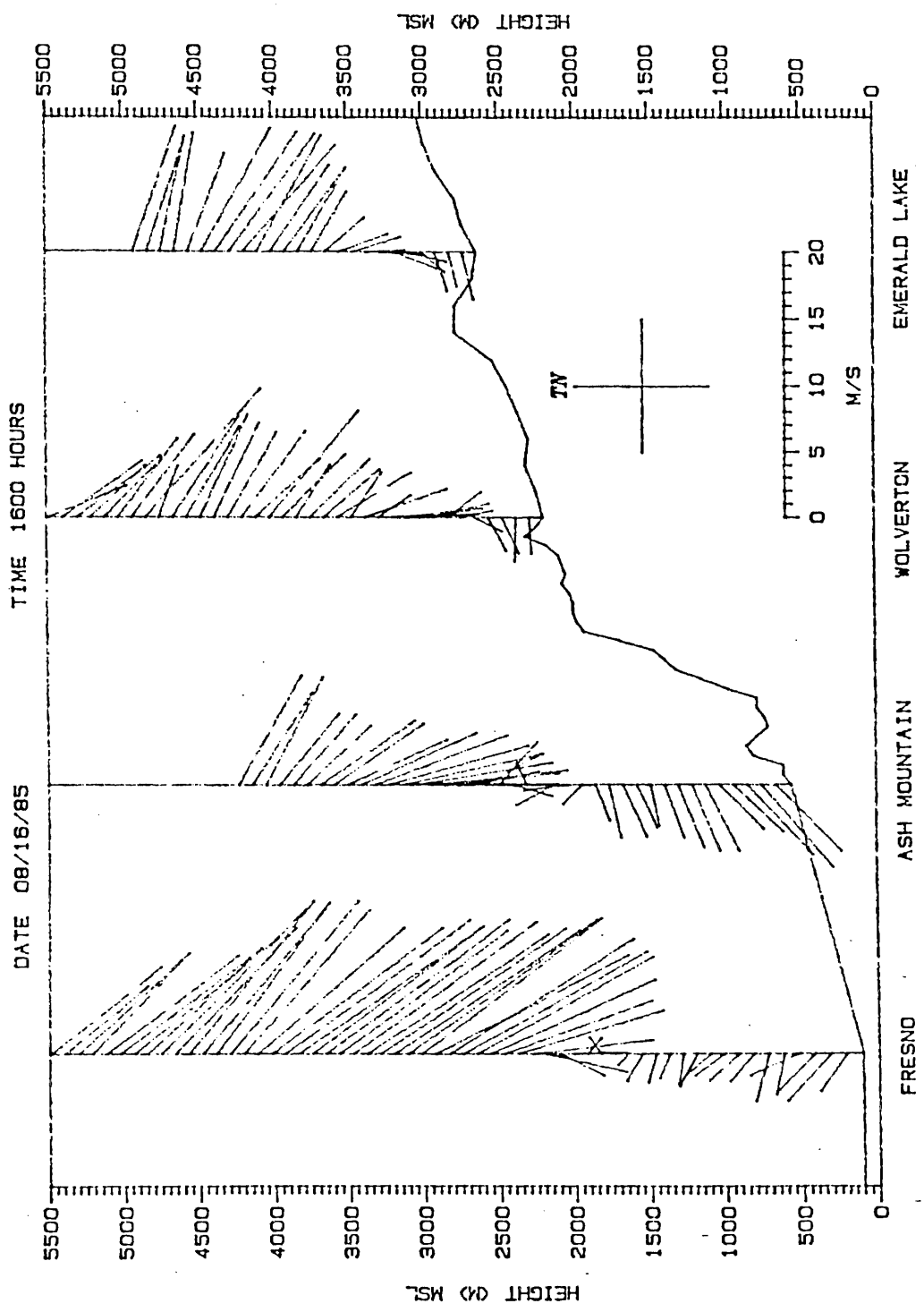


Figure 21: Pilot balloon wind profiles for August 16th, 1985, at 1600 PDT.

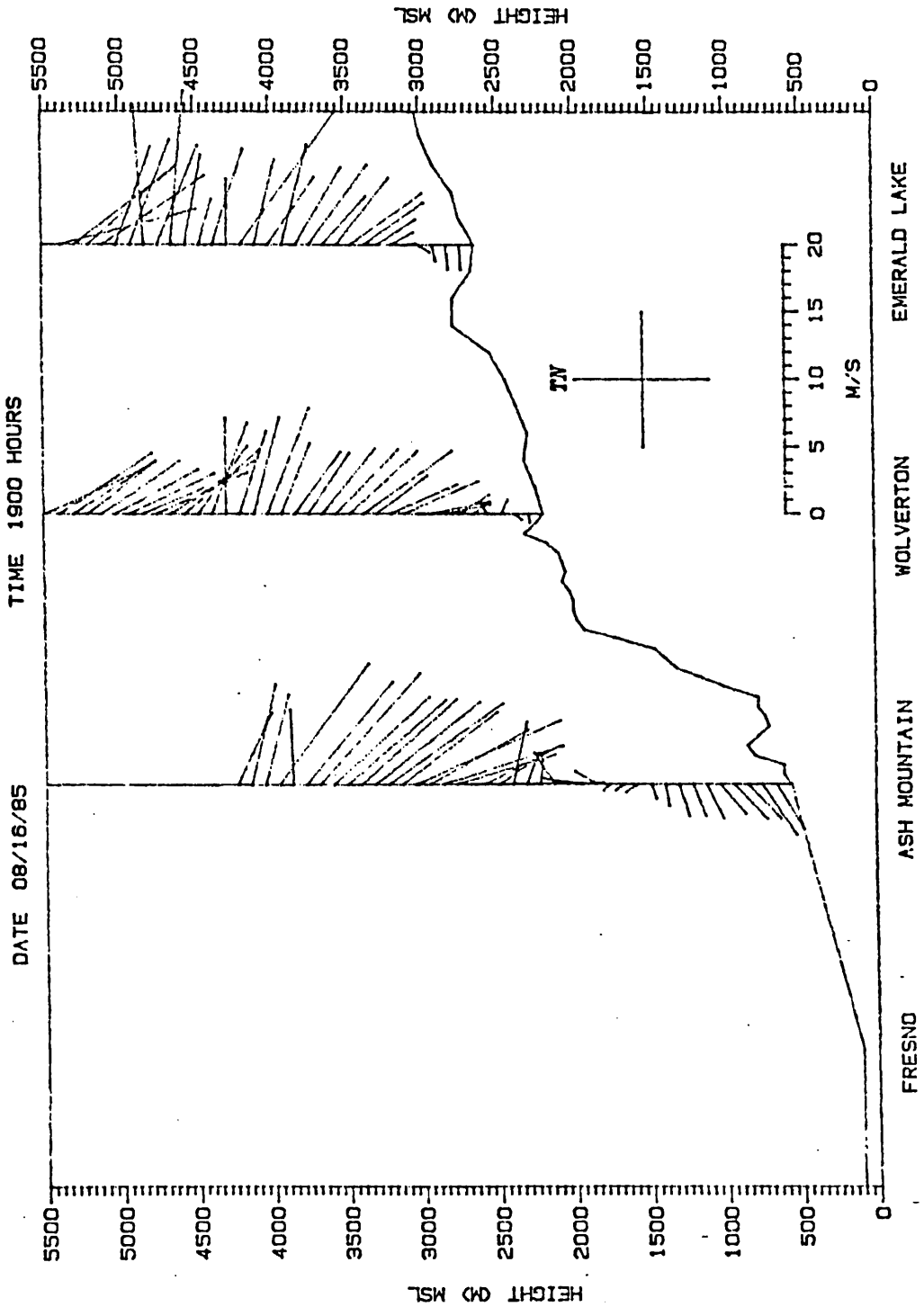


Figure 22: Pilot balloon wind profiles for August 16th, 1985, at 1900 PDT.

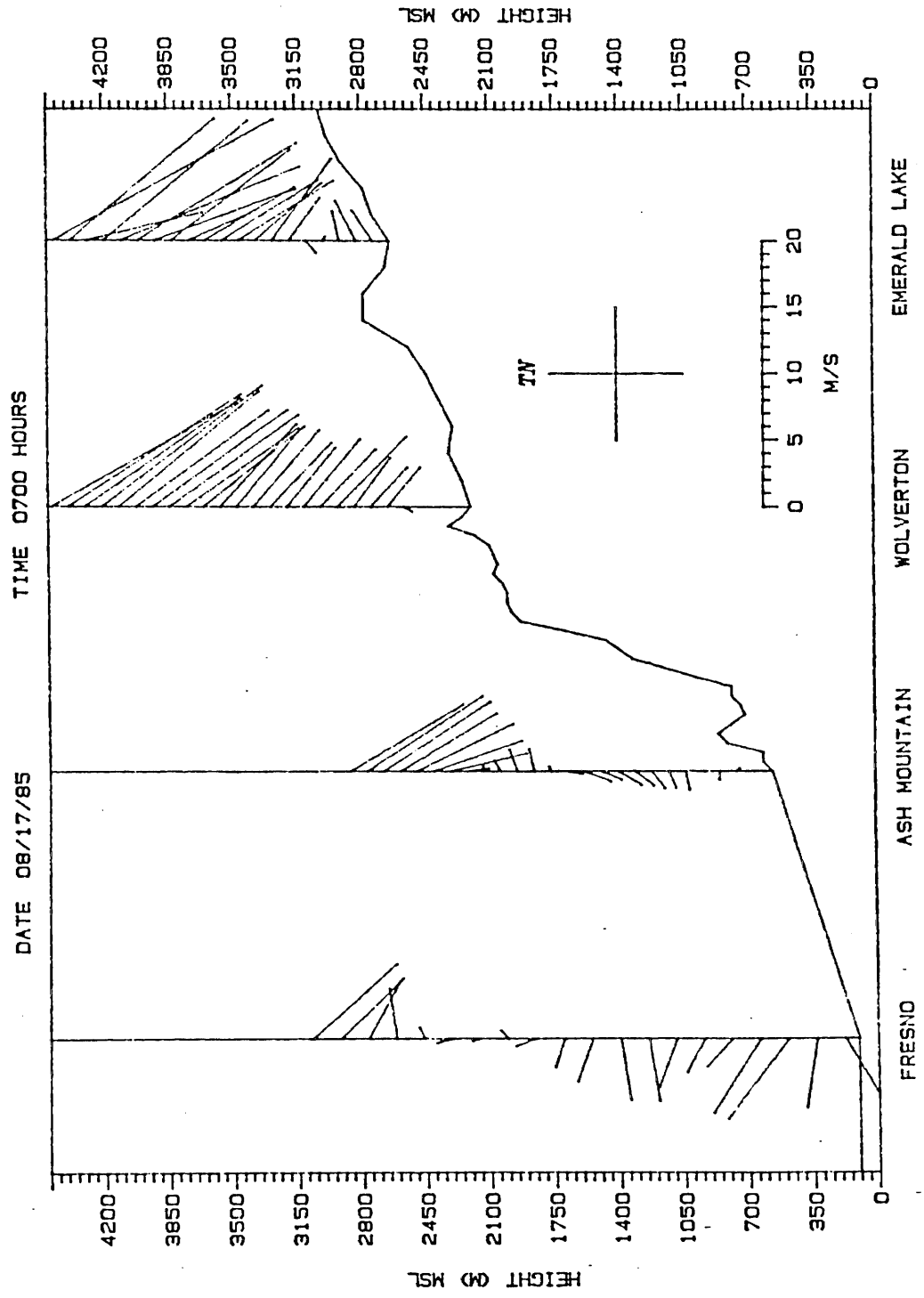


Figure 23: Pilot balloon wind profiles for August 17th, 1985, at 0700 PDT.

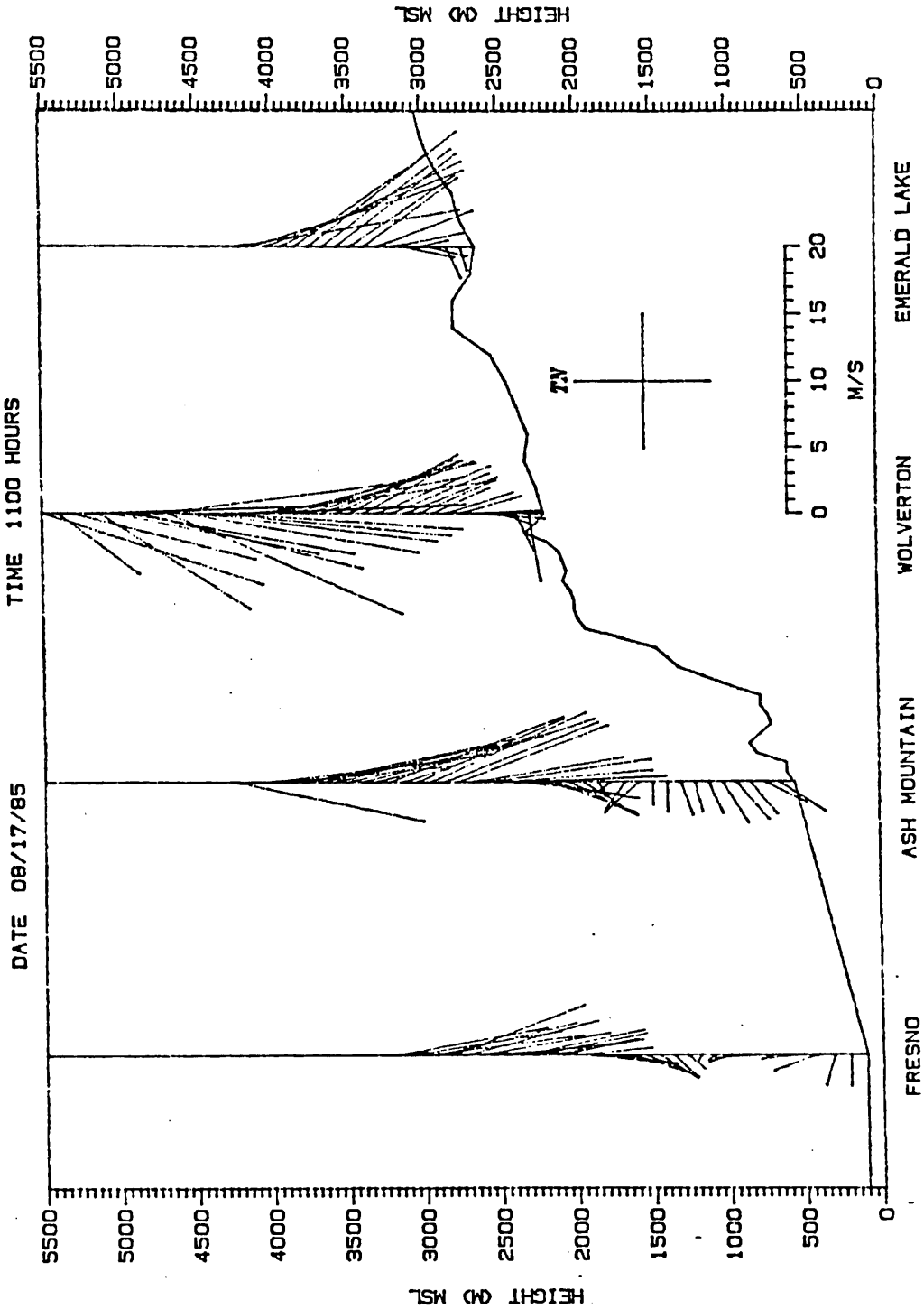


Figure 24: Pilot balloon wind profiles for August 17th, 1985, at 1100 PDT.

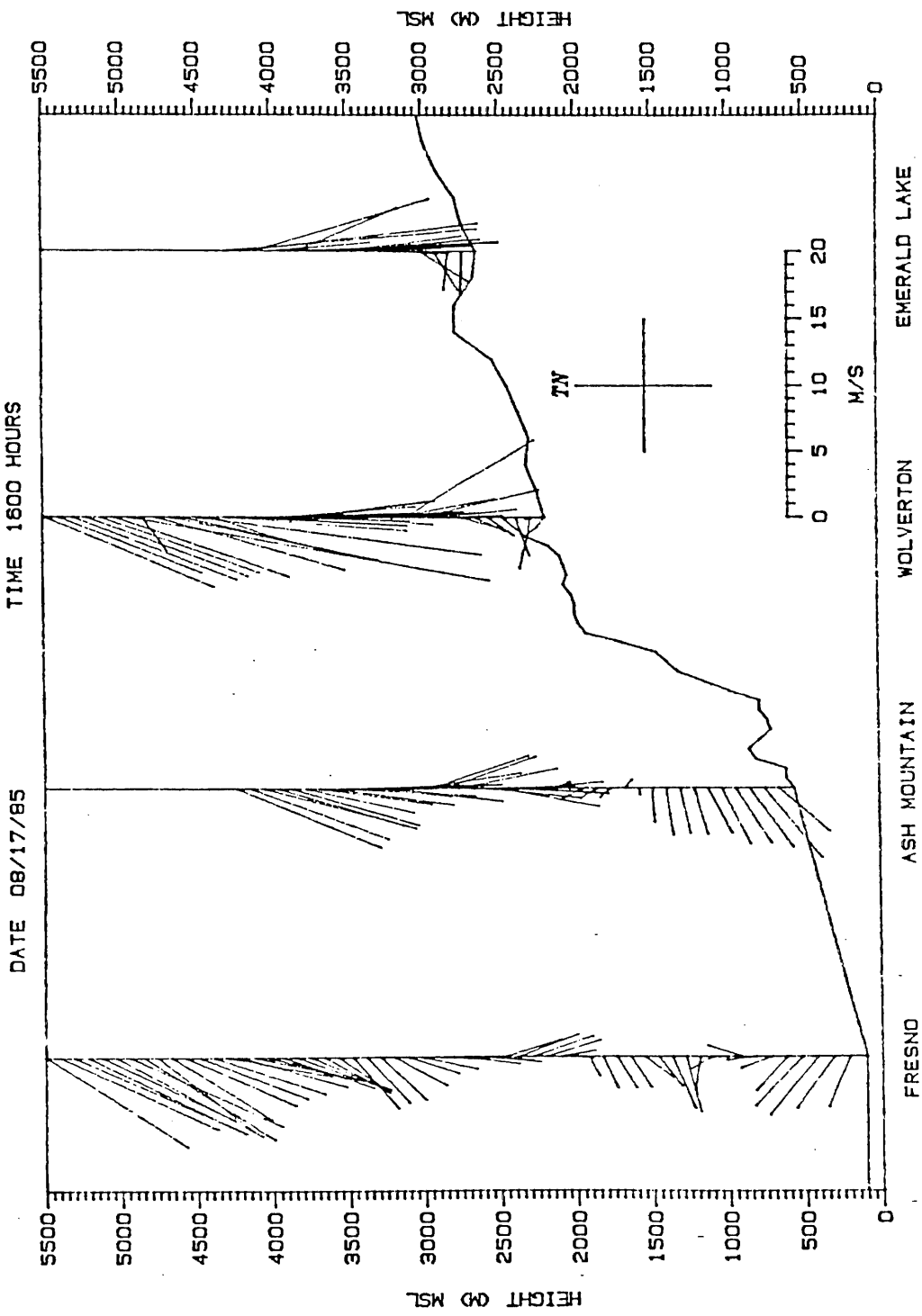


Figure 25: Pilot balloon wind profiles for August 17th, 1985, at 1600 PDT.

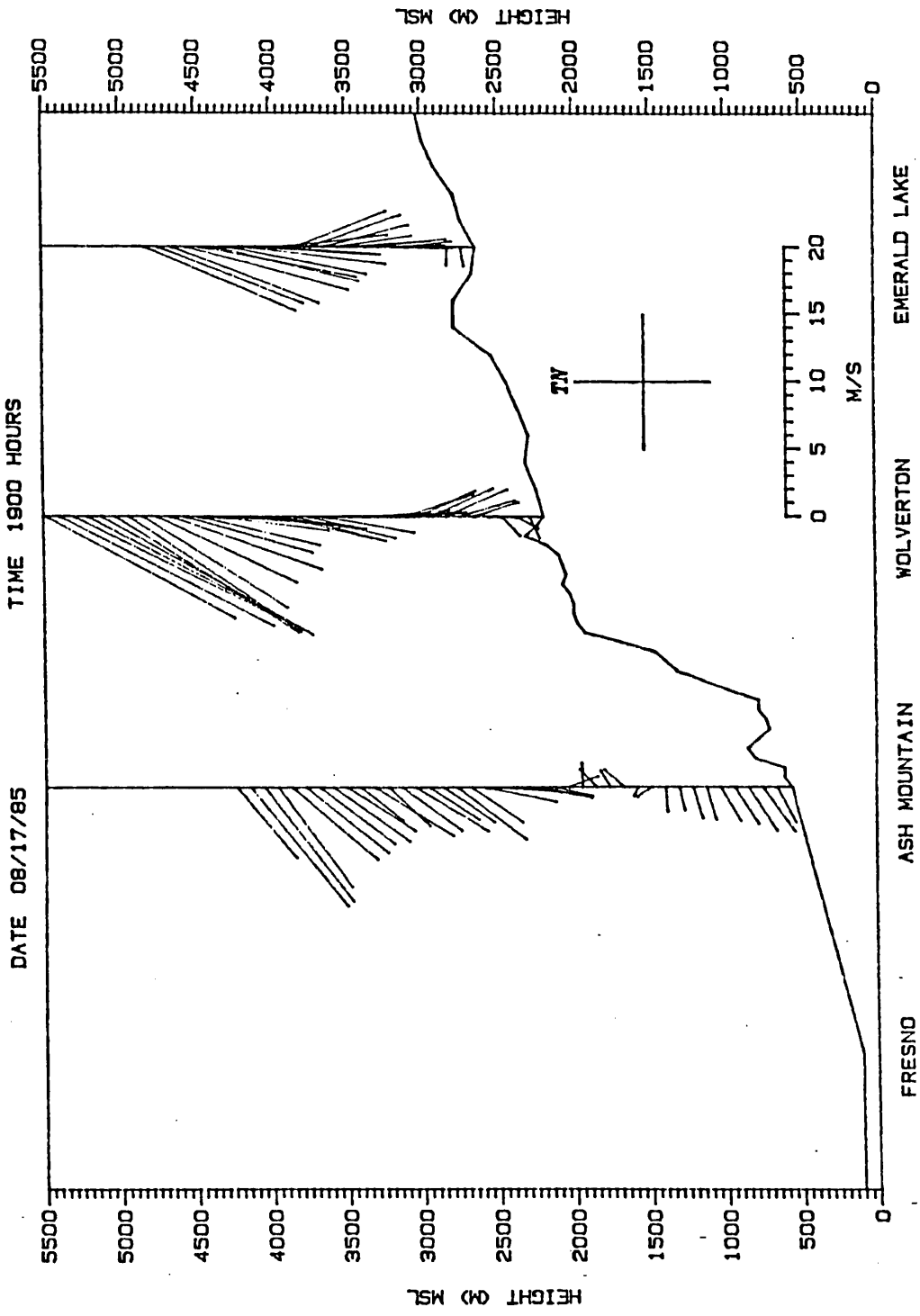


Figure 26: Pilot balloon wind profiles for August 17th, 1985, at 1900 PDT.

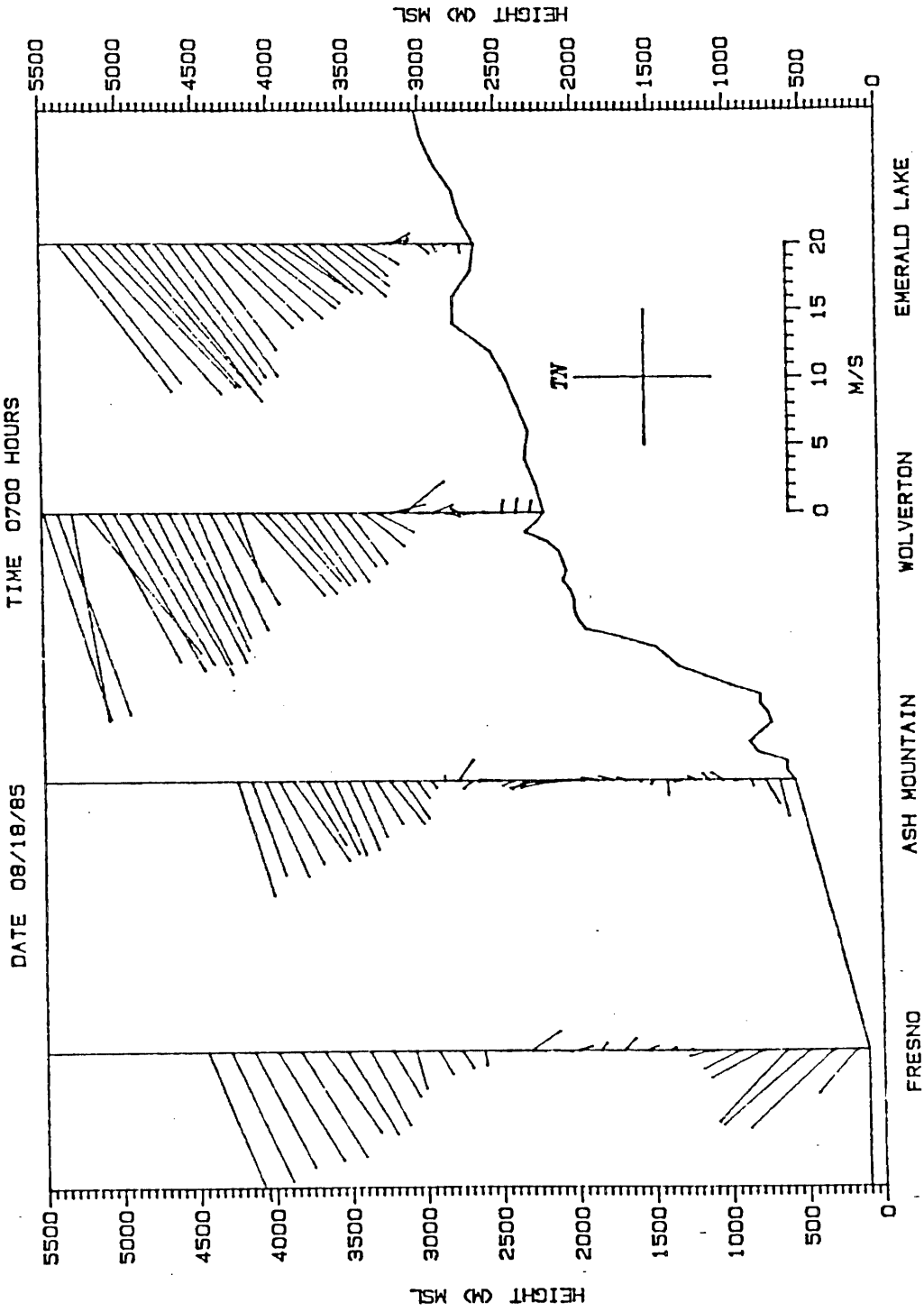


Figure 27: Pilot balloon wind profiles for August 18th, 1985, at 0700 PDT.

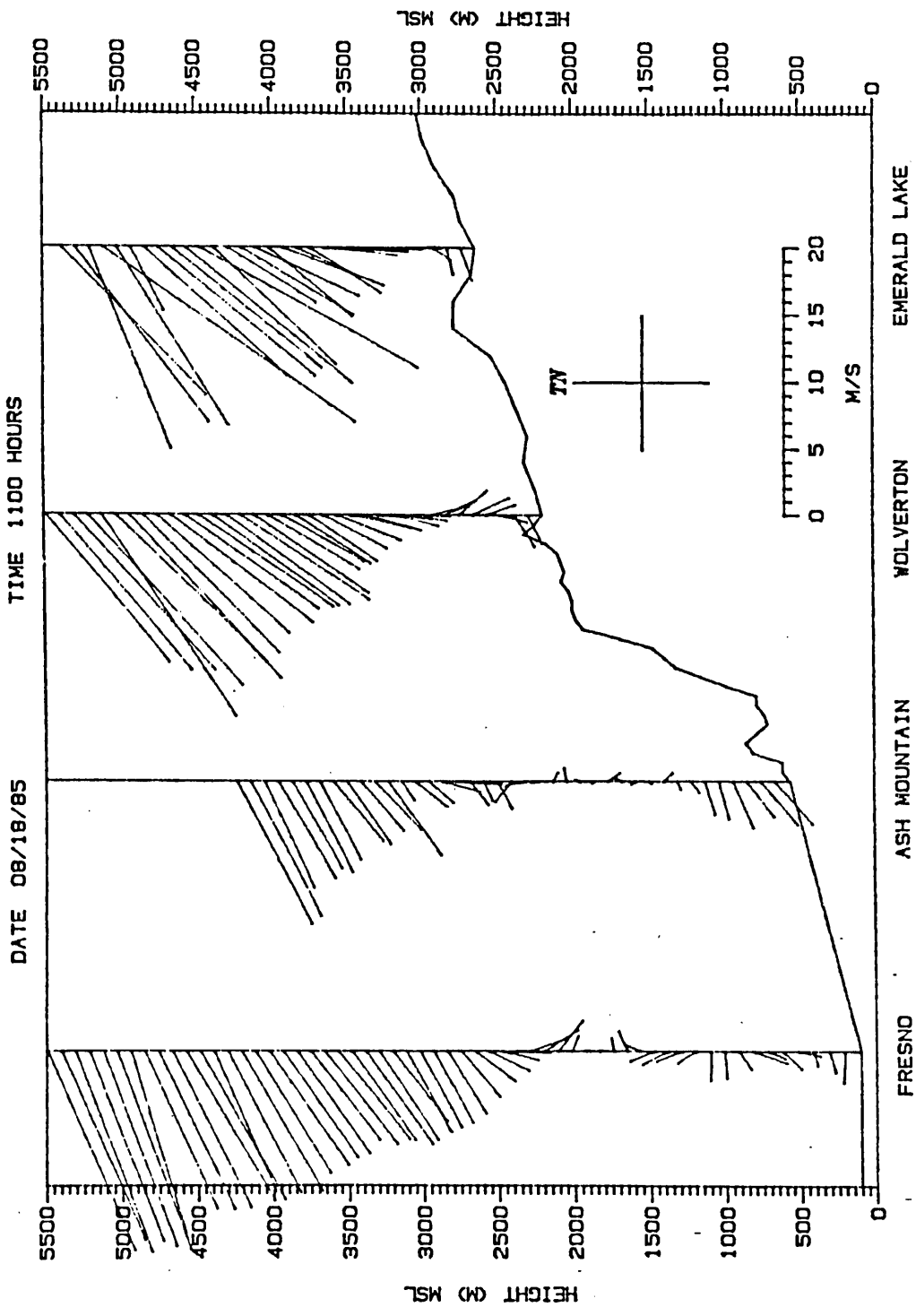


Figure 28: Pilot balloon wind profiles for August 18th, 1985, at 1100 PDT.

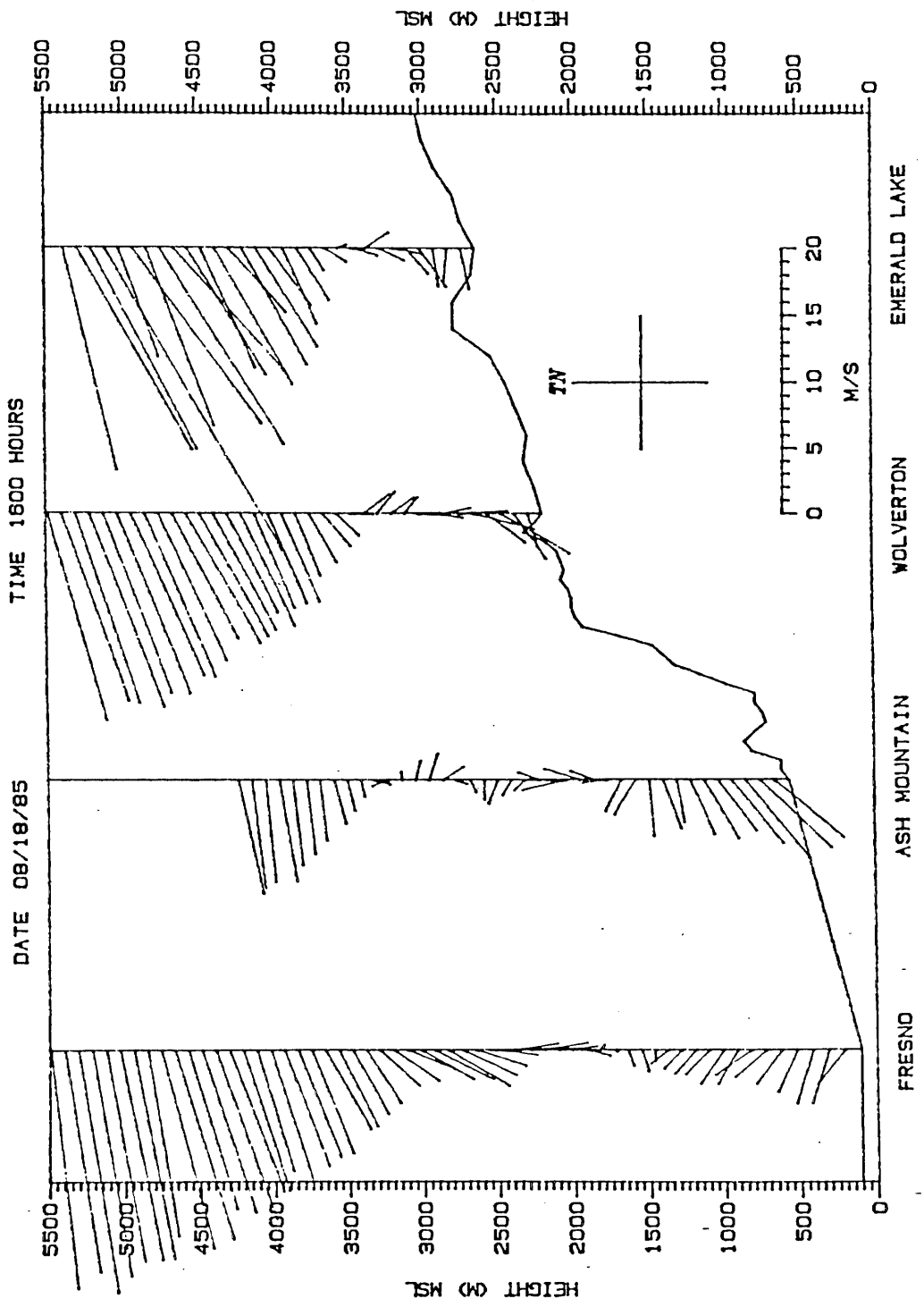


Figure 29: Pilot balloon wind profiles for August 18th, 1985, at 1600 PDT.

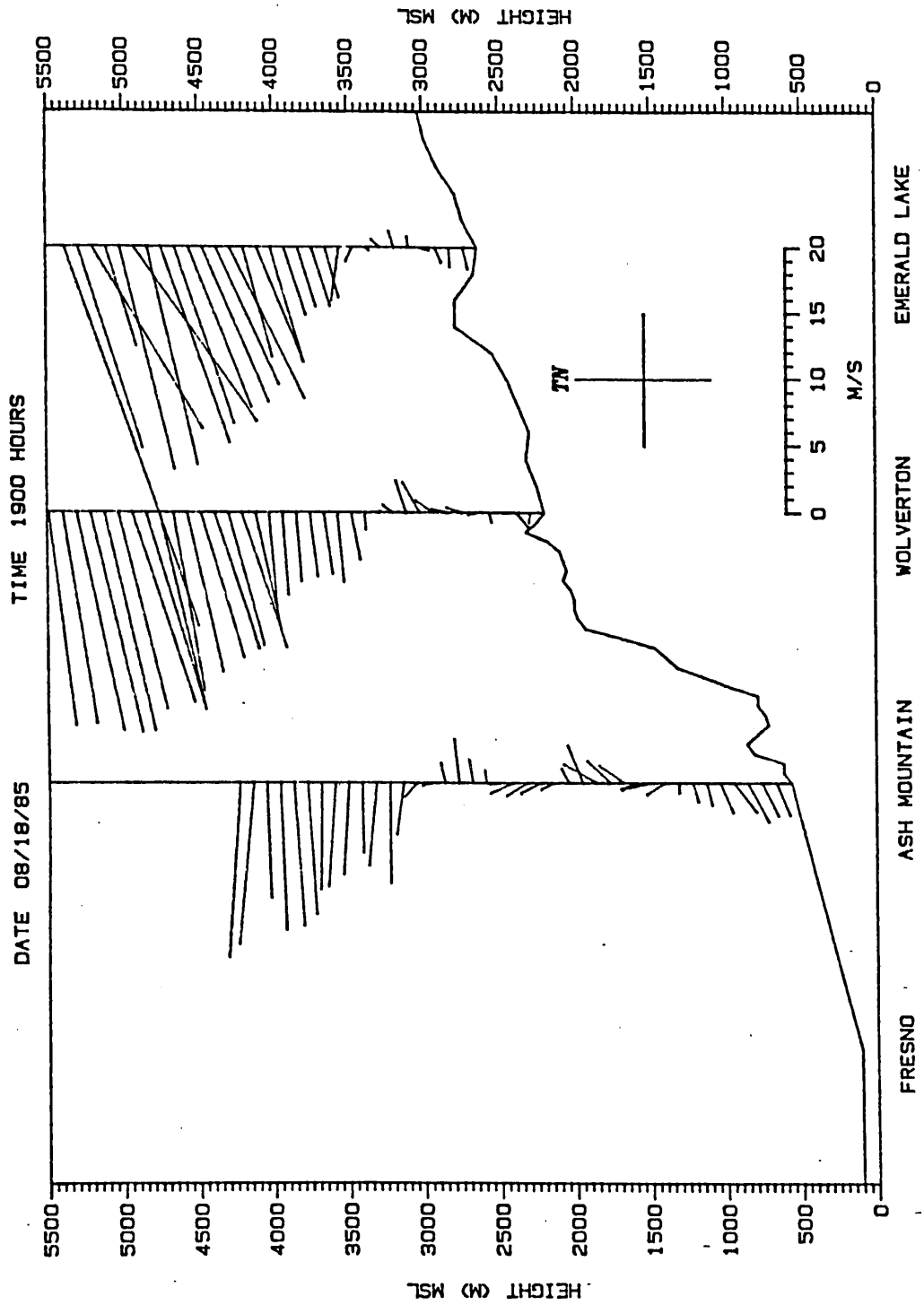


Figure 30: Pilot balloon wind profiles for August 18th, 1985, at 1900 PDT.

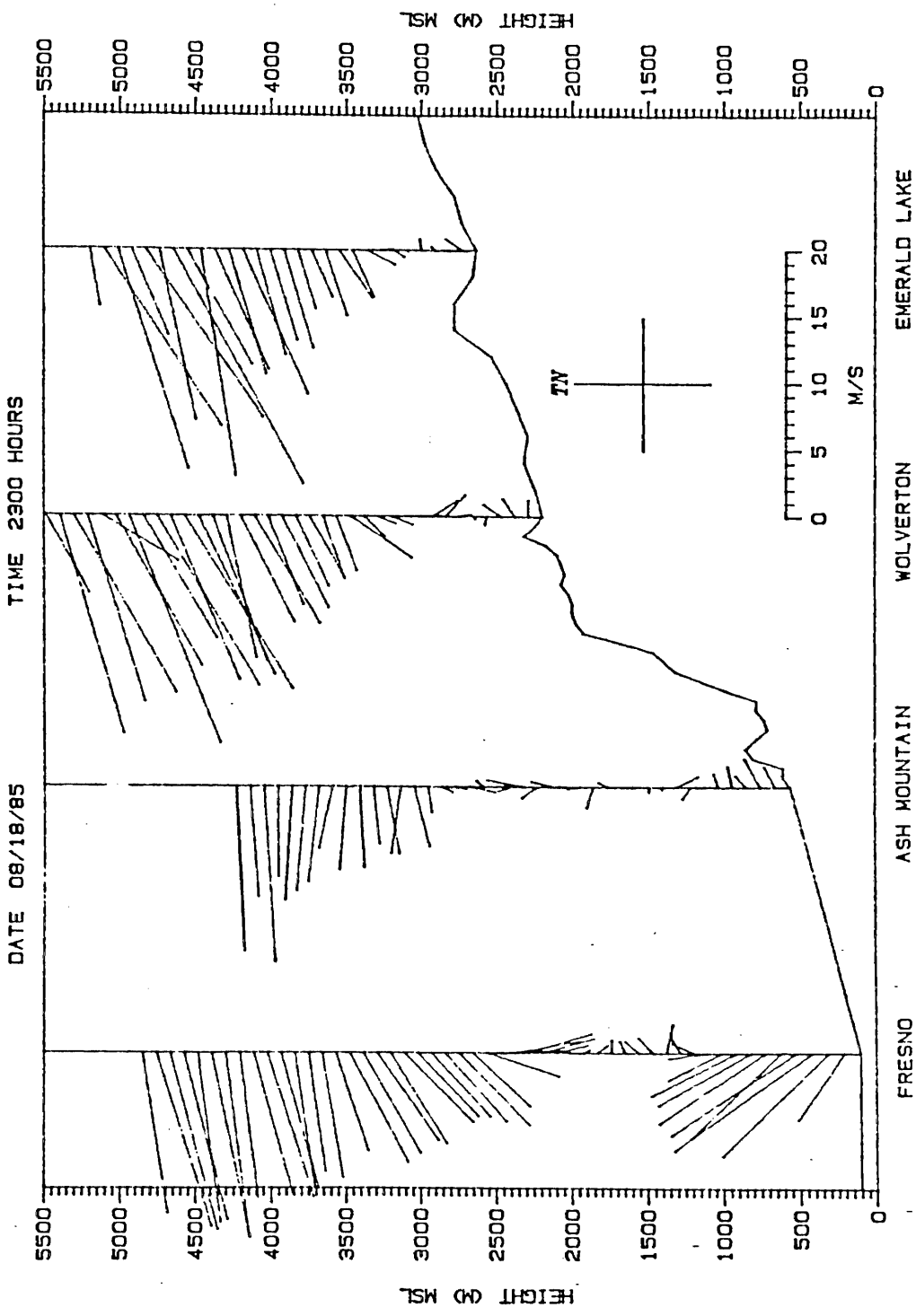


Figure 31: Pilot balloon wind profiles for August 18th, 1985, at 2300 PDT.

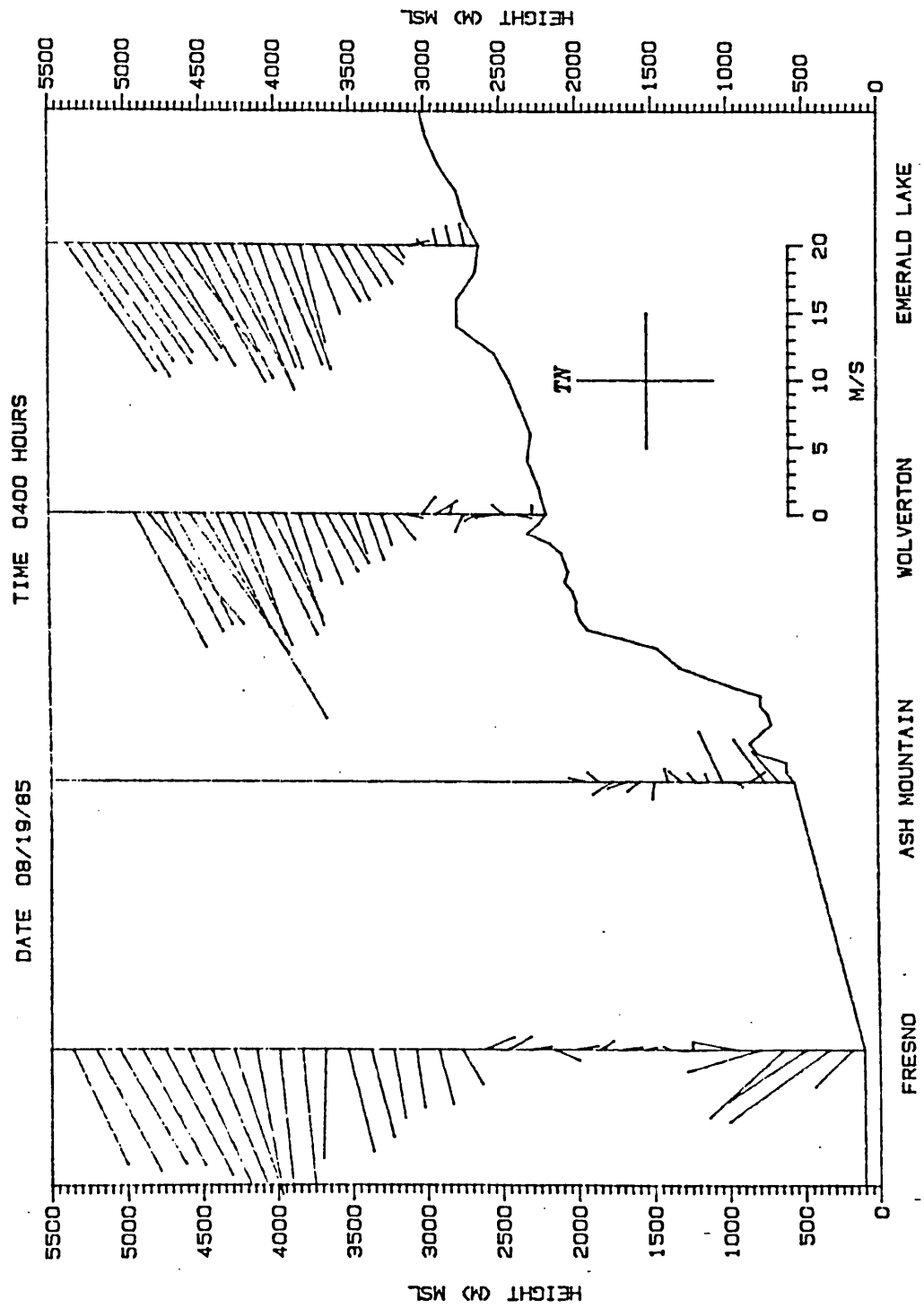


Figure 32: Pilot balloon wind profiles for August 19th, 1985, at 0400 PDT.

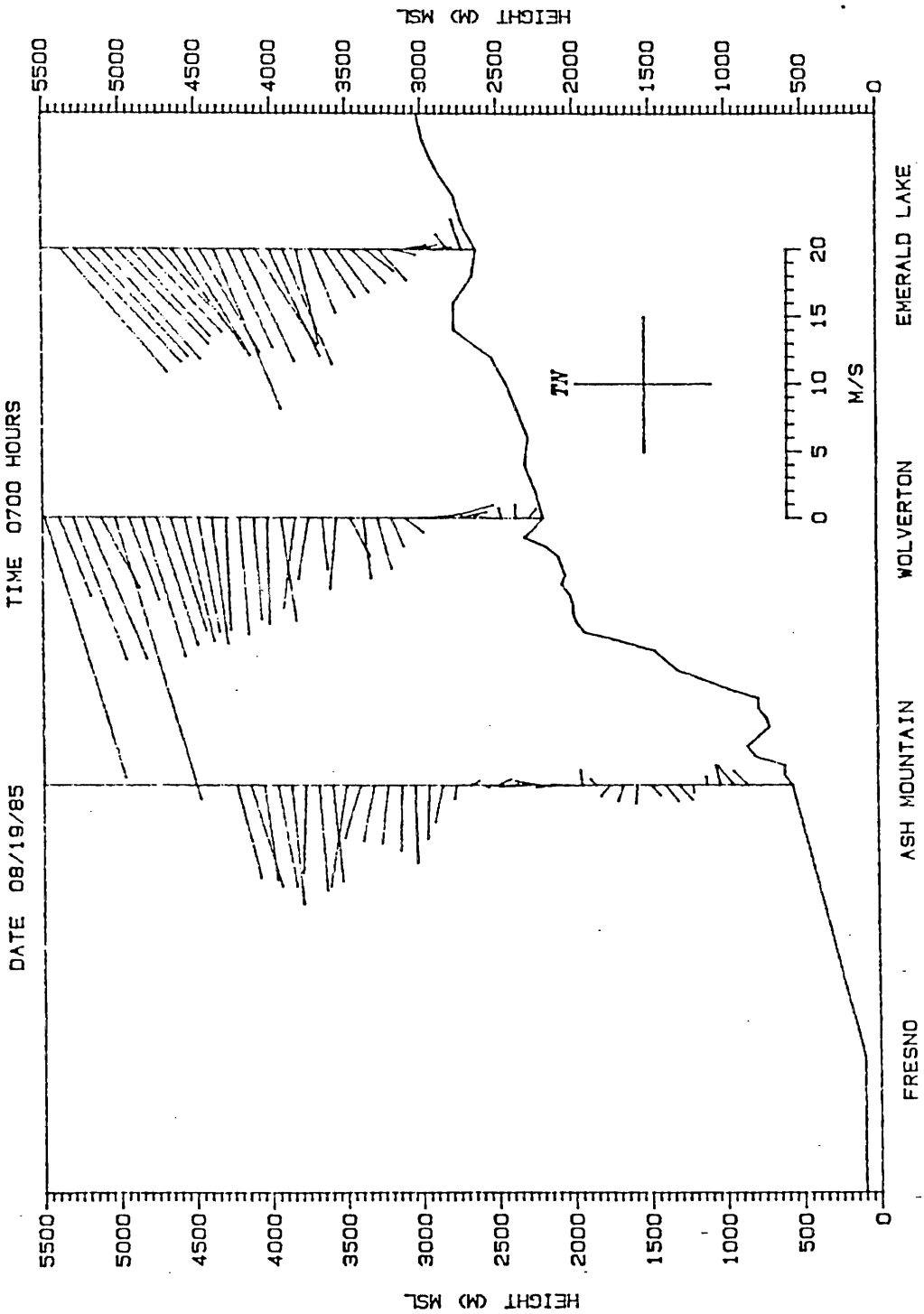


Figure 33: Pilot balloon wind profiles for August 19th, 1985, at 0700 PDT.

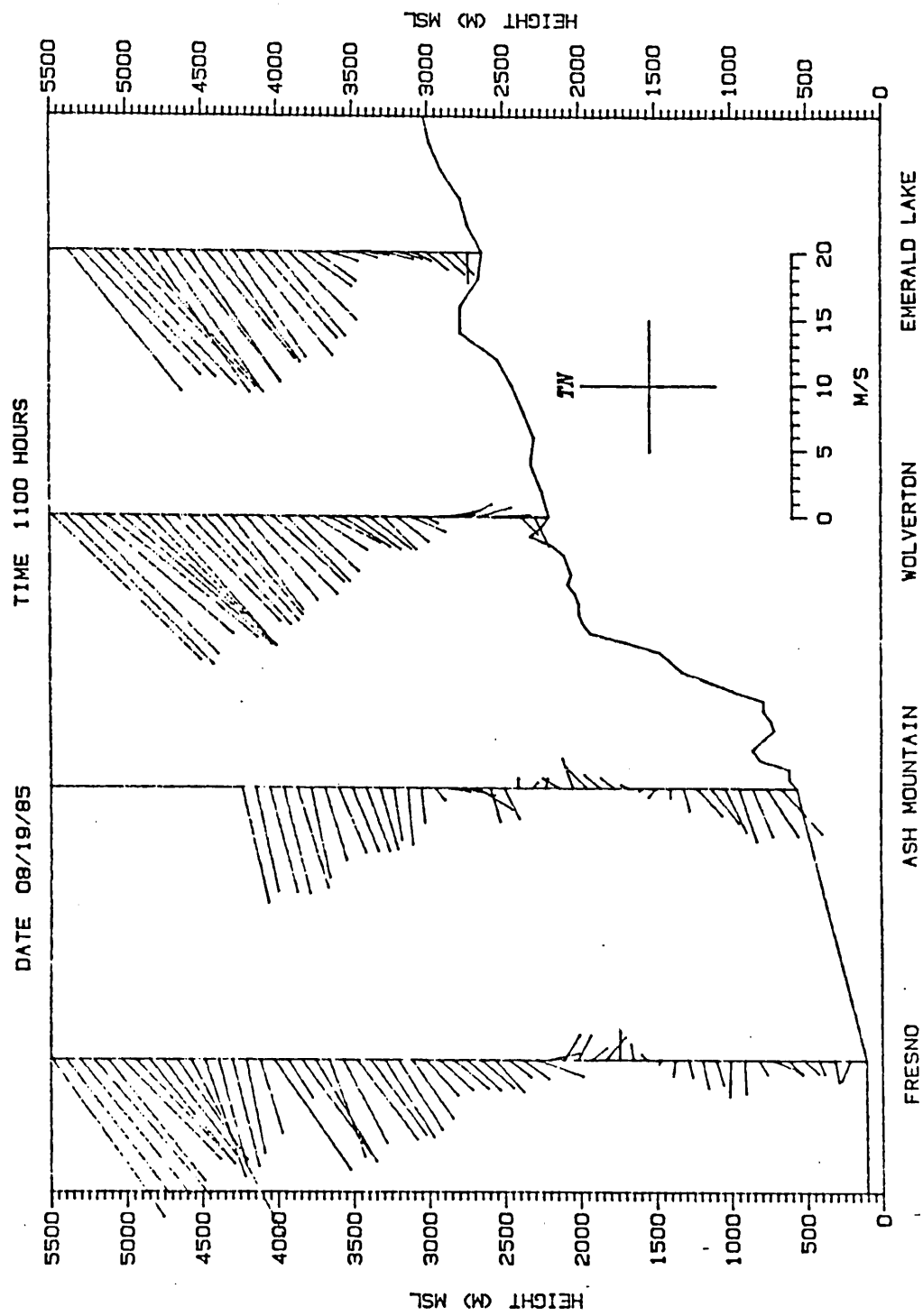


Figure 34: Pilot balloon wind profiles for August 19th, 1985, at 1100 PDT.

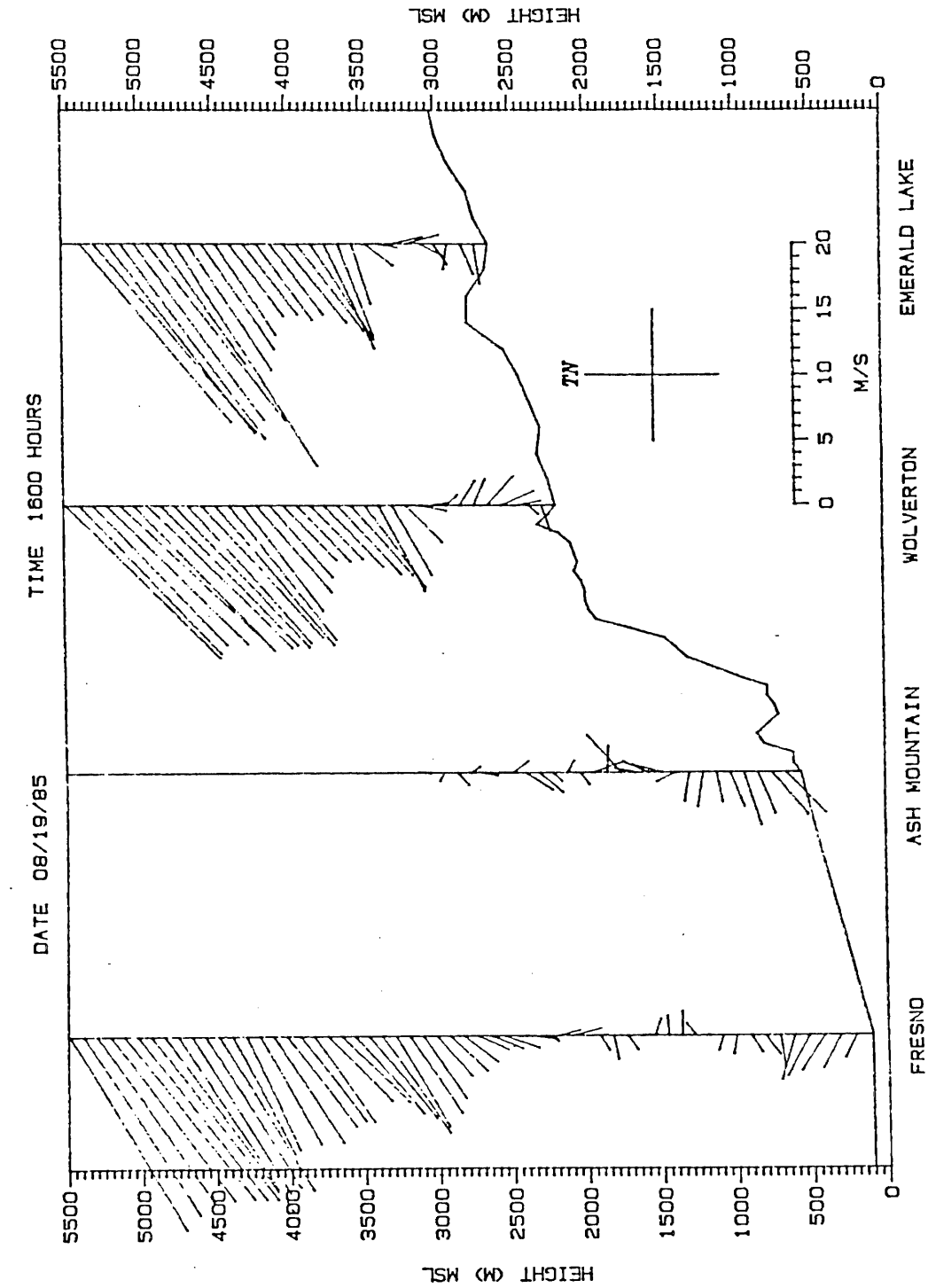


Figure 35: Pilot balloon wind profiles for August 19th, 1985, at 1600 PDT.

*00000949*
ASSET